UNIVERSITY OF CALIFORNIA
RIVERSIDE

Theory of Quantum Spin Liquids in Quasi–1D Systems

A Dissertation submitted in partial satisfaction
of the requirements for the degree of

Doctor of Philosophy

in

Physics

by

Amir Mohammadaghaei

September 2020

Dissertation Committee:

Professor Kirill Shtengel, Chairperson
Professor Shan–Wen Tsai
Professor Nathaniel Gabor

The Dissertation of Amir Mohammadaghaei is approved:

Committee Chairperson

University of California, Riverside

Acknowledgments

No achievement is a work of a single man and credit should be given where it is due. Almost all of this work would not have been possible without the help of all the people who through the years assisted me with my technical questions, understanding of fundamental theoretical aspects, and of course all forms of emotional, technical, and financial support.

First, I am, of course, grateful to my advisor, Kirill Shtengel, without whose help, I would not have been here. My PhD program was not drama–free. I went through months of difficulty coming back to the US due to visa issues. I had numerous occasions of feeling stuck in my research with very little progress. I experienced many stressful situations such as the time when my mother was traveling during the travel ban. I have been through irregularities with my teaching performance as a teaching assistant. Kirill always offered his support when I was in need and did not hesitate to give me life lessons as well. He was a mentor, not just in physics but in all ways of life.

In addition, I would like to especially thank Bela Bauer, and Ryan Mishmash for many hours of fun conversation which provided me with valuable insights toward my research.

Multiple people and institutions hosted me during my graduate program. In particular, I am thankful to Microsoft station Q, for an amazing internship and the opportunity to meet their quantum computing team, experience the environment of UCSB, and participate in KITP seminars. I also thank the organizers of the "Boulder School for Condensed Matter and Materials Physics" for the amazing 2018 summer school at the University of Colorado, Boulder, focused on quantum information and quantum computation, which led

to many good memories and lasting friendships. Furthermore, I thank organizers at the Max Plank Institute for Complex Systems in Dresden, Frank Pollmann at the Technical University of Munich, and Frank Verstraete at the University of Ghent, for hosting me as a research visitor.

As a graduate student at UCR, I learned a lot during the classes and conversations with the faculty of physics, especially those whom I shared a floor with, Shan–Wen Tsai, Michael Mulligan, Vivek Aji, Leonid Pryadko, Nathaniel Gabor, and Chandra Varma. I would also like to thank the mathematics faculty at UCR, especially, John Baez, Vyjayanthi Chari, and Carl Mautner for my foundational mathematical understanding. Additionally, I had numerous conversations with many graduate students in physics, mathematics, material science engineering, and other departments, each of which had great impact on my approach to physics and the graduate student life in general.

It is also very important to thank all the people who called me their friend. They showed me love despite my unstable, unorthodox, and often intolerable personality. Many people offered me the gift of their friendship, which is arguably the most valuable of all gifts. Here is an incomplete list: Shiva, Hamed, Ali, Shima, Siavash, Maryam, Raelynne, Silvia, Frank, Chai, Amartya, Steven, and Shane.

Lastly, I genuinely want to thank my family, extended and nuclear. I was a difficult child, and rarely respected family gatherings and traditions. Nevertheless, I was always loved, often unconditionally. I have never put the time to appreciate any of them. I am forever grateful for the best possible childhood I could have ever had.

The following publication is used in chapter 4 :

- *Signatures of gapless fermionic spinons on a strip of the kagome Heisenberg antiferromagnet*, Amir M-Aghaei, Bela Bauer, Kirill Shtengel, Ryan V. Mishmash, Phys. Rev. B 98, 054430 – Published 27 August 2018

To my mom, *Roya*, and my dad, *Arman*.

I was a terrible child; they loved me regardless!

ABSTRACT OF THE DISSERTATION

Theory of Quantum Spin Liquids in Quasi–1D Systems

by

Amir Mohammadaghaei

Doctor of Philosophy, Graduate Program in Physics
University of California, Riverside, September 2020
Professor Kirill Shtengel, Chairperson

Ever since the introduction of resonating valence bond states by P. W. Anderson in 1970s, the search for exotic many–body quantum behavior in peculiar states of matter known as quantum spin liquids has been a central challenge in the field of condensed matter physics. An important searching ground for such *quantum–ness* is the low energy physics of frustrated magnets. In a quantum system, frustration—the inability of a physical system to achieve a global state that consistently minimizes its energy locally—enables the unavoidable quantum fluctuations to hybridize an extensive number of classical states into highly entangled quantum states at low temperatures. It can be argued that this is the most practical approach to achieve genuine many–body quantum behavior at large scales.

The fundamental source of frustration in many physical systems, is the existence of local non–commuting terms. In the case of antiferromagnet spin theories the simplest examples are triangles of nearest–neighboring sites. Consequently, lattices with triangles as building blocks have long been studied in hopes of discovering spin liquids physics. In particular the kagome lattice, which is composed of corner–sharing triangles, has been the

center of at least four decades of spin liquid research. This is due to the underconstrained nature of system made out of corner–sharing triangles.

After the first three chapters, introduction in chapter 1, preliminary physics in chapter 2, and a brief introduction to spin–liquids in chapter 3, in chapter 4 I tackle a simpler version of the long-standing problem of spin–1/2 Heisenberg antiferromagnets by considering a quasi–1D lattice consisting entirely of corner–sharing triangles, *kagome strip*. I illustrate that the standard Heisenberg antiferromagnet Hamiltonian over kagome strip is an extended gapless quantum phase, that is well characterized by two fermionic/bosonic gapless modes and power–law decaying spin and bond–energy correlations. I also demonstrate that the correlation functions oscillate at tunably incommensurate wave vectors. It turns out that this phase can be identified by a particular marginal instability of a two-band spinon Fermi surface coupled to an emergent U(1) gauge field. This interpretation is supported by analytic Abelian bosonization and with extensive numerical large–scale density matrix renormalization group study as well as variational Monte Carlo calculations on Gutzwiller ansätz wave functions. This intriguing result is the first numerical demonstration of emergent fermionic spinons in a simple SU(2) invariant nearest-neighbor Heisenberg model beyond the strictly 1D (Bethe chain) limit.

The unexpected success of the fermionic spinons in describing the low energy physics of kagome antiferromagnet, reintroduces the questions about the validity of spinon physics as an effective theory of quantum spin liquids. However, numerical methods are still far behind the theoretical advances. And still even today, an accurate description of the quantum spin liquid states using tensor network methods is notoriously challenging. It

is known that for large quasi-1D systems, the density matrix renormalization group and related methods usually require significant computational resources and sometimes fail to converge to a satisfactory state. On the other hand, variational wavefunctions acquired from the Gutzwiller projection of gaussian fermionic theories have long served as both a theoretical starting point for the construction of such spin liquid states and as an inspiration for numerical variational Monte Carlo (VMC) to calculate observables of interest. Noting this observation I examine a different method by exploring the possibility of constructing a matrix product state (MPS) representation for a Gutzwiller–projected state from two given MPS representations of gaussian fermionic theories in the 5 chapter.

I investigate the complexity of different approaches to achieve Gutzwiller projection for MPSs and introduce the novel algorithm which we call the Guzwiller zipper method. The performance of the algorithm is tested against two copies of a single half-filled band of spin-1/2 fermionic spinons. In a successful attempt to describe the nature of spin liquid states on quasi-1D strips of triangular and kagome-like lattices, I apply this method to two MPS of multi-band fermionic spinon theories and compare with the complexity of the traditional VMC approach. In particular, we methodically disprove the conjecture of a spinon fermi surface spin liquid for the triangular lattice.

Finally, I conclude this thesis by laying out a bird's eye view of the current and future of spin liquid physics in kagome and triangular lattices and pointing out numerous possible applications of the novel Gutzwiller zipper method. In addition, I would also discuss its possible extensions to more complicated tensor networks as well as versions for higher spatial dimensions.

Contents

List of Figures

List of Tables

Chapter 1

Introduction

The advent of quantum theory has proved incredibly successful in giving an accurate description of the fundamental laws that govern nature. For example, quantum electrodynamics predicts fundamental physical constants with an impressive accuracy to a few parts per billion as confirmed by state–of–the–art research laboratories [107], and we are yet to observe an experiment in contradiction with its basic principles. Nevertheless, despite its undeniable contributions to the modern state of our society, its true power has yet to be fully exploited. In particular, the dream of building a device that performs a radically new form of computation solely based on the principles of quantum theory [38], i.e. the *quantum computer*, despite significant progress, has not yet been fully realized [103, 79, 5, 72]. One particularly challenging step is the development of a sufficiently descriptive theory for quantum systems consisting of thermodynamically many interacting particles. This problem is the main focus of condensed matter physics; where novel theoretical and numerical methods are used to explain experimental observations of systems that are assumed to function

according to the low–level description of quantum mechanics and therefore explore them for new possibilities.

As one might suspect, however, not every quantum model has the capacity to utilize the power of quantum mechanics in full. It turns out that one needs to search for the so–called *frustrated systems* [133, 136]. When the low–energy state of a quantum system is incapable of simultaneously satisfying a large number of enforced constraints, it remains frustrated. This scenario, together with the unavoidable quantum fluctuations[1], leaves an extensive portion of the Hilbert space available to the frustrated quantum system to explore. Under these same circumstances, even down to very low temperatures, a classical system manifestly violates the third law of thermodynamics approaching $T = 0$. However, a quantum system exhibits a highly entangled many–body liquid–like behavior at low temperatures [130, 90, 9]. That is why such states–*quantum liquids*–are good candidates for observations of purely quantum mechanical effects at large scales. Examples of condensed matter systems expected to have high degrees of frustration are those with kagome or triangular lattices. The two–dimensional version of various theories on these lattices are still debated despite 40 years of theoretical and computational effort.

A particularly interesting class of quantum liquids are the states of Hamiltonians made purely of spin degrees of freedom. These were originally studied in the field of quantum magnetism. Quantum spin liquids (QSL) are elusive states of quantum matter that defy usual ordering down to very low temperatures, may contain long–range quantum correlations, and exhibit nontrivial quasiparticle excitations [117, 9, 152, 19]. This surprising behavior is often caused by the inability of the system to minimize its energy locally.

[1]The quantum fluctuations are guaranteed by the uncertainty principle.

Such frustration thus makes the ground state (and its low–energy excitations) a system–wide compromise between extensively many quantum degrees of freedom. The resonating valence bond (RVB) state initially proposed by Anderson [4, 3] was the first example of a *gapped* QSL—such gapped spin liquids have since been long studied for their fundamentally interesting behavior as well as for their potential application to robustly store quantum information and perform fault–tolerant quantum computation [74, 75]. Despite their long–range entanglement, the gapped nature of these states make computational studies that are based on tensor networks more tractable, at least in low dimensions $D \leq 3$.

There are two main questions to answer when it comes to systems suspected of exhibiting quantum liquid behavior:

1. Do such systems at low temperature harbor *exotic* quantum phases that can be manipulated to make useful devices such as a quantum computer? If yes, how robust are these phases to external perturbations and the existence of impurities in experimentally relevant circumstances?

2. Is it possible, or practical, to extend such descriptions to systems beyond quasi-one-dimensions? For example, one can think of a relatively small one–dimensional periodic strip as a few one–dimensional cuts in the Brillouin zone of a theory corresponding to a two–dimensional system. This realization may reveal some hints toward the nature of two–dimensional theory.

We live in a three–dimensional space and we expect the physics to describe a three–dimensional world, however, it has been shown that many interesting physical phenomena arise in lower dimensions. Experimental and theoretical work restricted to two

spatial dimensions has uncovered revolutionary quantum physics, such as topological non-trivial phases with *anyonic* excitations [52, 74]. Additionally, the simplicity of working with only one spatial dimension often permits a complete theoretical investigation using techniques available from conformal field theory [14], Bosonization [42, 43], and exactly solvable models [15, 13]. Furthermore, the adaptation of efficient numerical techniques to verify underlying physics being studied, such as the possibility of performing exact diagonalization for decent sized systems [116], matrix product state based algorithm such as the density matrix renormalization group (DMRG) and the time–dependent variational principle (TDVP) [144, 145, 139, 94, 49, 48]. As a result, low–dimensional systems serve as a convenient playground for testing the ideas of theoretical physics in the realm of many–body systems. However, this should not lead to the confusion that the one–dimensional models are just fictitious objects in minds of theoretical physicists. But rather, materials can be engineered to behave effectively as one-dimensional objects, i.e. they are confined in the other two dimensions using potential barriers. These models also have critical importance for companies such as Microsoft that are basing their quantum computer design on such a quasi–one–dimensional system–the majorana qubit [72].

Due to the importance of quantum entanglement in identifying the phases of matter, it is now common to use theoretical and numerical techniques that are mainly derived from the field of *quantum information* to study condensed matter systems. In the early days of quantum theory, quantum information guilty of being too mathematical, was generally dismissed by theoretical physicists. However, more recently methods based on quantum information have become indispensable in the studies addressing the foundations of physics.

In addition to that, quantum information is the natural underlying language of a quantum computer. Utilizing tools from quantum information theory facilitates calculation of certain quantities related to quantum entanglement, such as von Neumann and Renyi entropies, entanglement spectrum, and other related quantities, in a straightforward manner. It is now well–established that the bipartite entanglement, i.e. the entanglement present in the density matrix corresponding to one part of the bipartition of the system, inherits important and revealing information about the nature of the state. In a set of works, Kitaev and Preskill as well as Levin and Wen, have shown that topological states are characterized by a non–trivial *topological entanglement entropy* which can be measured by simple formula involving the six possible choices of bipartitions for a state of a system divided into three parts [73, 86]. More recently it is been shown that at least in systems confined to one spatial dimension, bipartite entanglement reflects the topological properties of the quantum state under study [33, 135, 111].

Classical simulation of quantum many–body states with long–range massive entanglement remains an active field of research [116, 41, 134, 144, 145, 118]. This is due to the fact that despite recent claims and advances in building a programmable and reliable quantum computer [5, 25, 72], the classical methods are still the main gadget in a condensed matter physicist's toolbox. This is even more relevant in the case of QSLs due to their long–range massive entanglement. In the case of gapped QSLs, despite their long–range entanglement, the gapped nature of these states make studies based on tensor networks more tractable, at least in two spatial dimensions. However, our general understanding of the gapless QSLs is much more limited. This is in part because studies of gapless QSLs

have long been hampered by the inability of numerical tools to catch up with the theory and experiment. The main classical methods at our disposal all suffer from various shortcomings. In practice, typical simulations usually require a large number of spins to nail down the nature of the state. As a result, the finite-size scaling analysis is almost impossible using exact diagonalization methods and in practice they may only serve to rule out possible ordering, even if that. Additionally, the massive entanglement that grows with system size, prevents numerical approaches such as DMRG to converge entanglement–related quantities such as the von Neumann entropy (as in Refs. [148, 54]). Quantum Monte–Carlo methods usually involve a notorious sign problem leading to large errors in the calculations of correlation functions. Variational methods, as usual, suffer from apriori assumptions about the nature of states that may or may not reflect the true state, and finally, tensor network methods suffer from entanglement blow–ups. All of these shortcomings lead to the same issue, that is the conclusions are to some extent unreliable. Consequently, reaching conclusive conclusions based on well grounded evidence about the nature of the states presents an ongoing challenge, wherein some cases even the existence of the gap, have been debated for decades [115, 87, 67, 44, 63, 62, 91, 55, 149]. Nevertheless, to this day, methods based on tensor network states remain the main tools utilized for classical simulations of QSLs [147, 20, 50, 108, 96, 29, 120, 118, 138, 146, 137].

The coupling of fermionic theories to strong gauge fields has been proposed as a possible effective theory for spin liquid states [143], where the QSL is recovered by the integration of the gauge field. It is expected that the fundamental properties of the resulted QSLs are inherited from the fermionic theories. Examples are gapped states,

three–dimensional QED, and projected Fermi surfaces states. The variational Monte–Carlo method (VMC) has conventionally been used for numerical calculations of correlation functions for the resulted spin state [47, 26]. However, the VMC methodology suffers from various disadvantages. First, since the actual state is not known, only the calculation of the pre–selected set of correlation functions are available. Second, certain entanglement properties of states, for example, the entanglement spectrum is not readily achievable through VMC.

This motivates the continuous effort of exploiting the power of tensor networks ansätze to study the exotic behaviors in these strongly correlated systems. This is because, tensor network based tools when used with powerful computers give an almost faithful representation of the original state. Researchers in the community constantly develop new designs of tensor network tools and combine them with other classical methods to increase their efficiency as well as their descriptive power to study quantum many–body states with massive entanglement, such as QSLs, as well as topological states of interacting fermions featuring non–trivial bulk excitations [56, 22, 21, 121, 119, 30, 111, 135]. Tensor network state has also been employed in tracking the generic quantum states that arise from time evolution of classical un–entangled states under the action of non–integrable Hamiltonians with some promising results [34, 78, 109, 151, 147].

Chapter 2

Preliminary physics

2.1 The setup of condensed matter physics

The main field of condensed matter physics, tries to describe the macroscopic properties of matter, i.e. a large collection of individual particles packed together using their corresponding electromagnetic forces, based on the microscopic fundamental physics governing each particle. The field has historically emerged out of the solid state physics, however today condensed matter physicist study the broad range from complicated interactions in liquid–like materials to unconventional theories of quantum gravity. The current questions of "hard" condensed matter generally revolve around the electronic physics of solids as turned out to be more complicated to be simply described by the ordinary non–interacting physical theories.

The usual starting point for the physics of solid state matter is to describe the fundamental physics as the quantum mechanics of many particles interacting via the electromagnetic long–range interaction. The Hamiltonian is made out of the kinetic terms

for the nuclei and electrons, the Coloumb interaction between electrons and atoms and electron–electron Coloumb interaction.

$$\begin{aligned} \mathrm{H} = &\sum_a \frac{P_a}{2M_a} + \sum_i \frac{p_i}{2m_i} \\ &+ \sum_{a,b} \frac{Z^2 e^2}{|\mathbf{r}_a - \mathbf{r}_b|} - \sum_{i,a} \frac{Ze^2}{|\mathbf{r}_i - \mathbf{r}_a|} + \sum_{i,j} \frac{e^2}{|\mathbf{r}_i - \mathbf{r}_j|} \end{aligned} \tag{2.1}$$

This should not come as a surprise that the brute force approach to solving the Schroedinger's equation is a lost cause, because the space of possible solutions is uncontrollably large.

2.2 Many–Body Quantum Systems

2.2.1 Spins Models

Let us start by the simplest exmaple of a spin model, that is a chain of N sites where on each site $i = 1, \ldots, N$ resides a single two–dimensional Hilbert space h_i i.e. the spin-1/2 Hilbert space. We can choose a natural basis for each h_i,

$$|e_i^0\rangle \equiv e_i^0 \coloneqq \begin{pmatrix} 0 \\ \\ 1 \end{pmatrix}, \quad |e_i^1\rangle \equiv e_i^1 \coloneqq \begin{pmatrix} 1 \\ \\ 0 \end{pmatrix}. \tag{2.2}$$

We also choose a basis for the vector space of linear operators, $\mathrm{End}(h_i) = \langle 1_i, S_i^z, S_i^+, S_i^- \rangle$ defined as

$$S_i^z = \frac{1}{2}\sigma^z, \quad S_i^+ = \frac{1}{2}(\sigma^x + \mathrm{i}\sigma^y), \quad S_i^- = \frac{1}{2}(\sigma^x - \mathrm{i}\sigma^y), \tag{2.3}$$

where the σ operators represent the usual Pauli matrices:

$$\sigma^z = \begin{pmatrix} 1 & 0 \\ 0 & -1 \end{pmatrix}, \quad \sigma^x = \begin{pmatrix} 0 & 1 \\ 1 & 0 \end{pmatrix}, \quad \sigma^y = \begin{pmatrix} 0 & -\mathrm{i} \\ \mathrm{i} & 0 \end{pmatrix}. \tag{2.4}$$

Note that this definition in terms of Pauli matrices also defines an algebra with the usual matrix multiplication where the linear maps satisfy the following commutation relations

$$[S^z, S^+] = S^+, \quad [S^z, S^-] = -S^-, \quad [S^+, S^-] = 2S^z. \tag{2.5}$$

The total Hilbert space of the chain is the direct product of local Hilbert spaces, $\mathcal{H}_S = \bigotimes_i h_i$, and has the dimension: $\dim \mathcal{H}_S = 2^N$. We represent the basis of the total spin chain Hilbert space as the tensor product of the basis of local spins in ket notation,

$$|e_1, \ldots, e_i, \ldots, e_N\rangle \coloneqq e_1 \otimes \cdots \otimes e_i \otimes \cdots \otimes e_N. \tag{2.6}$$

The basis can also be constructed by defining a vacuum state for spins $|\mathrm{vac}\rangle \coloneqq e_1^0 \otimes \cdots \otimes e_N^0$ and generating all possible states by multiple application of S^+ operators, for exmaple,

$$|e_i^1, e_j^1, e_k^1, \ldots\rangle \equiv S_i^+ S_j^+ S_k^+ \cdots |\mathrm{vac}\rangle, \tag{2.7}$$

where we omit the e^0 vectors in the ket notation for convenience.

We can create linear maps over the chain Hilbert space by tensor product of local linear maps. We define the *support* of such linear map (operator) $O\colon \mathcal{H}_S \to \mathcal{H}_S$ as the set of sites on which the operator acts in a non-trivial way (i.e. it is not the identity map). We say an operator is *local* if its support is localized in space.

If the support of a linear map $S_i\colon \mathcal{H}_S \to \mathcal{H}_S$ is only site i we say it is a *hard-core boson* or *spin* operator. This justifies the sloppy notation of referring to the local operator

($S_i \in \operatorname{End} h_i$) and the global operator ($S_i \in \operatorname{End} \mathcal{H}_S$) with the same name. The usual matrix multiplication defines an algebra of spin operators and their product. Note that the spin operators with support on different sites commute and operators with the same support site obey the same algebra of local spin.

We say a linear *Hermitian* map, $H \colon \mathcal{H}_S \to \mathcal{H}_S$, is a *local spin Hamiltonian* if it is a sum of terms with local support. A famous example of a spin Hamiltonian is the XXZ model with periodic boundary conditions

$$H = J \sum_{i=1}^{N} \frac{1}{2}(S_i^+ S_{i+1}^- + S_i^+ S_{i+1}^-) + \Delta \sum_{i=1}^{N} S_i^z S_{i+1}^z. \tag{2.8}$$

The point $\Delta = J$ of this model is also called the Heisenberg model or Bethe chain. Another famous example is the quantum Ising with transverse field model

$$H = J \sum_{i=1}^{N} S_i^x S_{i+1}^x + B \sum_{i=1}^{N} S_i^z. \tag{2.9}$$

We can have multiple flavors of spins per site, but this is trivial as we just need to tensor product the two spin models. For example if we have a spin state for one flavor where the operators are shown by S and another spin state for another flavor where operators are shown by R, defining the total vacuum state as $|\mathrm{vac}\rangle \coloneqq |\mathrm{vac}\rangle_S \otimes |\mathrm{vac}\rangle_R$, the total state for the two flavors is just

$$S_i^+ S_j^+ \cdots R_k^+ R_l^+ \cdots |\mathrm{vac}\rangle = \left(S_i^+ S_j^+ \cdots |\mathrm{vac}\rangle_S\right) \otimes \left(R_k^+ R_l^+ \cdots |\mathrm{vac}\rangle_R\right) \tag{2.10}$$

Where the order of flavors is not important because they commute.

2.2.2 Fermion Models

Here we also have a chain (one–dimensional lattice) of N sites where each site has two possible states, it can either be empty or occupied. This gives the dimension of the chain Hilbert space, $\dim \mathcal{H}_F = 2^N$. A natural representation for the basis of the Hilbert space is by using the occupation numbers of each site $n_i = 0, 1$ as in the ket notation $|n_1, \ldots, n_i, \ldots, n_N\rangle$, but this turns out to be ambiguous. To see how we need to define the fermion operators.

$$|n_1, \ldots, n_i, \ldots, n_N\rangle, \tag{2.11}$$

for convenience we can also omit all the zeros when there is no ambiguity.

The adjoint linear operators $f_i^\dagger, f_i \colon \mathcal{H}_F \to \mathcal{H}_F$ defined for each site i which increase or decrease the occupation number and obey the following *fermionic anticommutation relations*:

$$\begin{aligned} \{f_i, f_j\} &= 0, \\ \{f_i^\dagger, f_j^\dagger\} &= 0, \\ \{f_i, f_j^\dagger\} &= \delta_{ij}. \end{aligned} \tag{2.12}$$

are called the *fermion creation* and *fermion annihilation* operators respectively. Their action on the *vaccum* state $|0\rangle$, i.e. the state where all sites are empty, is defined as

$$\begin{aligned} f_i|0\rangle &= 0 \\ f_i^\dagger|0\rangle &= |n_i = 1\rangle, \end{aligned} \tag{2.13}$$

however, their action on other states are not as well–defined due to the *non-local* anticommutation relations. The best way to address this issue is to define the Hilbert space basis

based on an arbitrary predefined order for the fermionic operators, which we call the Fock space convention. For the chain we pick the Fock space convention of listing all fermionic creation operators from left to right by their order in the ket notation (or the order they appear in the chain from left to right), this means the following definition for ket basis

$$|n_i = 1, n_j = 1, n_k = 1, \dots\rangle \coloneqq f_i^\dagger f_j^\dagger f_k^\dagger \cdots |0\rangle \qquad (i < j < k < \cdots). \tag{2.14}$$

This definition together with the anitcommutation relations unambiguously define the action of fermion operators on all the states of the Hilbert space.

With this convention a linear fermion operator of site i acts on a state with a minus if there is an odd number of occupied fermions on the left of site i and with a plus sign otherwise. In other words the fermion operators measure the leftmost fermion parity.

So, fermions are aware of the occupation numbers of other sites and hence are non–local by nature, i.e. cannot be written as linear combination of local linear maps (this is why we didn't define the local linear maps at all in case of fermions). Again note that this particular choice of the sign convention is arbitrary but very convenient.

Since the definition of the Hilbert space is in terms of fermion creation operators, we have an algebra for the fermion operators as linear maps $\operatorname{End} \mathcal{H}_F$.

An operator that is a multiplication of an even number of fermion operators that are localized in space, is a fermion operator with *local support*. This is because an even number of fermions with non–overlapping support commute with each other. We say that a *Hermitian* linear map $H\colon \mathcal{H}_F \to \mathcal{H}_F$ is a *local fermion Hamiltonian*, if it is a sum of terms with local support. A famous example is the spinless Hubbard model which consists of the fermion hopping terms plus the density–density interaction term (periodic boundary

condition) for on–site and neigherst neighbors

$$H = -t\sum_{i+1}^{N}(f_{i+1}^{\dagger}f_i + f_i^{\dagger}f_{i+1}) + \mu\sum_{i=1}^{N} n_i + V\sum_{i=1}^{N} n_i n_{i+1}, \tag{2.15}$$

another example is the hopping plus the pairing term

$$H = -t\sum_{i+1}^{N}(f_{i+1}^{\dagger}f_i + f_i^{\dagger}f_{i+1}) + \Delta\sum_{i=1}^{N}(f_{i+1}^{\dagger}f_i^{\dagger} - f_{i+1}f_i) \tag{2.16}$$

We can also have more than one flavor of fermions where each site can now be empty or occupied by fermions of several different flavors. The only nontrivial part is that different flavors of fermions anticommute, so the Hilbert space is not simply the tensor product space of different flavors, it has a sign to account for fermion anticommutations. For example if we have a flavor of fermions labeled by $f^{\dagger}$ and another flavor labeled by $c^{\dagger}$ and we pick the Fock space convention of $f^{\dagger}$ left of $c^{\dagger}$ for each site and sites left–to–right same as before, the total vacuum is $|0\rangle = |0\rangle_f \otimes |0\rangle_c$ and for an arbitrary state we need a $(-1)^p$ where p is the number of swaps required to bring the multiplication of fermion operators into the Fock space convention form, for example

$$\left(f_i^{\dagger}f_k^{\dagger}f_m^{\dagger}|0\rangle_f\right) \otimes \left(c_j^{\dagger}c_l^{\dagger}c_m^{\dagger}|0\rangle_c\right) = (-1)^3 f_i^{\dagger}c_j^{\dagger}f_k^{\dagger}c_l^{\dagger}f_m^{\dagger}c_m^{\dagger}|0\rangle \tag{2.17}$$

where we assumed $i < j < k < l < m$ which required 3 fermion operator swaps to bring this state to convention.

2.2.3 The Jordan–Wigner Transformation

The similarities between the fermion operators and spin operators hint a possible relation between the two. Indeed, in one spatial dimension we can define an isomorphism

between fermion operator algebra and spin operator algebra, which serves as a translation between local fermion theories and local spin theories.

The first step is to define an isomorphism between the Hilbert space of the spin theory and the Hilbert space of the fermion theory by defining it on the basis as follows

$$|\alpha_1, \ldots, \alpha_i, \ldots, \alpha_N\rangle \;\mapsto\; |e_1^{\alpha_1}, \ldots, e_i^{\alpha_i}, \ldots, e_N^{\alpha_N}\rangle, \tag{2.18}$$

where the αs are binary values. Note that some Fock space convenction is implicitely assumed already in this isomorphism, because the basis of the fermion Hilbert space is defined based on the choice of the convention.

This allows to establish an algebra isomorphism, the *Jordan-Wigner transformation*, between the spin operator algebra and fermion operator algebra as follows

$$\begin{aligned} f_i^\dagger &\mapsto K_i\, S_i^+, \\ f_i &\mapsto K_i\, S_i^-, \\ n_i = f_i^\dagger f_i &\equiv S_i^z + \tfrac{1}{2}, \end{aligned} \tag{2.19}$$

where K_i operator, which we call the *string* or *tail* operator, is a non–local spin operator that recover the non–local anitcommutation relation between fermions of different sites, because the spin operators at different sites are unable to do that as they simply commute with each other. The tail operator is defined as

$$K_i \coloneqq \prod_{j=1}^{i-1} \sigma_j^z. \tag{2.20}$$

A better way to think about the tail operator is by remembering the choice of the Fock space convention. In The chosen convention a fermionic operator of site i measure the fermion parity left of site i to determine the sign of it action. This procedure is now carried by the

tail operator, so, the particular form of the tail operator (left–to–right) is due to the choice of Fock space convention (left–to–right).

It is fruitful to explicitly show how the fermionic anticommutation relations are restored from the spin operator algebra due the introduction of the tail operator. For simplicity, assume $i \leq j$, and define $K_{i\to j} = \prod_{k=i}^{j-1} \sigma_k^z$. We have

$$\begin{aligned}\left\{f_i, f_j^\dagger\right\} &= \left\{S_i^-, K_{i\to j} S_j^+\right\} \\ &= \begin{cases} K_{(i+1)\to j}\left\{S_i^-, \sigma_i^z\right\} S_j^+ & i < j \\ \left\{S_i^-, S_i^+\right\} & i = j \end{cases} \\ &= \delta_{ij} \end{aligned} \tag{2.21}$$

and similarly,

$$\begin{aligned}\left\{f_i^\dagger, f_j^\dagger\right\} &= \left\{S_i^+, K_{i\to j} S_j^+\right\} \\ &= \begin{cases} K_{(i+1)\to j}\left\{S_i^+, \sigma_i^z\right\} S_j^+ & i < j \\ \left\{S_i^+, S_i^+\right\} & i = j \end{cases} \\ &= 0, \end{aligned} \tag{2.22}$$

and an identical calculation for $\{f_i, f_j\}$.

This transformation is almost useless if it takes local Hamiltonian to non-local counterparts. However a particulary nice feature of this transformation is that local Hamiltonian of spin system produce local fermionic Hamiltonian and vice versa. For example, the Jordan Wigner transformation of the XXZ model is

$$H_{\mathrm{XXZ}} \mapsto \sum_i \frac{1}{2}(f_i^\dagger f_{i+1} + f_{i+1}^\dagger f_i) + \Delta \sum_i (n_i - \frac{1}{2})(n_{i+1} - \frac{1}{2}) \tag{2.23}$$

which is the free fermion theory (the XY part) plus a nearest neighbor density–density interaction (the Ising part).

The isomorphism allows to switch between a fermion theory and a spin theory when convenient. For example, MPS-DMRG algorithm is designed to find the ground state of a spin Hamiltonian but the result can also be interpreted as the ground state of the corresponding fermion model. On the other hand, one way to reach to a field theoretic description of a spin system is to start by translating it into a fermion model and then study the fermionic field theory.

In the following section we answer the interesting question of whether the JW transformation technique can be generalized to more flavors of fermions as in the case of spinons for a spin-1/2 system, see section 3.5.

2.2.4 JW transformation for multiple flavors

To see how this works lets start with the simplest and most important example—the *spinful* Jordan-wigner transformation—where there are two flavors per site.

For two flavors of spin-1/2 per site labeled by $\uparrow, \downarrow$ the local Hilbert space is $h_i = h_{i\uparrow} \otimes h_{i\downarrow}$ and it has the dimension $d \coloneqq \dim h_i = 4$. We can also use the tensor product basis

$$\begin{aligned} e_i^0 &\coloneqq e_{i\uparrow}^0 \otimes e_{i\downarrow}^0 \\ e_i^1 &\coloneqq e_{i\uparrow}^1 \otimes e_{i\downarrow}^0 \\ e_i^2 &\coloneqq e_{i\uparrow}^0 \otimes e_{i\downarrow}^1 \\ e_i^3 &\coloneqq e_{i\uparrow}^1 \otimes e_{i\downarrow}^1 \end{aligned} \tag{2.24}$$

similarly the tensor product of spin operators works as spin operators for this basis. The total Hilbert space is 4^N–dimensional.

For the fermions, the Hilbert space is also 4^N–dimensional which we label using the occupation numbers. Same as before we also need to choose the Fock space convention of order of fermions that represent a certain state. Two natural options come to mind: (i) we can list all $\uparrow$ fermions left of all $\downarrow$ fermions and the same left–to–right convention for sites, (ii) or to list $\uparrow$ left of $\downarrow$ fermions of the same site and then the fermions of the next right site. It turn out that the second option is the one that gives a Jordan-Wigner transformation which leaves Hamiltonians local. So we list fermion operator each site $\uparrow$s left of $\downarrow$ and from lower site index to higher, which means

$$|(n_{1\uparrow}=1,n_{1\downarrow}=1),(n_{i\uparrow}=0,n_{i\downarrow}=1),\dots\rangle \coloneqq f^\dagger_{1\uparrow}f^\dagger_{1\downarrow}f^\dagger_{i\uparrow}f^\dagger_{i\downarrow}\cdots|0\rangle. \tag{2.25}$$

Exactly the same as for the case of one flavor, we define an isomorphism between the Hilbert space of spin system and the Hilbert space of fermion system through their basis vectors,

$$v_F \mapsto v_S \tag{2.26}$$

where v_F and v_S are generic basis vectors of the fermion system and spin system respectively,

$$\begin{aligned} v_F &\coloneqq |(n_{1\uparrow},n_{1\downarrow}),\dots,(n_{i\uparrow},n_{i\downarrow}),\dots,(n_{N\uparrow},n_{N\downarrow})\rangle \\ v_S &\coloneqq |e^{n_1}_{1\uparrow}\otimes e^{n_1}_{1\downarrow},\dots,e^{n_i}_{i\uparrow}\otimes e^{n_i}_{i\downarrow},\dots,e^{n_N}_{N\uparrow}\otimes e^{n_N}_{N\downarrow}\rangle, \end{aligned} \tag{2.27}$$

For the Jordan-Wigner transformation it is obvious that both flavors have to carry the tail operators $K_\uparrow, K_\downarrow$ at the same time, but since the covention puts the $\uparrow$ before down the latter has to measure the former density on the same site as well. So we have the

following isomorphism of algebras

$$\begin{aligned} f^\dagger_{i\uparrow} &\mapsto K_{i\uparrow}K_{i\downarrow}\, S^+_{i\uparrow}, \\ f_{i\uparrow} &\mapsto K_{i\uparrow}K_{i\downarrow}\, S^-_{i\uparrow}, \\ n_{i\uparrow} = f^\dagger_{i\uparrow}f_{i\uparrow} &\equiv S^z_{i\uparrow} + \tfrac{1}{2}, \end{aligned} \tag{2.28}$$

$$\begin{aligned} f^\dagger_{i\downarrow} &\mapsto K_{(i+1)\uparrow}K_{i\downarrow}\, S^+_{i\downarrow}, \\ f_{i\downarrow} &\mapsto K_{(i+1)\uparrow}K_{i\downarrow}\, S^-_{i\downarrow}, \\ n_{i\downarrow} = f^\dagger_{i\downarrow}f_{i\downarrow} &\equiv S^z_{i\downarrow} + \tfrac{1}{2}, \end{aligned} \tag{2.29}$$

Again we show explicitely how the fermionic anticommutation relations are restored from the spin algebra and the tail operators. Obviously each flavor of fermions obey the fermionic relations among themselves. For the anticommutation relations between flavors, for $i \leq j$ we have,

$$\begin{aligned} \left\{ f_{i\uparrow}, f^\dagger_{j\downarrow} \right\} &= \left\{ K_{i\uparrow}K_{i\downarrow}S^-_{i\uparrow}\ ,\ K_{j+1\uparrow}K_{j\downarrow}S^+_{j\downarrow} \right\} \\ &= \left\{ S^-_{i\uparrow}\ ,\ K_{(i\to j+1)\uparrow}K_{(i\to j)\downarrow}S^+_{j\downarrow} \right\} \\ &= \begin{cases} K_{(i+1\to j+1)\uparrow}K_{(i\to j)\downarrow} \left\{ S^-_{i\uparrow}, \sigma^z_{i\uparrow} \right\} S^+_{j\downarrow} & i < j \\ \left\{ S^-_{i\uparrow}, \sigma^z_{i\uparrow} \right\} S^+_{i\downarrow} & i = j \end{cases} \\ &= 0, \end{aligned} \tag{2.30}$$

and if $i > j$ we have,

$$\begin{aligned}\left\{f_{i\uparrow}, f_{j\downarrow}^{\dagger}\right\} &= \left\{K_{i\uparrow}K_{i\downarrow}S_{i\uparrow}^{-}\ ,\ K_{j+1\uparrow}K_{j\downarrow}S_{j\downarrow}^{+}\right\} \\ &= \left\{K_{(j\to i)\uparrow}K_{(j\to i)\downarrow}S_{i\uparrow}^{-}\ ,\ \sigma_{j\uparrow}^{z}S_{j\downarrow}^{+}\right\} \\ &= K_{(j+1\to i)\uparrow}K_{(j+1\to i)\downarrow}S_{i\uparrow}^{-}\left\{\sigma_{j\downarrow}^{z}, S_{j\downarrow}^{+}\right\} \\ &= 0. \end{aligned} \tag{2.31}$$

Similarly, an almost identical calculation also shows $\{f_{i\uparrow}, f_{j\downarrow}\} = 0$ and $\{f_{i\uparrow}^{\dagger}, f_{j\downarrow}^{\dagger}\} = 0$. This indicates that the map between fermion and spin algebras is indeed an algebra isomorphism.

It is now simple to generalize this approach to l number of flavors per site. We need to choose a Fock space convention for different flavors. First we decided on some order and then label the flavors from left to right by 1 through l. For the mth flavor at site i the full tail operator is simply given by

$$K_{(i+1)1}\cdots K_{(i+1)m-1}K_{(i)m}K_{(i)m+1}\cdots K_{(i)l}. \tag{2.32}$$

Again the interpretation of the tail operator is quite clear. For the normal Jordan–Wigner transformation a fermionic operator measure the parity of left fermions in order to determine the sign. For multiple flavors version, other than the parity of left sites, the mth flavor need to measure the $(m-1)$ previous flavors located on the same site as well. This is so that different flavors anticommute on the same site. Note that initial choice of the order of flavors is arbitrary but has to match the Fock space convention.

2.3 Bosonization

2.3.1 A brief introduction to Abelian bosonization

A particularly important challenge in condensed matter physics is to describe the behavior of fermions in the presence of interactions. Since we only know how to solve the free theory, formal approaches are usually limited to perturbative approaches to quantum field theories which are expected to fail for large interactions.

In one spatial dimension, there exist a powerful technique that reformulates a Quantum field theory of fermions in terms of bosonic fields, which are derived from fermionic current/density; this transformation is known as *bosonization* [42, 43, 71, 39]. It is possible to write the fermionic creation/annihilation operators in terms of *kinks* in the bosonic fields and rewrite any multi–fermion interaction in terms of the new bosons. The hope of the bosonization transformation is that the resulting interacting bosonic theory is simpler to study by the usual bosonic QFT.

The above description of fermions as kinks in a bosonic field and bosons as fermionic current/density hints to an interesting duality between fermions and bosons in one spatial dimension.

Below, I briefly illustrate the Abelian Bosonizaition in four steps:(i) linearize the dispersion (ii) calculate the commutation relations for currents/densities (iii) establish a duality between the fermionic theory and bosonic fields (iv) write the fermionic operators in terms of bosons. For further detailed discussion see books by Giamarchi, Nagaosa and Gogolin, as well as a short Boulder school lecture by Kane [42, 71, 43, 102].

Let us start with free fermions hopping on a 1D lattice of size L and lattice spacing a. We can think of the fermions as the starting theory, or possibly derivations from an underlying theory of hard–core bosons (spins). The translationally invariant system can be easily diagonalized in the momentum space where the fermionic states form a cosine band. Additionally, we can take the $a \to \infty$ limit to get a continuous space and infinitely large Brillouin zone; in this limit the energy dispersion reduces to that of the free particles, a parabola.

We can either enforce particle conservation at some fractional filling which determines the chemical potential μ or add a chemical potential term and fix that instead. In the second case the momentum space Hamiltonian is

$$\mathrm{H} = \sum_{k \in \mathrm{BZ}} (E_k + \mu) f_k^\dagger f_k. \tag{2.33}$$

The ground state is then described by the set of occupied momentum states which form a line segment in the momentum space, i.e. the *Fermi sea*. Here, the boundary of the Fermi sea—the *Fermi surface*—consists of two points at the *Fermi momentum*, k_F (see Fig).

Linearization

The first step is to *linearize* the Hamiltonian at the Fermi surface points; that is to replace the original dispersion relation with a linear dispersion. This new linear model is known as Tomonaga–Luttinger (TL) model (see Fig. 2.1). As expected, the general behavior of the TL model is quite different than the original model: (i) it has two bands (left–movers and right–movers) of fermions while we started with one fermion species in the original

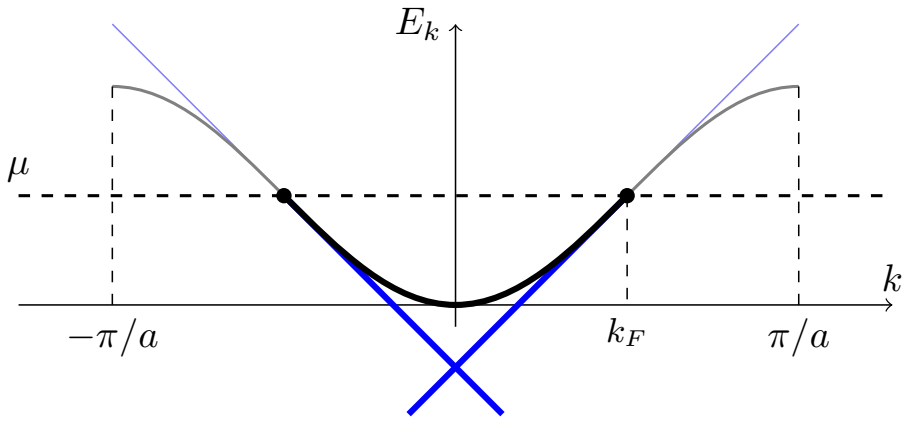

Figure 2.1: The ground state of the tight–binding model at fractional filling in the momentum space and its linearization—the Tomonaga–Luttinger model.

model[1], and (ii) each band has infinitely extended Fermi seas and therfore dramatically different high–energy excitations. However, about the linearization point, the two models exhibit the same low–energy behavior.

If we show the fermion operators living on the right(left) branch as f_P, where $P = R/L = +/-$, the momentum space Hamiltonian describing the TL model (up to a constant) is

$$\mathrm{H} = \sum_{k\in \mathrm{BZ}} v_f k \, \Big(f_R^\dagger(k) f_R(k) - f_L^\dagger(k) f_L(k) \Big). \tag{2.34}$$

In case of nonzero μ, the coefficient are given by $k-\mu$ and $-(k+\mu)$ for right and left branch respectively. By using the following Fourier transform convention

$$\begin{aligned} f_P(k) &= L^{-1/2} \int_L \mathrm{d}x \; \mathrm{e}^{-\mathrm{i}kx} \psi_P(x), \\ \psi_P(x) &= L^{-1/2} \sum_{\mathrm{BZ}} \mathrm{e}^{\mathrm{i}kx} f_P(k), \end{aligned} \tag{2.35}$$

[1]This is because chiral fermions come in pairs in a lattice model, i.e. the fermion doubling problem.

and defining the *Fermi velocity* as $v_F \equiv \partial E_k/\partial k$, we can identify the continuous real space Hamiltonian as the theory of 1+1D Dirac fermions:

$$\begin{aligned} \mathrm{H} &= \int_L \mathrm{d}x \ -\mathrm{i}v_F \Big(\psi_R^\dagger(x)\partial_x \psi_R(x) - \psi_L^\dagger(x)\partial_x \psi_L(x) \Big), \\ &= \int_L \mathrm{d}x \ -\mathrm{i}v_F \ \bar{\psi}\gamma_1 \partial_x \psi, \end{aligned} \tag{2.36}$$

where in the second representation we define the spinor operators as usual:

$$\psi \equiv \begin{pmatrix} \psi_R \\ \\ \psi_L \end{pmatrix}, \qquad \bar{\psi} \equiv \psi^\dagger \gamma_0, \tag{2.37}$$

and the 1+1D matrices, which obey the Clifford algebra, has the form $\gamma_0 \equiv \sigma_x$, and $\gamma_1 \equiv -\mathrm{i}\sigma_y$.

Fermion density as bosons

For the second step we need to show that the right/left density operators $\psi_P^\dagger(x)\psi_P(x)$ of the TL model behave like bosons. However, for the continuous TL model there exist infinite number of occupied states in the Fermi sea of each branch, which means divergence for the density. In the field theory approach usually people work around this issue by introducing the notion of *normal ordering* which hides the singularities into the ground state expectation value and separate from the study of fluctuations. Since we would like to study the low–energy fluctuations of the density/current operators about their TL ground state expectation value (which coincide with the low–energy density/current fluctuations of our original lattice model), we intorduce normal ordering of an operator O as

$$: O : \ \equiv O - \langle \Omega | O | \Omega \rangle \tag{2.38}$$

where by Ω we represent the set of occupied states in the Fermi sea of the TL model. Since all operators of interest are given in terms of fermion bilinears, it is intersting to note what normal ordering does for femion bilinear operator

$$: f_k^\dagger f_k : \; = \begin{cases} f_k^\dagger f_k & k \notin \Omega \\ -f_k f_k^\dagger & k \in \Omega \end{cases} \tag{2.39}$$

This should also make clear why the term "normal ordering" is used to refer to this operation, as the operation enforces a paritcular ordering depending on whether or not the state is inside the Fermi sea.

We first try to calculate the commutation relation for the Fourier modes of the density operator, defined as

$$\rho_P(q) \equiv L^{-1/2} \int \mathrm{d}x \; \mathrm{e}^{-\mathrm{i}qx} \rho_P(x) = L^{-1/2} \sum_k f_P^\dagger(k+q) f_P(k). \tag{2.40}$$

An explicit calculation of the commutation relation results in

$$\begin{aligned} \left[\rho_P(-q), \rho_P(q')\right] &= \frac{1}{L} \sum_{k,k'} \left[f_P^\dagger(k-q) f_P(k), f_P^\dagger(k'+q') f_P(k') \right] \\ &= \frac{1}{L} \sum_k \left(f_P^\dagger(k-q) f_P(k-q') - f_P^\dagger(k-q+q') f_P(k) \right). \end{aligned} \tag{2.41}$$

The above expression should not be naively evaluated as it is the difference of two infinity terms; we should first replace each term by thier respetive normal ordering plus their expectation value. The normal ordering terms (fluctuations) now simply cancel (because they are finite terms and we can rename the dummy index) and the difference in the ground state expectation values, $\sum_k \langle n(k-q)\rangle - \langle n(k)\rangle$, will be the number of states on a segment of size q, and gives a $P \times q(L/2\pi)$ factor. Therefore, the density operators obey the following

commutation relations

$$\left[\rho_P(-q), \rho_P(q')\right] = P\frac{q}{2\pi}\delta_{pp'}, \tag{2.42}$$

The fact that the Fourier modes of fermionic density obey bosonic commutation relations naturally lead us to the definition of momentum space bosons with creation and annihilation operators, $b_q^\dagger, b_q$ define as

$$b_q^\dagger = \sqrt{\frac{2\pi}{|q|}} \times \begin{cases} \rho_R(q) & q > 0 \\ \\ \rho_L(q) & q < 0 \end{cases}, \tag{2.43}$$

$$b_q = \sqrt{\frac{2\pi}{|q|}} \times \begin{cases} \rho_R(-q) & q > 0 \\ \\ \rho_L(-q) & q < 0 \end{cases}. \tag{2.44}$$

The $q = 0$ is excluded as it doesn't satisfy bosonic commutators and it corresponds to the total number of fermions which is a conserved quantity due the chiral symmetry of the original model. The dream is now realized since the density–density interactions can now be written as boson bilinears. These bosons can now be used to define real space bosonic field operators but here we take a more natural approach for derivation of the real space fields.

The real space commutation relation can also be derived using the inverse Fourier transform formula,

$$\left[\rho_P(x), \rho_P(x')\right] = -P\frac{\mathrm{i}}{2\pi}\partial_x\delta(x - x'). \tag{2.45}$$

It is more natural to write the commutation relations for the fermionic *chiral current* opertors, $j_\mu = \bar{\psi}\gamma_\mu\psi$. The chiral current components j_0, j_1 correspond to the total fermionic

density and total fermionic right–moving current,

$$j_0(x) = \rho_R(x) + \rho_L(x), \qquad j_1(x) = \rho_R(x) - \rho_L(x), \tag{2.46}$$

and the obey the commuation relation,

$$\big[j_0(x), j_1(x')\big] = -\frac{\mathrm{i}}{\pi}\partial_x \delta(x - x'). \tag{2.47}$$

Duality, the bosonic fields

We are now ready for the third step. The above commutation relation strongly suggests a duality between the fermionic field theory and the theory of a bosonic field. Recall that a bosonic field $\varphi(x)$ with its conjugate field $\Pi(x) \equiv \partial_t \varphi(x)$ obey the commutation relation $[\varphi(x), \Pi(x')] = \mathrm{i}\delta(x - x')$. This allows us to establish a precise connection between the components of the fermionic chiral current and the bosonic field, say φ, using the identifications:

$$j_0 \equiv \pi^{-1/2}\ \partial_x \varphi(x), \qquad j_1 \equiv -\pi^{-1/2}\ \Pi(x) = -\pi^{-1/2}\ \partial_t \varphi(x). \tag{2.48}$$

An important implication of this identification is that a step-function-like kink in the boson field corresponds to a delta-like peak (particle) in the fermionic density. This is why we referred to fermions as a "kink" in bosonic field.

Alternatively, we could have identified j_1 with the spatial derivative of a different bosonic field, say ϑ, and j_0 with its temporal derivative (conjugate field Ξ), that is

$$j_0 \equiv -\pi^{-1/2}\ \Xi(x) = -\pi^{-1/2}\ \partial_t \vartheta(x), \qquad j_1 \equiv -\pi^{-1/2}\ \partial_x \vartheta(x). \tag{2.49}$$

With this particular choice of identification and signs the two boson fields satisfy the *Cauchy–Riemann* equations with φ as the first field, and ϑ as the second field

$$\partial_t \varphi = \partial_x \vartheta, \qquad \partial_x \varphi = -\partial_t \vartheta. \tag{2.50}$$

so the field $\varphi(x,t) + \mathrm{i}\vartheta(x,t)$ is an analytic field of $x + \mathrm{i}t$!

It is in this manner that the fields ϑ and φ are considered as conjugate fields, in particular their commutator reads

$$\big[\varphi(x), \vartheta(x')\big] = -\mathrm{i}\Theta(x - x'), \tag{2.51}$$

where Θ is the normal Heaviside step function. We will see that it is generally simpler to bosonize the fermionic theories using the φ and ϑ field instead of their conjugates.

Fermions as vertex operators

For the fourth and final step, we learned that fermions can be considered as kinks in the bosonic filed φ, so we try for the operator exchange of the non–local *soliton* operators defined as $\psi(x) \equiv \exp\big(\mathrm{i}\alpha\varphi(x) + \mathrm{i}\beta \int_{-\infty}^{x} \Pi(x')\ \mathrm{d}x'\big)$,

$$\psi(x)\psi(y) = \psi(y)\psi(x) \exp\left(\alpha\beta \int_{-\infty}^{y} \mathrm{d}y' \left[\varphi(x), \Pi(y')\right] + \alpha\beta \int_{-\infty}^{x} \mathrm{d}x' \ \left[\Pi(x'), \varphi(y)\right]\right)$$

which means choosing $\beta = \pm\pi/\alpha$, they behave like fermions.

We can now express the right(left) moving Dirac operators,

$$\psi_+(x) = \frac{1}{\sqrt{2\pi a}} \ :\mathrm{e}^{+\mathrm{i}\sqrt{\pi}(\varphi - \vartheta)}:$$
$$\psi_-(x) = \frac{1}{\sqrt{2\pi a}} \ :\mathrm{e}^{-\mathrm{i}\sqrt{\pi}(\varphi + \vartheta)}:$$

Different notations can be found throughout the literature which includes different choice of letters for the bosonic fields, different choice of sign, different placement of the π factors, and different definition for the Luttinger liquid parameter. It is thus useful to have a conversion table.

	j_0	j_1
Gogolin [43]	$\frac{1}{\sqrt{\pi}}\partial_x\Phi$	$-\frac{1}{\sqrt{\pi}}\partial_x\Theta$
Giamarchi [42]	$-\frac{1}{\pi}\partial_x\phi$	$\frac{1}{\pi}\partial_x\theta$
Kane, Fisher [71, 39]	$\partial_x\theta$	$-\partial_x\phi$
Nagaosa [102]	$\frac{1}{2\pi}\partial_x\theta_+$	$\frac{1}{2\pi}\partial_x\theta_-$

For the rest of this thesis, we chose to use the conventions of Kane and Fisher and replace ϕ with φ. This is mainly to remain consistent with other references [125] and the problems we address in this thesis.

It is now easy to translate possible fermion interaction terms into the boson langauage and discuss their renormalization around the free theory fixed point. Let us start with the interaction operator $\psi_+^\dagger\psi_-$,

$$\psi_+^\dagger\psi_- = \frac{1}{2\pi a} :\mathrm{e}^{-4\pi[\phi_+,\phi_-]}: \; :\mathrm{e}^{-\mathrm{i}2\sqrt{\pi}\varphi}:$$

So the mass term will be represented as a cosine

$$\psi_+^\dagger\psi_- + \psi_-^\dagger\psi_+ = -\frac{1}{\pi a} : \cos\left(2\sqrt{\pi}\varphi\right): .$$

Another important four particle interaction term is the umklapp interaction of left(right) scatter into two right(left) particles which is the result of half filling and the Fermi momentum of π. The Umklapp interaction term can be represented in the bosonized language as follows

$$(\psi_+^\dagger\psi_-)^2 + (\psi_-^\dagger\psi_+)^2 = \frac{1}{2\pi^2 a^2} : \cos\left(4\sqrt{\pi}\varphi\right): .$$

2.4 Sine–Gordon theory

We would use the Eucleadian path integral formalism, where $\tau = \mathrm{i}t$. The sine–Gordon theory Lagrangian is

$$\mathcal{L} \equiv \frac{1}{2\pi g}\left[\frac{1}{v}(\partial_\tau\theta)^2 + v(\partial_x\theta)^2\right] + \alpha\cos(\beta\theta) \tag{2.52}$$

where v is the velocity of the field, g is the Luttinger liquid parameter, i.e. the ratio of the kinetic term to potential term.

2.4.1 Correlation fucntions and scaling dimension of vertex operator

To check the SBM theory we need to treat the allowed interaction terms using RG. We have seen that the Hermitian fermion interaction terms are expressed in terms of cos, sin of boson fields. So we need to calculate the scaling dimension of the operator $V(x) \equiv \exp\left(\mathrm{i}\alpha\theta(x)\right)$ at the fixed point of the free theory given by the partition function

$$\mathcal{Z}[0] = \int \mathcal{D}\theta\ \exp\left(-\int \mathcal{L}_0(\tau,x)\ \mathrm{d}\tau\mathrm{d}x\right), \qquad \mathcal{L}_0 \equiv \frac{1}{2\pi g}\left[\frac{1}{v}(\partial_\tau\theta)^2 + v(\partial_x\theta)^2\right] \tag{2.53}$$

For simplicity we can define $\mathbf{r} = (v\tau, x)$. In this new variable the Lagrangian is simply $\mathcal{L}_0 = (\nabla\mathbf{r})^2/2\pi g$. To find the correlation function $\langle\theta(\mathbf{r})\theta(\mathbf{r}')\rangle$ we need to define the partition function with a source field $J(\mathbf{r})$,

$$\mathcal{Z}[J] \equiv \int \mathcal{D}\theta\ \exp\left(-\int \mathrm{d}^2\mathbf{r}\ \left[\mathcal{L}_0 - J(\mathbf{r})\theta(\mathbf{r})\right]\right), \tag{2.54}$$

we will therefore have

$$\frac{\mathcal{Z}[J]}{\mathcal{Z}[0]} = \left\langle \exp\left(\int \mathrm{d}^2\mathbf{r}\ J(\mathbf{r})\theta(\mathbf{r})\right)\right\rangle$$
$$= \exp\left(\frac{1}{2}\int J(\mathbf{r})G(|\mathbf{r}-\mathbf{r}'|)J(\mathbf{r}')\ \mathrm{d}^2\mathbf{r}\mathrm{d}^2\mathbf{r}'\right) \tag{2.55}$$
$$= \exp\left(\frac{1}{2}\int J(\mathbf{k})G(k)J(-\mathbf{k})\ \mathrm{d}^2\mathbf{k}\right) \tag{2.56}$$

to see note that the interacting Lagrangian written in momentum space

$$\mathcal{L} = \int \mathrm{d}^2\mathbf{k}\ \left(\frac{k^2}{2\pi g}\theta'(\mathbf{k})\theta'(-\mathbf{k}) + \frac{1}{2}J(\mathbf{k})\ \frac{\pi g}{k^2}\ J(-\mathbf{k})\right) \tag{2.57}$$

where we complete the square with the new field $\theta'(\mathbf{k}) = \theta(\mathbf{k}) - \pi g/k^2 J(\mathbf{k})$. From symmetry considerations as well as the above result we see that the Green's function $G(\mathbf{r},\mathbf{r}')$ only depends on the distance $|\mathbf{r}-\mathbf{r}'|$ and is the inverse of the operator $\nabla^2/\pi g$. Therefore, the Green's function is the solution to the differential equation

$$\nabla^2 G(|\mathbf{r}-\mathbf{r}'|) = \pi g\delta(\mathbf{r}-\mathbf{r}') \tag{2.58}$$

which has the solution

$$G(|\mathbf{r}-\mathbf{r}'|) = \frac{g}{2}\ln|\mathbf{r}-\mathbf{r}'| \tag{2.59}$$

The correlation functions are also related to the derivatives of the source field partition function and the Green's function simply

$$\langle\theta(\mathbf{r})\theta(\mathbf{r}')\rangle = \frac{\partial}{\partial J(\mathbf{r})}\frac{\partial}{\partial J(\mathbf{r}')}\frac{\mathcal{Z}[J]}{\mathcal{Z}[0]} = G(\mathbf{r},\mathbf{r}'). \tag{2.60}$$

We are now ready to discuss the scaling dimension of $V(\mathbf{r})$ operator. Defining $f(\mathbf{r}'') \equiv \mathrm{i}\beta(\delta(\mathrm{r}''-\mathrm{r}) + \delta(\mathrm{r}''-\mathrm{r}'))$, we can easily calculate the correlation

$$\langle \mathrm{e}^{\mathrm{i}\beta\theta(\mathbf{r})}\ \mathrm{e}^{\mathrm{i}\beta\theta(\mathbf{r}')}\rangle = \frac{\mathcal{Z}[f]}{\mathcal{Z}[0]} = \mathrm{e}^{-\beta^2(G(0)+G(|\mathbf{r}-\mathbf{r}'|))} \propto \frac{1}{|\mathbf{r}-\mathbf{r}'|^{g\beta^2/2}}, \tag{2.61}$$

and read the scaling dimension of operator $V(\mathbf{r})$, that is

$$\Delta[\mathrm{e}^{\mathrm{i}\beta\theta(\mathbf{r})}] = \frac{g\beta^2}{4}. \tag{2.62}$$

2.4.2 The Renormalization group study

In order to perform the renormalization group study we introduce the cut–off field $\theta_\Lambda(\mathbf{r})$ that represents only the field in the modes slower than a cut–off Λ. That is

$$\theta_\Lambda(\mathbf{r}) = \int_{0<|\mathbf{k}|<\Lambda} \frac{\mathrm{d}^2k}{(2\pi)^2}\ \theta(\mathbf{k}). \tag{2.63}$$

We would then study the Lagrangian under the change of cut–off and rescaling of the fields. For a given $b = 1+\epsilon$ with $\epsilon > 0$ we will then split the field $\theta_{b\Lambda}$ to the slow and fast moving parts

$$\theta_{b\Lambda}(\mathbf{r}) = \theta_\Lambda(\mathbf{r}) + h_\Lambda(\mathbf{r}), \qquad h_\Lambda(\mathbf{r}) = \int_{\Lambda<|\mathbf{k}|<b\Lambda} \frac{\mathrm{d}^2k}{(2\pi)^2}\ \theta(\mathbf{k}). \tag{2.64}$$

We would like to write down the parition function upon the rescaling of the field and integration of the fast modes:

$$\mathcal{Z}_{b\Lambda} = \int \mathcal{D}\theta_{b\Lambda}\ e^{-\mathcal{S}[\theta_{b\Lambda}]} = \int \mathcal{D}\theta_\Lambda\ e^{-\tilde{\mathcal{S}}[\theta_\Lambda]}. \tag{2.65}$$

Labling the interaction term as $F(\mathbf{r}) \equiv \cos(\beta[\theta_\Lambda(\mathbf{r}) + h_\Lambda(\mathbf{r})])$, we have

$$\mathcal{S}[\theta_{b\Lambda}] = \mathcal{S}_0[\theta_\Lambda] + \mathcal{S}_0[h_\Lambda] + \alpha \int \mathrm{d}\mathbf{r}\ F(\mathbf{r}) \tag{2.66}$$

we now integrate out the fast fields h_Λ we find the modified action as (up to a constant)

$$\tilde{\mathcal{S}}[\theta_\Lambda] = \mathcal{S}_0[\theta_\Lambda] - \ln\left\langle \mathrm{e}^{-\alpha\int \mathrm{d}\mathbf{r}\ F(\mathbf{r})}\right\rangle_h \tag{2.67}$$

$$\begin{aligned}\approx \mathcal{S}_0[\theta_\Lambda] &+ \alpha\int \mathrm{d}\mathbf{r}\ \langle F(\mathbf{r})\rangle_h \\ &- \frac{\alpha^2}{2}\iint \mathrm{d}\mathbf{r}\mathrm{d}\mathbf{r}'\Big(\langle F(\mathbf{r})F(\mathbf{r}')\rangle_h - \langle F(\mathbf{r})\rangle_h\langle F(\mathbf{r}')\rangle_h\Big) \\ &+\cdots\end{aligned} \tag{2.68}$$

which in the last step we used the first two terms of the cumulant expansion for small α. Defining the Green's function only in the narrow band of momenta $\Lambda < k < b\Lambda$ as

$$G_h(r) = \int_{\Lambda<k<b\Lambda}\frac{\mathrm{d}^2\mathbf{k}}{(2\pi)^2}\mathrm{e}^{\mathrm{i}\mathbf{k}\cdot\mathbf{r}}\ \frac{\pi g}{k^2}, \tag{2.69}$$

for small change of the cut–off that is for $b = 1+\ell$ the narrow band Green's function is

$$G_h(r) \approx \frac{g\ell}{2}\ \frac{1}{2\pi}\int_0^{2\pi}\mathrm{e}^{ikr\cos\phi}\ \mathrm{d}\phi = \frac{g\ell}{2}J_0(\Lambda r) \tag{2.70}$$

where J_0 is the 0th Bessel function.

We get for the expectation value, choosing $J(\mathbf{r}') = \mathrm{i}\beta\delta(\mathbf{r}'-\mathbf{r})$, or in Fourier $J(\mathbf{k}) = \mathrm{i}\beta\mathrm{e}^{-\mathrm{i}\mathbf{k}\cdot\mathbf{r}}/2\pi$ we have

$$\langle \mathrm{e}^{\mathrm{i}\beta h(\mathbf{r})}\rangle_h = \frac{\mathcal{Z}_h[J]}{\mathcal{Z}_h[0]} = \mathrm{e}^{-\frac{\beta^2}{2}G_h(0)} \tag{2.71}$$

and similarly choosing $J(\mathbf{r}'') = \mathrm{i}\beta[\delta(\mathbf{r}''-\mathbf{r}) \pm \delta(\mathbf{r}''-\mathbf{r}')]$, or in Fourier $J(\mathbf{k}) = \mathrm{i}\beta[\mathrm{e}^{-\mathrm{i}\mathbf{k}\cdot\mathbf{r}} \pm \mathrm{e}^{-\mathrm{i}\mathbf{k}\cdot\mathbf{r}'}]/2\pi$ we have

$$\langle \mathrm{e}^{\mathrm{i}\beta h(\mathbf{r})}\ \mathrm{e}^{\pm\mathrm{i}\beta h(\mathbf{r}')}\rangle_h = \frac{\mathcal{Z}_h[J]}{\mathcal{Z}_h[0]} = \mathrm{e}^{-\beta^2(G_h(0)\pm G_h(|\mathbf{r}-\mathbf{r}'|)} \tag{2.72}$$

We can now evaluate the first two order of the Eq. (2.68) using the above calcualtion of expectation values.

$$\tilde{\mathcal{S}}[\theta_\Lambda] = \mathcal{S}_0[\theta_\Lambda] + \mathcal{S}^{(1)}[\theta_\Lambda] + \mathcal{S}^{(2)}[\theta_\Lambda] + \cdots \tag{2.73}$$

where the first order of expansion is

$$\mathcal{S}^{(1)}[\theta_\Lambda] = \alpha \mathrm{e}^{-\frac{\beta^2}{2}G_h(0)} \int \mathrm{d}\mathbf{r}\ \cos(\beta\theta_\Lambda(\mathbf{r})) \tag{2.74}$$

up to first order of expansion (one loop normalization group) considering small ℓ, we can write $e^{-\beta^2 G_h(0)/2} = 1 - g\beta^2/4$. So, we have the flow equation

$$\frac{\mathrm{d}\alpha}{\mathrm{d}\ell} = -\frac{g\beta^2}{4} \tag{2.75}$$

note that this is consistant with the scaling dimension of the vertex operator!

And for the second order of expansion we have

$$\begin{aligned}\mathcal{S}^{(2)}[\theta_\Lambda] = -\frac{\alpha^2 \mathrm{e}^{-\beta^2 G_h(0)}}{4} \iint \mathrm{d}\mathbf{r}\mathrm{d}\mathbf{r}' \Big(\mathrm{e}^{-\beta^2 G_h(|\mathbf{r}-\mathbf{r}'|)} - 1\Big) \cos(\theta_\Lambda(\mathbf{r}) + \theta_\Lambda(\mathbf{r}')) \\ + \Big(\mathrm{e}^{\beta^2 G_h(|\mathbf{r}-\mathbf{r}'|)} - 1\Big) \cos(\theta_\Lambda(\mathbf{r}) - \theta_\Lambda(\mathbf{r}'))\end{aligned} \tag{2.76}$$

The Green's function is generally strongly decaying, specifically since only a narrow region of modes contribute to G_h. Therefore only $|\mathbf{r} - \mathbf{r}'| < \Lambda^{-1}$ contribute to this integral. The field θ_Λ is also varying slowly in that region, as it only has modes up to Λ, therefore the cosine in second terms can be approaximated by $1 - \frac{1}{2}(|\mathbf{r} - \mathbf{r}'| \cdot \nabla\theta_\Lambda)^2$. Redefining r as the center of mass coordinates, $\mathbf{r} = (\mathbf{r} + \mathbf{r}')/2$, and the difference $\mathbf{x} = \mathbf{r} - \mathbf{r}'$

$$\mathcal{S}^{(2)}[\theta_\Lambda] \approx \frac{\alpha^2\beta^2 \mathrm{e}^{-\beta^2 G_h(0)}}{8} \iint \mathrm{d}\mathbf{r}\mathrm{d}\mathbf{x} \Big(\mathrm{e}^{\beta^2 G_h(\mathbf{x})} - 1\Big)(\mathbf{x} \cdot \nabla\theta_\Lambda(\mathbf{r}))^2 \tag{2.77}$$

With these approximations we can see that the coefficient of $(\nabla\theta)^2$ has changed in the Lagrangian, we can rescale the field to get back the original form of free Lagrangian

$$\tilde{\theta} = \left(1 + \frac{A}{8}\frac{\pi^2 g^2}{\Lambda^4}\alpha^2\beta^4\ell\right)^{1/2} \theta \tag{2.78}$$

where A represent $\int_0^\infty x^3 J_0(x)\,\mathrm{d}x$. If we now replace the interaction term with the rescaled field as well, we will see that

$$\tilde{\beta} = \beta\left(1 + \frac{A}{8}\frac{\pi^2 g^2}{\Lambda^4}\alpha^2\beta^4\ell\right)^{-1/2}. \tag{2.79}$$

So to second order we get the following flow equation

$$\frac{\mathrm{d}\beta}{\mathrm{d}\ell} = -\frac{A}{16}\frac{\pi^2 g^2}{\Lambda^4}\alpha^2\beta^5 \tag{2.80}$$

2.5 Conformal Field Theory

2.5.1 Motivation

Classical critical phenomena

It has been shown that second order phase transition corresponding to $T \neq 0$, is characterized by blow–up of the correlation function, $\xi \to \infty$, and is described by a field theory that remains invariant under conformal transformation. This is because at least for 2D theories, if the theory that is invariant under the global scale transformation, it is also invariant under the larger symmetry group–the conformal group.

Wilson Renormalization group

In the language of field theory we usually assume that all terms respecting the symmetry in the action are possible for the field degrees of freedom of the system $phi(x)$. Each term will be added by a coupling g_i. Upon renormalization the flow of the couplings in the space of operators are governed by the flow equation,

$$\frac{\mathrm{d}g_i}{\mathrm{d}\log E} = \beta_i(g) \tag{2.81}$$

The flows are generally toward or away from a *fixed sub–manifolds* at which the β function vanishes. Since Renormalization procedure can be thought of as an scale change, the fixed sub–manifolds are by definition scale invariant.

Why not more?

The Coleman–Mandula theorem states that the largest possible symmetry group for a non–trivial field theory is the conformal symmetry [31]. However, superconformal symmetries could be thought of as a counterexample.

2.5.2 Classical Conformal Invariance

Conformal map

Consider a smooth manifold M equipped with metric g, a diffeomorphism $\varphi\colon M \to M$ is called a *conformal map* if the pullback metric equals to the original metric *up to scale*, which means the resulted metric from the transformation is a real–valued function times the original metric,

$$g' \coloneqq \varphi^* g = \Lambda(x) g$$

For the flat space with the metric $\eta_{\mu\nu} = \mathrm{diag}(-1, \cdots, +1, \cdots)$, and its conformally equivalent metrics we have

$$\eta_{\rho\sigma} \frac{\partial x'^{\rho}}{\partial x^{\mu}} \frac{\partial x'^{\sigma}}{\partial x^{\nu}} = \Lambda(x) \eta_{\mu\nu} \tag{2.82}$$

To derive the condition for an infinitesimal transformation, $x^\mu \mapsto x'^\mu = x^\mu + \epsilon^\mu$, to be conformal we expand up to first order in ϵ

$$\big(1+\lambda(x)\big)\eta_{\mu\nu} = \eta_{\rho\sigma}\left(\delta^\rho_\mu + \partial_\mu\epsilon^\rho\right)\left(\delta^\sigma_\nu + \partial_\nu\epsilon^\sigma\right) = \eta_{\mu\nu} + (\partial_\nu\epsilon_\mu + \partial_\mu\epsilon_\nu)$$

multiplying the above equation with $\eta^{\mu\nu}$ we reach the condition,

$$(\partial_\nu\epsilon_\mu + \partial_\mu\epsilon_\nu) = \frac{2}{D}(\partial\cdot\epsilon)\eta_{\mu\nu} \tag{2.83}$$

Conformal Group and Conformal Algebra in D=2

In $D=2$, using $g_{\mu\nu} = \delta_{\mu\nu}$ the infinitesimal condition for conformal transformation becomes the Cauchy–Riemann equations,

$$\partial_1\epsilon_1 = \partial_2\epsilon_2, \qquad \partial_1\epsilon_2 = -\partial_2\epsilon_1$$

As a result, it makes sense to define the usual complex coordinates here,

$$z = x^1 + \mathrm{i}x^2, \quad \partial_z = \tfrac{1}{2}(\partial_1 - \mathrm{i}\partial_2), \quad \epsilon(z) = \epsilon^1 + \mathrm{i}\epsilon^2 \tag{2.84}$$

$$\bar{z} = x^1 - \mathrm{i}x^2, \quad \partial_{\bar{z}} = \tfrac{1}{2}(\partial_1 + \mathrm{i}\partial_2), \quad \bar{\epsilon}(\bar{z}) = \epsilon^1 - \mathrm{i}\epsilon^2, \tag{2.85}$$

Note that here $z, \bar{z}$ are treated as two independent variables which means that we are working in $\mathbb{C}^2$ instead of the original $\mathbb{R}^2$ space. This is a standard trick which simplifies the treatment in the sense that we can limit the discussion to the un–bared part and the bared will follow, however, when necessary we have to make sure to work in the *real contour*, which is defined as the $2D$ surface in $\mathbb{C}^2$ that z and $\bar{z}$ are complex conjugates.

In the complex plane, the infinitesimal conformal transformation $\epsilon(z)$ and $\bar{\epsilon}(\bar{z})$ are only a function of z and $\bar{z}$ respectively, since $\partial_{\bar{z}}\epsilon = \partial_z\bar{\epsilon} = 0$.

From the condition it follows that for the transformation to be conformal, we only need $\epsilon(z)$ to be a holomorphic function and thus, any holomorphic function, $f(z) = z+\epsilon(z)$, is an infinitesimal conformal transformation with scale factor of $\Lambda = |\frac{\partial f}{\partial z}|^2$. So we now can perform the Laurent expansion of $\epsilon(z), \bar{\epsilon}(\bar{z})$,

$$z \mapsto f(z) = z + \sum_n \epsilon_n(-z^{n+1}), \qquad \bar{z} \mapsto \bar{f}(\bar{z}) = \bar{z} + \sum_n \bar{\epsilon}_n(-\bar{z}^{n+1})$$

and read the generators of infinitesimal transformation $l, \bar{l}$ as,

$$l_n = -z^{n+1}\partial_z, \qquad \bar{l}_n = -\bar{z}^{n+1}\partial_{\bar{z}}$$

It is straightforward to check that the generators satisfy two independent algebras $\mathfrak{A}$ and $\bar{\mathfrak{A}}$ known as the *Witt algebra*,

$$[l_m, l_n] = (m-n)l_{m+n}, \qquad \left[\bar{l}_m, \bar{l}_n\right] = (m-n)\bar{l}_{m+n} \qquad \left[l_m, \bar{l}_n\right] = 0 \tag{2.86}$$

Again note that the direct product of the two algebra, $\mathfrak{A} \otimes \bar{\mathfrak{A}}$, lives in $\mathbb{C}^2$. For our original $\mathbb{R}^2$ space , when the algebra is concerned, we consider the subalgebra $\mathfrak{A} \oplus \bar{\mathfrak{A}}$ generated by $l_n + \bar{l}_n$ and $\mathrm{i}(l_n - \bar{l}_n)$.

These generators are called the *local conformal algebra* in a sense that they have been defined on the $\mathbb{R}^2$ space (or any open set of that). However, since inversions are conformal, in a conformal field theory we do not want to consider the infinity as a special point and we would like to work in $S^2 \sim \mathbb{R}^2 \oplus \{\infty\}$. So, considering the whole vector field $\mathcal{V}(z) = -\sum z^{n+1}\partial_z$ we can ask what subset of the local algebra is well defined globally?

Obviously there are only two points that $\mathcal{V}$ could have poles. At the limit $z \to 0$ only $n \geq -1$ are well defined and for the limit $z \to \infty$, we have to go to local coordinates,

using the change of variable $w = -\frac{1}{z}$,

$$l_n = -\left(-\frac{1}{w}\right)^{n+1} \times (-w^2\partial_w) = -\left(-\frac{1}{w}\right)^{n-1} \partial_w$$

only $n \leq 1$ are well defined. So, for the whole space of Riemann sphere only the set of $\{l_{-1}, l_0, l_1\}$ together with their anti–holomorphic counterparts $\{\bar{l}_{-1}, \bar{l}_0, \bar{l}_1\}$ are well define. This subalgebra of local algebra is called the *global conformal algebra.*

- $l_{-1} \oplus \bar{l}_{-1}$ are the generators of translations in $2D$.

- l_0 generates the transformation $z \mapsto (1+\epsilon)z$, using the standard r, ϕ for complex variable $z = r\mathrm{e}^{\mathrm{i}\phi}$ we have.

  $$l_0 = -z\partial_z = -\frac{1}{2}\left(r\partial_r - \mathrm{i}\partial_\phi\right), \qquad \bar{l}_0 = -\bar{z}\partial_{\bar{z}} = -\frac{1}{2}\left(r\partial_r + \mathrm{i}\partial_\phi\right)$$

  So, together they are the generators of dilatation and $2D$ rotation.

  $$(l_0 + \bar{l}_0) = -r\partial_r, \qquad \mathrm{i}(l_0 - \bar{l}_0) = -\partial_\phi$$

- $l_1 \oplus \bar{l}_1$ are the special conformal generators which can be thought of as the translations for the inverse variable $w = -\frac{1}{z}$,

  $$l_1 = -z^2\partial_z = -\left(-\frac{1}{w}\right)^2 (w^2\partial_w)2 = -\partial_w$$

The *global conformal group* generated by exponentiation of this algebra is the $\mathrm{SL}(2,\mathbb{C})/\mathbb{Z}_2$

$$z \mapsto \frac{az+b}{cz+d}, \qquad \bar{z} \mapsto \frac{a\bar{z}+b}{c\bar{z}+d}$$

The $\mathbb{Z}_2$ is due to the fact that multiplying the a, b, c, d by -1 does not change the transformation. There are 4 interesting subgroups,

- Translation: $z \mapsto z + B$, $\begin{pmatrix} 1 & B \\ 0 & 1 \end{pmatrix}$
- Rotation: $z \mapsto \mathrm{e}^{\mathrm{i}\theta} z$, $\begin{pmatrix} \mathrm{e}^{\mathrm{i}\theta} & 0 \\ 0 & \mathrm{e}^{-\mathrm{i}\theta} \end{pmatrix}$
- Dilatation: $z \mapsto \lambda z$, $\begin{pmatrix} \lambda & 0 \\ 0 & \lambda^{-1} \end{pmatrix}$
- Special conformal: $z \mapsto \frac{1}{Cz+1}$, $\begin{pmatrix} 1 & 0 \\ C & 1 \end{pmatrix}$

As expected the group $\mathrm{SL}(2,\mathbb{C})$ is isomorphic to $\mathrm{SO}(3,1)$.

2.5.3 Conformal QFTs

For a general conformal invariant field theory we demand the following properties:

- A set of fields $\{A_i\}$ which contains all the fields and their derivatives.
- A subset of fields $\{\phi_j\} \subset \{A_i\}$ called "quasi–primary" which under global conformal transformations, will transform like

$$\phi_j(x) \mapsto \left|\frac{\partial x'}{\partial x}\right|^{\Delta_j/d} \phi_j(x')$$

- All the fields can be represented in terms of linear combination of quasi primary fields and their derivatives.
- There exist a vacuum $|0\rangle$ invariant under global conformal transformation.

Radial Quantization

Lets start with flat Euclidean time σ^0 and space σ^1 coordinates and compactify the space $\sigma^1 = \sigma^1 + 2\pi$ to get rid of unavoidable IR divergences in 2D. Defining $\zeta, \bar{\zeta} = \sigma^0 \pm \sigma^1$ they now live on a cylinder.

We can now consider the conformal map $\zeta \mapsto z = \mathrm{e}^{\zeta}$, to map the cylinder to a plane of z. The radial direction of the plane is now the time direction and The equal time circles on the cyclinder map to concentric circles on the plane. In particular,

- The infinite past and future $\sigma^0 = \pm\infty$ will now correspond to $z = 0, \infty$.
- The time–reversal operation $\sigma^0 \mapsto -\sigma^0$ is now $z \mapsto 1/z^*$.
- Rotations on the plane $z \mapsto \mathrm{e}^{\mathrm{i}\theta} z$ are just the space translations on cylinder $\sigma^1 \mapsto \sigma^1 + \theta$
- Dilatation on the plane $z \mapsto \mathrm{e}^{a} z$ are just the time translation on the cylinder $\sigma^0 \mapsto \sigma^0 + a$

So, the generator of dilatation on the plane can be considered as the Hamiltonian, i.e. the generator of time translation in our cylinder spacetime, and the Hilbert space can be built up on the surfaces of constant radius on the plane. This definition of quantum theory on the plane is called the *Radial Quantization*.

Following the above discussion, it makes sense to define the physical states as the eigenvectors of the Dilatation operator. if we denote the eigenvalues of $l_0, \bar{l}_0$ by $h, \bar{h}$, the eigenvalues of Dilatation operator , also known as the *scaling dimension* Δ ,will then be $h + \bar{h}$ and the eigenvalues of Rotation operator will be $h - \bar{h}$, also known as *spin* s.

$$\Delta = h + \bar{h}, \qquad s = h - \bar{h}$$

The physical requirement for the $h, \bar{h}$ is then to be real numbers.

Field Operators

Translating the notion of quasi–primary fields to $2D$, we define a quasi–primary field of dimension $(h, \bar{h})$ to transform according to the following rule under global conformal transformations,

$$\Phi(z, \bar{z}) \mapsto \left|\frac{\partial f}{\partial z}\right|^{h} \left|\frac{\partial \bar{f}}{\partial \bar{z}}\right|^{\bar{h}} \Phi\big(f(z), \bar{f}(\bar{z})\big)$$

This is equivalent to the statement that the differential $\Phi(z, \bar{z})\ \mathrm{d}z^{h}\mathrm{d}\bar{z}^{\bar{h}}$ is invariant. If the field Φ transform with same rule under local conformal transformations we call it a primary field of conformal weight $(h, \bar{h})$. It is useful to calculate the variation of a primary field under an infinitesimal conformal transformation, $z \mapsto z + \epsilon(z)$

$$\begin{aligned}\delta_{\epsilon,\bar{\epsilon}}\Phi(z, \bar{z}) &= (1 + \partial_z\epsilon)^{h}(1 + \partial_{\bar{z}}\bar{\epsilon})^{\bar{h}}\Big((1 + \epsilon\partial_z + \bar{\epsilon}\partial_{\bar{z}})\Phi(z, \bar{z})\Big) - \Phi(z, \bar{z}) \\ &= \Big((h\partial_z\epsilon + \epsilon\partial_z) + (\bar{h}\partial_{\bar{z}}\bar{\epsilon} + \bar{\epsilon}\partial_{\bar{z}})\Big)\Phi(z, \bar{z}) \qquad (2.87)\end{aligned}$$

Conformal invariance imposes important constraints on the form of the correlation functions of quasi–primary fields. For the two point correlation function the invariance under symmetry will for the result to be only a function of distances $z_{ij} = z_i - z_j, \bar{z}_{ij} = \bar{z}_i - \bar{z}_j$ and the invariance under scaling will lead to,

$$G(z_i, \bar{z}_i, z_j, \bar{z}_j) \coloneqq \langle \Phi_i(z_i, \bar{z}_i)\Phi_j(z_j, \bar{z}_j)\rangle = \frac{d_{ij}}{z_{ij}^{h_i+h_j}\ \bar{z}_{ij}^{\bar{h}_i+\bar{h}_j}}$$

To examine the invariance under special conformal transformation, it suffices to only consider the invariance under inversion,

$$\begin{aligned} G(z_i,\bar{z}_i,z_j,\bar{z}_j) &= \frac{1}{z_i^{2h_i}}\frac{1}{z_j^{2h_j}}\frac{1}{\bar{z}_i^{2\bar{h}_i}}\frac{1}{\bar{z}_j^{2\bar{h}_j}}G(\tfrac{1}{z_i},\tfrac{1}{\bar{z}_i},\tfrac{1}{z_j},\tfrac{1}{\bar{z}_j}) \\ &= \frac{1}{z_i^{2h_i}}\frac{1}{z_j^{2h_j}}\frac{1}{\bar{z}_i^{2\bar{h}_i}}\frac{1}{\bar{z}_j^{2\bar{h}_j}}\frac{d_{ij}}{(\frac{-1}{z_i}+\frac{-1}{z_j})^{h_i+h_j}(\frac{-1}{\bar{z}_i}+\frac{-1}{\bar{z}_j})^{\bar{h}_i+\bar{h}_j}} \end{aligned}$$

Which can only be satisfied when $h_i = h_j$ and $\bar{h}_i = \bar{h}_j$, so the final form of the two point functions of quasi primary fields is

$$G(z_i,\bar{z}_i,z_j,\bar{z}_j) = \begin{cases} \frac{d_{ij}}{z_{ij}^{2h_i}\,\bar{z}_{ij}^{2\bar{h}_i}} & h_i = h_j, \bar{h}_i = \bar{h}_j \\ 0 & \text{otherwise} \end{cases} \tag{2.88}$$

Global Symmetries of QFTs

A transformation of the fields that leaves the action, $\mathcal{S}$, invariant (even when the EOM is not satisfied) is called a global symmetry,

$$\Phi^a(x) \mapsto \Phi^a(x) + \mathrm{i}\epsilon\mathcal{N}^a(x), \quad \text{s.t.} \quad \delta\mathcal{S} = \mathrm{i}\epsilon\int \mathrm{d}^D x\ \frac{\delta\mathcal{S}}{\delta\Phi^a(x)}\mathcal{N}^a(x) = 0$$

The standard trick of Noether's theorem is to enhance the ϵ to a smooth but arbitrary function of coordinates. The variation of action is then, generally, nonzero but if we now require the satisfaction of EOM, $\delta\mathcal{S}$ vanishes for arbitrary variations due to the stationary condition of $\mathcal{S}$. This leads to a *conserved current*,

$$0 = \delta\mathcal{S} = \int \mathrm{d}^D x\ j^\mu \frac{\partial\epsilon(x)}{\partial x^\mu} \quad \Longrightarrow \quad \partial_\mu j^\mu = 0$$

We can make another set of conserved quantities out of the currents, known as the conserved charge which serve as the Quantum generators of transformation,

$$Q = \int \underbrace{\mathrm{d}^{D-1}x}_{\text{spatial}}\ j_0$$

If the symmetry is now the symmetry of Lagrangian density, it is straightforward to show that for the current and charge we have,

$$j^\mu = \frac{\partial \mathscr{L}}{\partial(\partial_\mu \Phi^a)}\mathcal{N}^a \quad \Longrightarrow \quad Q = \int \mathrm{d}^{D-1}x\ \frac{\partial \mathscr{L}}{\partial(\partial_t \Phi^a)}\mathcal{N}^a$$

remembering that $\partial\mathscr{L}/\partial(\partial_t\Phi)$ was defined as conjugate momentum, it is now easy to see in what sense the conserved charge is the generator of transformation,

$$\big[Q, \Phi^a\big] = \int \mathrm{d}^{D-1}x\ \big[\Pi_b, \Phi^a\big]\mathcal{N}^b = -\mathrm{i}\mathcal{N}^a$$

It is fruitful to define the current in terms of the *energy–momentum stress tensor* $j_\mu = T_{\mu\nu}\epsilon^\nu$ which is in general a symmetric(Belifante stree tensor) divergence free tensor (since for a constant ϵ^μ, we have $0 = \partial^\mu j_\mu = \partial^\mu T_{\mu\nu}$). In particular for a conformal transformation $T_{\mu\nu}$ is also traceless, because

$$0 = \partial^\mu j_\mu = T_{\mu\nu}(\partial^\mu \epsilon^\nu) = \frac{1}{d}T_{\mu\nu}\eta^{\mu\nu}(\partial\cdot\epsilon) = \frac{1}{d}(\partial\cdot\epsilon)T^\mu{}_\mu$$

To realize the consequence of traceless property we can write the stress tensor in $z, \bar{z}$ coordinates in terms of standard coordinates of the plane $x^0 = \frac{1}{2}(z+\bar{z})$, $x^1 = \frac{1}{2\mathrm{i}}(z-\bar{z})$ with Euclidean metric $\delta_{\mu\nu}$. The metric for $z, \bar{z}$ coordinates is then,

$$g_{\mu\nu} = \begin{array}{c} \\ x^0 \\ x^1 \end{array}\begin{array}{c} \begin{array}{cc} x^0 & x^1 \end{array} \\ \begin{pmatrix} 1 & 0 \\ 0 & 1 \end{pmatrix} \end{array} \quad \Longrightarrow \quad g_{\mu\nu} = \begin{array}{c} \\ z \\ \bar{z} \end{array}\begin{array}{c} \begin{array}{cc} z & \bar{z} \end{array} \\ \begin{pmatrix} 0 & \frac{1}{2} \\ \frac{1}{2} & 1 \end{pmatrix} \end{array}$$

and for the components of stress tensor,

$$T_{zz} = \frac{1}{4}(T_{00} - 2\mathrm{i}\ T_{01} - T_{11}) = \frac{1}{2}(T_{00} - \mathrm{i}T_{01})$$
$$T_{\bar{z}\bar{z}} = \frac{1}{4}(T_{00} + 2\mathrm{i}\ T_{01} - T_{11}) = \frac{1}{2}(T_{00} + \mathrm{i}T_{01})$$
$$T_{z\bar{z}} = T_{\bar{z}z} = \frac{1}{4}(T_{00} + T_{11}) = 0$$

using the divergence–free property,

$$\begin{aligned}\partial_{\bar{z}} T_{zz} &= \frac{1}{4}(\partial_0 + \mathrm{i}\partial_1)(T_{00} - \mathrm{i}T_{10}) \\ &= \frac{1}{4}\Big((\underbrace{\partial_0 T_{00} + \partial_1 T_{10}}_{\partial_\mu T_{\mu 0}}) + \mathrm{i}(\underbrace{\partial_1 T_{00} - \partial_0 T_{10}}_{\partial_\mu T_{\mu 1}})\Big) = 0\end{aligned}$$

So the two non–vanishing components of stress tensor have only holomorphic and antiholomorphic dependence respectively, So for simplicity we can write,

$$T(z) \coloneqq T_{zz}(z), \qquad \bar{T}(\bar{z}) \coloneqq T_{\bar{z}\bar{z}}(\bar{z})$$

So, we have a holomorphic $j_z = T(z)\epsilon(z)$ and an antiholomorphic current, $\bar{j}_{\bar{z}} = \bar{T}(\bar{z})\bar{\epsilon}(\bar{z})$. The conserved charge (integral of orthogonal component of current to surface of equal time) becomes $\int \mathrm{d}\theta\ j_r(\theta)$, so we are only interesting in the $\mathrm{i}(j_z + \bar{j}_{\bar{z}})$ component of current. If we make the convention of integrating counterclockwise and normalize the size of space 2π we can define the conserved charge as

$$Q_{\epsilon,\bar{\epsilon}} = \frac{1}{2\pi\mathrm{i}} \oint \Big(\mathrm{d}z\ T(z)\epsilon(z) + \mathrm{d}\bar{z}\ \bar{T}(\bar{z})\bar{\epsilon}(\bar{z})\Big) \tag{2.89}$$

Note that we can not calculate this integral until we mention what fields it is acting on (are present inside of the contour) For the infinitesimal transformation of any field we then have

$$\delta_{\epsilon,\bar{\epsilon}}\phi(w,\bar{w}) = \frac{1}{2\pi\mathrm{i}}\left(\oint \mathrm{d}z\ \epsilon(z)\Big[T(z), \phi(w,\bar{w})\Big] + \oint \mathrm{d}\bar{z}\ \bar{\epsilon}(\bar{z})\Big[\bar{T}(\bar{z}), \phi(w,\bar{w})\Big]\right)$$

Operator Product Expansion

We now turn into the calculation of variation of a field under infinitesimal conformal transformation. For Quantum fields we have to impose the regular time ordering which on the plane will translate to the notion of *Radial Ordering*. We define the radial ordering of operators,

$$R\Big(A(z)B(w)\Big) = \begin{cases} A(z)B(w) & |z| > |w| \\ \\ B(w)A(z) & |w| > |z| \end{cases}$$

Using the radial ordering definition, we can decipher the meaning of equal time commutator. Considering only holomorphic part

$$\begin{aligned} \oint_{\text{E.T.}} \mathrm{d}z\,[A(z), B(w)] &= \oint_{|z|>|w|} \mathrm{d}z A(z)B(w) - \oint_{|w|>|z|} \mathrm{d}z A(z)B(w) \\ &= \oint_{C(w)} R\Big(A(z)B(w)\Big) \end{aligned}$$

where $C(w)$ is a circle of infinitesimal radius around w traversed counterclockwise.

Comparing the holomorphic part of primary field transformation with the transformation from the conserved charge,

$$\frac{1}{2\pi \mathrm{i}} \oint \mathrm{d}z\ \epsilon(z) R\Big(T(z)\Phi(w,\bar{w})\Big) = (h\partial_w \epsilon + \epsilon\partial_w)\Phi(w,\bar{w})$$

using the following identities,

$$\begin{aligned} \epsilon(w)\partial_w \Phi(w,\bar{w}) &= \frac{1}{2\pi \mathrm{i}} \oint_{C(w)} \mathrm{d}z\ \frac{\epsilon(z)}{z-w} \partial_w \Phi(w,\bar{w}) \\ h\partial_w \epsilon(w)\Phi(w,\bar{w}) &= \frac{1}{2\pi \mathrm{i}} \oint_{C(w)} \mathrm{d}z\ \frac{h\epsilon(z)}{(z-w)^2} \Phi(w,\bar{w}) \end{aligned}$$

we find the Operator Product Expansion (OPE) of a primary field with the energy momentum tensor (we drop the radial ordering and consider the products as the radially ordered products from now on),

$$T(z)\Phi(w,\bar{w}) = \frac{h}{(z-w)^2}\Phi(w,\bar{w}) + \frac{1}{z-w}\partial_w\Phi(w,\bar{w}) + \cdots(\text{reg.}) \tag{2.90a}$$

$$\bar{T}(\bar{z})\Phi(w,\bar{w}) = \frac{\bar{h}}{(\bar{z}-\bar{w})^2}\Phi(w,\bar{w}) + \frac{1}{\bar{z}-\bar{w}}\partial_{\bar{w}}\Phi(w,\bar{w}) + \cdots(\text{reg.}) \tag{2.90b}$$

This OPE can be taken for the definition of primary fields as well.

Quantum Correction to Conformal Algebra

A secondary (or descendant) field is a field that has higher poles in its OPE with T or $\bar{T}$. As an example, by taking the derivative of a primary field one can see that the derivatives of primary fields are not primary.

An important secondary field is the stress tensor itself, to see that we have to look at the conformal transformations of the stress tensor. From the OPE of primary fields it is apparent that T has conformal weight (2,0). Given that stress tensor is bosonic, we can write down the TT OPE upto a constant c,

$$T(z)T(w) = \frac{c/2}{(z-w)^4} + \frac{2}{(z-w)^2}T(w) + \frac{1}{z-w}\partial_w T(w) + \cdots(\text{reg.}) \tag{2.91}$$

Here c, the central charge, is a number that depends on the theory. Using the OPE we can now derive the infinitesimal conformal transformation for the stress tensor,

$$\delta_\epsilon T(z) = 2\partial\epsilon T(z) + \epsilon\partial T(z) + \frac{c}{12}\partial^3\epsilon$$

Virasoro algebra

We now derive the algebra of the generators of conformal transformation of a Quantum theory. The Laurent expansion of $T(z)$ reads,

$$T(z) = \sum_{n\in\mathbb{Z}} z^{-n-2} L_n \quad \Longrightarrow \quad L_n = \frac{1}{2\pi \mathrm{i}} \oint \mathrm{d}z \; z^{n+1} T(z)$$

The 2 in the exponent is chosen so that L_n operators have the scaling dimension of n. We first show that the Laurent modes of stress tensor are indeed the generators of infinitesimal conformal transformation. Choosing the specific transformation $\epsilon(z) = -\epsilon_n z^{n+1}$ for the conserved charge we have,

$$Q_n = \oint \frac{\mathrm{d}z}{2\pi \mathrm{i}} \; T(z)\epsilon_n z^{n+1} = -\epsilon_n \sum_{m\in\mathbb{Z}} \oint \frac{\mathrm{d}z}{2\pi \mathrm{i}} \; L_m z^{n-m-1} = -\epsilon_n L_n$$

So, to calculate the algebra,

$$\begin{aligned}
[L_m, L_n] &= \oint \frac{\mathrm{d}z}{2\pi \mathrm{i}} \oint \frac{\mathrm{d}w}{2\pi \mathrm{i}} \; z^{m+1} w^{n+1} \left[T(z), T(w)\right] \\
&= \oint_{C(0)} \frac{\mathrm{d}w}{2\pi \mathrm{i}} \; w^{n+1} \oint_{C(w)} \frac{\mathrm{d}z}{2\pi \mathrm{i}} \; z^{m+1} T(z)T(w) \\
&= \oint_{C(0)} \frac{\mathrm{d}w}{2\pi \mathrm{i}} \; w^{n+1} \oint_{C(w)} \frac{\mathrm{d}z}{2\pi \mathrm{i}} \; z^{m+1} \left(\frac{c/2}{(z-w)^4} + \frac{2T(w)}{(z-w)^2} + \frac{\partial_w T(w)}{z-w} \right) \\
&= \oint_{C(0)} \frac{\mathrm{d}w}{2\pi \mathrm{i}} \; w^{n+1} \left(\frac{c}{12} m(m^2-1) w^{m-2} + 2(m+1) w^m T(w) + w^{m+1} \partial_w T(w) \right) \\
&= \frac{c}{12} m(m^2-1)\delta_{m+n,0} + 2(m+1)L_{m+n} - (m+n+2)L_{m+n} \\
&= (m-n)L_{m+n} + \frac{c}{12} m(m^2-1)\delta_{m+n,0}
\end{aligned}$$

Which is known as the *Virasoro Algebra*.

2.5.4 The free boson/fermion theory

The free massless boson action is conformally invariant in $D = 2$, the action for a 2D massless bosonic field $X(x^0, x^1)$ defined on the cylinder $x^1 = x^1 + 2\pi$ with metric

$h = \mathrm{diag}(+1, +1)$ would be,

$$\mathcal{S} = \frac{1}{4\pi\kappa} \int \mathrm{d}x^0 \mathrm{d}x^1 \sqrt{|h|}\ h^{\alpha\beta} \partial_\alpha X \partial_\beta X$$

Following the usual mapping to the complex plane, $z = \mathrm{e}^{x^0 + \mathrm{i}x^1}$, the metric of the complex plane is,

$$g = \begin{pmatrix} 0 & \frac{1}{2z\bar{z}} \\ \frac{1}{2z\bar{z}} & 0 \end{pmatrix}, \qquad g^{-1} = \begin{pmatrix} 0 & 2z\bar{z} \\ 2z\bar{z} & 0 \end{pmatrix}$$

So for the $X(z, \bar{z})$ filed the action will be,

$$\begin{aligned} \mathcal{S} &= \frac{1}{4\pi\kappa} \int \mathrm{d}z \mathrm{d}\bar{z}\ \sqrt{|g|} g^{ab} \partial_a X \partial_b X \\ &= \frac{1}{2\pi\kappa} \int \mathrm{d}z \mathrm{d}\bar{z}\ \partial X \bar{\partial} X \end{aligned}$$

from the equation of motion $\partial\bar{\partial} X(z, \bar{z}) = 0$ it is apparent that $X(z, \bar{z})$ splits into holomorphic and antiholomorphic parts which correspond to massless left–movers and right–movers.

2.6 Exact solution of the XXZ model

2.6.1 Integrability

A particularly fruitful approach in theoretical physics is to introduce exactly solvable *toy models* to achieve a stronger understanding of the underlying physics of many–body phenomena. These toy models generally posses an extensive set of *local* constants of motion, or symmetries of the theory, which allow for a complete solution. It is in this sense that we describe *integrability* as the ultimate form of symmetry. Note that *the theory of nature* might not necessarily respect this symmetry, and probably doesn't, therefore the conclusions from toy models should not be naively extended to all possible theories. In this section we

follow Hans Bethe's solution to one dimensional interacting systems in the context of one dimensional XXZ chain. This surprising solution is a consequence of existence of solitons in the theory, despite complexity any non–linear system with solitons is integrable.

2.6.2 Bethe ansatz for spin chains

Spin chains

For a periodic chain of length L with a single spin-$\frac{1}{2}$, which is a two dimensional Hilbert space $h^{\frac{1}{2}}$, at every site the total Hilbert space is

$$\mathcal{H} = \bigotimes^{L} h^{\frac{1}{2}}, \qquad \dim \mathcal{H}' = 2^L$$

If the Hamiltonian satisfies

- *Translational invariance*, that is $[\mathrm{T}, \mathrm{H}]$. The translation operator T is defined by its action on the Ising configuration states,

  $$\mathrm{T}\,|m_1, \ldots, m_{L-1}, m_L\rangle = |m_L, m_1, \ldots, m_{L-1}\rangle$$

  it is therefore a non–local unitary operator with eigenvalues $\mathrm{e}^{\mathrm{i}k}$ with the allowed values of *momentum*, $k = \frac{2\pi}{L} \times (-\frac{L}{2}, \ldots, 0, \ldots, \frac{L}{2} - 1)$, are prescribed by the periodicity.

- *Short ranged*, that is the Hamiltonian is a sum of short ranged operators that have only local support.

- *Conservation of the third component of total spin*, which means $[S^z_{\mathrm{tot}}, \mathrm{H}]$,

the total Hilbert space can be split into different sectors and hence be exactly solved.

The first step is to make use of the conservation of total magnetization $m = \sum S_i^z + \frac{1}{2}$, which leads to division of Hilbert space (and hence the Hamiltonian) into different magnetization sectors. Defining m as the count of the number of up spins in an Ising configuration,

$$\mathcal{H} = \bigoplus \mathcal{H}_m, \qquad \dim \mathcal{H}_m = \binom{L}{m}$$

For the case of Heisenberg Hamiltonian the total spin operator, $\mathrm{S}_{\mathrm{tot}}$ is also conserved (because each Heisenberg term commutes with the complete graph Heisenberg Hamiltonian) and as a result the Hilbert space can be divided into total spin blocks. Since for total spin of s there are $2s+1$ possible eigenvalues for the third component of spin, namely $\mathrm{S}^z_{\mathrm{tot}} = s, s-1, \ldots, -s$, the number of possible total spin–s that can be generated from a chain of length L is easy to calculate

$$N_s = \binom{L}{\frac{L}{2}+s} - \binom{L}{\frac{L}{2}+s+1}$$

so the total Hilbert space in terms of total spin blocks are

$$\mathcal{H} = \bigoplus_{s=0}^{L/2} \mathcal{H}_s \quad \text{where} \quad \mathcal{H}_s = \bigoplus^{N_s} h^s$$

Bethe basis

Going back to the magnetization blocks, the $m = 0$ sector has only one state, i.e. the Ising configuration of all L spins down, known as the *Bethe reference state*, ψ_0. Obviously, this state is also an eigenstate of the translation operator with the trivial momentum of $k = 0$. This state is the lowest weight of the total spin–$\frac{L}{2}$ sector.

For the sake of notation simplicity, from now on I only use the position of up spins to represent any Ising configuration, for example the state $|i, j, k\rangle$ where $1 \leq i < j < k \leq L$

represents all spins in the down state except for the three sites at i, j, k. The action of the translation operator in this new notation is

$$\mathrm{T}\,|i,j,k\rangle = |(i+1),(j+1),(k+1)\rangle \mod L$$

The $m = 1$ sector has L states which we can expand in terms of the Ising basis as,

$$\psi_{1,\alpha} = \sum_{x=1}^{L} c_\alpha(x)\ |x\rangle, \qquad \alpha = 1, 2, \ldots, L$$

If we now impose the translational invariance on the states,

$$\mathrm{T}\,\psi_1(k) = \mathrm{e}^{\mathrm{i}k}\psi_1(k) \quad \Longrightarrow \quad \psi_1(k) = \frac{1}{\sqrt{L}}\sum_{x=1}^{L} \mathrm{e}^{-\mathrm{i}kx}\ |x\rangle$$

So the spin wave states label with the good Quantum number, the total momentum k, are all the L translational invariant states in this sector. It is worthy to talk about the total spin of these states. The action of the $\mathrm{S}^-_{\mathrm{tot}}$ on these states, shows that the $k = 0$ state belongs to the total spin of $\frac{L}{2}$ and the rest are lowest weights of $L-1$ distinct spin–$(\frac{L}{2}-1)$ sectors.

$$\mathrm{S}^-_{\mathrm{tot}}\,\psi_1(k) = \frac{1}{\sqrt{L}}\sum_{x=1}^{L} \mathrm{e}^{-\mathrm{i}kx}\ \mathrm{S}^-_x\,|x\rangle = \sqrt{L}\psi_0\ \delta_{k,0}$$

For $m = 2$ sector we can again write the desired states in terms of the Ising configuration basis

$$\psi_{2,\alpha} = \sum_{1\le x_1<x_2\le L} c_\alpha(x_1, x_2)\ |x_1, x_2\rangle$$

As a first guess one might think that the product of single spin waves with quasi–momenta $\mathrm{e}^{-\mathrm{i}(k_1x_1+k_2x_2)}$ is an eigenstate of translation operator with momentum $k_1 + k_2$, however for the Ising configuration when one of the up spins wraps around the periodic boundary condition due to the action of the translation operator we can see that

$$\mathrm{T}\,\mathrm{e}^{-\mathrm{i}(k_1x_1+k_2L)}\ |x_1, L\rangle \neq \mathrm{e}^{\mathrm{i}(k_1+k_2)}\mathrm{e}^{\mathrm{i}(k_1+k_2(x_1+1))}\ |1, x_1+1\rangle$$

and as a result the simple product of spin waves are not the desired states. However, the following ansatz

$$c_\alpha(x_1, x_2) = A_{12}\ \mathrm{e}^{-\mathrm{i}(k_1 x_1 + k_2 x_2)} + A_{21}\ \mathrm{e}^{-\mathrm{i}(k_2 x_1 + k_1 x_2)}$$

is a translationally invariant state with the total momentum of $k_1 + k_2$ if the following two conditions hold

$$A_{12} = A_{21}\mathrm{e}^{-\mathrm{i}k_1 L}, \qquad A_{21} = A_{12}\mathrm{e}^{-\mathrm{i}k_2 L}$$

defining the scattering amplitude as $S_{12} \equiv A_{21}/A_{12}$ we can rewrite the above ansatz

$$c_\alpha(x_1, x_2) = A_{12}\ (\mathrm{e}^{-\mathrm{i}(k_1 x_1 + k_2 x_2)} + S_{12}\ \mathrm{e}^{-\mathrm{i}(k_2 x_1 + k_1 x_2)}), \quad S_{12} = \mathrm{e}^{-\mathrm{i}k_2 L} \tag{2.92}$$

To see if the number of ansatz states are equal to the dimension of Hilbert space in this sector we need to explore the possible values for k_1, k_2. The periodicity implies $k \equiv k_1 + k_2 = 2\pi n$. Assuming that the scattering amplitude is just a phase so defining $S_{12} \equiv \mathrm{e}^{\mathrm{i}\phi}$ we have

$$k_1 L = +\phi + 2\pi n_1, \quad k_2 L = -\phi + 2\pi n_2$$

with all n_1, n_2, n can be of values $0, \ldots, L-1$. Notice that since k_1, k_2 are interchangeable not all L^2 possible choices lead to different ansatz states and we are left with $L(L+1)/2$ choices for $n_1 \leq n_2$. This is still L states larger than the size of the Hilbert space, so one would expect that depending on the value of S_{12}, calculated for specific models, some of these states either vanish or not be linearly independent.

We can now generalize the same concept for the higher value of m all the way up to $m = L/2$ (we can use particle–hole symmetry for larger m) and introduce the ansatz

$$\psi_{m,\alpha} = \sum_{1 \leq x_1 < \cdots < x_m \leq L} c_\alpha(x_1, \ldots, x_m)\ |x_1, \ldots, x_m\rangle$$

with the coefficients defined as

$$c_{\{k\}}(x_1,\ldots,x_m) \equiv \sum_{P\in S_m} A_P \prod_{n=1}^{m} \mathrm{e}^{-\mathrm{i}k_{P(n)}x_n}$$

where P is a permutation of m elements, i.e. a member of the symmetric group S_m. We want for this state to be an eigenstate of translation operator with total momentum $k = \sum_i^m k_i$. As in the simpler case of $m = 2$ here too we need to consider the nontrivial effect of translation operator on the Ising configurations that need to transfer the last spin around the periodic boundary. So, we require

$$c_{\{k\}}(x_1,\ldots,x_{m-1},L) = \mathrm{e}^{\mathrm{i}k} c_{\{k\}}(1,x_1+1,\ldots,x_{m-1}+1)$$

or equivalently for each term in the sum,

$$A_P\ \mathrm{e}^{-\mathrm{i}(k_{P(1)}x_1+\cdots+k_{P(m)}L)} = A_{P'}\ \mathrm{e}^{-\mathrm{i}(k_{P'(1)}0+\cdots+k_{P'(m)}x_{m-1})}.$$

to satisfy this equation we need to have $P(1,2,\ldots,m) = P'(2,\ldots,m,1)$. Now by defining the shift permutation P_s, we can write down a simple version of general condition on the coefficients of the ansatz.

$$A_{PP_s} = A_P\ \mathrm{e}^{-\mathrm{i}k_{P(m)}L}, \qquad P_s(1,2,\ldots,m) \equiv (m,1,\ldots,m-1) \tag{2.93}$$

To unwrap the underlying mathematics of these equations lets try to explore the $m = 3$ case. Here, the translational invariant condition leads to six equations

$$\begin{aligned}
\frac{A_{312}}{A_{123}} &= \frac{A_{321}}{A_{213}} = \mathrm{e}^{-\mathrm{i}k_3L},\\
\frac{A_{231}}{A_{312}} &= \frac{A_{213}}{A_{132}} = \mathrm{e}^{-\mathrm{i}k_2L},\\
\frac{A_{123}}{A_{231}} &= \frac{A_{132}}{A_{321}} = \mathrm{e}^{-\mathrm{i}k_1L}.
\end{aligned}$$

The first important implication of these equations is that the exchange of two particles, i.e. scattering, is independent of the position of other particles, for example from the first equation we have $A_{123}/A_{213} = A_{312}/A_{321}$ which indicates that the exchange of $1, 2$ is independent of where 3 is. This is equivalent to factorization of an m–particle scattering matrix into $\binom{m}{2}$ two–particle scatterings in an integrable systems. Using this property it now make sense to only talk about two–particles scattering amplitudes without talking about the order of the rest of the particle. An interesting implication is the existence of a Yang–Baxtor relation between the two–particle scatterings. To see this notice that we can get from A_{123} to A_{321} by the application of each of the following three exchange operators

$$\mathrm{S}_{23}\,\mathrm{S}_{13}\,\mathrm{S}_{12} = \mathrm{S}_{12}\,\mathrm{S}_{13}\,\mathrm{S}_{23}$$

The general form of the scattering matrices depends on the specifics of the system under study. Generally given the Hamiltonian, we have to solve for the following eigenvalue problem

$$\sum_{\{x'\}} c(x'_1, \ldots, x'_m)\langle x_1, \ldots, x_m|\,\mathrm{H}\,|x'_1, \ldots, x'_m\rangle = E\ c(x_1, \ldots, x_m) \tag{2.94}$$

XXZ model

To see this basis in action, lets start with the easy example of ferromagnetic XXZ model with the anisotropy of $\Delta = J_z/J_{\mathrm{XY}}$ and fixing $J_{\mathrm{XY}} = 1$ for convenience,

$$\mathrm{H} = \sum_i^L \Big[\frac{1}{2}\ (\mathrm{S}_i^+\,\mathrm{S}_{i+1}^- + \mathrm{S}_i^-\,\mathrm{S}_{i+1}^+) + \Delta\ \ \mathrm{S}_i^z\,\mathrm{S}_{i+1}^z\Big]$$

The $m = 0$ sector has just one state, which is the ground state for $\Delta > 1$,

$$\mathrm{H}\,\psi_0 = E_0\ \psi_0, \quad \text{where} \quad E_0 = \frac{\Delta}{4}L.$$

For $m = 1$, the spin waves will have a cosine dispersion,

$$\begin{aligned} \mathrm{H}\,\psi_1(k) &= \frac{1}{\sqrt{L}} \sum \mathrm{e}^{-\mathrm{i}kx} \Big(\frac{\Delta}{4}(L-4)|x\rangle + \frac{1}{2}(|x-1\rangle + |x+1\rangle) \Big) \\ &= (E_0 - \Delta + \cos k)\, \psi_1(k). \end{aligned}$$

To solve the eigenvalue problem in the $m = 2$ sector, we start with a generic Ising configuration $|x_1, x_2\rangle$ where $x_1 + 1 \neq x_2$, there are five different way to generate this configuration when we apply the XXZ Hamiltonian, namely $(x_1 - 1, x_2), (x_1, x_2 - 1), (x_1 + 1, x_2), (x_1, x_2 + 1)$ from the XY part and (x_1, x_2) from the Ising part. If we demand the anstaz to be the eigenstate,

$$\begin{aligned} E\ c(x_1, x_2) = \frac{A_{12}}{2} \times \\ \Big((\mathrm{e}^{\mathrm{i}k_1} + \mathrm{e}^{\mathrm{i}k_2} + \mathrm{e}^{-\mathrm{i}k_1} + \mathrm{e}^{-\mathrm{i}k_2} + 2E_0 + 4\Delta)\ \mathrm{e}^{-\mathrm{i}(k_1 x_1 + k_2 x_2)} + \\ (\mathrm{e}^{\mathrm{i}k_2} + \mathrm{e}^{\mathrm{i}k_1} + \mathrm{e}^{-\mathrm{i}k_2} + \mathrm{e}^{-\mathrm{i}k_1} + 2E_0 + 4\Delta)\ S_{12}\ \mathrm{e}^{-\mathrm{i}(k_2 x_1 + k_1 x_2)} \Big) \end{aligned}$$

To make sure the ansatz is an eigenstate we also need to check the specific Ising configuration $|x_1, x_2\rangle$ when x_1 and x_2 are nearest neighbors. In this case two of the above five terms won't contribute and we can solve for the scattering amplitude S_{12}. Defining $q \equiv k_1 - k_2$

$$S_{12} = -\frac{1 - 2\Delta \mathrm{e}^{-\mathrm{i}k_2} + \mathrm{e}^{-\mathrm{i}(k_1 - k_2)}}{1 - 2\Delta \mathrm{e}^{-\mathrm{i}k_1} + \mathrm{e}^{+\mathrm{i}(k_1 - k_2)}} = -\frac{\cos\frac{k}{2} - \Delta \mathrm{e}^{+\mathrm{i}\frac{q}{2}}}{\cos\frac{k}{2} - \Delta \mathrm{e}^{-\mathrm{i}\frac{q}{2}}}$$

so with this scattering amplitude the ansatz is now an eigenstate with the energy spectrum for two spin waves of

$$E = E_0 - 2\Delta + \cos k_1 + \cos k_2 = E_0 - 2(\Delta - \cos\frac{k}{2}\cos\frac{q}{2})$$

The scattering amplitude is just a phase $S_{12} = \mathrm{e}^{\mathrm{i}\phi}$, from the constraint we can solve for the phase

$$\cot\frac{\phi}{2} = \frac{\Delta \sin\frac{q}{2}}{\cos\frac{k}{2} - \Delta\cos\frac{q}{2}}$$

this equation has to be consistently solved for ϕ given different choice of k_1, k_2.

2.7 Quantum Information

The field of quantum information theory revolves around the fundamental properties of quantum state such as quantum entanglement [105]. The entanglement in a quantum state of a quantum system is *the* property of quantum mechanics that makes is fundamentally different than classcial physics. In very loose terms, it describes how much (and in what sense) an operation on a part of a quantum system affect the rest of that system. It is then necessary to define more clearly what we mean by *operation* and *influence* in the previous sentence.

2.7.1 The setup of quantum information theory

The setup of quantum information consists of multiple parties, e.g. Alice(A), Bob(B), Charlie(C), etc., that share a *quantum system*. This means a *natural* tensor product structure is defined on the total Hilbert space of the system, namely $\mathcal{H} = \bigotimes_i \mathcal{H}_i$ where i goes over all parties. The parties are assumed to reside on separate locations in real space which mean each party only has access to their *local* Hilbert space, so they are only allowed to apply local quantum operations and measurements on their local part of system. Furthermore, there exist a classical communication line/channel between the parties such that

they can inform each other of operations they perform and the outcome of their measurements. This motivates the definition of a class of operations on the total Hilbert space of the system known as *local operations and classical communication* or in short LOCC [28].

2.7.2 Bipartite entanglement

Here, the Hilbert space has the tensor product structure of $\mathcal{H} = \mathcal{H}_A \otimes \mathcal{H}_B = \mathbb{C}^a \otimes \mathbb{C}^b$ where the A, B are the labels for the two partitions of the quantum system and with their respective Hilbert space dimensions $a \coloneqq \dim \mathcal{H}_A$ and $b \coloneqq \dim \mathcal{H}_B$.

A *pure state* is described via a vector $\psi \in \mathcal{H}$. A *mixed state* (an statistical ensemble of several pure states) is described through a Hermitian matrix ρ with the properties $\rho \geq 0$ and $\operatorname{Tr} \rho = 1$.

2.7.3 Pure state bipartite entanglement

In this case we have two classes of states: product states and entangled states. We say a pure state $|\psi\rangle \in \mathcal{H}$ is a *product state* iff there exist $|\psi_A\rangle \in \mathcal{H}_A$ and $|\psi_B\rangle \in \mathcal{H}_B$ such that $|\psi\rangle = |\psi_A\rangle \otimes |\psi_B\rangle$. If a state is not a product state, we say it is an *entangled state*. Note that this classification is not particularly useful, because in practice we are not interested in whethere or not a state is engtangled but instead we would like to know how much is the *entanglement content* of a given state. So, we need to quantify the entanglement!

Thm (Schmidt decomposition): For any vector $|\psi\rangle \in \mathcal{H}$ there exist orthonormal sets $\{|\psi_A^i\rangle\} \subset \mathcal{H}_A$ and $\{|\psi_B^i\rangle\} \subset \mathcal{H}_B$ such that

$$|\psi\rangle = \sum_i^{\min(a,b)} \sqrt{\lambda_i}\, |\psi_A^i\rangle \otimes |\psi_B^i\rangle \tag{2.95}$$

here the $\sqrt{\lambda_i}$ are called *Schmidt values*. They are real and non–negative and their square sum up to 1 (normalization). Schmidt decomposition is closely realted to singular value decomposition (SVD), because any vector on a tensor product can be reinterpreted as a linear map $\tilde{\psi}\colon \mathcal{H}_A \to \mathcal{H}_B$.

From the definition it is obvious that a product state has a single nonzero Schmidt value. This suggests that a functional of Schmidt values can be used to quantify bipartite entanglement for pure states.

We can write a pure state as a density matrix $\rho = |\psi\rangle\langle\psi|$, written in terms of the Schmit decomposition and tracing over the B part (partial trace) we find the *reduce* density matrix for subsystem A

$$\rho_A \coloneqq \mathrm{Tr}_B\, \rho = \sum_i \lambda_i\ |\psi_A^i\rangle\langle\psi_A^i| \tag{2.96}$$

We use the entropy of λ_i to quantify entanglement. In paricular, for any density matrix we can define the Tsallis(T), Renyi(R) entropies respeictively as follows

$$S_T^\alpha(\rho) \coloneqq \frac{1}{1-\alpha}(\mathrm{Tr}\,\rho^\alpha - 1) \tag{2.97}$$

$$S_R^\alpha(\rho) \coloneqq \frac{1}{1-\alpha}\log \mathrm{Tr}\,\rho^\alpha \tag{2.98}$$

The Tsallis entropy is also called the *linear* entropy for $\alpha = 2$ and both Renyi and Tsallis entropies at the limit of $\alpha \to 1$ approach the von Neumann entropy

$$S(\rho) \coloneqq \lim_{\alpha\to 1} S_{T,R}^\alpha = -\,\mathrm{Tr}(\rho\log\rho) \tag{2.99}$$

It is customary to use the von Neumann entropy to quantify pure state bipartite entanglement, it is also called the *entanglement entropy*.

An important note here is that the entanglement entropy (as a map from the state space to the real numbers) naturally defines a preorder for the set of states, so every pair of states are comparable and we have a notion of how one state is *better* (say, for quantum information purposes) than an another state. We will see that defining a preorder is not meaningful for mutli–partite entanglement [37].

2.7.4 Mixed state bipartite entanglement

A mixed state is describe by a density matrix, so we need to action of LOCC on a density matrix. We can not describe LOCC mathematically but we can define a new class of operations, separable operations or SEP. We say an operation Λ is SEP if its action on a density matrix is given as follows

$$\sum_k (A_k \otimes B_k)\rho(A_k \otimes B_k)^\dagger \tag{2.100}$$

Chapter 3

Quantum Spin Liquids

The quantum spin liquids are a class of phases of matter that evade conventional (symmetry breaking order) and embody many–body long range entanglement. The entanglement is mainfested throught topological properites, such as non–local excitations, and fractionalization. There are various fantastic reviews on spin-liquids, for a few of them see for example Refs. [9, 152, 117]

3.1 The QSL History

Quantum spin liquids have an intriguing history. They were originally suggested by P. W. Anderson [3, 4] in the context of resonating valence bond (RVB) states. Soon after it was realized that these classes of states carry a massive amount of entanglement.

3.2 Materials and Experimental efforts

A particular class of organic compounds are the κ-(BEDT-TTF)$_2$X with X represents some inorganic anion. The dimer of organic material has strong interaction and could be considered as a single site where the effective Hamiltonian is Hubbard model on square lattice or when the diagonal interaction is strong, anisotropic triangular lattice. A famious example of almost isotropic triangular ($t'/t \approx 1.06$) lattice is the organic compound κ-(BEDT-TTF)$_2$Cu$_2$(CN)$_3$ where despite large Heisenberg coupleing of $J = 250$ K the system does not order down to $T \approx 30$ mK [127]. It is therefore suggested that spin liquid phase is realized in this material. Motrunich using the variational wavefunctions for Heisenberg model augmented by ring exchange has suggested that the projected Fermi–sea spin liquid is a candidate for the ground state of this material close to the metalic phase [101].

3.3 Frustrated systems

A key property of most experimental system that are candidates of harboring QSL ground states, is the existance of a frustrated Hamiltonian. Frustration, in rudimentary terms, is the inability of a system to satify local constraints. In the case of Hamiltonians, frustration is the inability of the Hamiltonian to minimize its energy locally.

It is a common practice to introduce frustration with *classical frustration*, or the geometrical frustration. Imagine a triangle with classical Heisenberg spins (3D arrows of size $|\mathbf{S}|$) on the corner and an Hamiltonian of the form

$$\mathrm{H} = J(\mathbf{S}_1 \cdot \mathbf{S}_2 + \mathbf{S}_2 \cdot \mathbf{S}_3 + \mathbf{S}_1 \cdot \mathbf{S}_3) \tag{3.1}$$

The ferromagnetic case, negative J, the classical solution is all spin aligned (with a remaining global rotatoin redundancy). The This solution minimizes every single term in the Hamiltonian and consequently minimizes the whole Hamiltonian as a whole.

The antiferromagnetic or the frustrated case is more interesting. Every single term requires the spins to be opposite direction to each other, but that is obviously impossible to satisfy for all three bonds. Let us reformulate the Hamiltonian (up to const), it can be written as H $\propto (\mathbf{S}_1 + \mathbf{S}_2 + \mathbf{S}_3)^2$ which means the classical ground state is where the sum of all three spin vectors has the lowest magnitude, that is $\mathbf{S}_1 + \mathbf{S}_2 + \mathbf{S}_3 = 0$ this is simply satisfied if the three vectors form a 120° angle with each others (or equivalently, reside on the sides of an equilateral triangle). Defining local unit vector $\hat{n}_i$ where $\hat{n}_i \cdot \hat{n}_j = -\frac{1}{2}$ for $i \neq j$ the classical anti–ferromagnetic ground state is

$$|\Psi_0\rangle_{\text{classical}} = \bigotimes_i \left|\mathbf{S}_i \cdot \hat{n}_i = |\mathbf{S}|\right\rangle \tag{3.2}$$

with an energy of $\varepsilon_{\text{bond}} = -\frac{|\mathbf{S}|^2}{2} J$ per bond.

Let us consider the kagome lattice for spin–1/2. The ground state for just a single bond of two spins is simply the singlet state

$$= \frac{1}{\sqrt{2}}\Big(|\uparrow\downarrow\rangle - |\downarrow\uparrow\rangle\Big) \tag{3.3}$$

where the singlet is depicted as a thick line with an arrow representing the direction of the minus sign (we drop the minus sign when it doesn't matter). The singlet has a $\varepsilon_{\text{bond}} = -\frac{3J}{4}$ energy per bond. As for a trianglet a single singlet bond is the lowest possible energy. So, if possible, a singlet bond for all triangles of the kagome lattice could be the ground state. However a simple counting shows that this is not possible. If we show the the number of

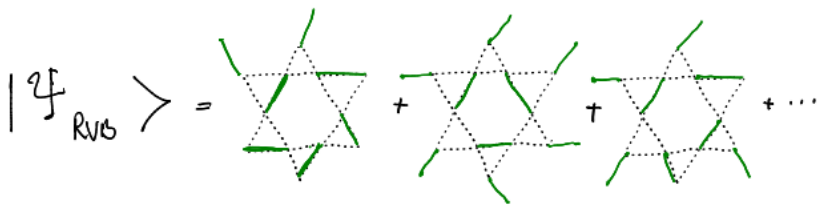

Figure 3.1: Schematic of the resonating valence bond state

site by N, then the number of singlet is $N_s = N/2$. In the kagome lattice each site has four bonds (shared with other sites), so we have two bonds per site $N_b = 2N$ and there are three triangles per bond $N_b = 3N_t$ therefore we see that

$$N_s = \frac{1}{2}N = \frac{1}{4}N_b = \frac{3}{4}N_t \tag{3.4}$$

Therefore a complete dimer covering leaves a quarter of the trinagles unsatisfied. Since the expectation value of the Heisenberg bond term for all non-singlet terms in a dimer covering is zero, the total dimer covering energy is $\varepsilon_{\text{site}} = -\frac{3}{8}J$ compared to the classical energy of $\varepsilon_{\text{site}} = -\frac{1}{4}J$. Therefore the dimer covering has a better energy, however note that none of them are even a ground state. The dimer covering is still not a very entangled state, because as a many–body state it is basically a product state of singlet, if we show a paif of sites (i, j) as a dimer in the set of all dimers D for a specific covering

$$|\Psi_D\rangle = \bigotimes_{(i,j)\in D} |\bullet\!\!-\!\!\bullet\rangle_{i,j} \tag{3.5}$$

It was Paul Anderson who came up with the idea of superposition of all dimer coverings as a potential state[3, 4], the so–called RVB states.

3.4 Exactly solvable QSLs

3.4.1 the toric code model

A famous example of a non–frustrated commuting quantum spin liquid is the Alexei Kitaev original suggestion of the toric code as an error–correcting quantum code for the purpose of fault–tolerant quantum computation [75, 46]. However, the physics of emergent fractionalized excitations were studied even before that [113]. Here we briefly introduce the model as an example of an exactly solvable quantum spin liquid. The system is made of spin–1/2 site residing on the *edges* of a square lattice. The Hamiltonian reads

$$H = -J_e \sum_v A_v - J_m \sum_p B_p \tag{3.6}$$

where A_v is the star or vertex term defined for every four spin around a vertex of the lattice and B_p is the plaquette term define for every four spin in each plaquette of the square lattice.

$$A_v = \prod_{i \in v} \sigma_i^x, \tag{3.7}$$

$$B_p = \prod_{i \in p} \sigma_i^z. \tag{3.8}$$

Since all vertex and plaquette terms share and even number of sites, they manifestly commute with each other and hence the theory is exactly solvable.

3.4.2 The Kitaev's honeycomb model

We define the model on a lattice that is a three-colorable (Tait colorable) trivalent [1] graph, i.e. where every vertex has degree three, we label every color edge as either Z-link,

[1] also called cubic, note that not every cubic lattice is three-colorable

X-link, or Y-link and define the follwoing Hamiltonian

$$H = -J_x \sum_{X\text{-link}} \sigma_i^x \sigma_j^x - J_y \sum_{Y\text{-link}} \sigma_i^y \sigma_j^y - J_z \sum_{Z\text{-link}} \sigma_i^z \sigma_j^z \tag{3.9}$$

where σs are the usual Pauli operators, $\sigma_i \sigma_j = 2\mathrm{i}\epsilon^{ijk}\sigma_k$.

The above Hamiltonian is a sum of bi-spin terms $K_{ij}^{\alpha} \equiv \sigma_i^{\alpha}\sigma_j^{\alpha}$. While the K^{α} terms are not themselves constants of motions (because links that share a site do not commute), it is clear that the product of these operators on any loop commutes with any of these terms. That is for a loop $\mathcal{L}$ of size N going throught sites $1, 2, \ldots, N$ we have

$$[W_{\mathcal{L}}, K_{ij}^{\alpha}] = 0, \qquad W_{\mathcal{L}} \equiv K_{12}^{\alpha} K_{23}^{\beta} \cdots K_{(N-1)N}^{\gamma} \tag{3.10}$$

therefore, there is a constant of motion $W_{\mathcal{L}}$ associated with any loop $\mathcal{L}$ in the graph, because they commute with each other and the Hamiltonian.

Brief introduction to Majoranas

Attempts at solving the above Hamiltonian mostly depend on the fermionization of the spins. More precisly to write the spin in terms of Majoranas. We therefore spend some time introducing the Majoranas and then talk abour the Majorana represenation of spins.

For any fermion we can write it in terms of its real and imaginary part. The two resulting real fermions are known as Majoranas. So we define

$$a_i = \frac{1}{2}(\eta_i + \mathrm{i}\zeta_i), \qquad a_i^{\dagger} = \frac{1}{2}(\eta_i - \mathrm{i}\zeta_i) \tag{3.11}$$

We can also write the Majoranas in terms of fermions as follows

$$\eta = a^{\dagger} + a, \qquad \zeta = \mathrm{i}(a^{\dagger} - a) \tag{3.12}$$

it is then straightforward to check that the Majoranas are self-adjont $\eta^\dagger = \eta$ and $\zeta^\dagger = \zeta$ and they satisfy the fermionic anticommutation relations as follows

$$\{\eta_i, \zeta_j\} = 0, \qquad \{\eta_i, \eta_j\} = \{\zeta_i, \zeta_j\} = 2\delta_{ij} \tag{3.13}$$

defining a new fermion by $b^\dagger \equiv -\mathrm{i}a$ and $b \equiv \mathrm{i}a^\dagger$ we see that η, ζ are switched in the new fermion and $b^\dagger b = -a^\dagger a$. So for any pair of Majoranas we should pick which one is the real part and which imaginary to define the fermion. The fermionic sign operator can be written in terms of Majoranas

$$\mathrm{e}^{\mathrm{i}\pi a^\dagger a} = 1 - 2a^\dagger a = -\mathrm{i}\eta\zeta \tag{3.14}$$

Original Kitaev solution and extensions

Originally Kitaev has chosen four majornas per site (effectively doubling the Hilbert space) to solve the problem on the Honeycomb lattice [74]. The idea that the σ_z operator can be writen in terms of $-i\eta\zeta$ suggests the definition of four Majorana operators per spin $\eta^x, \eta^y, \eta^z, \zeta$ such that each spin operator can be written as

$$\sigma_i^\alpha = -\mathrm{i}\eta^\alpha\zeta \tag{3.15}$$

This definition automatically satisfies the anti-commutation relations between spin operators. However to satisfy also the commuitation relation we would need

$$[\sigma^\alpha, \sigma^\beta] = -2\eta^\alpha\eta^\beta = 2\mathrm{i}\epsilon^{\alpha\beta\gamma}\sigma^\gamma = -2\mathrm{i}\epsilon^{\alpha\beta\gamma}\eta^\gamma\zeta \tag{3.16}$$

Therefore we would need the operators $D_i = -\mathrm{i}\eta_i^\alpha\eta_i^\beta\eta_i^\gamma\zeta_i$ to be $+1$ in order to satisfy the commutation relations. We would therefore call $D_i = +1$ the physical space and $D_i = -1$

the unphysical part of the doubled Hilbert space. The projection operator to the physical space is then

$$\mathcal{P} = \prod_i \frac{1 + D_i}{2} \tag{3.17}$$

Let note that the eq. (3.16) hints that when we restrict to the physical subspace the spin operators can also be written as

$$\sigma_i^\alpha = -\mathrm{i}\eta^\beta \eta^\gamma \tag{3.18}$$

which automatically satisfies the commutation and anticommutation relations. This indeed suggests that we did not need to define the extra *zeta* operator at all. This approach of using $SO(3)$ representation of spin is actually much older than the 4 Majorana representation. In this representation the previous physical indicator operator turns into $\tau_i = -\mathrm{i}\eta_i^\alpha \eta_i^\beta \eta_i^\gamma$ is no longer a two dimensional operator but a Majorana constant at each site that commutes with spins

$$[\tau_i, \sigma_i^\alpha] = 0 \tag{3.19}$$

since only two Majoranas where required to make a two-dimensional space for the spin, the τ Majorana can be thought of as the remaining extra Majorana degree of freedom. The strategy then is to pick any pair of spins in the system (at will) and use the pairs of τ Majorana of them to build a two dimensional space and set it to ± 1 at will to get back the physical Hilbert space. In this approach no projection to physical subspace is required as opposed to the Kitaev four Majorana represenation.

We can use the Kitaev four Majorana representation to rewrite the Hamiltonian of eq. (3.9)

$$H = -J_x \sum_{X\text{-link}} (-\mathrm{i}\eta_i^x \eta_j^x)\ \mathrm{i}\zeta_i\zeta_j - J_y \sum_{Y\text{-link}} (-\mathrm{i}\eta_i^y \eta_j^y)\ \mathrm{i}\zeta_i\zeta_j - J_z \sum_{Z\text{-link}} (-\mathrm{i}\eta_i^z \eta_j^z)\ \mathrm{i}\zeta_i\zeta_j \tag{3.20}$$

The remarkable property of using the kitaev four Majorana representation for lattice like this is that the link operators $u_{ij} = -\mathrm{i}\eta_i^\alpha \eta_j^\alpha$ all commute with each other and the Hamiltonian, so are all constants of motion. The only complication remained in the problem is that the u_{ij} operators are not physical (they don't commute with the gauge operator). Regardless of the difficulty remained in the problem (as far as the actual state is concerned), the energy spectrum can be deduced by diagonalizing the Hamiltonian for each sector of $u_{ij} = \pm 1$ since the remaining Hamiltonian will simply turn into a mojarana free Hamiltonian of type

$$H = \sum_{\langle i,j\rangle} \mathrm{i}\frac{A_{ij}}{4}\ \zeta_i\zeta_j \tag{3.21}$$

Where A is a real anti–symmetric matrix which gives a positive and negative version of Hermtian complex fermionic spectrum effectively. The factor of 4 is simply introduced for simplicity.

The states, however, are not just the free Majoranas. Since the u_{ij} operators don't commute with Ds, therefore one has to project into the physical subspace. As usual, this is the step that generates spin–liquid entanglement. The u_{ij} are not relevant themselves, but the equivalnece classes of them that leave the product of u_{ij}s over loops constant.

For the case of the original Kitaev model, the honeycomb lattice, it turns out that happens in the sector with no flux meaning that the product of all u_{ij} operators around any loop (plaquette) is $+1$. One can therefore choose a positive u_{ij} and solve for the translationally invariant free Majorana theory.

Jordan–Wigner transformation of Kitaev model

If we now pick an ordering for the vertices, starting from the beggining of an X-link and follow until the loops closes. It is possible to have open boundary or inifintly large system as well. For the open boundary conition we loosen the requirement of degree of three for vertices on the boundary. Based on this ordering we now define a Jordan-Wigner transformation from spins to fermions following the usual anti–commutation relation, $\{a_i^\dagger, a_j\} = \delta_{ij}$, as follows

$$\sigma_i^z = 1 - 2a_i^\dagger a_i = \mathrm{e}^{\mathrm{i}\pi a_i^\dagger a_i}, \qquad \sigma^\pm = \frac{1}{2}(\sigma^x \pm \mathrm{i}\sigma^y) = a_i^\pm \prod_{j<i} \mathrm{e}^{\mathrm{i}\pi a_j^\dagger a_j} \tag{3.22}$$

Note that in order to combine two equations into one we have used the convention $a^+ \equiv a^\dagger$ and $a^- \equiv a$. Using this transformation for any loop of alternating X-links and Y-links the X-link terms in the Hamiltonian simplify to

$$\sigma_i^x \sigma_{i+1}^x = (\sigma_i^+ + \sigma_i^-)\ (\sigma_{i+1}^+ + \sigma_{i+1}^-) \tag{3.23}$$

$$= (a_i^\dagger + a_i)\ \mathrm{e}^{\mathrm{i}\pi a_i^\dagger a_i}\ (a_{i+1}^\dagger + a_{i+1}) \tag{3.24}$$

$$= (a_i^\dagger - a_i)\ (a_{i+1}^\dagger + a_{i+1}) \tag{3.25}$$

the same is true for the Y-link terms (execpt for the last term of the loop). They simplify to

$$\sigma_i^y \sigma_{i+1}^y = -(\sigma_i^+ - \sigma_i^-)\ (\sigma_{i+1}^+ - \sigma_{i+1}^-) \tag{3.26}$$

$$= -(a_i^\dagger - a_i)\ \mathrm{e}^{\mathrm{i}\pi a_i^\dagger a_i}\ (a_{i+1}^\dagger - a_{i+1}) \tag{3.27}$$

$$= -(a_i^\dagger + a_i)\ (a_{i+1}^\dagger - a_{i+1}) \tag{3.28}$$

for the final Y-link of the loop of size $2m$ (for simplicity here starting at index 1) we have

$$\sigma^y_{2m}\sigma^y_1 = -(\sigma^+_{2m} - \sigma^-_{2m})\ (\sigma^+_1 - \sigma^-_1) \tag{3.29}$$

$$= -(a^\dagger_{2m} - a_{2m})\ \prod_{j=1}^{2m-1} \mathrm{e}^{\mathrm{i}\pi a^\dagger_j a_j}\ (a^\dagger_1 - a_1) \tag{3.30}$$

$$= \prod_{j=1}^{2m} \mathrm{e}^{\mathrm{i}\pi a^\dagger_j a_j}\ (a^\dagger_{2m} + a_{2m})\ (a^\dagger_1 - a_1) \tag{3.31}$$

So the final Y-link also carries the information about the total number of fermions in the loops. Note that this problem doesn't exist in the infinite or open boundary condition.

Kitaev model in terms of Jordan–Wigner Majoranas

Since every alternating loops (or chain) of X and Y links has even number of sites and we have chosen to start X-links on odd numbers and Y-links on even numbers. The equations (3.23) and (3.26) suggest to define opposite labeled Majoranas for even and odd sites. Therefore for the odd sites

$$\begin{cases} a_i = \frac{1}{2}(\eta_i + \mathrm{i}\zeta_i), \qquad a^\dagger_i = \frac{1}{2}(\eta_i - \mathrm{i}\zeta_i) \qquad (i \text{ odd}) \\ a_i = \frac{1}{2}(\zeta_i + \mathrm{i}\eta_i), \qquad a^\dagger_i = \frac{1}{2}(\zeta_i - \mathrm{i}\eta_i) \qquad (i \text{ even}) \end{cases} \tag{3.32}$$

with this definitions the different part of Hamiltonian can be written as

$$\sigma^x_i\sigma^x_{i+1} = -\mathrm{i}\zeta_i\zeta_{i+1}, \qquad (X\text{-links}) \tag{3.33}$$

$$\sigma^y_i\sigma^y_{i+1} = +\mathrm{i}\zeta_i\zeta_{i+1}, \qquad (Y\text{-links}) \tag{3.34}$$

$$\sigma^y_{2m}\sigma^y_1 = \left(\prod_{i=1}^{m}(-\mathrm{i}\eta_{2i-1}\zeta_{2i-1})(\mathrm{i}\eta_{2i}\zeta_{2i})\right)\ (-\mathrm{i}\zeta_{2m}\zeta_1) \tag{3.35}$$

$$\sigma^z_i\sigma^z_j = (-1)^{i+j-1}(-\mathrm{i}\eta_i\eta_j)(-\mathrm{i}\zeta_i\zeta_j) \qquad (Z\text{-links}) \tag{3.36}$$

If we now assume we have a lattice with open boundary conitions and no $X-Y$ loops, then the closing Y-link never shows up and the theory becomes a free theory of ζ_i Majoranas with $-\mathrm{i}\eta_i\eta_j$ operators at every Z-link as constants of motion.

In the presence of $X-Y$ loops product of $-\mathrm{i}\eta_i\eta_j$ operators of Z-links that touches every envolved loops an even number of times are constants of motion. That means any path or plaquette that start from a Z-link and ends at the same Z-link gives a constanct of motions multiplying the $-\mathrm{i}\eta_i\eta_j$ operators at all the visited Z-links. This includes zeros paths, Z-links that don't start and end on any loops and also one Z-link paths for Z-links that start and end on the same loop.

This now suggest to rewrite the theory in terms new fermions living on Z-links. We define two fermions at each Z-link. The $f^\dagger, f$ fermion which is made by η_i, η_j Majoranas

$$f_\alpha = \frac{1}{2}(\eta_{\alpha,1} + \mathrm{i}\eta_{\alpha,2}), \qquad f_\alpha^\dagger = \frac{1}{2}(\eta_{\alpha,1} - \mathrm{i}\eta_{\alpha,2}) \tag{3.37}$$

and $c^\dagger, c$ fermions which are made by ζ_i, ζ_j as follows

$$c_\alpha = \frac{1}{2}(\zeta_{\alpha,1} + \mathrm{i}\zeta_{\alpha,2}), \qquad c_\alpha^\dagger = \frac{1}{2}(\zeta_{\alpha,1} - \mathrm{i}\zeta_{\alpha,2}) \tag{3.38}$$

3.5 Parton construction of QSLs

3.5.1 The spinon

A common method to construct QSLs is to assign a separate identity to each of the Abrikosov fermions—spinons or more generally *partons*. The spin–1/2 operator in terms of spinons is given by

$$\mathbf{S}_i = \frac{1}{2}\sum_{\alpha,\beta=\uparrow,\downarrow} f_{i,\alpha}^\dagger \boldsymbol{\sigma}_{\alpha,\beta} f_{i,\beta}. \tag{3.39}$$

Where the fermions obey the usual fermionic anti–commutation relations

$$\{f_{i\alpha}, f^{\dagger}_{j\beta}\} = \delta_{ij}\delta_{\alpha\beta}, \quad \{f_{i\alpha}, f_{j\beta}\} = 0. \tag{3.40}$$

Assigning a separate identity for each flavor of fermion effectively doubles the dimension of the local Hilbert space. This issue can be remedied by the introduction of a local constraints at every site. That is to require *one and only one* fermion per site, i.e. $n_i \equiv \sum_\alpha f^{\dagger}_{i,\alpha} f_{i,\alpha} = 1$, and identifying $|n_\uparrow = 1\rangle \leftarrow |\uparrow\rangle$ and $|n_\downarrow = 1\rangle \leftarrow |\downarrow\rangle$.

If one considers the state as the low energy description of a fermionic theory, the above argument translates to the introduction of local constants of motion, or gauge symmetries, into the free theory. Therefore, the Gaussian fermionic theories are coupled to a gauge theory and strongly interact through that. Since the free fermion hopping theories respect the U(1) symmetry, the fermionic theory is coupled to a U(1) gauge field. An important question is whether or not this fermionic theory coupled to gauge field is the correct effective theory for the spins. This questions ultimately translates to the confinement/deconfinement problem of the gauge theory. For a thorough discussion see ref. [143].

The classical simulation of the gauge theories is still in its early stages [cite] and a faithful numerical understanding remains out of reach. Instead, it is common to start with ground states of fermionic theories, that live in corresponding Hilbert spaces $\mathcal{H}_\uparrow$, $\mathcal{H}_\downarrow$, and then *project* them down into the spin theory $\mathcal{H}_{1/2}$. This procedure is known as the *Gutzwiller projection.*

3.5.2 The Gutzwiller projection

Let us assume the fermionic states are ground states of Gaussian Hamiltonians $H_\uparrow$ and $H_\downarrow$ where each of them can be represented as Slater determinant states of the form

$$|\psi_\uparrow\rangle = \prod_k c^\dagger_{k,\uparrow}|0_\uparrow\rangle \tag{3.41}$$

$$|\psi_\uparrow\rangle = \prod_k c^\dagger_{k,\downarrow}|0_\downarrow\rangle \tag{3.42}$$

where k labels the filled orbitals of the free fermion theories. The spin theory state is know constructed by projecting down the tensor product state

$$|\psi_s\rangle = \mathcal{P}_G \left(\prod_{k,k'} c^\dagger_{k,\uparrow} c^\dagger_{k',\downarrow} |0_{\uparrow\downarrow}\rangle \right) \tag{3.43}$$

where $\mathcal{P}_G$ denotes the Gutzwiller projection operator

$$\mathcal{P}_G = \prod_i n_i(2-n_i), \qquad n_i = n_{i\uparrow} + n_{i\downarrow}. \tag{3.44}$$

3.5.3 Mean–field treatment of Heisenberg spin–1/2

For a lattice with spin-1/2 residing on every site and the an exchange interaction on every edge

$$H = \sum_{(i,j)\in \text{edges}} J_{ij}\ \mathbf{S}_i \cdot \mathbf{S}_j$$

While the size of the Hilbert space at each site is only two, this is not a fermionic model because the spins at different sites commute with each other. However, we can use the parton/spinon construction as before and rewrite the Hamiltonian in terms of the spinons as

$$H = \sum_{(i,j)\in \text{edges}} -\frac{1}{2} J_{ij}\ f^\dagger_{i\alpha} f_{j\alpha} f^\dagger_{j\beta} f_{i\beta} + \sum_{i,j\in \text{edges}} J_{ij}(\frac{1}{2} n_i - \frac{1}{4} n_i n_j) \tag{3.45}$$

This new Hamiltonian has two ($\uparrow$ and $\downarrow$) fermion species per site. As a result the size of the Hilbert space at each site is now four instead of the original two. To retain the original Hilbert space we can enforce one and only one fermion(spinon) on every site as a constraint, $n_i = f^\dagger_{i\alpha} f_{i\alpha} = 1$, by introducing Lagrange multipliers μ_i which can be thought of as on site chemical potential. The second term in the Hamiltonian is also no longer relevant as it reduces to just a constant.

At the mean–field level we can replace the hopping operator by its average $\langle f^\dagger_{i\alpha} f_{j\alpha} \rangle = t_{ij}$ and add the fluctuations later. So we can try to solve the simple spinon hopping model

$$H = \sum_{(i,j)\in \text{edges}} -\frac{1}{2} J_{ij}\ t_{ji} f^\dagger_{i\alpha} f_{j\alpha} + \sum_{i \in \text{sites}} \mu_i (f^\dagger_{i\alpha} f_{i\alpha} - 1) \tag{3.46}$$

The above mean–field consideration justifies the spinon construction and Gutzwiller projection procedure at least when Heisenberg–like Hamiltonians are involved. It is however an important questions, whether or not the mean–field physics survives the constraint. We can continue this treatment as a field theoretical approach and go beyond mean–field, for further details and a thorough treatment of the theory consult Ref. [143].

3.6 The spin–Bose metal

3.6.1 Single band spinful theory, the Bethe chain

The single band bosonization is described in section 2.3. If we now consider spin, the free theory is simply two separate theories for each species of fermions denoted by the spin label $\alpha = \uparrow, \downarrow$. The bosonization procedure is the same for each species, except the introduction of the Klein factors $\{\eta_\alpha, \eta_\beta\} = 2\delta_{\alpha\beta}$ in order to impose the fermionic

anticommutation relations between different species. We may express the fermions in terms of boson field as

$$\psi_{P\alpha} = \eta_\alpha \, \mathrm{e}^{\mathrm{i}(\varphi_\alpha + P\theta_\alpha)} \tag{3.47}$$

which leads to a free imaginary time Lagrangian that reads

$$\mathcal{L}_0 = \sum_{a\alpha} \frac{1}{2\pi} \left[\frac{1}{v_F} (\partial_\tau \theta)^2 + v_F (\partial_x \theta)^2 \right].$$

Here we are ultimately interested to study the spin model. Following the spinon approach, the corresponding constraint on the number of fermions per site enters the boson theory in the form of a compact $U(1)$ gauge field which couples to the density operator of all species. So it makes sense to define the *charge* and *spin* fields by

$$\theta_{\rho/\sigma} \equiv \frac{1}{\sqrt{2}} (\theta_\uparrow \pm \theta_\downarrow)$$

Now because of $\sum_\alpha \theta_\alpha^2 = \theta_\rho^2 + \theta_\sigma^2$ we can express the same free theory for the newly defined charge and spin fields. In this language the gauge field couples to θ_ρ. Here, the trick is to introduce the kinetic term with a $1/m$ coupling constant, to control the fluctuations of the gauge field. The original theory can be recovered as $m \to \infty$. The gauge field Lagrangian takes the form

$$\mathcal{L}_A = \frac{1}{m} (\partial_x A/\pi)^2 + \mathrm{i} A \rho, \quad \rho = \sqrt{2} \partial_x \theta_\rho / \pi$$

The gauge field can now be integrated out and eliminated from the Lagrangian leaving behind a mass term for field related to total density $m(\theta_\rho - \theta_\rho^0)^2$.

The low–energy physics can be achieved by integrating out the pinned charge (θ_ρ) sector. The remaining theory is a free theory of fermions in the spin sector that can

be identified with the fermions derived from the spin theory by means of Jordan–Wigner transformation. This theory of gapless excitations in the spin sector corresponds to the low energy theory of the Heisenberg AF chain which is in the Bethe–chain phase.

3.6.2 Two–Band Spinful Theory

We now introduce the two–band spinful model, where there exist two Fermi seas labeled by a with their corresponding Fermi momentum k_{Fa}. Examples are the two–leg triangular ladder discussed in Ref. [125] and chapter. 5 as well as the kagome strip model we introduce in chapter. 4. There are two possibilities for the half–filling constraint

$$k_{F_1} + k_{F_2} = \pi/2 \qquad \text{or} \qquad k_{F_1} + k_{F_2} = 3\pi/2.$$

Same as before, we linearize at the Fermi surface (point) which gives a Dirac theory for each species of fermions determined by the band label $a = 1, 2$, and the spin label $\alpha =\uparrow, \downarrow$. Introducing $\{\eta_{a\alpha}, \eta_{b\beta}\} = 2\delta_{ab}\delta_{\alpha\beta}$, we may express fermion operators in terms of boson fields as

$$\psi_{Pa\alpha} = \eta_{a\alpha}\ \mathrm{e}^{\mathrm{i}(\varphi_{a\alpha} + P\theta_{a\alpha})} \tag{3.48}$$

At this point for each species of fermions we have a free boson field. The Fermi velocities are in general different for each band with the exception of two equally filled bands. So, the free imaginary time Lagrangian density in terms of θ fields reads

$$\mathcal{L}_0 = \sum_{a\alpha} \frac{1}{2\pi} \left[\frac{1}{v_a} (\partial_\tau \theta_{a\alpha})^2 + v_a (\partial_x \theta_{a\alpha})^2 \right]$$

Again to study the spin model, in the spinon approach, the compact $U(1)$ gauge field couples to the density operator of all species. Here other the previous charge/spin

sectors it is convenient to also define even/odd combinations of bands for each sector as follows

$$\theta_{\rho(\sigma)\pm} \equiv \frac{1}{\sqrt{2}}(\theta_{1\rho(\sigma)} \pm \theta_{2\rho(\sigma)}),$$

In this language the gauge field couples to the $\theta_{\rho+}$ field. Adding the kinetic term to suppress the gauge fluctuation, the gauge field Lagrangian takes the form

$$\mathcal{L}_A = \frac{1}{m}(\partial_x A/\pi)^2 + \mathrm{i}A(\rho), \quad \rho = 2\partial_x \theta_{\rho+}/\pi$$

Integrating the gauge adds a mass term, $m(\theta_{\rho+} - \theta^0_{\rho+})^2$, and integrating the now massive $\theta_{\rho+}$ results to the following low energy theory known as the Spin–Bose Metal (SBM) theory

$$\mathcal{L}_0 = \frac{1}{2\pi g}\left[\frac{1}{v}(\partial_\tau \theta_{\rho-})^2 + v(\partial_x \theta_{\rho-})^2\right] + \mathcal{L}_0^\sigma$$

The $\mathcal{L}_0^\sigma$ is the original free theory for the spin sector, the new Fermi velocity for the odd charge sector is $v \equiv \sqrt{v_1 v_2}$, and the coupling constant is $g \equiv 2v/(v_1 + v_2)$.

We refer to this theories as CαSβ denotes a state with α (β) gapless charge (spin) modes [10, 89].

Chapter 4

The Heisenberg antiferromagnet on a strip of kagome

4.1 Introduction

Beginning with Anderson's seminal proposal of the resonating valence bond state [3, 4], physicists have been actively searching for exotic ground states of spin-1/2 quantum antiferromagnets for more than four decades [9, 117, 152]. While there have been numerous theoretical and numerical sightings of such quantum spin liquid states over the years, the most convincing demonstrations have typically required going beyond the simplest SU(2)–invariant nearest–neighbor Heisenberg model—examples of success include quantum dimer models [114, 100] or spin models with some combination of, for example, extended two-spin interactions, spin-exchange anisotropy, special conservation laws, and/or multi-site ring-exchange interactions [8, 131, 132, 74, 150, 66, 12, 45, 101, 17].

The single unique example of a simplest possible nearest neighbor SU(2)–invariant Heisenberg model that can possibly host spin liquid physics has always been suspected to be the kagome. For the infamous two-dimensional (2D) kagome Heisenberg antiferromagnet, spin liquid physics was theoretically predicted in the early 1990s [115] with unconfined excitations as, spin–1/2 bosonic, spinons. Recent numerical calculations [149, 35] indicate that even the simplest model with SU(2)–invariant nearest-neighbor two-spin interactions exhibits spin liquid behavior. Consequently most recent studies on kagome systems has been focused on approaching the 2D limit [149, 35, 67, 69, 56, 77, 44, 55, 70, 87, 64, 63, 62, 61, 65, 27].

In this chapter, we address a particular quasi-one-dimensional (quasi-1D) version of kagome lattice that has remarkably evaded both complete numerical characterization and theoretical understanding. An interesting approach is to think of the narrowest wrapping of the kagome lattice on a cylinder that consists purely of corner-sharing triangles (see Fig. 4.2), i.e., the *kagome strip*. It is important to point out that the term *kagome strip* has been used for a different lattice in the past [6, 140]. This lattice has also been called the *three-spin ladder* [140] or the *bow-tie ladder* [93]. The bulk of this chapter has been published in Physical Reviews B [91].

The main purpose of this chapter is to argue that that for $0.8 \lesssim J \lesssim 1.3$ this model harbors an exotic phase with $c = 2$ gapless modes and power-law spin correlations and bond-energy textures which oscillate at incommensurate wave vectors tunable by J. We will argue that this phase—which respects all symmetries, including lattice translations and time reversal—can be understood as a marginal instability of a two-band U(1)

spinon Fermi surface state, i.e., "spin Bose metal" (SBM) [125], on this kagome strip. (Unlike in the U(1) Dirac spin liquid —which has been studied intensely in the context of kagome antiferromagnets for many years [53, 58, 112, 57, 64, 63, 62, 61, 65, 55], the spinons in our state see zero flux.) The physics of spinon Fermi surface state has been considered before [112, 92] in the context of the 2D kagome antiferromagnet and its associated prototypical experimental realization herbertsmithite (see Ref. [106] for a review); however, it is most famous as a proposed theory for several triangular-lattice spin-liquid materials [101, 85, 122, 99]—and more recently for the spin–orbit coupled triangular-lattice spin–liquid candidate $YbMgGaO_4$ [124].

It is quite remarkable that a simple model such as this quasi–1D descendant of the nearest-neighbor kagome antiferromagnet gives rise to the exotic physics of multiple bands of fermionic spinons. While it is well–known that one such band can faithfully describe the Bethe chain phase of the 1D Heisenberg model [51, 123], other numerically well-established realizations of emergent gapless fermionic slave particles beyond strictly 1D have typically required complicated interactions in the Hamiltonian [126, 125, 18, 17, 98, 68].

4.2 The Hamiltonian

We start by describing the Hamiltonian for kagome strip model. The kagome strip lattice is seen in 4.2. As advertised, for the Hamiltonian, let us pick the simplest SU(2)–invariant nearest-neighbor spin-1/2 Heisenberg antiferromagnet,

$$\mathrm{H} = \sum_{\langle i,j \rangle} J_{ij}\, \mathbf{S}_i \cdot \mathbf{S}_j, \tag{4.1}$$

on this lattice with antiferromagetic leg and cross couplings (the leg–cross model) $J_\ell = 1$ exchange for bonds on the top and bottom legs, and $J_c \equiv J \geq 0$ for bonds between middle spins and the ones on the two legs of the ladder. The respected exchange interactions are also depicted in Fig. 4.2. The Hamiltonian, can therefore be written as

$$H = \sum_{\substack{i\in\{2\} \\ j\in\{1,3\}}} J_c \, \mathbf{S}_i \cdot \mathbf{S}_j + \sum_{\substack{i,j\in\{1\} \\ i,j\in\{3\}}} J_\ell \, \mathbf{S}_i \cdot \mathbf{S}_j$$

For $J = 0$, the model consists of two decoupled Bethe chains (with free spins in the middle chain), while for $J \to \infty$ the model is bipartite and exhibits a conventional ferrimagnetic phase [88, 140]. Our main interest is the region $0.8 \lesssim J \lesssim 2.0$, where in an early study Waldtmann et al. [140] provided numerical evidence for a gapless ground state but were unable to fully clarify its nature (Similar conclusions were also reached more recently by Lüscher, McCulloch, and Läuchli, which served as one of the motivations in pursuing this path more rigorously.

4.2.1 The mean–field treatment

For a basic understanding of the possible spinon physics on kagome strip, we follow the procedure described in section 3.5, introducing two fermions per site. The kagome strip unit cell contains three sites. So we need three species of spinful fermions which we define according to the labeling of top, bottom, and middle in 4.2. The most general hopping

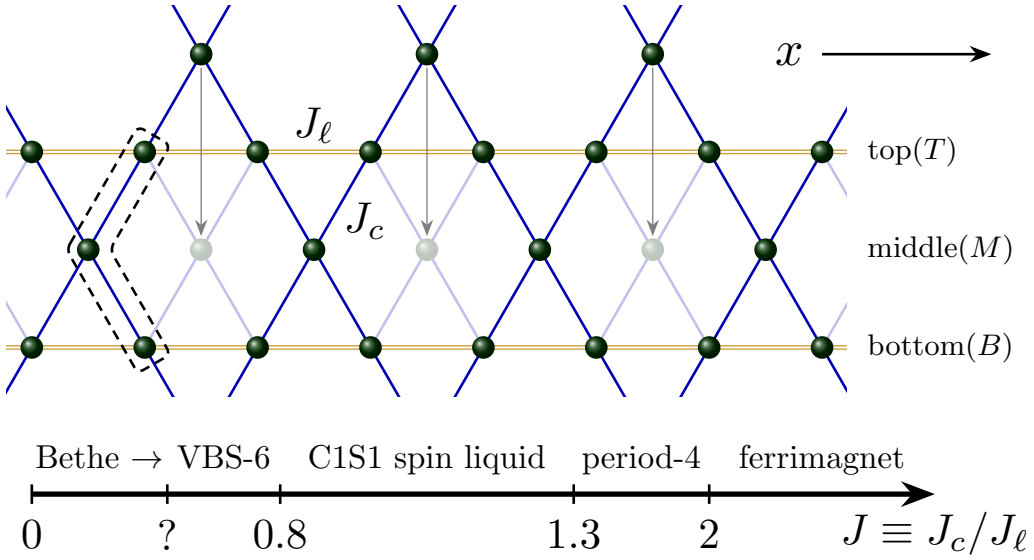

Figure 4.1: The kagome strip ladder. The numerically obtained phase diagram is also shown on the bottom. It has three–site unit cell that is boxed by a dashed line. We identify a phase with two 1D gapless modes resulting from gapless bands of fermionic spinons in the regime $0.8 \lesssim J \lesssim 1.3$.

Hamiltonian on kagome strip is

$$H = -\sum_x \quad \Big(t_2\ f_3^\dagger(x) f_3(x+1) + \text{h.c.}\Big) \tag{4.2}$$

$$+ \Big(t_1\ f_1^\dagger(x) f_1(x+1) + \text{h.c.}\Big) \tag{4.3}$$

$$+ \Big(t_5\ f_1^\dagger(x) f_2(x+1) + \text{h.c.}\Big) \tag{4.4}$$

$$+ \Big(t_6\ f_3^\dagger(x) f_2(x+1) + \text{h.c.}\Big) \tag{4.5}$$

$$+ \Big(t_3\ f_1^\dagger(x) f_2(x) + \text{h.c.}\Big) \tag{4.6}$$

$$+ \Big(t_4\ f_3^\dagger(x) f_2(x) + \text{h.c.}\Big) \tag{4.7}$$

$$+\mu_1\ f_1^\dagger(x) f_1(x) + \mu_2\ f_2^\dagger(x) f_2(x) + \mu_3\ f_3^\dagger(x) f_3(x) \tag{4.8}$$

defining the Fourier transform of the spinon operators as $f(k) = \frac{1}{\sqrt{L}} \sum_x \mathrm{e}^{-\mathrm{i}kx} f(x)$, the Hamiltonian in k–space is

$$H = -\sum_k \begin{pmatrix} f_1^\dagger(k) & f_2^\dagger(k) & f_3^\dagger(k) \end{pmatrix} H_k \begin{pmatrix} f_1(k) \\ f_2(k) \\ f_3(k) \end{pmatrix}$$

$$H_k \equiv \begin{pmatrix} \mathrm{Re}(t_1 \mathrm{e}^{\mathrm{i}k}) + \mu_1 & t_3 + t_5 \mathrm{e}^{\mathrm{i}k} & 0 \\ t_3^* + t_5^* \mathrm{e}^{-\mathrm{i}k} & \mu_2 & t_4^* + t_6^* \mathrm{e}^{-\mathrm{i}k} \\ 0 & t_4 + t_6 \mathrm{e}^{\mathrm{i}k} & \mathrm{Re}(t_2 \mathrm{e}^{\mathrm{i}k}) + \mu_3 \end{pmatrix}$$

For the specific case of what we call the leg–cross (LC) model, the up–down and left–right reflection symmetry implies that $t_1 = t_2 := t_l = t_l^*$ for orange bonds in Fig. 4.7 and Fig. 4.2, $\mu_1 = \mu_3 = \mu_0$ and $t_3 = t_4 = t_5 = t_6 = t_c$ for blue bond in Fig. 4.7 and Fig. 4.2. Now defining $\mu = \mu_2 - \mu_0$, the chemical potential μ_0 is now just a constant in the Hamiltonian and can be set to 0. This choice of chemical potential maintains the leg–interchange symmetry between the top and bottom legs. Therefore, for the LC model we have

$$H_k^{\mathrm{LC}} = \begin{pmatrix} 2t_l \cos k & t_c(1 + \mathrm{e}^{\mathrm{i}k}) & 0 \\ t_c^*(1 + \mathrm{e}^{-\mathrm{i}k}) & \mu & t_c^*(1 + \mathrm{e}^{-\mathrm{i}k}) \\ 0 & t_c(1 + \mathrm{e}^{\mathrm{i}k}) & 2t_l \cos k \end{pmatrix}$$

We take hopping the amplitude of $t_\ell = 1$. The choice of real values for t_ℓ and t_c is justified by the lack of time–reversal symmetry breaking in the DMRG ground state illustrated by Fig. 4.11. For a translationally invariant system, we have a three-site unit cell and H_{MF} can be diagonalized analytically resulting in the following band energies as

functions of momentum k along the x direction:

$$\epsilon_a(k) = -2t_\ell \cos(k), \tag{4.9}$$

$$\epsilon_s^{\pm}(k) = -\frac{1}{2}\left(\mu - \epsilon_a(k) \mp \sqrt{[\mu + \epsilon_a(k)]^2 + 16t_c^2[1+\cos(k)]}\right). \tag{4.10}$$

These bands are shown in Fig. 4.3, where there we denote the lower band $\epsilon_s^-(k) \equiv \epsilon_s(k)$. (We also show these dispersions again below in Fig. 4.13, where we discuss the precise state VMC state used in Fig. 4.5.) The corresponding wave functions (with the basis states ordered as "top", "middle", "bottom") are given by

$$\psi_a(k) = \frac{1}{\sqrt{2}}\begin{pmatrix} 1 \\ 0 \\ -1 \end{pmatrix}, \tag{4.11}$$

$$\psi_s^{\pm}(k) = \frac{1}{\sqrt{2+|\alpha_\pm(k)|^2}}\begin{pmatrix} 1 \\ \alpha_\pm(k) \\ 1 \end{pmatrix}, \tag{4.12}$$

where $\alpha_\pm(k) \equiv [\epsilon_a(k) - \epsilon_s^{\pm}(k)]/[t_c(1+e^{ik})]$.

With this diagonalization, we can define new fermion operators and write a simple 3–band ($b \in \{0,+,-\}$) free Hamiltonian.

$$\mathrm{H_{MF}} = -\sum_{\substack{k \\ b\in\{0,+,-\}}} \epsilon_b(k) c_b^\dagger(k) c_b(k), \qquad \begin{aligned} c_0(k) &\equiv A_0(f_1 - f_3) \\ c_\pm(k) &\equiv A_\pm(f_1 + \alpha_\pm^* f_2 + f_3) \end{aligned}$$

where A_0 and $A_\pm$ are the appropriate normalization factors of the calculated eigenvectors.

To ensure the constraint, the first step is to find the half–filling for this 3–band model. All possible scenarios for half–filling are shown in Fig. 4.2.1. For $\mu > 0$, we have

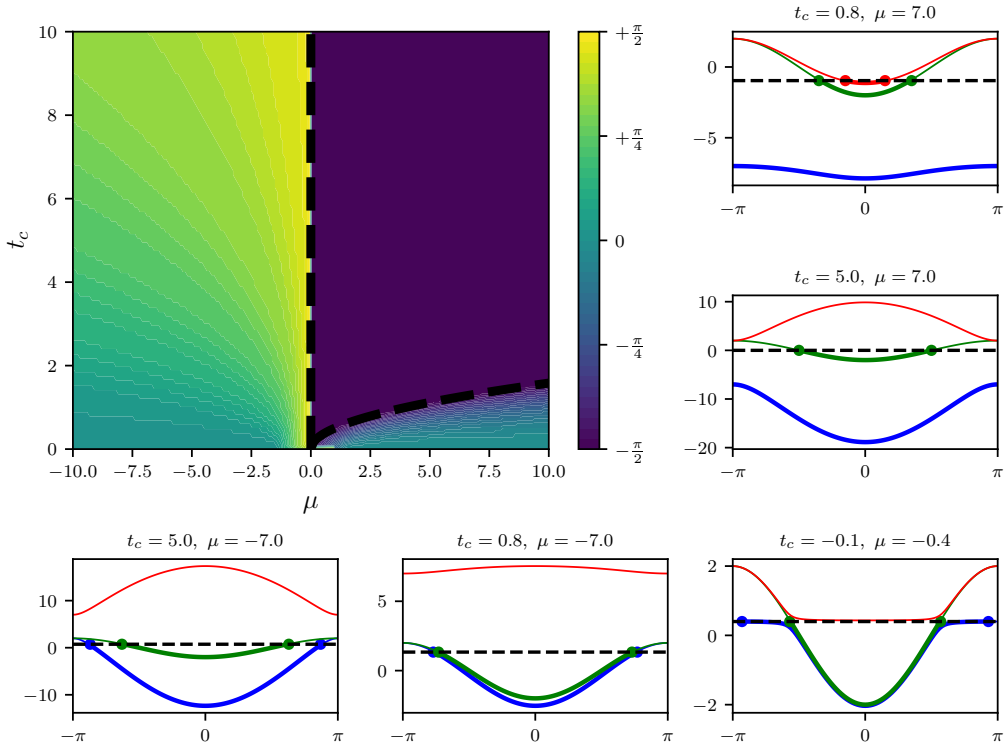

Figure 4.2: The possible scenarios for half–filling of the spinon hopping Hamiltonian. The color plot shows the difference between k_F values of the two Fermi seas (FS). The dark dashed line separates the one single Fermi sea region from the double Fermi sea region.

mostly single Fermi sea regions except for a narrow space inside the parabola,

$$\epsilon_-(k=0) = 0 \quad \Longrightarrow \quad \mu - \frac{4t_c^2}{t_l} = 0$$

So for small enough t_c we can get two Fermi seas, k_f^- and k_f^0 that satisfy $k_f^0 \geq k_f^-$ and $k_f^- + k_f^0 = \pi/2$. For $\mu < 0$ we have always two Fermi seas, k_f^+ and k_f^0 that satisfy $k_f^+ \geq k_f^0$ and $k_f^+ + k_f^0 = 3\pi/2$. For the same μ, smaller t_c leads to smaller difference between the two k_F and the line of $t_c = 0$ which means to decouple the top and bottom chains corresponds to two equal size Fermi seas.

We will focus on the case $\mu < 0$, which leads to partial filling of the lowest two bands (see Fig. 4.3), hence producing a state with $c = 4$ (two spin & two charge) gapless

modes at the mean-field level. As we will see, this regime provides a natural starting point for explaining the phenomenology of the kagome strip Heisenberg model for $0.8 \lesssim J \lesssim 1.3$.

To continue with the mean–field approach, it is possible to write the original f fermions in terms of c_b and require that $f_i^\dagger f_i = 1$. This will give two equations involving N_0, N_+, N_- that with the hopping average $f_i^\dagger f_j = t$ will fix the filling of each band and value of t_c. However, we already know that the mean–field result is not capable of correctly describing the original spin model so we need other approaches to deal with the spinon theory.

Since the DMRG results suggest a possible gapping of the symmetric band, here we try to add pairing for the symmetric band. If we add pairing for band b with amplitude Δ_b we can translate that into real space

$$\begin{aligned}\Delta_b \sum_k c_{b\uparrow}^\dagger(k) c_{b\downarrow}^\dagger(-k) &= \Delta_b \sum_k \alpha_{bi}^* f_{i\uparrow}^\dagger(k) \alpha_{bj}^* f_{j\downarrow}^\dagger(-k) \\ &= \sum_{x,x'} \underbrace{\left(\frac{\Delta}{L_x} \sum_k \alpha_{bi}^* \alpha_{bj}^* \mathrm{e}^{\mathrm{i}k(x-x')} \right)}_{\Delta_{x,x'}} f_{i\uparrow}^\dagger(x) f_{j\uparrow}^\dagger(x') \end{aligned} \tag{4.13}$$

where there is also a sum over i, j, which are the site index in the unit cell. If we now add this term to the mean–field Hamiltonian, we can diagonlize it using the Bogoliubov procedure and project to the space of $N_\uparrow = N_\downarrow = N/2$ and write the BCS wavefunction as follows

$$|\mathrm{BCS}\rangle = \left(\sum_{x,x'} \phi(x,x') f_{x\uparrow}^\dagger f_{x'\downarrow}^\dagger \right)^{N/2} |0\rangle \tag{4.14}$$

4.3 The spin liquid ground state

To go beyond mean field, we can couple the spinons for our two–band situation depicted in Fig. 4.3 to a U(1) gauge field as described in 3.6. While the corresponding 2D theory of coupling a Fermi surface to a U(1) gauge field is notoriously challenging [82, 83, 84, 95], including U(1) gauge fluctuations at long wavelengths along a quasi–1D ladder can be readily achieved via bosonization [126, 125, 42]. Specifically, integrating out the gauge field produces a mass term for the particular linear combination of bosonized fields corresponding to the overall (gauge) charge mode $\theta_{\rho+}$, thus implementing a coarse-grained version of the on–site constraint mentioned above.

The resulting theory is a highly unconventional $c = 3$ Luttinger liquid with one gapless *relative* charge mode $\theta_{\rho-}$ and two gapless spin modes $\theta_{s\sigma}$ and $\theta_{a\sigma}$, i.e., a C1S2 SBM state (here as in section 3.6, CαSβ denotes a state with α (β) gapless charge (spin) modes [89, 10]). In what follows, we present evidence that the kagome strip Heisenberg model realizes a particular instability of the SBM in which one of the two spin modes is gapped while $c = 2$ gapless modes remain: a C1S1 state.

Note that the low–energy theory of fermionic spinons coupled to a U(1) gauge field on the kagome strip for $\mu < 0$ is basically identical to that described in Ref. [125] (on a 2–leg triangular strip or the zig–zag ladder) using the translation $1 \leftrightarrow a$ and $2 \leftrightarrow s$, where 1 and 2 denote the two band labels in Ref. [125] However, there is in general no reason to expect *a priori* that such an exotic state would produce a faithful description of the low–energy physics of a given microscopic model.

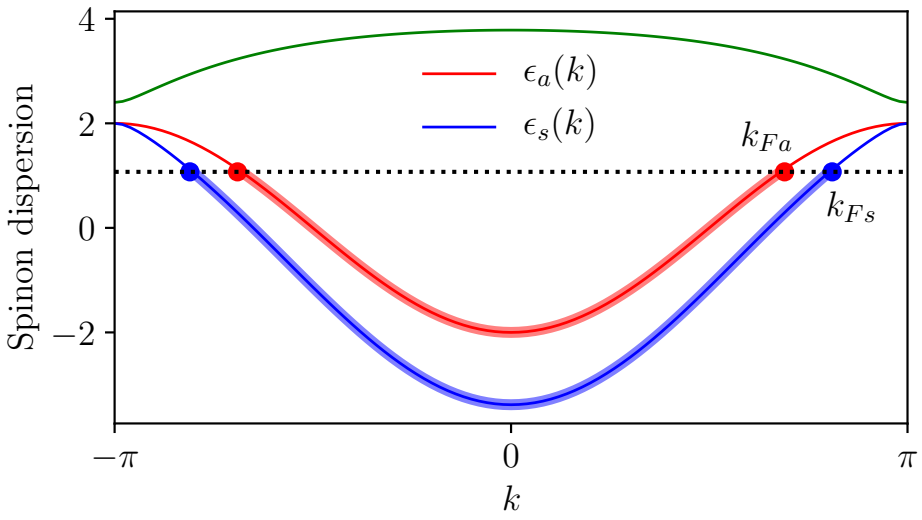

Figure 4.3: Characteristic spinon band structure for states with $\mu < 0$ (here $t_c = 1.0$, $\mu = -2.4$). There are two partially filled 1D bands, one symmetric (s) and one antisymmetric (a) under leg interchange. The DMRG ground state for $0.8 \lesssim J \lesssim 1.3$ on the kagome strip can be well-described as follows: (1) take this $c = 4$ mean-field state, (2) include gauge fluctuations, and (3) gap out the spin mode $\theta_{s\sigma}$ for the symmetric band, thereby producing a C1S1 spin liquid state with $c = 2$.

4.3.1 Evidence of C1S2 ground state for $0.8 \lesssim J \lesssim 1.3$

In this section we rule out the evidence for the unconventional ground state of the kagome strip at the parameter regime $0.8 \lesssim J \lesssim 1.3$. We begin the argument with calculations of bond–energy textures induced by open boundary conditions (OBC) [104, 80]. Specifically, we consider the Fourier transform of local nearest-neighbor spin-spin correlations along the bottom leg: $\mathcal{B}_q \equiv \sum_x \mathrm{e}^{-iqx} \langle \mathbf{S}^B_x \cdot \mathbf{S}^B_{x+1} \rangle$, where here and in what follows $\mathbf{S}^\lambda_x$ is the spin operator at horizontal position x and vertical position $\lambda = T, M, B$ (for "top", "middle", and "bottom"; see Fig. 4.2). Such quantities contain content similar to the dimer structure factor [80, 125], yet are less formidable to compute on large systems. In Fig. 4.4, we show DMRG measurements of $\mathcal{B}_q$ on an OBC system of length $L = 60$ as illustrated in section 4.4. We see that $\mathcal{B}_q$ generically shows two prominent features centered symmetri-

cally about wave vector $\pi/2$. These features are power-law singularities for $0.8 \lesssim J \lesssim 1.3$; we will later discuss the Bragg peaks observed at $J = 0.78$. Defining $q_<$ ($q_>$) as the smaller (larger) wave vector, notice that $q_<$ ($q_>$) increases (decreases) with increasing J, but the two wave vectors always satisfy $q_< + q_> = \pi$.

The presence of such power–law singularities at wave vectors tunable by a coupling parameter, yet obeying particular sum rules, is suggestive of multiple bands of gapless fermionic spinons [126, 125, 18, 17, 98, 68]. In Fig. 4.4, we also include VMC calculations on wave functions obtained by Gutzwiller projecting the free fermion states of the form shown in Fig. 4.3—these are model wave functions for the SBM [101, 125, 17] and section 4.6. Such wave functions exhibit power-law singularities in physical quantities at various "$2k_F$" wave vectors, i.e., wave vectors obtained by connecting sets of Fermi points in Fig. 4.3. Specifically, for the SBM states considered, we expect and observe features in $\mathcal{B}_q$ at wave vectors $q = 2k_{Fs}$ and $2k_{Fa}$, where $2k_{Fs}+2k_{Fa} = \pi \mod 2\pi$ due to the half-filling condition. The overall qualitative agreement between VMC and DMRG measurements of $\mathcal{B}_q$ in Fig. 4.4 is notable; recall that the VMC states have only two free parameters. We can now make the following identification with the wave vectors $q_<$ and $q_>$ discussed earlier: $q_< = 2k_{Fs}$ and $q_> = 2k_{Fa}$.

The next argument is based on the measurements of the spin structure factor. Defining $\mathbf{S}_x^{s/a} \equiv \frac{1}{\sqrt{2}} \left(\mathbf{S}_x^T \pm \mathbf{S}_x^B \right)$, we consider 1D structure factors obtained by Fourier transforming real-space spin-spin correlation functions composed from the spin operators $\mathbf{S}_x^s$, $\mathbf{S}_x^M$, and $\mathbf{S}_x^a$, i.e., $\langle \mathbf{S}_q^s \cdot \mathbf{S}_{-q}^s \rangle$, $\langle \mathbf{S}_q^M \cdot \mathbf{S}_{-q}^M \rangle$, and $\langle \mathbf{S}_q^a \cdot \mathbf{S}_{-q}^a \rangle$. The former two spin operators are symmetric under leg interchange ($T \leftrightarrow B$), while $\mathbf{S}_x^a$ is antisymmetric. To characterize

correlations between the outer chains and the middle sites, we also consider the analogous 1D structure factor $\langle \mathbf{S}^B_q \cdot \mathbf{S}^M_{-q} \rangle = \langle \mathbf{S}^T_q \cdot \mathbf{S}^M_{-q} \rangle$. In Fig. 4.5, we show DMRG calculations of these four quantities on a system of length $L = 32$ with periodic boundary conditions (PBC) at coupling $J = 0.9$, which is characteristic of the observed behavior throughout $0.8 \lesssim J \lesssim 1.3$. As calculated by DMRG, the three structure factors $\langle \mathbf{S}^s_q \cdot \mathbf{S}^s_{-q} \rangle$, $\langle \mathbf{S}^M_q \cdot \mathbf{S}^M_{-q} \rangle$, and $\langle \mathbf{S}^B_q \cdot \mathbf{S}^M_{-q} \rangle$ all reveal clear power-law singularities at a particular incommensurate wave vector $q_> = 10 \cdot \frac{2\pi}{32}$, while $\langle \mathbf{S}^a_q \cdot \mathbf{S}^a_{-q} \rangle$ is completely smooth hence indicating exponential decay in real space. Also shown in Fig. 4.5 are VMC calculations for an appropriate SBM state satisfying $2k_{Fa} = q_>$. As expected, the VMC data shows singular features in $\langle \mathbf{S}^s_q \cdot \mathbf{S}^s_{-q} \rangle$, $\langle \mathbf{S}^M_q \cdot \mathbf{S}^M_{-q} \rangle$, and $\langle \mathbf{S}^B_q \cdot \mathbf{S}^M_{-q} \rangle$ at wave vectors $q_< = 2k_{Fs}$ and $q_> = 2k_{Fa}$ and in $\langle \mathbf{S}^a_q \cdot \mathbf{S}^a_{-q} \rangle$ at wave vector $\pi/2$. In this case, the qualitative agreement between VMC and DMRG remains intact only near the wave vector $q_> = 2k_{Fa}$: the DMRG data is completely lacking any structure at both $q_< = 2k_{Fs}$ (symmetric cases) and at $\pi/2$ (antisymmetric case).

We perform large–scale density matrix renormalization group (DMRG) calculations on Eq. (4.1) using the DMRG-MPS routines from the ALPS package [11, 36], and compare these results to variational Monte Carlo (VMC) calculations [47, 26] on Gutzwiller-projected wave functions based on the above SBM theory. While the VMC calculations oftentimes provide a semiquantitative description of the DMRG data, here VMC is mainly used as a cross–check on the analytic theory and to demonstrate that simple—albeit exotic—wave functions can qualitatively describe the intricate behavior observed in the DMRG. The DMRG is performed on ladders of length L in the x direction and employ both open and periodic boundary conditions detailed in 4.4.

This discrepancy can be explained universally by postulating that the spin mode $\theta_{s\sigma}$ is gapped in the DMRG state. Indeed, in the low-energy SBM theory, there is an allowed four-fermion single-band $2k_F$ backscattering interaction which, upon bosonization, contains a nonlinear cosine potential [10, 76, 81, 125]:

$$V_{ss}^{\perp} = \lambda_{ss}^{\sigma} \cos(2\sqrt{2}\theta_{s\sigma}). \tag{4.15}$$

If $\lambda_{ss}^{\sigma} < 0$, this term is marginally relevant, and the field $\theta_{s\sigma}$ becomes pinned [10, 125]. Assuming all other allowed interactions are irrelevant or marginally irrelevant, the resulting state is an unconventional C1S1 Luttinger liquid with two gapless modes, $\theta_{\rho-}$ and $\theta_{a\sigma}$, and one nontrivial Luttinger parameter $g_{\rho-} < 2/3$ (see section 4.5 and Ref. [125]). Unfortunately, faithfully describing our proposed C1S1 state via projected variational wave functions cannot be done in a straightforward way (see section 4.6). However, based on our theoretical understanding, we can be certain that a C1S1 state would resolve all qualitative differences between the (C1S2 SBM) VMC data and the DMRG data in Figs. 4.4 and 4.5. Firstly, this state would have short-ranged correlations in the spin structure factor measurements at wave vectors $q_< = 2k_{Fs}$ and $\pi/2$, while retaining power-law behavior at $q_> = 2k_{Fa}$—completely consistent with the DMRG data in Fig. 4.5. Secondly, since the long-wavelength component of the bond energy at wave vector $2k_{Fs}$ is proportional to $e^{-i\theta_{\rho-}} \cos(\sqrt{2}\theta_{s\sigma})$, the corresponding feature at $q_< = 2k_{Fs}$ in $\mathcal{B}_q$ would actually be *enhanced* relative to the SBM upon pinning of $\theta_{s\sigma}$. This indeed occurs in the DMRG data of Fig. 4.4, where the feature at $q_< = 2k_{Fs}$ in $\mathcal{B}_q$ is significantly more pronounced than that at $q_> = 2k_{Fa}$. Finally, as we show in section 4.5.2, the *spin chirality structure factor* as obtained by DMRG is featureless at finite wave vectors. While the C1S2 state would

exhibit power-law decaying chirality correlations at various finite wave vectors due to *interband* $2k_F$ processes [125], decay at these wavevectors become short-ranged in the C1S1 state with its gapped spin mode $\theta_{s\sigma}$—this is fully consistent with the DMRG results of section 4.5.2. Furthermore, we observe no Bragg peaks in the chirality structure factor measurements thereby allowing us to clearly rule out spontaneous breaking of time–reversal symmetry in this model . This rules at possible relations of the realized state to the gapless chiral U(1) spin liquid states studied in Ref. [16].

We next describe *instabilities* of the putative C1S1 phase realized in the DMRG for $0.8 \lesssim J \lesssim 1.3$. On one side, in a narrow window $0.75 \lesssim J \lesssim 0.8$, we find a state with (dominant) period-6 long-range valence bond solid (VBS) order—see the Bragg peaks in the DMRG measurements of $\mathcal{B}_q$ at $J = 0.78$ in Fig. 4.4. Remarkably, this VBS-6 phase can be naturally understood by analyzing the C1S1 theory at the special commensurate point corresponding to $2k_{Fs} = \pi/3$ and $2k_{Fa} = 2\pi/3$. Here, there exists an additional symmetry-allowed six-fermion umklapp-type interaction which is necessarily relevant with respect to the C1S1 fixed point, thereby providing a natural explanation for the observed VBS state bordering the C1S1. On the other side, we observe a strong first-order phase transition (and possibly intervening phase) in the region $J \simeq 1.3 - 1.4$ before entering a phase at still larger J with period-4 bond-energy textures (likely) decaying as a power-law.

The last evidence is the measurements of the bipartite entanglement entropy, the scaling of which gives access to perhaps the most important universal number characterizing 1D and quasi-1D systems: the central charge c, which in our case is equivalent to the number of 1D gapless modes of the realized Luttinger liquid [23]. We perform DMRG calculations

on large $x \leftrightarrow -x$ reflection-symmetric OBC systems as illustrated in section 4.4, up to length $L = 160$ ($3L + 1 = 481$ total sites), and as is clearly evident in Fig. 4.6, fits to the usual scaling form [23] strongly suggest $c = 2$ for $0.8 \lesssim J \lesssim 1.3$. This is precisely the number of 1D gapless modes expected for the C1S1 state.

4.4 The DMRG calculation results

In this section we present resulting data from the DMRG calculations and ellaborate on the details of the DMRG calculations, including lattice geometries, measurements, and convergence properties of the wavefunctions.

The DMRG calculations are performed on the kagome strip Heisenberg model [see Eq. (4.1)] for finite-size systems with either periodic (PBC) or open (OBC) boundary conditions in the x direction. The precise lattice geometries we use are shown in Fig. 4.7. For the PBC setup, a unit cell (of which there are L) is boxed by a dashed line. For OBC systems, we consider two different setups, OBC(<<) and OBC(<>), where the direction of the two angle brackets indicates the type of boundary termination at the left and right ends of the ladder (see Fig. 4.7). Note that the OBC(<>) configuration exhibits $x \leftrightarrow -x$ reflection symmetry about the middle site, while OBC(<<) does not. In all cases, L refers to the number of sites along the bottom (top) chain so that the total number of sites is $N_{\text{sites}} = 3L$ for both PBC and OBC(<<), while $N_{\text{sites}} = 3L + 1$ for OBC(<>).

For our DMRG simulations, we generally retain a bond dimension of between about $m = 1{,}600$ and 4,000 states and perform about 10 to 30 finite-size sweeps, resulting

in a density matrix truncation error of 10^{-6} or smaller. All measurements are converged to an accuracy of the order of the symbol size or smaller in the presented plots.

The operator measurements are focused on (1) bond-energy textures, (2) spin structure factors, and (3) bipartite entanglement entropy. Throughout, we define $\mathbf{S}_x^\lambda$ as the spin operator at horizontal position x and vertical position $\lambda = T, M, B$ (for the "top", "middle", and "bottom" rows of sites; see Fig. 4.2). For simplicity, we define symmetric and antisymmetric combinations of $\mathbf{S}_x^T$ and $\mathbf{S}_x^B$:

$$\mathbf{S}_x^{s/a} \equiv \frac{1}{\sqrt{2}} \left(\mathbf{S}_x^T \pm \mathbf{S}_x^B \right). \tag{4.16}$$

For the bond–energy texture calculations, we employ OBC and compute the Fourier transform of the nearest–neighbor bond-energy expectation value along one of the horizontal legs (say the bottom chain):

$$\mathcal{B}_q \equiv \mathcal{B}_q^{\text{leg}} \equiv \sum_{x=1}^{L} \mathrm{e}^{-iqx} \langle \mathbf{S}_x^B \cdot \mathbf{S}_{x+1}^B \rangle. \tag{4.17}$$

For both OBC configurations, a system of length L has L sites—and thus $L-1$ bonds—along the bottom chain. Thus, we define $\langle \mathbf{S}_L^B \cdot \mathbf{S}_{L+1}^B \rangle \equiv 0$ when computing $\mathcal{B}_q^{\text{leg}}$ in Eq. (4.17) so that $\langle \mathbf{S}_x^B \cdot \mathbf{S}_{x+1}^B \rangle$ is effectively L-periodic [for OBC(<<) in practice we append the 0 to the *beginning* of the real-space vector, $\langle \mathbf{S}_0^B \cdot \mathbf{S}_1^B \rangle \equiv 0$, before performing the Fourier transform]. Below in Figs. 4.10 and 4.12, we present additional data on the analogous (parallel) cross-bond bond-energy textures:

$$\mathcal{B}_q^{\text{cross}} \equiv \sum_{x=1}^{L} \mathrm{e}^{-iqx} \langle \mathbf{S}_x^B \cdot \mathbf{S}_{x-\frac{1}{2}}^M \rangle. \tag{4.18}$$

Since the real–space data used to generate $\mathcal{B}_q^{\text{leg/cross}}$ does not generally exhibit $x \leftrightarrow -x$ symmetry [e.g., due to use of OBC(<<)], our Fourier-space data is in general complex. For

simplicity, we thus plot only the real part: $\Re\,(\mathcal{B}_q^{\text{leg/cross}})$. Finally, we have confirmed that using OBC(<<) versus OBC(<>) does not make a qualitative difference in these bond-energy texture calculations; for presentation in Fig. 4.4 and in Fig. 4.10 below, we use the OBC(<<) setup. The DMRG result for the bond energy textures for a variety of parameters are shown in Fig. 4.8.

For the spin structure factor calculations, we use PBC and compute the following four momentum-space spin-spin correlation functions:

$$\langle \mathbf{S}_q^s \cdot \mathbf{S}_{-q}^s \rangle \equiv \frac{1}{L} \sum_{x,x'} e^{-iq(x-x')} \langle \mathbf{S}_x^s \cdot \mathbf{S}_{x'}^s \rangle, \tag{4.19}$$

$$\langle \mathbf{S}_q^M \cdot \mathbf{S}_{-q}^M \rangle \equiv \frac{1}{L} \sum_{x,x'} e^{-iq(x-x')} \langle \mathbf{S}_x^M \cdot \mathbf{S}_{x'}^M \rangle, \tag{4.20}$$

$$\langle \mathbf{S}_q^a \cdot \mathbf{S}_{-q}^a \rangle \equiv \frac{1}{L} \sum_{x,x'} e^{-iq(x-x')} \langle \mathbf{S}_x^a \cdot \mathbf{S}_{x'}^a \rangle, \tag{4.21}$$

$$\langle \mathbf{S}_q^B \cdot \mathbf{S}_{-q}^M \rangle \equiv \frac{1}{L} \sum_{x,x'} e^{-iq(x-x')} \langle \mathbf{S}_x^B \cdot \mathbf{S}_{x'}^M \rangle. \tag{4.22}$$

When using PBC, we must necessarily work on smaller systems due to its well-known convergence problems in the DMRG, for example, the largest PBC system discussed here is for $L = 32$, that is $N_{\text{sites}} = 96$ total spins. Within the putative C1S1 state, for $1.0 \lesssim J \lesssim 1.3$ a relatively small bond dimensions of $m = 3{,}000$ results in a converged and almost translationally invariant system, while for $0.8 \lesssim J \lesssim 1.0$ a perfectly translationally invariant ground state is difficult to achieve even for m as large as 4,800. In principle, this can be an artifact of finite-momentum in the ground-state wave function [125]. Another culprit could be the near-ordering tendencies of the state at wave vector $q_<$ in the bond energy (see Fig. 4.4).

At the specific point $J = 0.9$, on smaller PBC systems of length $L = 18, 20, 24$, we were able to eventually converge to a translationally invariant state by increasing m and the number of sweeps. In all of these cases, when measured for a stable but not fully translationally invariant system, we can confirm that measurement of the spin structure factors in Eqs. (4.19)–(4.22) (which effectively average L one-dimensional Fourier transforms over all "origins" of the system) are identical to those performed on the final translationally invariant states. Hence, we are confident that the final spin structure factor measurements such as those presented in Fig. 4.5 are fully converged, accurate representations of the spin correlations in the ground-state wave function.

In section 4.5.2 additional DMRG data on spin chirality structure factor measurements, also obtained with PBC, is also presented. Specifically, we calculate

$$\langle \chi^B_q \chi^B_{-q} \rangle \equiv \frac{1}{L} \sum_{x,x'} e^{-iq(x-x')} \langle \chi^B_x \chi^B_{x'} \rangle, \tag{4.23}$$

$$\langle \chi^B_q \chi^T_{-q} \rangle \equiv \frac{1}{L} \sum_{x,x'} e^{-iq(x-x')} \langle \chi^B_x \chi^T_{x'} \rangle, \tag{4.24}$$

where

$$\chi^{B/T}_x \equiv \mathbf{S}^{B/T}_x \cdot (\mathbf{S}^M_{x+\frac{1}{2}} \times \mathbf{S}^{B/T}_{x+1}). \tag{4.25}$$

For simplicity, we take the convention that the real-space two-point correlation functions $\langle \chi^B_x \chi^B_{x'} \rangle$, $\langle \chi^B_x \chi^T_{x'} \rangle$ are zero if the two chirality operators share any common sites.

Note that the same convergence considerations described above for the spin structure factors apply similarly to these measurements of the chirality structure factors.

For the entanglement entropy calculations, we present data on the $x \leftrightarrow -x$ reflection-symmetric OBC(<>) system. We use a progression of bipartitions as indicated by

the site labels in the bottommost panel of Fig. 4.7. That is, the first subsystem considered contains the site labeled 1, the second subsystem contains sites 1 and 2, and so on. Using DMRG we compute the von Neumann entanglement entropy,

$$S_1(\rho_A) = -\mathrm{Tr}\left(\rho_A \log \rho_A\right), \tag{4.26}$$

where ρ_A is the reduced density matrix for a subsystem A. Note that the chosen progression of bipartitions produces data of S_1 versus subsystem size $\ell = 1, 2, \ldots, N_{\mathrm{sites}} - 1$ which is symmetric about the middle of the ladder in the x direction. We then perform fits to the calculated entanglement entropy data using the well-known Calabrese-Cardy formula [24, 23] to determine the central charge, c. Specifically, we fit to the scaling form

$$S_1(\ell, L) = \frac{c}{6} \log\left(\frac{3L+1}{\pi} \sin\frac{\pi\ell}{3L+1}\right) + A, \tag{4.27}$$

where $3L+1 = N_{\mathrm{sites}}$ is the total number of sites for OBC(<>). In our fits, we omit $O(10)$ of the smallest/largest subsystems near the ends of the ladder. The mid-system entanglement entropy data shown in the inset of Fig. 4.6 is simply the raw S_1 data for subregions spanning half the system according to the above labeling. For OBC(<>) systems with L even (N_{sites} odd), as presented in Fig. 4.6, we must work in the sector with $S^z_{\mathrm{tot}} = \frac{1}{2}$; we have confirmed that this detail makes no difference in the central charge determination. In addition, we have performed analogous calculations for both PBC and OBC(<<) systems where pure "unit-cell bipartitions" are natural, and we have indeed been able to confirm in those setups as well the result $c = 2$ in the putative C1S1 state for $0.8 \lesssim J \lesssim 1.3$ (data not shown).

We conclude this section by presenting additional data on the spin excitation gaps in the putative C1S1 phase. In Fig. 4.9, we plot the triplet excitation gap, $E_0(S=1) - E_0$, as

well as the singlet excitation gap, $E_1(S=0)-E_0$, versus inverse system length $1/L$ obtained with OBC(<<) at the characteristic point $J = 1.0$. (In the entire interval $0.75 \lesssim J \lesssim 2.0$, we find that the ground state is a spin singlet with total spin $S = 0$; see also Ref. [140].) We show fits to the simple scaling form $\Delta E = a/L$ (not considering log corrections [104, 140]) to show overall consistency with both gaps vanishing in the thermodynamic limit. This conclusion is in agreement with previous work [140]. Note that the smallest system size ($L = 30$) in Fig. 4.9 is comparable to the largest sizes considered in the early work of Ref. [140] which also argued for a gapless phase; thus, eventual small spin triplet gaps seem exceedingly unlikely on this kagome strip.

4.5 The C1S2 SBM theory and the C1S1 states

The long-wavelength description of two gapless 1D bands of spin-1/2 fermions (spinons) coupled to a U(1) gauge field has been extensively studied [125, 81, 80, 76, 99]. For completeness and brevity, we here only summarize the construction of the theory and highlight those aspects which are most relevant to our results on the kagome strip.

4.5.1 Bosonization description

The basics of bosonization procedure is described in section 2.3. Here we label the two partially filled bands in Fig. 4.3 as $b = a, s$, where band a (s) has associated wave functions which are antisymmetric (symmetric) under interchange of the top and bottom legs of the kagome strip. To import results from Ref. [125], we use the band-mapping dictionary $1 \leftrightarrow a$ and $2 \leftrightarrow s$ and follow the associated bosonization conventions. Taking

the low-energy continuum limit, we expand the spinon operators in terms of slowly varying continuum fields $f_{Pb\alpha}$ near the Fermi points [42]; $P = R/L = +/-$ denotes right and left moving fermion fields, $b = a, s$ is a band index, and $\alpha = \uparrow, \downarrow$ is the spin index. At the mean-field level (before introducing gauge fluctuations), we thus have a state with $c = 4$ 1D gapless (nonchiral) modes, which in terms of bosonized fields can be expressed as in section 3.6

$$f_{Pb\alpha} = \eta_{b\alpha} e^{i(\varphi_{b\alpha} + P\theta_{b\alpha})}, \tag{4.28}$$

where $\varphi_{b\alpha}$ and $\theta_{b\alpha}$ are the canonically conjugate bosonic phase and phonon fields, respectively, and $\eta_{b\alpha}$ are the Klein factors satisfying Majorana anticommutation relations, $\{\eta_{b\alpha}, \eta_{b'\beta}\} = 2\delta_{bb'}\delta_{\alpha\beta}$ [43, 125]. It is natural in this context to take linear combinations of the original four bosonic fields $\theta_{b\alpha}$ which correspond to "charge" (ρ) and "spin" (σ) modes for each band b:

$$\theta_{b\rho/\sigma} = \frac{1}{\sqrt{2}}(\theta_{b\uparrow} \pm \theta_{b\downarrow}), \tag{4.29}$$

as well as "overall" and "relative" combinations with respect to the two bands:

$$\theta_{\mu\pm} = \frac{1}{\sqrt{2}}(\theta_{a\mu} \pm \theta_{s\mu}), \tag{4.30}$$

where $\mu = \rho, \sigma$. Analogous definitions also hold for the φ fields.

As usual, inclusion of gauge fluctuations leads to a mass term for the overall (gauge) charge mode $\theta_{\rho+}$, thus essentially implementing a coarse-grained version of the microscopic on-site constraint $\sum_\alpha f^\dagger_{i\alpha} f_{i\alpha} = 1$. From now on we will thus assume that, up to massive quadratic fluctuations, the field $\theta_{\rho+}$ is pinned. The final resulting state is a two-band analog of the U(1) spinon Fermi surface state (i.e., "spin Bose metal" or SBM): It is a highly unconventional (insulating) C1S2 Luttinger liquid with one gapless

"relative charge" mode, $\theta_{\rho-}$, and two gapless spin modes, $\theta_{s\sigma}$ and $\theta_{a\sigma}$ ($c = 3$ total 1D gapless modes). The field $\theta_{\rho-}$ has an associated nontrivial Luttinger parameter $g_{\rho-}$, while SU(2) symmetry dictates trivial Luttinger parameters in the spin sector ($g_{a\sigma} = g_{s\sigma} = 1$). The specific quadratic Lagrangian for the SBM fixed point, and the relevant bosonization conventions are described in section 3.6 and a complete bible of two band theory can be found in Ref. [125].

Considering the symmetries present in our kagome strip Heisenberg model—i.e., SU(2) spin rotation, time reversal, $x \leftrightarrow -x$ reflection (mirror), top-bottom leg interchange, and spatial translations along x by one unit cell—the set of allowed (nonchiral) short-range four-fermion interactions of the spinons *at generic band-filling configuations* (k_{Fa} and k_{Fs}) are identical to those listed in Ref. [125] (see also Refs. [89, 10, 101, 81]). In terms of the so-called chiral currents,

$$J_{Pbb'} = f^\dagger_{Pb\alpha} f_{Pb'\alpha}\,, \quad \mathbf{J}_{Pbb'} = \frac{1}{2} f^\dagger_{Pb\alpha} \boldsymbol{\sigma}_{\alpha\beta} f_{Pb'\beta}, \tag{4.31}$$

these interactions can be written as follows:

$$\mathcal{H}^\rho_w = \sum_{b,b'} w^\rho_{bb'} J_{Rbb'} J_{Lbb'}, \tag{4.32}$$

$$\mathcal{H}^\rho_\lambda = \sum_{b,b'} \lambda^\rho_{bb'} J_{Rbb} J_{Lb'b'}, \tag{4.33}$$

$$\mathcal{H}^\sigma_w = -\sum_{b,b'} w^\sigma_{bb'} \mathbf{J}_{Rbb'} \cdot \mathbf{J}_{Lbb'}, \tag{4.34}$$

$$\mathcal{H}^\sigma_\lambda = -\sum_{b,b'} \lambda^\sigma_{bb'} \mathbf{J}_{Rbb} \cdot \mathbf{J}_{Lb'b'}, \tag{4.35}$$

where $w^{\rho/\sigma}_{aa} = w^{\rho/\sigma}_{ss} = 0$ (convention / absorbed into λ terms), $w^{\rho/\sigma}_{as} = w^{\rho/\sigma}_{sa}$ (from Hermiticity), and $\lambda^{\rho/\sigma}_{as} = \lambda^{\rho/\sigma}_{sa}$ (from $R \leftrightarrow L$ symmetry).

A potentially harmful interaction is the so-called W term composed of $\mathcal{H}_w^\rho + \mathcal{H}_w^\sigma$ [125, 81]:

$$\begin{aligned} W &\equiv (w_{as}^\rho J_{Ras} J_{Las} - w_{as}^\sigma \mathbf{J}_{Ras} \cdot \mathbf{J}_{Las}) + \text{H.c.} \\ &= \cos(2\varphi_{\rho-})\{4w_{as}^\rho[\cos(2\varphi_{\sigma-}) - \hat{\Gamma}\cos(2\theta_{\sigma-})] \\ &- w_{as}^\sigma[\cos(2\varphi_{\sigma-}) + \hat{\Gamma}\cos(2\theta_{\sigma-}) + 2\hat{\Gamma}\cos(2\theta_{\sigma+})]\}, \end{aligned} \tag{4.36}$$

where

$$\hat{\Gamma} \equiv \eta_{1\uparrow}\eta_{1\downarrow}\eta_{2\uparrow}\eta_{2\downarrow}. \tag{4.37}$$

The W term thus has a scaling dimension of $\Delta[W] = 1 + \Delta[\cos(2\varphi_{\rho-})] = 1 + \frac{1}{g_{\rho-}}$, and if it is relevant ($\Delta[W] < 2$), all three gapless modes present in the C1S2 become gapped leading to some fully gapped C0S0 paramagnet. Hence, stability of the parent C1S2 state at generic k_{Fa}, k_{Fs} necessarily requires the condition $g_{\rho-} \leq 1$.

Based on the characteristics of the DMRG data in the regime $0.8 \lesssim J \lesssim 1.3$, it is natural to explore the situation in which the single-band $2k_F$ backscattering interaction λ_{ss}^σ is marginally relevant, while the analogous terms λ_{aa}^σ and λ_{as}^σ are marginally irrelevant. This occurs given that $\lambda_{ss}^\sigma < 0$, while $\lambda_{aa}^\sigma > 0$ and $\lambda_{as}^\sigma > 0$ [10, 125]. We currently have little microscopic intuition for why this might be the case in our model but proceed based on the scenario's appealing phenomenology. In terms of bosonized fields, the term λ_{ss}^σ contains a cosine potential,

$$V_{ss}^\perp = \lambda_{ss}^\sigma \cos(2\sqrt{2}\theta_{s\sigma}), \tag{4.38}$$

so that relevance of λ_{ss}^σ pins the field $\theta_{s\sigma}$ associated with the spin mode of band s. The resulting state is a C1S1 Luttinger liquid with $c = 2$ 1D gapless modes, $\theta_{\rho-}$ and $\theta_{a\sigma}$. We

must still require that the W term is irrelevant for C1S1 to be a stable phase. Given that $\theta_{s\sigma}$ is pinned (hence $\varphi_{s\sigma}$ is fluctuating wildly), the important part of the W interaction in terms of bosonized fields reads [125]

$$W = -(4w_{as}^{\rho} + 3w_{as}^{\sigma})\cos(\sqrt{2}\theta_{a\sigma})\cos(\sqrt{2}\theta_{s\sigma})\cos(2\varphi_{\rho-}), \tag{4.39}$$

where now $\theta_{s\sigma}$ is pinned, while $\theta_{a\sigma}$ and $\varphi_{\rho-}$ are both fluctuating. The scaling dimension of the W term with respect to the C1S1 fixed point is thus $\Delta[W] = \frac{1}{2} + \frac{1}{g_{\rho-}}$, so that stability of the C1S1 state at generic k_{Fa}, k_{Fs} further requires $g_{\rho-} < 2/3$.

4.5.2 Observables

To connect to the DMRG measurements of bond-energy textures and spin-spin correlations functions, we now turn to bosonized expressions of the bond-energy and spin operators at finite wave vectors. We first consider fermion bilinears and focus on those composed of a (spinon) particle and hole moving in opposite directions, i.e., Amperean-enhanced contributions [82, 125]. For spin operators symmetric under leg interchange, e.g., $\mathbf{S}_x^s$ and $\mathbf{S}_x^M$, by symmetry we can write down the following contributions at wave vectors $2k_{Fb}$:

$$\mathbf{S}_{2k_{Fb}} = \frac{1}{2} f_{Lb\alpha}^{\dagger} \boldsymbol{\sigma}_{\alpha\beta} f_{Rb\beta}, \tag{4.40}$$

$$S_{2k_{Fb}}^{x} \propto e^{i\theta_{\rho+}} e^{\pm i\theta_{\rho-}} \sin(\sqrt{2}\varphi_{b\sigma}), \tag{4.41}$$

$$S_{2k_{Fb}}^{y} \propto e^{i\theta_{\rho+}} e^{\pm i\theta_{\rho-}} \cos(\sqrt{2}\varphi_{b\sigma}), \tag{4.42}$$

$$S_{2k_{Fb}}^{z} \propto e^{i\theta_{\rho+}} e^{\pm i\theta_{\rho-}} \sin(\sqrt{2}\theta_{b\sigma}), \tag{4.43}$$

	c	$\Delta[\mathcal{B}_{2k_{Fs}}]$	$\Delta[\mathcal{B}_{2k_{Fa}}]$	$\Delta[\mathbf{S}_{2k_{Fs}}]$	$\Delta[\mathbf{S}_{2k_{Fa}}]$
C1S2 (SBM)	3	$\frac{1}{2}+\frac{g_{\rho-}}{4}$	$\frac{1}{2}+\frac{g_{\rho-}}{4}$	$\frac{1}{2}+\frac{g_{\rho-}}{4}$	$\frac{1}{2}+\frac{g_{\rho-}}{4}$
C1S1 (realized)	2	$\frac{g_{\rho-}}{4}$	$\frac{1}{2}+\frac{g_{\rho-}}{4}$	∞	$\frac{1}{2}+\frac{g_{\rho-}}{4}$
C0S1 (BCS wf)	1	∞	$\frac{1}{2}$	∞	$\frac{1}{2}$

Table 4.1: Central charge, c, and scaling dimensions of the bond-energy and spin operators at wave vectors $q_< = 2k_{Fs}$ and $q_> = 2k_{Fa}$ for the C1S2, C1S1, and C0S1 states. C1S2 is the SBM theory whose wave functions we compare directly with the DMRG. C1S1 is the phase which we argue is actually realized in the DMRG. Finally, C0S1 refers to the BCS wave function described below in section 4.6 which would (relative to the DMRG) correctly capture short-ranged ($\Delta = \infty$) spin correlations at wave vector $q_< = 2k_{Fs}$, but it would also incorrectly (and tragically) give rise to short-ranged bond-energy correlations at wave vector $q_< = 2k_{Fs}$ as well as central charge $c = 1 < 2$, both of which are qualitatively inconsistent with C1S1 and the DMRG. The dominant feature in the C1S1 phase is in fact that in the bond energy at $q_< = 2k_{Fs}$; cf. the DMRG data in Fig. 4.4.

while for the bond energy at $2k_{Fb}$, we have

$$\varepsilon_{2k_{Fb}} = \frac{1}{2} f^\dagger_{Lb\alpha} f_{Rb\alpha}, \tag{4.44}$$

$$\mathcal{B}_{2k_{Fb}} \propto \varepsilon_{2k_{Fb}} \propto e^{i\theta_{\rho+}} e^{\pm i\theta_{\rho-}} \cos(\sqrt{2}\theta_{b\sigma}). \tag{4.45}$$

(In these expressions, $\pm$ corresponds to band $b = a/s$.) Note that at the C1S2 and C1S1 fixed points, the overall charge mode is pinned in the above expressions, i.e., $\theta_{\rho+} = \text{const}$.

On the other hand, for the spin operator $\mathbf{S}^a_x$, which is antisymmetric under leg interchange, we have analogous contributions at wave vector $\pi/2$. In addition, the bottom-leg bond-energy texture $\mathcal{B}_q$ defined above, which has no simple transformation property under leg interchange, would also have a contribution at $\pi/2$. (We refer the reader to Ref. [125] for the detailed expressions in each case.)

From the above discussion, it is clear that in the C1S2 (SBM) state we should in general expect power-law singularities in $\langle \mathbf{S}^s_q \cdot \mathbf{S}^s_{-q} \rangle$ and $\langle \mathbf{S}^M_q \cdot \mathbf{S}^M_{-q} \rangle$ at wave vectors $q_< = 2k_{Fs}$

and $q_> = 2k_{Fa}$ and similarly in $\langle \mathbf{S}^a_q \cdot \mathbf{S}^a_{-q} \rangle$ at wave vector $\pi/2$. This is fully consistent with our VMC calculations, as shown, for example, in Fig. 4.5. The structure factor $\langle \mathbf{S}^B_q \cdot \mathbf{S}^M_{-q} \rangle$ could in principle have contributions at all three wave vectors $2k_{Fs}, 2k_{Fa}$, and $\pi/2$ (although the VMC measurements only show the first two). The same expectations arise for the Fourier transform of the bond-energy textures $\mathcal{B}^{\text{leg}}_q$ and $\mathcal{B}^{\text{cross}}_q$ (see, for example, Eqs. (4.44)–(4.45) and Ref. [80]). As displayed in Fig. 4.4, the VMC clearly shows features in $\mathcal{B}_q$ at $q_< = 2k_{Fs}$ and $q_> = 2k_{Fa}$.

If the term λ^σ_{ss} is relevant—as is putatively realized in the DMRG state—then subsequent pinning of $\theta_{s\sigma}$ will affect physical operators such as the spin and bond energy in a qualitative way. By Eqs. (4.41)–(4.43), one obvious effect is to eliminate the power-law feature in the structure factors $\langle \mathbf{S}^s_q \cdot \mathbf{S}^s_{-q} \rangle$ and $\langle \mathbf{S}^M_q \cdot \mathbf{S}^M_{-q} \rangle$ at wave vector $q_< = 2k_{Fs}$. All features at $q = \pi/2$ in both $\langle \mathbf{S}^a_q \cdot \mathbf{S}^a_{-q} \rangle$ and $\mathcal{B}_q$ are similarly eliminated. In all these cases, the operator in question contains the wildly fluctuating field $\varphi_{s\sigma}$, thus leading to exponential decay in real space. On the other hand, as can be inferred from Eq. (4.45), the bond energy at wave vector $q_< = 2k_{Fs}$ actually gets *enhanced* upon pinning of $\theta_{s\sigma}$, i.e., slower decay in real space with concomitant stronger feature in momentum space. We summarize these points in Table 4.1 where we list the scaling dimensions of the $2k_F$ contributions to the bond-energy and spin operators with respect to both the C1S2 (SBM) and C1S1 fixed points. All in all, a C1S1 state obtained by (marginal) relevance of λ^σ_{ss} would qualitatively agree with all features observed in the DMRG data in Figs. 4.4 and 4.5. Unfortunately, as we discuss in section 4.6, faithfully representing such a C1S1 state with a Gutzwiller-projected variational wave function cannot be accomplished in a straightforward way.

In addition, we note that there are potential *four-fermion* contributions to the spin operator at wave vector π and to the bond energy at wave vectors $4k_{Fa} = -4k_{Fs}$ and π [125] (these basically arise from *two* $2k_F$ processes). For the spin correlations at $q = \pi$ (see Fig. 4.5), there are no such features in either the DMRG data nor VMC data except for the "bottom-middle" structure factor $\langle \mathbf{S}^B_q \cdot \mathbf{S}^M_{-q} \rangle$, where both the DMRG and VMC show a possible singularity. Turning to the bond-energy textures, we see in Fig. 4.4 that neither the DMRG data nor the VMC data possess any obviously noticeable features at $q = 4k_{Fa}$ nor at $q = \pi$ in $\mathcal{B}^{\text{leg}}_q$ (although the DMRG may indeed show a weaker feature at $4k_{Fa}$). By a scaling dimension analysis alone, singular structure at $4k_{Fa}$ may be expected to be comparable to that at $q_> = 2k_{Fa}$: the scaling dimensions of the bond energy at the two wave vectors are $g_{\rho-}$ and $\frac{1}{2} + \frac{g_{\rho-}}{4}$, respectively, with $g_{\rho-} < 2/3$ required for a stable C1S1. However, nonuniversal amplitudes—which are impossible to predict with the bosonized gauge theory—also strongly dictate the visibility of a state's power-law singularities. Such effects are likely to be at play here in describing, for example, why the VMC state itself shows no singular structure at $q = 4k_{Fa}$ in $\mathcal{B}^{\text{leg}}_q$ (and similarly for the DMRG).

In Fig. 4.10, we present data on cross-bond bond-energy textures $\mathcal{B}^{\text{cross}}_q$ [see Eq. (4.18)]. This data is analogous to the $\mathcal{B}^{\text{leg}}_q$ data of Fig. 4.4, and it was also obtained with OBC(<<). In this case, the VMC data does exhibit features at $q = 4k_{Fa}$ and $q = \pi$, while the DMRG clearly shows a feature only at $q = \pi$. (Although, as in $\mathcal{B}^{\text{leg}}_q$, the DMRG data may have a weak feature at $4k_{Fa}$ if one looks closely—the fact that it is not stronger is plausibly due to the amplitude effect described above). Note that the features at $q_> = 2k_{Fa}$ have opposite signs in the DMRG and VMC data sets. However, the amplitudes and phases of

these bond-energy textures are known to be nonuniversal and strongly dependent on the details of the pinning conditions at the boundary [80]. For our VMC calculations with open boundaries, we form a Gutzwiller-projected Fermi sea wave function obtained by simply diagonalizing a free spinon hopping Hamiltonian with uniform hopping amplitudes along the x direction (see section 4.6 below) but with hard-wall boundary conditions. We have attempted tuning the details of this hopping Hamiltonian (e.g., magnitudes and signs of the hopping amplitudes) near the boundary with the hope of flipping the sign of the $q_> = 2k_{Fa}$ feature in $\mathcal{B}_q^{\text{cross}}$. Although by doing so we were able to drastically alter the magnitudes of the features, we were unsuccessful in flipping the sign of the $q_> = 2k_{Fa}$ feature. Still, this should be possible in principle. As an explicit example of how the signs of such singular features are nonuniversal, we would like to point out the following observation about the behavior at $q = \pi$ in Fig. 4.10: In the DMRG data itself, the feature at $q = \pi$ actually appears to flip sign as one tunes through the phase from $J = 0.9$ (where the feature has "negative" sign) to $J = 1.2$ (where it has "positive" sign).

As a final characterization of the DMRG ground state in the regime $0.8 \lesssim J \lesssim 1.3$, we present in Fig. 4.11 measurements of the chirality structure factors defined in Eqs. (4.23)–(4.24) at the representative point $J = 0.9$. We see that these Fourier-space measurements (1) are featureless at finite wave vectors and (2) exhibit no Bragg peaks. Both of these properties are predicted by the C1S1 theory: (1) Gapping of the spin mode $\theta_{s\sigma}$ will result in short-ranged decay of the chirality-chirality correlations at all finite wave vectors (see discussion in the main text and Appendix A of Ref. [125]), and (2) the theory respects time-reversal symmetry. Note, however, that the $\rho-$ part of the theory can still produce $1/x^2$ decay

at zero momentum with nonuniversal prefactors [125]. There are noticeable corresponding slope discontinuities at $q = 0$ in the data in Fig. 4.11—we believe the relatively small slopes are merely a quantitative matter. In fact there are similarly weak $q = 0$ slope discontinuities in the spin structure factor measurements (even in some of the VMC data), while we know with absolute certainty that the spin sector is gapless; furthermore, weak slope discontinuities in $\langle \chi_q \chi_{-q} \rangle$ at $q = 0$ were likewise observed in the C1S2 SBM phase of Ref. [125] (see e.g. their Fig. 5). All in all, the chirality structure factors exhibited by the DMRG are fully consistent with the universal properties of the spin chirality sector of the C1S1 phase.

4.5.3 Instabilities of C1S1

In this section, we describe the states bordering the region $0.8 \lesssim J \lesssim 1.3$. Notably, the instability for $J \lesssim 0.8$ can be very naturally described within the C1S1 theory, while that for $J \gtrsim 1.3$ occurs via a strong first-order phase transition—possibly even intervening phase—and likely lies outside of our theoretical framework.

In the DMRG, we observe a state with long-range (dominant) period-6 VBS order (VBS-6) for $0.75 \lesssim J \lesssim 0.8$. Tracking the singular wave vectors in the DMRG, we expect this state to correspond to $q_< = 2k_{Fs} = \pi/3, q_> = 2k_{Fa} = 2\pi/3$ ($k_{Fs} = 5\pi/6, k_{Fa} = 2\pi/3$). Note that all such equalities involving wave vectors are implied to mean so, up to signs and $\mathrm{mod}\, 2\pi$. Indeed, when the theory is at the special commensurate point corresponding to $k_{Fs} = 5\pi/6$ and $k_{Fa} = 2\pi/3$, there is an additional symmetry-allowed six-fermion umklapp-

type interaction which needs to be considered:

$$V_6 = u_6(f^\dagger_{Rs\uparrow} f^\dagger_{Rs\downarrow} f^\dagger_{La\alpha} f_{Ls\uparrow} f_{Ls\downarrow} f_{Ra\alpha} + \text{H.c.}) \tag{4.46}$$

$$= -4u_6 \cos(\sqrt{2}\theta_{a\sigma}) \sin(3\theta_{\rho-} - \theta_{\rho+}). \tag{4.47}$$

This term has scaling dimension of $\Delta[V_6] = \frac{1}{2} + \frac{9}{4} g_{\rho-}$ with respect to the C1S1 (and C1S2) fixed point and is thus relevant given $g_{\rho-} < 2/3$. Since this is precisely the condition required for the W term to be irrelevant and thus C1S1 to be a stable phase at generic k_{Fs} and k_{Fa}, a C1S1 state tuned to the point $k_{Fs} = 5\pi/6$ and $k_{Fa} = 2\pi/3$ must necessarily be unstable to this interaction. The relevance of V_6 thus pins both of the remaining gapless modes, $\theta_{a\sigma}$ and $\theta_{\rho-}$, in the C1S1 phase. Inspection of Eq. (4.45) reveals that the resulting fully gapped C0S0 state would have coexisting period-6 and period-3 VBS order (with the former being dominant).

As remarked above, we would anticipate this state to be realized in the kagome strip Heisenberg model for values of J just below 0.8. Remarkably, we indeed find evidence for a state with long-range period-6 and period-3 VBS order in the narrow region $0.75 \lesssim J \lesssim 0.8$. In Fig. 4.12, we show bond-energy texture data ($\mathcal{B}_q^{\text{leg/cross}}$) taken with DMRG at a characteristic point $J = 0.78$ within this narrow window for a sequence of system sizes on the OBC(<<) geometry. We see clear development of Bragg peaks at wave vectors $q = 2\pi/6$ and $q = 2\pi/3$ in both $\mathcal{B}_q^{\text{leg}}$ and $\mathcal{B}_q^{\text{cross}}$ as advertised. We also see a potential Bragg peak at wave vector $q = \pi$ in $\mathcal{B}_q^{\text{cross}}$—as discussed above, such period-2 activity also naturally arises from the theory [125]. Convergence of the DMRG in this region of the phase diagram is challenging, and we have thus not been able to conclusively determine that the system is fully gapped (e.g., through explicit spin gap calculations, spin-spin correlation

functions, or entanglement entropy measurements), although indications are that it likely is (also consistent with the unpublished work of Lauchli). Near $J \simeq 0.75$, a first-order phase transition occurs, and for $J \lesssim 0.75$, it appears our theory based on two bands of fermionic spinons no longer applies. We experience strange convergence difficulties in the DMRG for $0.5 \lesssim J \lesssim 0.75$, and we have not thoroughly examined the situation for $J \lesssim 0.5$. In fact, it is even an interesting open question whether or not the decoupled Bethe chain phase at $J = 0$ persists to any finite J.

Next we discuss the behavior for $J \gtrsim 1.3$. For $1.3 \lesssim J \lesssim 1.4$, the system exhibits strange behavior (and DMRG convergence difficulties) consistent with a strong-first order phase transition, while for $1.4 \lesssim J \lesssim 2.0$ the DMRG state displays (likely) power-law decaying bond-energy textures with period-4. There does exist an additional four-fermion momentum-conserving interaction at the special point of the theory when $k_{Fs} = k_{Fa} = 3\pi/4$. [This term is closely resembling the W term in Eq. (4.36)—the two have equivalent operator forms upon taking $a \leftrightarrow s$ in the band indices for $J_{Lbb'}$ and $\mathbf{J}_{Lbb'}$.] One can show that this interaction has scaling dimensions with respect to the C1S2 and C1S1 fixed points of $1 + g_{\rho-}$ and $\frac{1}{2} + g_{\rho-}$, respectively, and is thus always relevant if the generic states are stable (i.e., if W is irrelevant). The resulting state is a fully gapped C0S0 paramagnet with long-range period-4 VBS order. This is not consistent with the DMRG data for $1.4 \lesssim J \lesssim 2.0$ which is (likely) gapless Ref. [140] with power-law decaying bond-energy correlations, however, the unpublished work by Lauchli does find a finite VBS-4 order parameter, and we cannot rule out eventual small gaps. In Fig. 4.12, we show bond-energy texture data for $J = 1.6$, which is representative of the behavior in this period-4 phase.

Again, since this state is entered through a strong first-order phase transition near $J \simeq 1.3$ (the DMRG exhibits convergence difficulties for $J \simeq 1.3 - 14$), it is thus not surprising that the realized period-4 phase is not naturally accessible starting from the C1S1 theory. Finally, for $J \gtrsim 2.0$, the ground state is a conventional quasi-1D ferrimagnet continuously connected to that realized for $J \to \infty$ [140].

We conclude by remarking that the bond-energy textures in the putative C1S1 phase itself ($0.8 \lesssim J \lesssim 1.3$) definitively exhibit power-law decay; this can be gleaned from the Fourier-space data in Figs. 4.4 and 4.10, and we have also performed a complementary real-space analysis. Within this phase, there is no VBS ordering tendency: For example, the $L = 60$ system would be able to accommodate potential VBS states with periods 4, 5, or 6, but for $0.8 \lesssim J \lesssim 1.3$ the singular wave vectors are incommensurate and fully tunable.

4.5.4 Comparison to other $c = 2$ states

Reference [7, 6] described a $c = 2$ fixed point in a frustrated three-leg spin ladder, and it is natural to explore the relationship between this fixed point and our C1S1 phase. Ultimately, however, our C1S1 state cannot be accessed in any meaningful way from the ladder model discussed in Ref. [7, 6]. Firstly, the fixed point at the focus of Ref. [7, 6] is accessed *perturbatively* via weakly coupling three Heisenberg (Bethe) chains. This is in sharp contrast to our results in which the underlying lattice does not consist of three decoupled chains in any limit; more generally, our C1S1 theory clearly cannot be accessed via weakly coupled chains—one needs to start with incommensurate filling of multiple fermionic spinon bands. The fixed point of Ref. [7, 6], in contrast to the C1S1 phase, exhibits only commensurate correlations. While it is in principle possible to reach a phase with incommensurate

wavevectors starting from decoupled Heisenberg chains, in general such approaches require terms that manifestly break the SU(2) symmetry of the Hamiltonian [7]. The intriguing point about our results is the observation that a simple nearest-neighbor Heisenberg Hamiltonian that retains SU(2) symmetry harbors a phase at low energies with incommensurate wavevectors obeying "Fermi-like" sum rules. Furthermore, our C1S1 state is observed over an extended region of parameter space and is thus a *stable quantum phase*. This means that all short-range interactions that are allowed by symmetry are either irrelevant or marginally irrelevant. This is markedly different from an *unstable fixed point* such as the one discussed in Ref. [6], where gapless behavior requires relevant perturbations be fine-tuned to zero.

$$\begin{aligned} V_4 &\equiv (v^{\rho}_{as} J_{Ras} J_{Lsa} - v^{\sigma}_{as} \mathbf{J}_{Ras} \cdot \mathbf{J}_{Lsa}) + \text{H.c.} \\ &= \cos(2\theta_{\rho-})\{4v^{\rho}_{as}[\hat{\Gamma}\cos(2\varphi_{\sigma-}) - \cos(2\theta_{\sigma-})] \\ &+ v^{\sigma}_{as}[\hat{\Gamma}\cos(2\varphi_{\sigma-}) + \cos(2\theta_{\sigma-}) + 2\cos(2\theta_{\sigma+})]\}. \end{aligned} \tag{4.48}$$

At the C1S1 fixed point, the important part of V_4 reads [cf. Eq. (4.39)]

$$V_4 = -(4v^{\rho}_{as} - 3v^{\sigma}_{as})\cos(\sqrt{2}\theta_{a\sigma})\cos(\sqrt{2}\theta_{s\sigma})\cos(2\theta_{\rho-}). \tag{4.49}$$

4.6 The VMC calculations

We have also perfromed variational Monte Carlo calculations by constructing a given trial wave function in the standard way by projecting out doubly-occupied sites, i.e. Gutzwiller projection, from the ground state of a free-fermion Hamiltonian. In the case of the SBM, this procedure is particularly simple as the mean-field Hamiltonian is a pure

hopping model that was discussed in section 4.2.1

$$\mathrm{H}_{\mathrm{MF}} = -\sum_{i,j} t_{ij} f^{\dagger}_{i\alpha} f_{j\alpha}. \tag{4.50}$$

Again, the sum over spin indices $\alpha = \uparrow, \downarrow$ is implied, hermiticity leads to $t_{ij} = t^{*}_{ji}$, and the on–site "chemical potential" terms are given by the diagonal elements: $t_{ii} \equiv \mu_i$. We then diagonalize H_{MF}, construct a spin-singlet free-fermion Slater determinant, $|\Psi_0(\{t_{ij}\})\rangle$, at half filling from the $N_{\uparrow} = N_{\downarrow} = N_{\mathrm{sites}}/2$ lowest-energy single-particle eigenstates of H_{MF}, and finally apply the Gutzwiller projection as (see section 3.5.2)

$$|\Psi_{\mathrm{SBM}}(\{t_{ij}\})\rangle = \mathcal{P}_G |\Psi_0(\{t_{ij}\})\rangle. \tag{4.51}$$

The set of hopping amplitudes $\{t_{ij}\}$ defining H_{MF} thus constitute the variational parameters of SBM trial states. These are what we refer to as the "bare" Gutwiller states, and are sampled efficiently using the standard VMC techniques [47, 26]. See also section 4.6 for a brief review of the VMC methodology.

Note that since we are manually filling up the Fermi sea, the overall chemical potential in H_{MF} is arbitrary. The ansatz thus contains two (real) variational parameters: t_c and μ. From the diagonlaization of the mean–field Hamiltonian, band "a" in Eq. 4.11 is antisymmetric under leg interchange, while both bands "s" in Eq. 4.12 are symmetric. At $\mu = 0$, the bottommost (symmetric) band is completely filled, while the middle (anti-symmetric) band is exactly half filled; this state does not give rise to the incommensurate structure observed in the DMRG. Hence, we focus on the regime $\mu < 0$ which produces two partially filled 1D bands (see Fig. 4.3 and Fig. 4.13 below). This is the VMC setup with open boundary conditions, discussed in section 4.5.2.

The above SBM states are model wavefunctions for the C1S2 phase, however the suspected ground state of the kagome strip heisenberg model is the argued C1S1 state. A natural question thus concerns how to faithfully described the C1S1 phase via variational wave functions.

Unfortunately, this appears to be nontrivial within the standard paradigm of constructing trial states by applying Gutzwiller projection to noninteracting mean-field states, but here we describe our unsuccessful attempts at doing so. In our case, again referring to the two active bands as simply s and a, we want to gap out the *spin mode only* for only the symmetric band s. A natural, potentially fruitful way to generalize the simple SBM is to add BCS pairing to the mean-field hopping Hamiltonian in Eq. (4.51), $H_{\mathrm{MF}} \to H_{\mathrm{MF}} + \hat{\Delta}$, and project the mean-field ground state to $N_{\mathrm{particles}} = N_\uparrow + N_\downarrow = N_{\mathrm{sites}}$ total particles before Gutzwiller projection. Working in momentum space, we could consider the following form for the pairing term:

$$\hat{\Delta} = \sum_k \left[\Delta_s f^\dagger_{s,\uparrow}(k) f^\dagger_{s,\downarrow}(-k) + \Delta_a f^\dagger_{a,\uparrow}(k) f^\dagger_{a,\downarrow}(-k) + \mathrm{H.c.} \right], \tag{4.52}$$

where $f^\dagger_{b,\alpha}(k)$ creates single-particle states given by the wave functions in Eqs. (4.11)–(4.12). Then by taking $\Delta_s \neq 0$ and $\Delta_a = 0$ we can selectively gap out band s at the mean-field level. However, doing so not only gaps out the corresponding spin mode (by pinning $\theta_{s\sigma}$), but it also disturbingly gaps out the corresponding charge mode (by pinning $\varphi_{s\rho}$).

To understand the latter, it is instructive to consider what happens when one adds BCS spin-singlet pairing to a single 1D band of spin-1/2 fermions and projects the ground-state wave function to N total particles (at some generic density). In this case, one will arrive at a BCS wave function with finite superconducting order parameter (see, e.g.,

Ref. [47]), regardless of the fact that the Mermin-Wagner theorem prohibits such a ground state for a Hamiltonian that preserves particle number. What is the fate of the system in terms of the bosonized fields? The (singlet) superconducting pair operator reads

$$f^{\dagger}_{R\uparrow} f^{\dagger}_{L\downarrow} + f^{\dagger}_{L\uparrow} f^{\dagger}_{R\downarrow} \propto e^{-i\sqrt{2}\varphi_{\rho}} \cos(\sqrt{2}\theta_{\sigma}). \tag{4.53}$$

This operator would take on a finite expectation value in the proposed wave function (in the sense of having finite two-point Cooper pair correlation functions at long distances). Hence, both θ_{σ} and φ_{ρ} would be pinned. That is, we have constructed some pathological C0S0 state where the spin sector is indeed gapped, but the charge sector is "soft" ($g_{\rho} \to \infty$ in fact), as opposed to a bona fide C1S0 Luttinger liquid with finite g_{ρ} (i.e., a Luther-Emery liquid).

For the two-band situation on the kagome strip, at the mean field level upon taking $\Delta_s \neq 0$ and $\Delta_a = 0$, we would therefore have pinned $\theta_{s\sigma}$ and $\varphi_{s\rho}$ fields. Gutzwiller projecting the BCS wave function would then naturally simply pin the remaining charge mode $\theta_{a\rho}$, thereby leaving a C0S1 state with $c = 1$. The scaling dimensions of the bond-energy and spin operators with respect to this fixed point are listed in the last row of Table 4.1 shown above. Insofar as representing C1S1, this C0S1 BCS wave function is thus arguably qualitatively worse than the C1S2 SBM wave function itself. Most importantly, the bond-energy at wave vector $q_{<} = 2k_{Fs}$ is *short-ranged* even at the mean-field level (scaling dimension $\Delta = \infty$), whereas this is actually the most prominent feature of the true C1S1 phase with its very slow power-law decay ($\Delta = g_{\rho -}/4$). Given this catastrophic qualitative discrepancy, we have not pursued numerical calculations of such BCS wave functions, and thus must leave robust wave-function modeling of C1S1 for future work.

Returning to the SBM wave functions, we show in Fig. 4.13 the exact VMC state used for the spin structure factor calculations in Fig. 4.5 ($L = 32$ PBC system with DMRG data taken at at $J = 0.9$). Specifically, we choose $t_c = 1.0, \mu = -2.4$, and antiperiodic boundary conditions for the spinons in the x direction. This produces a state whose $2k_F$ wave vectors match the singular features in the DMRG data. Aside from having the extra feature in the spin structure factors at wave vectors $q_< = 2k_{Fs}$ (symmetric cases) and $\pi/2$ (antisymmetric case) as well as exhibiting a quantitatively weak feature (in momentum space) in the bond-energy at wave vector $q_< = 2k_{Fs}$, such VMC states capture the long-distance properties of the putative C1S1 phase reasonably well. (The relatively prominent feature shown by the VMC state at wave vector $q_< = 2k_{Fs}$ in the "middle-middle" structure factor $\langle \mathbf{S}^M_q \cdot \mathbf{S}^M_{-q} \rangle$ is likely some nonuniversal property of the given projected wave function; recall this feature will be eliminated entirely in a true C1S1 state.)

Finally, we discuss the energetics of our simple SBM trial states in the kagome strip Heisenberg model; for concreteness, we continue to focus on the point $J = 0.9$ as in Fig. 4.5. Within this class of SBM states, the state at $t_c = 1.0, \mu = -2.4$ shown in Fig. 4.13 is not quite the energy-optimized VMC state. However, the lowest-energy variational state is not far off at $t_c = 0.9, \mu = -0.5$ [see Fig. 4.14 for the energy landscape at $J = 0.9$ of our SBM trial states in the variational space (t_c, μ)]. This latter state has incorrect values of k_{Fs} and k_{Fa} however (error $\sim 2\pi/L$). As for the energies themselves, on the length $L = 32$ PBC system at $J = 0.9$, the DMRG ground state has energy -39.8 (in units of the leg coupling J_ℓ). On the other hand, the energy-optimized VMC state ($t_c = 0.9, \mu = -0.5$) has energy -38.3, while the state chosen for presentation ($t_c = 1.0, \mu = -2.4$) has energy

-30.6 (this can be improved somewhat by tuning t_c and μ at fixed values of k_{Fs} and k_{Fa}, e.g., $t_c = 0.9, \mu = -1.5$ gives energy -32.0). However, the latter is likely due to the state having inaccuracies in its (nonuniversal) amplitudes and short-range properties. It should be possible to remedy this deficiency by, for example, using the "improved Gutzwiller" wave functions of Ref. [125]; these are essentially Gutzwiller-projected fully gapless superconducting wave functions, although empirically even they only have tunable amplitudes with fixed Luttinger parameter $g_{\rho-} = 1$. Even more importantly, recall that such SBM trial states are not even in the correct quantum phase (C1S2 instead of putative C1S1), so extremely accurate energetics should not be anticipated. Again note that the VMC wave functions are mainly meant to serve as a numerical representation/cross-check of the analytic parent C1S2 theory, as opposed to being quantitatively accurate trial states to describe all (including short-distance) properties of the DMRG data. Still, our simple VMC states do reasonably well qualitatively, even semi–quantitatively, with regards to those universal features shared between C1S2 and C1S1.

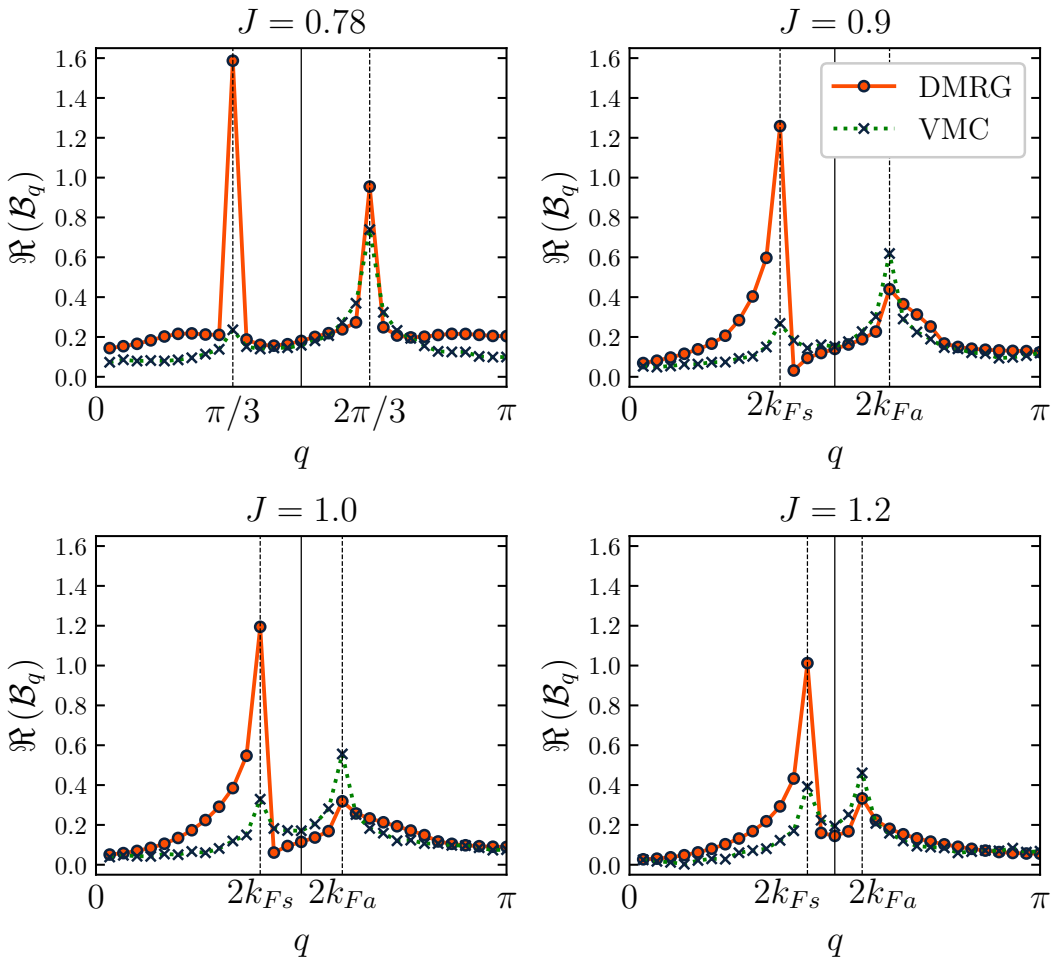

Figure 4.4: Fourier transform of (leg-bond) bond-energy textures induced by OBC on a length $L = 60$ kagome strip at $J = 0.78, 0.9, 1.0$, and 1.2. We show both DMRG data and VMC data for bare Gutzwiller SBM states. A wave function for the proposed C1S1 state would appear similar to the SBM except it would have a more prominent feature at $q_< = 2k_{Fs}$ due to lowering of the scaling dimension of the associated operator upon pinning of $\theta_{s\sigma}$. At $J = 0.78$, the DMRG ground state is a fully gapped period-6 VBS phase. For analogous data of bond-energy textures involving the *cross bonds*, please see Fig. 4.10 in section 4.5.2.

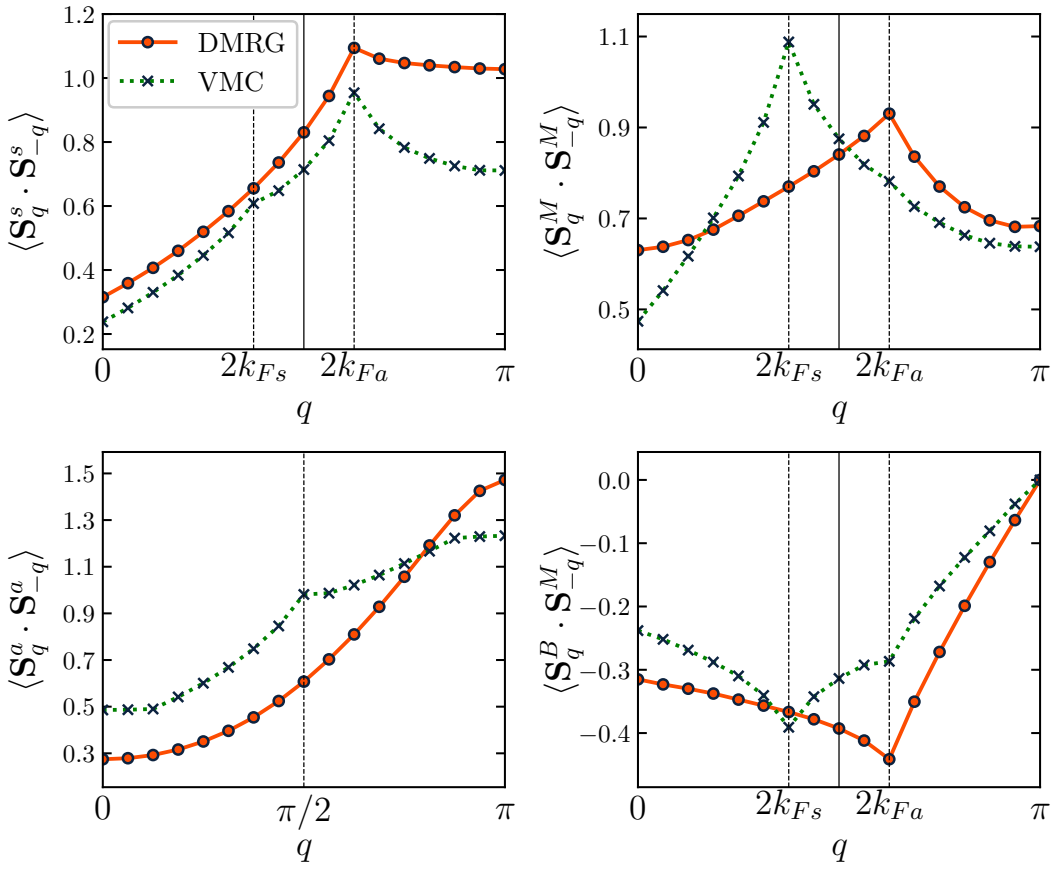

Figure 4.5: Spin structure factors at $J = 0.9$ on a $L = 32$ system with PBC. As in Fig. 4.4, we show both DMRG and bare Gutzwiller (SBM) VMC calculations. All features at wave vectors $q_< = 2k_{Fs}$ and $\pi/2$ would be absent in a wave function for the proposed C1S1 state—indeed these features are absent in the DMRG data.

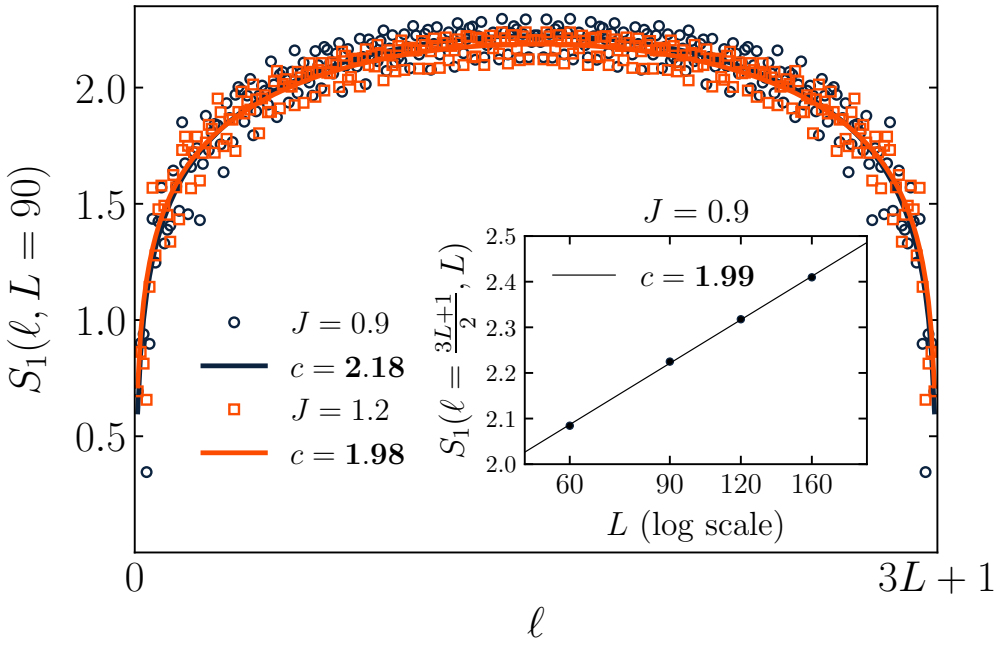

Figure 4.6: Scaling of the von Neumann entanglement entropy S_1 versus subsystem size ℓ as calculated by DMRG on an OBC system of length $L = 90$ at $J = 0.9$ and 1.2. In the inset, we show for $J = 0.9$ the mid-system entanglement entropy as we vary L. The solid curves are fits to the scaling form [23], strongly indicating $c = 2$ as expected for C1S1.

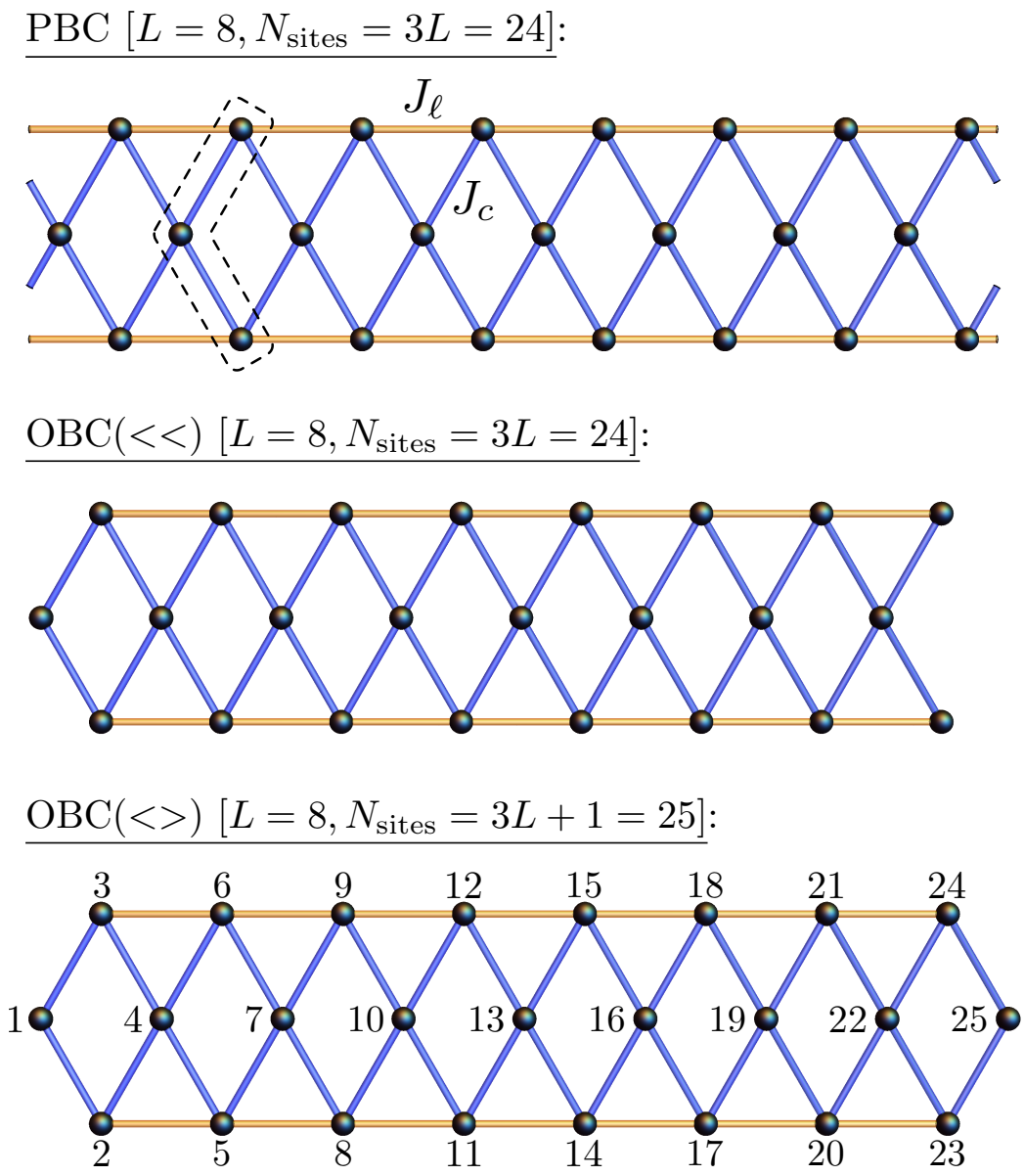

Figure 4.7: Kagome strip clusters with different boundary conditions (from top to bottom): PBC, OBC(<<), and OBC(<>). The relation to the 2D kagome lattice structure is illustrated in Fig. 4.2. The "leg" bonds are orange with associated coupling strength $J_\ell = 1$ in the Hamiltonian, while the "cross" bonds are blue with coupling $J_c \equiv J \geq 0$. In each case, the example lattice corresponds to a length $L = 8$ system. The site labels in the OBC(<>) case indicate the progression of subsystem bipartitions used in our entanglement entropy analysis (see Fig. 4.6).

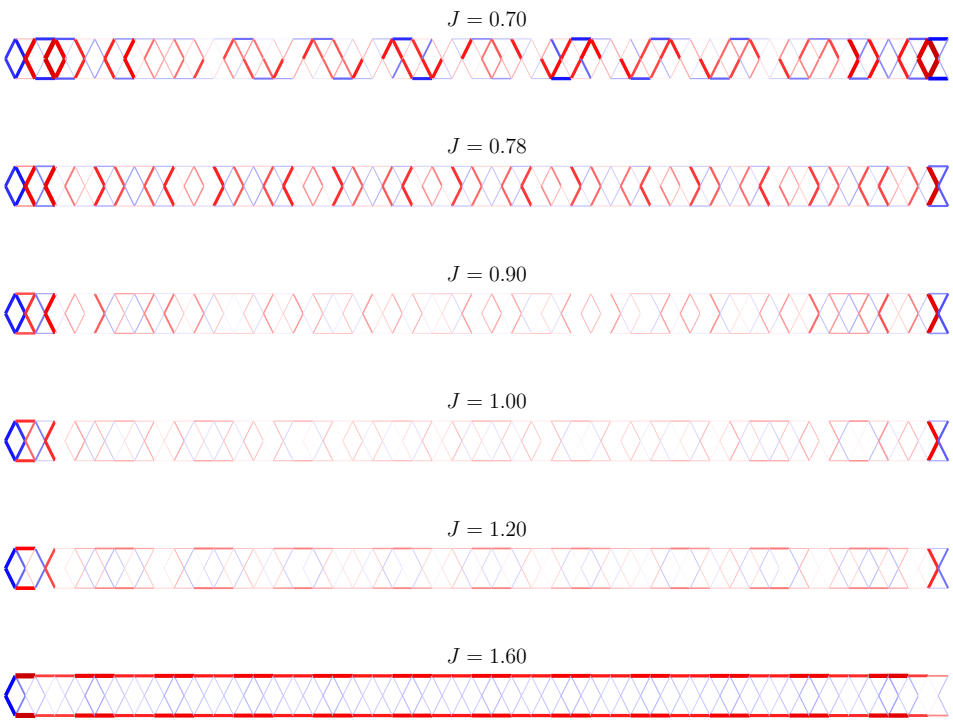

Figure 4.8: The bond energy textures in real space for a variety of parameters.

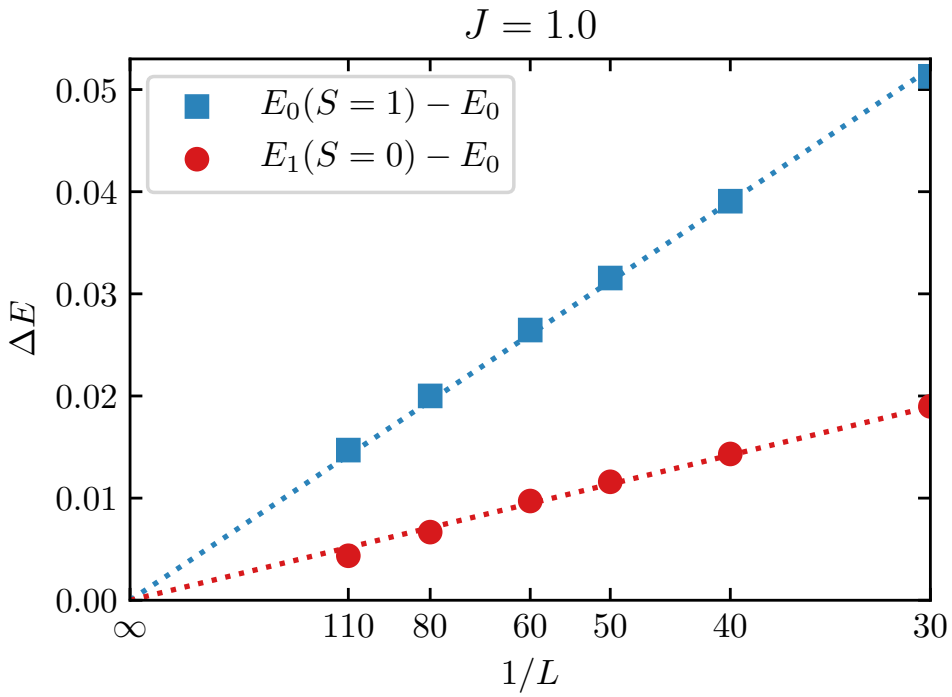

Figure 4.9: Spin triplet and singlet excitation gaps [$E_0(S=1) - E_0$ and $E_1(S=0) - E_0$, respectively] versus $1/L$ calculated with DMRG on the OBC(<<) system at $J = 1.0$. For generic L, the energies/gaps exhibit some nonmonotonic behavior with $1/L$—consistent with finite-size "shell-filling" effects for the spinons [125, 68, 97] or, relatedly, some system sizes being more compatible with the dominant $q_<$ feature in the bond-energy textures than others—therefore, here we only plot sizes at local minima versus $1/L$. The lines are fits to the simple linear scaling form $\Delta E = a/L$.

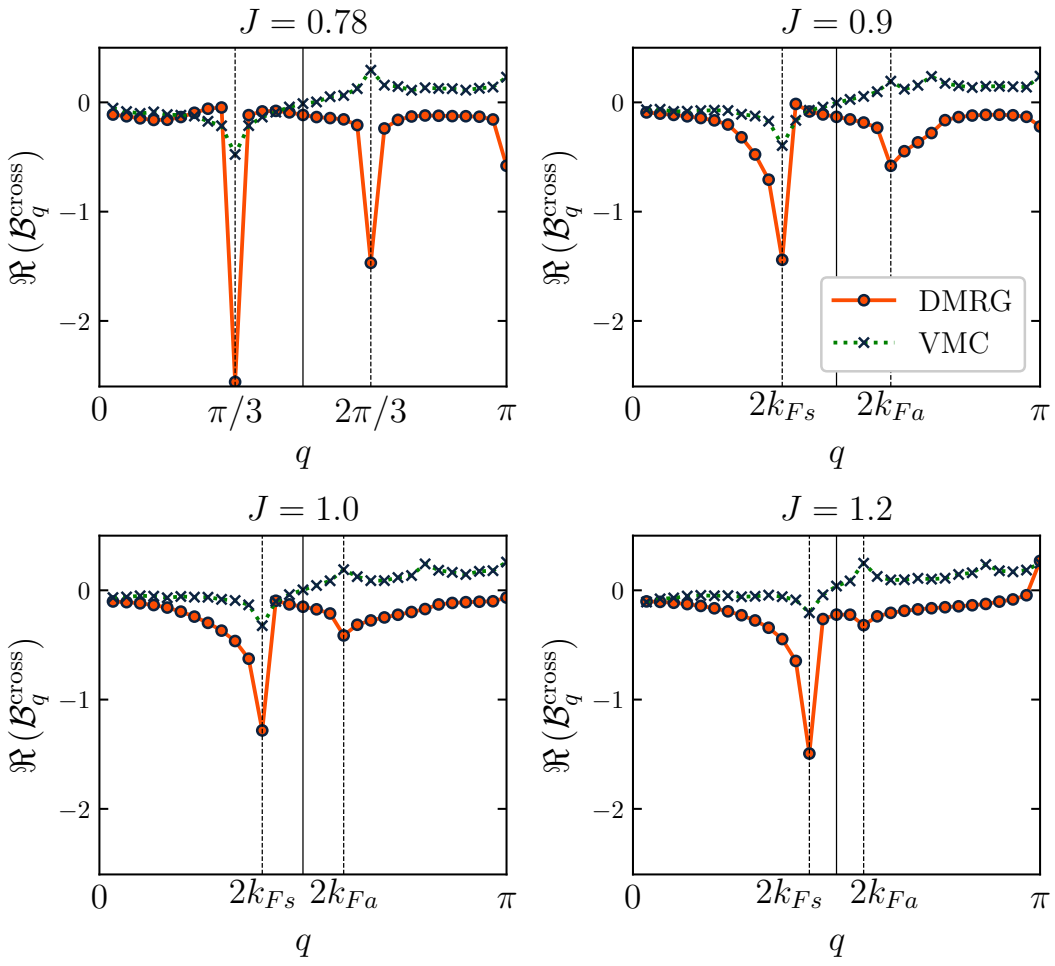

Figure 4.10: Data analogous to Fig. 4.4, but now taking the Fourier transform of the *cross-bond* bond-energy textures [see Eq. (4.18)]. The parameters chosen for the VMC states in these calculations (and in the analogous calculations of $\mathcal{B}_q \equiv \mathcal{B}_q^{\rm leg}$ in Fig. 4.4) are $t_c = 1.0$ and $\mu = -1.8, -2.4, -3.1, -4.8$ for $J = 0.78, 0.9, 1.0, 1.2$, respectively. (For details of our VMC calculations, please see section 4.6.) Recall that the DMRG ground state at $J = 0.78$ is a period-6 VBS (C0S0), but we still show a corresponding VMC state (C1S2) for comparison. The discrepancies in signs of the features at, for example, $q_> = 2k_{Fa}$ between the DMRG and VMC results can plausibly be explained by nonuniversal amplitudes/phases of the bond texture's oscillatory components.

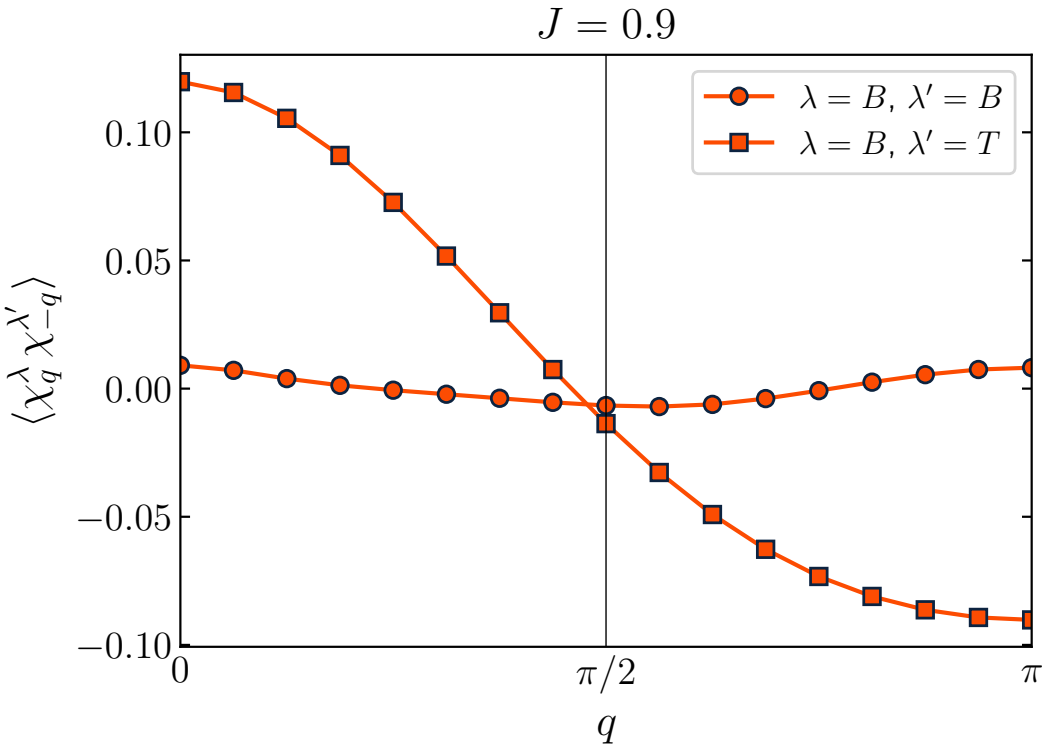

Figure 4.11: Chirality structure factors obtained with DMRG at the point $J = 0.9$ on a PBC system of length $L = 32$; the specific quantities being plotted are detailed in Eqs. (4.23)–(4.25). The lack of Bragg peaks implies that the DMRG ground state respects time-reversal symmetry (which we have also verified with complex-valued DMRG simulations); and the lack of power-law singularities at finite wave vectors indicates short-ranged behavior at those wave vectors in the chirality sector. This behavior is consistent with the proposed C1S1 theory.

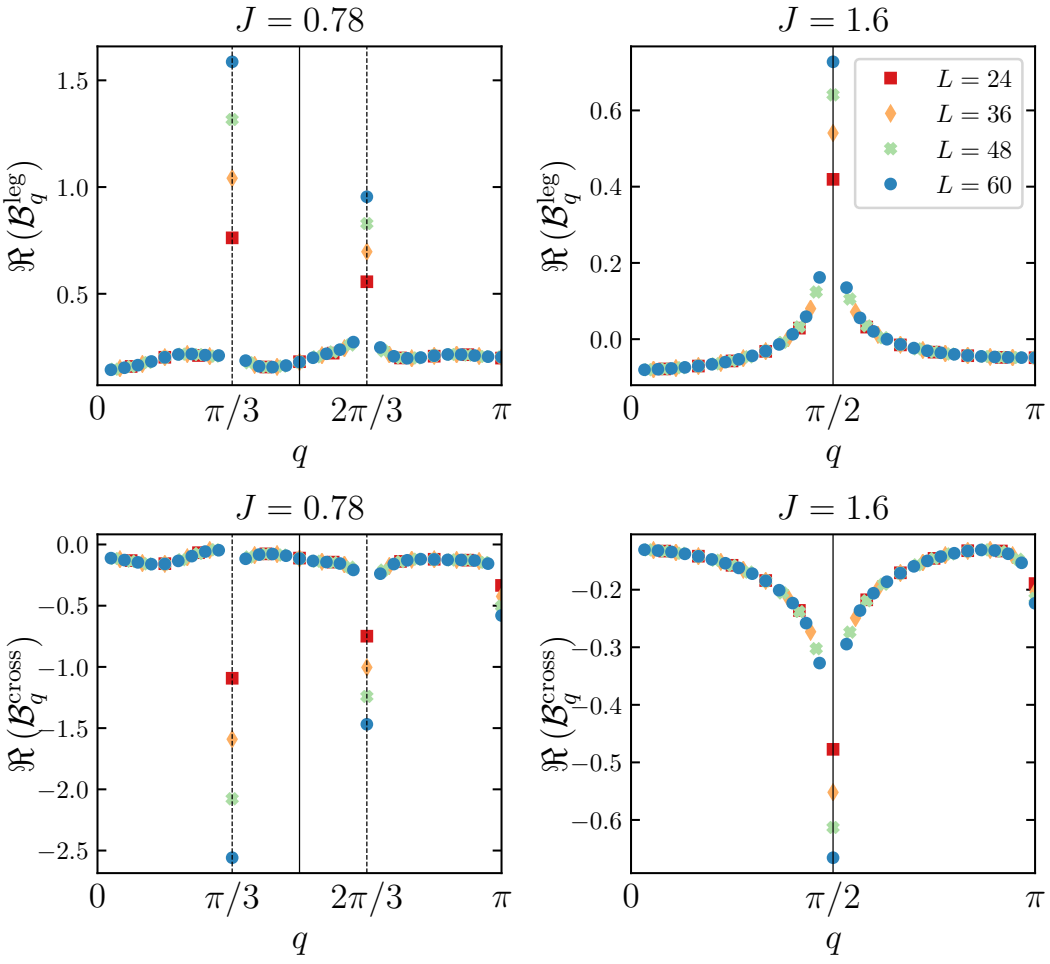

Figure 4.12: Leg-bond (top row) and cross-bond (bottom row) bond-energy texture data for a sequence of lengths L in the period-6 VBS phase at $J = 0.78$ (left column) and in the period-4 phase at $J = 1.6$ (right column). Development of Bragg peaks in the former case is evident. These calculations were performed with DMRG using the OBC(<<) geometry.

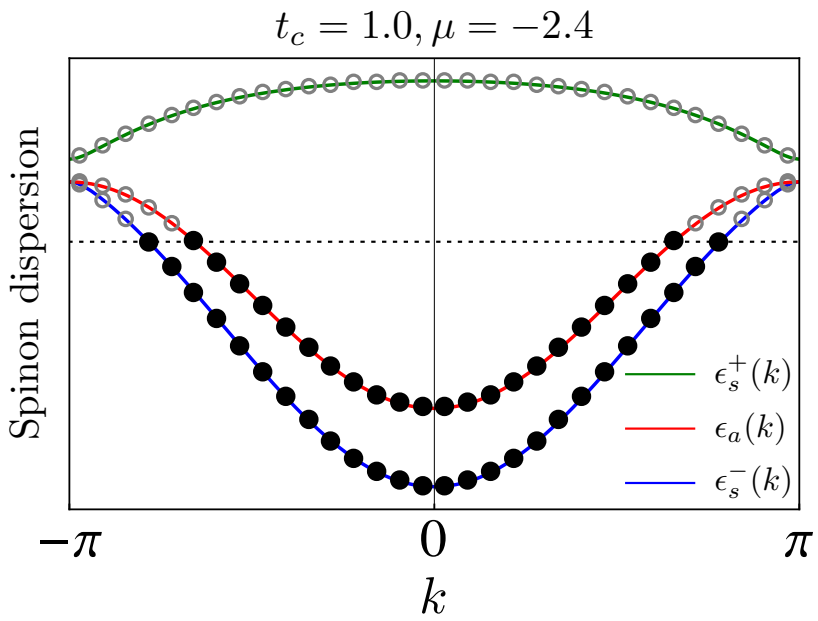

Figure 4.13: Specific SBM trial state used for the VMC data in Fig. 4.5. The boundary conditions in the x direction for the spinons are taken to be antiperiodic; this produces a spin wave function with periodic boundary conditions.

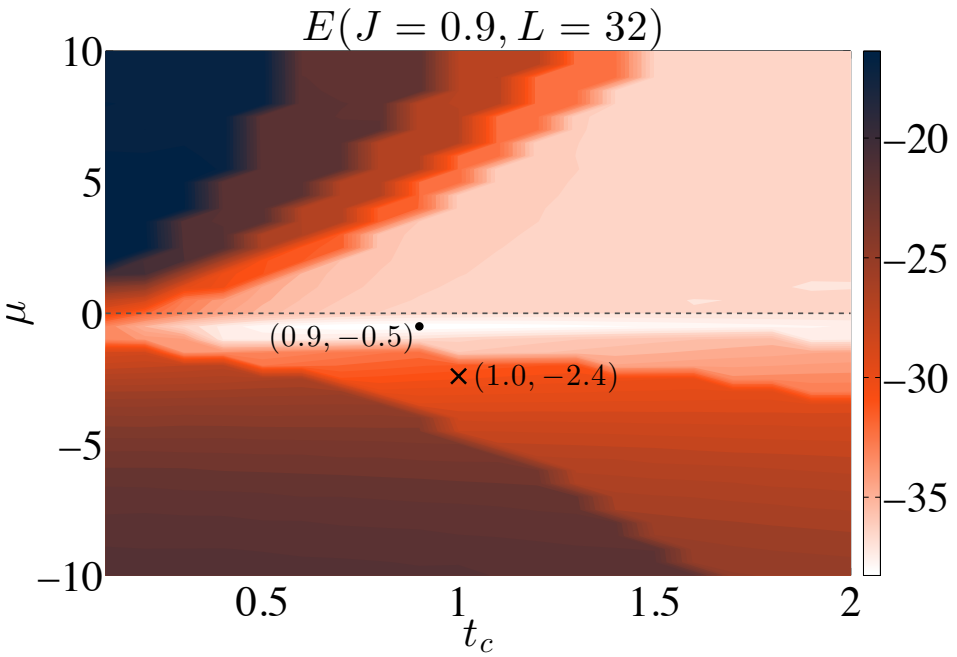

Figure 4.14: Energy landscape of SBM trial states versus t_c and μ for a $L = 32$ PBC system at $J = 0.9$. The point marked by $\cdot$ is the energy-optimized state, while the point marked by $\times$ is the state shown in Fig. 4.5 (see also Fig. 4.13).

Chapter 5

The MPS representation of the Gutzwiller variational wavefunctions

In this chapter, we investigate a new approach to the Gutzwiller projection formalism for QSLs. We introduce a new tensor network method, in which we combine the illustrative nature of the fermionic variational methods with the strength of tensor networks to capture the properties of the exact state. This is achieved by generating an efficient matrix product state (MPS) representation of the variational wavefunction. The MPS representation could then be used in any MPS–based tensor network algorithm such as the usual DMRG. In addition to its theoretical appeal, the remarkable efficiency of this method makes it a powerful tool to attack both gapped and gapless QSLs.

5.1 MPS for Gutzwiller projected states

In this section we discuss possible approaches to generate MPS representations for Gutzwiller projected variational wavefunctions. We introduce an efficient method which we call *Gutzwiller zipper* and comment on the complexity, scaling and shortcomings of the methods.

Let us start by describing the setup in more detail. The system has L sites labeled by $i = 1, \ldots, L$, where each site hosts a spin–1/2 local Hilbert space $h_{1/2} = \{|\uparrow\rangle, |\downarrow\rangle\}$. We would like to describe a particular variational spin state defined through the Gutzwiller projection over the Hilbert space of the system $\mathcal{H}_{1/2} = \bigotimes_i h_{i,1/2}$. That is to define two distinct two dimensional local Hilbert spaces, *parton Hilbert space* $h_{i,\uparrow}, h_{i,\downarrow}$ on each site with the corresponding global Hilbert spaces $\mathcal{H}_\uparrow = \bigotimes_i h_{i,\uparrow}$ and $\mathcal{H}_\downarrow = \bigotimes_i h_{i,\downarrow}$.

The starting point is two MPS representaion of spin-less fermionic theories over the two parton Hilbert spaces, which here we refer to as *parton MPS*s. The process of Gutzwiller projection works regardless of the nature of parton MPSs. The parton MPSs can be copies of the same guassian fermionic theories as were used traditionally to construct spin liquid states or different states as long as the entanglement is relatively contained (area law or similar). Indeed, in our work and for the purpose of illustrations we only consider copies of ground states of Gaussian fermionic theories. These parton MPSs have been derived using a unitary circuit applied to some initial tensor product configuration, for example in the z-component basis of the spin-1/2. The simple unitary quantum circuits relation between given Gaussian states and trivial tensor product states have been studied in state preparation quantum information community [40, 141] and tensor network community [60].

The detail of the process in the context of MPS is outlined in ref. [142], where the NN unitary operators found from approximate diagonalization of the correlation matrix $\Lambda_{ij} = \langle c_i^\dagger c_j \rangle$ are called Gaussian MPS or GMPS. For our purposes we consider this representation to be almost exact. This is because with little computational effort the error at this stage can be chosen to be orders of magnitude smaller than the truncation errors occur at later stages of the method. The truncation becomes necessary during the application of unitary operators on the initial configuration MPS that unavoidably increase the bond dimension of MPS. The parton MPSs are given as

$$\mathcal{H}_\uparrow \ni |\psi_\uparrow\rangle = \sum_{\{\alpha\}} A_1^{\alpha_1} \cdots A_L^{\alpha_L} |\alpha_1 \ldots \alpha_L\rangle \tag{5.1}$$

$$\mathcal{H}_\downarrow \ni |\psi_\downarrow\rangle = \sum_{\{\beta\}} B_1^{\beta_1} \cdots B_L^{\beta_L} |\beta_1 \ldots \beta_L\rangle \tag{5.2}$$

The parameter that controls the truncation here is the bond dimension of the parton MPSs, which we denote by m. The final entanglement of the Gutzwiller projected MPS is inherited from the original entanglement in the MPS representation for Slater determinants, as a result the parton MPSs should be reasonably converged. The measure of convergence should be the entanglement in the state and not convergence of some small support correlation function. This is because small support correlation functions are expected to converge much faster (even more so if some averaging is performed, as in when one is looking at them in the Fourier space) than total entanglement. However, the entanglement convergence guarantees the convergence of all correlation functions. In practice, a bond dimension of a few hundreds appears to be sufficient for the QSLs that we use here for the illustrations on cylindrical boundary conditions (open boundary condition in x–direction, and periodic in y–direction). Particularly, for the 4–leg triangular ladder of size $L = 4 \times 50$ a

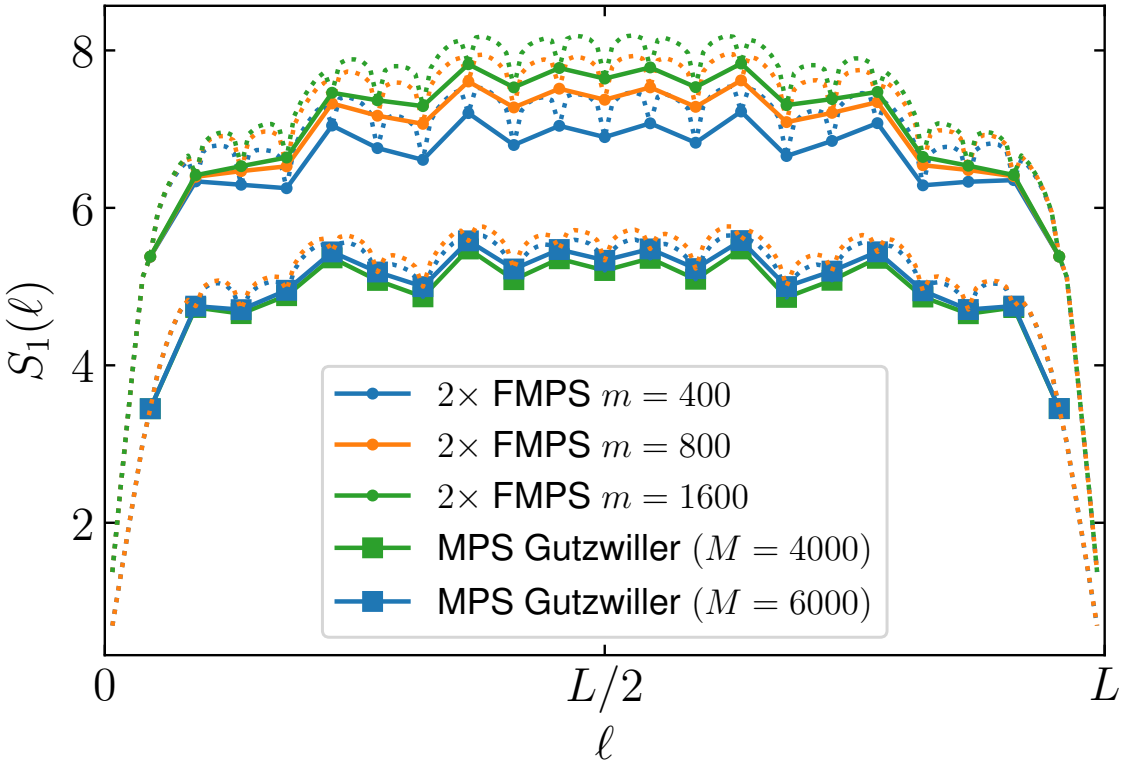

Figure 5.1: The entanglement entropy for two species of the ground state of isotropic hopping on a triangular lattice of size 6×22 with cylinder boundary condition for $m = 400, 800, 1600$ and the Gutzwiller projected MPS with $M = 6000$ for $m = 400, 800$. Note that the entanglement of the Guzwiller projected state is inherited. Hence choosing parton MPSs with converged high entanglement is important to achieve a highly entanglement Gutzwiller projected states.

mere bond dimension of $m \lesssim 400$ seems to keep the truncation error $\epsilon \lesssim 10^{-6}$. For systems of roughly the same size the 6–leg ladder requires $m \approx 1000$ to achieve reasonable results (see Fig. 5.1).

The generic process is as follows. We have to first calculate the tensor product MPS while respecting the fermionic anti–comutation relations. The anti–commutation relations are implemented by a fermionic *swap* gate. The swap inserts a minus sign at sectors where the MPS corresponding to both flavors of fermions have odd parity on the remaining tail of

the tensor [32]. It is therefore necessary for the MPS matrices to at least be aware of the $\mathbb{Z}_2$ symmetry sectors corresponding to the fermionic parity. If the theory respects (is expected to respect) a larger symmetry group and efficient tensor network algorithms exist, it is also beneficial to make use of the larger symmetry group. For example, making use of symmetries in tensor networks, specifically MPS/DMRG is now quite standard [144, 145, 34, 128, 129] and free fermion theories without pairing respect a global U(1) symmetry, $f_i \to \mathrm{e}^{\mathrm{i}\phi} f_i$, that labels different sectors of the Hilbert space corresponding to a constant number of fermions. From Jordan–Wigner transformation the global symmetry corresponds to the total magnetization $S^z_{\mathrm{tot}} = \sum_i S^z_i$ sectors of the spin theories. We therefore employ U(1) symmetric tensors to construct such states.

The Gutzwiller projection tensor is then applied on each site reducing the local physical dimension from 4 to 2. The Gutzwiller projection combined with the identification of two single occupancy local states with spin states, $\mathcal{P}_G$ tensor is given by

$$\mathcal{P}_G = |\uparrow\rangle\langle n_\uparrow = 1| + |\downarrow\rangle\langle n_\downarrow = 1|. \tag{5.3}$$

The resulted MPS is then brought back into the canonical form using singular value decomposition. That is to bring all tensors into right– or left–isometry form except for a single tensor that contains the singular values in the center. This tensor is now the center of orthogonality because the set of Schmidt states on the right and left of this tensor form an orthonormal set respectively [118]. One can also follow by a usual approximation step, that is a SVD at the center of orthogonality accompanied by a singular value truncation step. The sum of the truncated singular values is called the truncation error. It corresponds to amplitude of the dismissed states compared to the remaining state.

If the truncation error of the preparation of the parton MPS are ϵ then the tensor product MPS will inherit the same error of ϵ. It seems reasonable to assume that the error of Gutzwiller project state is also of order ϵ. This is not trivial, can we argue that the Gutzwiller singular values have some equal density in the singular values of the original state. [A better argument needs to be made for truncation error of Gutzwiller projected states]. In order to test the truncation error of the Gutzwiller projected state we have tested the fidelity of different Gutzwiller projected states for different values of initial MPS truncation errors, from the Fig () it is clear that the truncation error of Gutzwiller projection grows linearly with parton MPS error.

The above outlined procedure is quite inefficient. To illustrate this let's pick a parton MPSs of bond dimension m. The tensor product MPS has bond dimension m^2 which requires memory of $\mathcal{O}(Ldm^4)$ to store the state. After the Gutzwiller projection the canonicalization step requires SVD which takes $\mathcal{O}(Ldm^6)$. The canonical MPS can then be approximated into a much smaller MPS by truncation. Thus this straightforward approach is near impossible on an ordinary computers even for moderate values of m, that is about a few hundreds. For example, for our available computer with 64GB of memory and 16core - 3GHZ CPU power, we have only tried the $m = 100$ case for a small system of 64 sites for comparison purposes. The interesting question is: can we achieve an approximated state of much smaller size without generating the large tensor product MPS?

In the following we will consider an efficient approach at the expense of introducing more errors in the Gutzwiller projected state.

As long as the tensor product without projection is concerned, there exists an efficient approach that leads to the same final truncated tensor product MPS. The key observation is that if the two starting MPS are in canonical form with the same center of orthogonlaity, then so is the resulting tensor product MPS. That is because the tensor product of two right–/left–isometries is a right–/left–isometry. This allows for a much more efficient but still straightforward method to approximate the tensor product MPS.

We start with the two MPSs in canonical form with the orthogonality center at the first site and bond dimensions m_ℓ at bond ℓ. The final result is an approximation to the tensor product MPS with a bond dimension M_ℓ. At any step ℓ, we follow these steps

(i) (**zip**) Make the matrix C'_ℓ that is the tensor contraction of parton MPSs A_ℓ, B_ℓ, that are tensors with dimensions $(m_{\ell-1} \times d \times m_\ell)$, and the carry from previous step $E_{\ell-1}$ that is a $(M_{\ell-1} \times m_{\ell-1} \times m_{\ell-1})$ tensor as in figure Fig. 5.2 (excluding the Gutzwiller projection). This is just a multiplication step which for the best choice of multiplication order takes approximately $\mathcal{O}(Mm^3)$ or more precisely

$$\mathcal{O}(M_{\ell-1}m_{\ell-1}^2 m_\ell d + M_{\ell-1}m_{\ell-1}m_\ell^2 d^2). \tag{5.4}$$

(ii) (**truncate**) Bundle the physical dimension with the left index of C'_ℓ, perform SVD, $C'_\ell = U_\ell S_\ell V_\ell^\dagger$ and truncate. The SVD is on a $(dM_{\ell-1} \times m_\ell^2)$ matrix, which at best takes

$$\mathcal{O}(\min(d^2 M_{\ell-1}^2 m_\ell^2, dM_{\ell-1}m_\ell^4)) \approx \mathcal{O}(m^2 M^2) \tag{5.5}$$

(iii) Identify U_ℓ as the MPS tensor corresponding to the truncated tensor product MPS at site ℓ, that is $C_\ell \coloneqq U_\ell$,

(iv) Identify $S_\ell V_\ell^\dagger$ as the carry matrix for the next step, that is $E_\ell \coloneqq S_\ell V_\ell^\dagger$

The procedure is initialized by defining $E_0 = I$ and is terminated by reaching the last step and defining $C_L \coloneqq C'_L$. The resulted tensor product MPS is canonical with center at the last site L.

We note that one may be tempted to avoid performing SVD on the full C' matrix by defining the matrix–vector multiplication functions and then feed it to a sparse SVD solver. To analyze the scaling of the matrix–vector multiplication and the sparse SVD method, we start with the best tensor contraction possible for the multiplication to the right vector (see Fig 5.2 bottom part). It can be done in approximately $\mathcal{O}(m^2M)$ or more precisely

$$\mathcal{O}(dm_{\ell-1}m_\ell^2 + d^2m_{\ell-1}^2m_\ell + d^2m_{\ell-1}^2M_{\ell-1}) \tag{5.6}$$

The same multiplication to the left vector again takes approximately $\mathcal{O}(m^2M)$ or more precisely

$$\mathcal{O}(M_{\ell-1}m_{\ell-1}^2 + dm_{\ell-1}^2m_\ell + d^2m_{\ell-1}m_\ell^2) \tag{5.7}$$

so both direction can be done in $\mathcal{O}(m^2M)$ but since we require M_ℓ singular values, we have to perform at least $\mathcal{O}(M)$ number of the above multiplications, which leaves us again with $\mathcal{O}(M^2m^2)$. In practice, this approach works worse than the straightforward method! Generally such approaches are only useful if making the large matrix is more memory consuming or if better scaling matrix–vector multiplication function are available compared to that of the straightforward approach. None of the two reasons applies to the current situation.

We now consider the application of the Gutzwiller projection. For the tensor product MPS, the efficient method is also exactly the correct scheme to approximate the state. For an efficient generation of Gutzwiller projected MPS the following two approaches comes to mind:

1. Generate the truncated tensor product MPS first (by the same method described above) and then apply the Gutzwiller projection tensor.

2. Apply the Gutzwiller projection at the same time during the zip and truncation procedure. That is to include the multiplication by the Guzwiller projection tensor into the definition of C'_{ell} tensor (see Fig. 5.2).

Both of the suggested approaches suffer from some shortcomings. Note that only a tiny part of the wavefunction survives the Gutzwiller projection, because the overlap of the Gutzwiller projected wavefunction with the tensor product state is exponentially small in system size (about $1/2^L$). In the first approach, The effect of this premature truncation of MPS before projection is in general not trivial. Therefore, in a careful study the application of the projection before the truncation step should be preferred. However, we do expect the Gutzwiller projection to require a smaller bond dimension (to achieve up to the same approximation) since it reduces the complexity of the tensor product state.

The second approach performs the truncation after projection but it introduces a source of uncontrolled errors. The problem here is that while the original MPS and the tensor product are all in the canonical form, the Gutzwiller projected part is not. So, in principle the SVD performed at each step is not a Schmidt decomposition of the final wavefunction because the right vectors do not form an orthonormal basis. However, if one

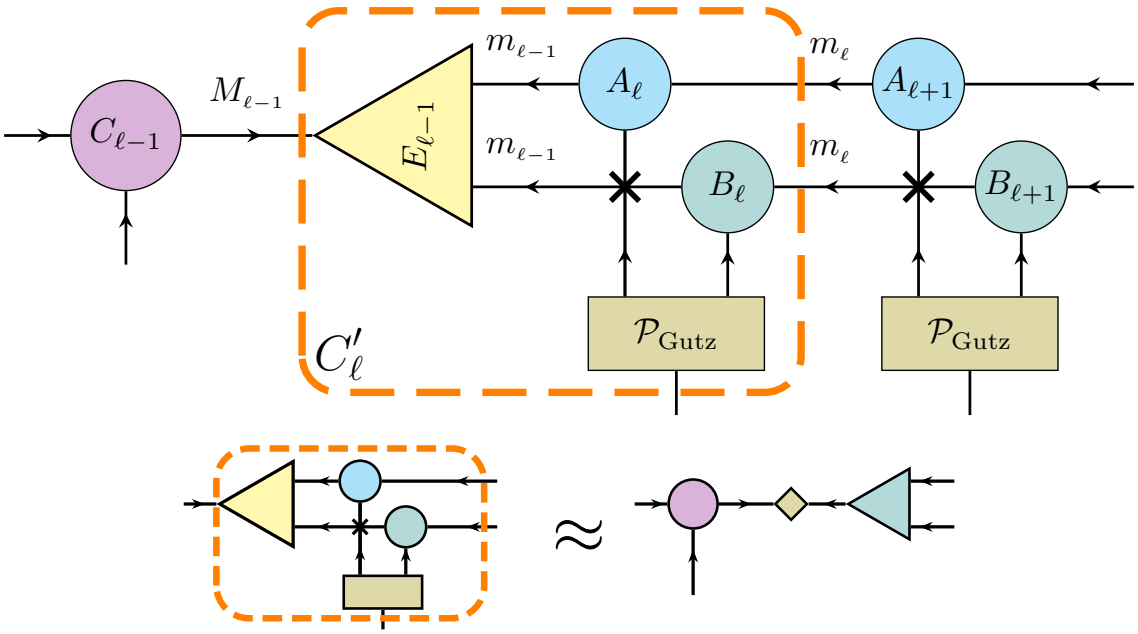

Figure 5.2: Illustration of the ℓth step of the Gutzwiller zipper method. The C'_ℓ tensor is formed by contracting the tensors inside of the dashed box and the undergoes SVD and truncation to make C_ℓ and E_ℓ. Thick cross-out operator indicates the position of fermionic swap. Arrows indicate the isometry direction (The carry tensor E_ℓ is not an isometry). The left part of site ℓ are all left–isometry tensors, however note that while the parton tensors are chosen to be right isometry on the right side of side ℓ, the right part of the full MPS is not right–isometry due to the presence of the non-trivial Gutzwiller projection operator. Therefore we are not at the center of orthogonality of the Gutzwiller MPS. This is the main source of uncontrolled errors. The svd–truncation step is shown underneath.

fixes the threshold for the truncation error to a small enough value, in practice, the final MPS wavefunction could be found close enough to the target MPS, reducing the magnitude of uncontrolled errors to a reasonable amount.

We will consider the source of errors and a more comprehensive discussion to the section on error analysis.

5.2 The tentative Gapless QSL on traingular lattice

In this section we present some numerical results for the study of gapless spin–liquids using the introduced Gutzwiller zipper method. We comment on the entanglement properties of the generated Gutzwiller state, as well as the state after performing one or two steps of the usual DMRG. Other local properties such as spin–spin correlation functions are also reported. For the DMRG studies the size of the Krylov space is chosen to be small; the number of multiplication for each Lanczos step has been limited to a maximum of 20. A choice of a small size of the Krylov space achieves two important goals. It prevents local over–minimization before a global minimization in the system is reached, and makes the illustration of the convergence more clear, as longer number of operations are required for convergence.

A good example to illustrate the power of Gutzwiller zipper method in practice, is to investigate the tentative gapless quantum spin liquid on triangular lattice. The SU(2)–symmetric spin model Hamiltonian consists of NN Heisenberg AF augmented by the four–spin ring exchange interaction defined on every possible diamond of triangular lattice. There are three possible diamonds per unit cell that are shown in Fig. 5.3. The ring exchange operator is defined by its circular shift action on the spins. For any chosen basis, the action is $P_{ijkl}|\sigma_i\sigma_j\sigma_k\sigma_l\rangle = |\sigma_l\sigma_i\sigma_j\sigma_k\rangle$. We define the Hamiltonian (following the convention of ref. [17]) as

$$H = \sum_{\langle i,j\rangle} 2J_{ij}\ \mathbf{S}_i \cdot \mathbf{S}_j + \sum_{ijkl\in\Diamond} K_{\Diamond}\ (P_{ijkl} + \text{h.c.}) \tag{5.8}$$

Where we study 4–leg and 6–leg lattices for the fully isotropic model where all Js and all Ks are equal. A well–known result for the 2–leg ladder is also included for comparison purposes. At $K = 0$ the Heisenberg AF model on the triangular lattice is known to be in 120 degree ordered phase. With the introduction of K terms it has been suggested that the model initialy transitions into a valence bond solid where patterns of single strong bond (close to singlet) per each triangle form on the lattice. As we increase K/J, it is reasonable to expect that the ring exchange term provides enough quantum fluctuation for the singlets to disseminate and realize a spin liquid phase. Indeed, a number of studies suggested that around $K/J \gtrsim 0.3$ this model realizes a gapless quantum spin liquid with incommensurate wavevectors, the so–called spin–Bose metal (SBM) [101, 17]. The quasi-1D systems are then considered to be cuts into the Fermi sea where each cut will correspond to a partially filled 1D band. These theories are labeled as SBM–n where n is the number of partially filled bands.

Since the suggested spin–liquid is a projected Fermi surface spin–liquid, the parton theories are chosen to be described by free fermion hoppings on the same lattice. For a non–chiral periodic spin theory we have the choice of periodic and anti-periodic boundary condition for the fermionic spinons (since the spin is made out of two copies). For systems on a torus (periodic in both directions) the anti–periodic boundary conditions along the larger direction (x) is chosen to avoid degeneracy of fermion theories at half–filling. The anti–periodic boundary condition corresponds to spinons exposed to a π–flux when hopping along a loop in that particular direction. It is worth noting that chiral spin theories can also be generated for an arbitrary boundary condition at the expense of breaking the time–

reversal symmetry, where the two flavors of spinon experience opposite fluxes, i.e. one flavor experiences a θ–flux and the other $(-\theta)$–flux for any $\theta \in [0, \pi]$. For the systems on cylinder, here we only consider periodic boundary condition in the shorter direction (y).

The general scheme of our study is as follows. We first build the spinon MPSs and use the method explained above to build the Gutzwiller projected MPS. We will then perform the regular DMRG initialized by the Gutzwiller MPS and monitor the behavior of the state.

Let us start with the 2–leg ladder where it is well–established that the SBM phase with the central charge of $c = 3$ is realized and is stable in an extended region of the phase diagram [125]. We have picked $t = 1.0, 0.7$ for the Gutzwiller state model and $J = 1.0$, $K = 1.6$ for the spin model to compare the results. The advantage of initializing DMRG with the Gutzwiller state is quite remarkable as is shown in Fig. 5.4. Note that since the entanglement of the Gutzwiller MPS is already high and the MPS is in the right phase, it is quite incredible that only two sweeps of DMRG capture all long and short range properties of the ground state with relatively good accuracy. Meanwhile even 6 sweeps of DMRG has difficulty capturing the entanglement. This is expected because DMRG is a local iterative method, which naturally captures the short range correlations more accurately while it struggles to converge to complicated long range correlation functions. We note that if conclusive studies did not exist for the 2–leg ladder, this behavior could have been taken as strong evidence that the ground state of this Hamiltonian for the 2–leg ladder is the suggested SBM–2 quantum spin liquid. This is indeed the approach we take for this model on wider ladders of size 4, and 6 legs.

We now try to reproduce the previous results found for the of 4–leg triangular ladders. For the parton theories we pick the isotropic hopping $t_1 = t_2 = t_3$. The quasi–1D system has three filled 1D bands so the spin–less theories have a central charge of $c = 3$. The resulting Gutzwiller projected state thus is expected to have $c = 6 - 1 = 5$ where the single species is subtracted because the integration of the gauge field pins the field corresponding to the total charge fluctuations. In Fig. 5.5 we show that decent number of kept states for open boundary conditions suggest the $c = 5$ value for central charge.

As the SBM phase is suggested for $K/J > 0.3$ we pick $J = 1.0$ and $K = 0.6$ that is well inside of the SBM region of phase diagram. If the suggested projected Fermi surface is the correct ground state of the spin model, same as in the 2–leg ladder, we expect that the first few sweeps of DMRG only correct the short–range terms in the Hamiltonian and minimize the energy while keeping the entanglement, the generic long–range property of the state, at the same level. Contrary to the expected behavior for the ground state of a gapless theory we observe the flattening of entanglement entropies cuts in Fig. 5.6. This is a strong evidence that in contrast to the suggested phase diagram, the ground state of this spin model is not the projected Fermi surface. Moreover, the flattening of entanglement entropies for different system sizes is evidence for existence of a gapped state.

5.3 Error analysis of the Gutzwiller zipper method

As we have already mentioned, the efficient Gutzwiller zipper method introduced in this chapter suffers from a mathematical limitation. At any step during the zipping

process the right part of the MPS tensor network does not form an orthonormal basis which is a consequence of the Gutzwiller projection. As a result, the singular values of the tensor at site ℓ are not Schmidt values of actual Gutzwiller projected states and truncating them introduced uncontrolled errors in the process. It is therefore important to analyse the error produced by this method.

Here, we chose to perform the zipping from left to right at each step, ℓ, and keep the left unitary of singular value decomposition as the local MPS tensor the that site. This means that at each step the left part of the tensor is already orthonormal by construction. So in order to find the error generated at that step we need to exactly SVD the tensor network from right and bring the center of orthogonality to site ℓ, that is to make the Gutzwiller contraction and subsequent SVDs exactly on the right side of site ℓ. We will then end up with a tensor of the form shown in Fig. 5.7. This tensor contraction measures the uncontrolled error introduced in this process.

5.4 SBM theory for triangular lattice

A simple chain corresponds to a single cut in the BZ of the 2D system, it should have two Fermi points at $k_f = \pi \mod 2\pi$, and a central charge of $c = 1$. For the two–leg triangular ladder (zig–zag ladder) there are two cuts into the BZ, which correspond to two Fermi seas with two pairs of Fermi points at $\pm k_{f1}, \pm k_{f2}$. Again the Fermi surface has to satsify the sum rule $k_{f1} + k_{f2} = \pi \mod 2\pi$. The two–Fermi–sea SBM theory has been fully studied with its instabilities and it has been shown that the SBM physics is realized on a

two–leg triangular ladder of Heisenberg spin-1/2 in the presence of a sufficiently strong ring exchange interaction.

In Fig. 5.8 we show the BZ of the 4–leg and 6–leg triangular ladders. Based on the above discussion, since we see 3 and 5 cuts into the BZ respectively, it is reasonable to expect that the Gutzwiller state should have the central charge of $c_{(l_y=4)} = 5$ and $c_{(l_y=6)} = 9$. Large scale DMRG calculations can in principle probe these large central charges, however in practice only $c = 5$ is reasonably accessible. Nevertheless, we have shown that for $l_y = 6$ some evidence that the $c = 9$ is indeed the observed Gutzwiller state.

5.5 Gutzwiller zipper in action

For the calculations of the spin structure factors we have mainly used open boundary conditions. However, we have since due to the averaging of the structure factors, there is not a significant difference between open and periodic system. The structure factors are defined as

$$\langle \mathbf{S}_q \cdot \mathbf{S}_{-q} \rangle = \frac{1}{L} \sum_x \mathrm{e}^{-\mathrm{i}qx} \sum_i \langle \mathbf{S}_i \cdot \mathbf{S}_{i+x} \rangle \tag{5.9}$$

The central charge has been calculated using the fitting of the scaling of von Neumann entanglement entropy cuts to the Calabrese–Cardy [23] formula

$$S(\ell, L) = \frac{c}{6} \log \left(\frac{L}{\pi} \sin \frac{\ell \pi}{L} \right) + \cdots \tag{5.10}$$

for the open boundary condition and twice that for system with periodic boundary condition.

5.5.1 Simple 1D chain

In this section we test and benchmark the Gutzwiller tensor network method on a simple chain of spin–1/2 Heisenberg antiferromagnet. The Gutzwiller state in this example is known to be the ground state of the Haldane–Shastry model [123, 51] and is in the same phase as the ground state of Heisenberg antiferromagnet. The model has a long range interacting spin–1/2 interaction on a chain of size L

$$H_{\mathrm{HS}} = \sum_{\ell} \left(\frac{\pi}{L \sin(\pi \ell / L)} \right)^2 \sum_{i} \mathbf{S}_i \cdot \mathbf{S}_{i+\ell} \tag{5.11}$$

Both models are gapless and have a central charge of $c = 1$, and both show a feature of algebraically decaying correlations at the wavevector $k_F = \pi$ which is consistent with the theoretical and numerical prediction of Ref. [125].

5.5.2 The 2–leg triangular ladder (zig–zag ladder)

In this section we try to find the phase diagram of the 2–leg ladder given in detail in Ref. [125] starting from the Gutzwiller mother state. We demonstrate that all the phase diagram of the 2–leg ladder can be achieved despite the fact that the correct parent double–parton fermi surface is not exactly constructed. In principle, one should first minimize the energy (using VMC for example) and construct the correct parent state with the correct(!) fermi surface(points) and perfrom the DMRG on that. However, as we see this is not necessary as the correct state is picked up by the DMRG even without the energy minimization step. This is because all the phase diagram could be though of as an instability of mother state (as long as the correct number bands are filled) and the exact wavevector is not important and it will be picked by a few sweeps of DMRG.

Four of the possible phases in the 2–leg ladder is shown in Fig 5.9. Note that the signature of all phases with apparent from the structure factors and the entanglement entropy, even for very small bond dimensions $M = 300$.

5.5.3 Wider ladders of triangular lattice

Going to larger width ladders, the conjectured phase diagram of 4–leg ladder in Ref. [17] has three separate phases, for isotropic J which we also considered here. The Rung phase which we consider for parameters $K/J = 0.1$, the VBS phase which we consider for parameters $K/J = 0.25$ and the tentative SBM phase which we consier for parameters $K/J = 0.6$.

The different possible conjectured phases of the 4–leg ladder is shown in Fig 5.10. Based on the behavior of entanglement entropy cuts, we conclude that the ground state of the Heisenberg model augmented with the ring exchange is not the SBM theory which is realized for the Gutzwiller state.

For the 4–leg ladder we have also calculated the central charge of the Gutzwiller state for periodic boundary conditions. Despite keeping up to 7200 states for the MPS, the entanglement entropy did not fully converge. However, it seems that the central charge is approaching the expected $c = 5$, see Fig. 5.12

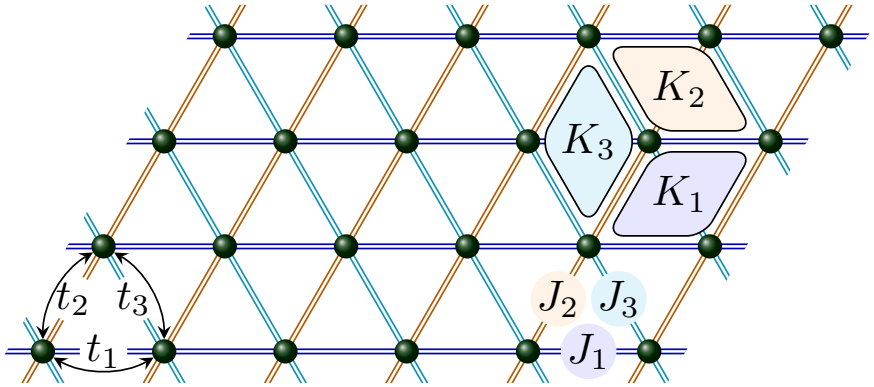

Figure 5.3: The triangular lattice drawn for the size of $L = 4 \times 6$ with periodic boundary conditions. Schematic representation of spin theory operators are depicted on the right. It is believed that this spin model harbors a gapless QSL which well described by a projected Fermi surface. The schematics of hopping amplitudes for the fermionic spinons are shown on the left.

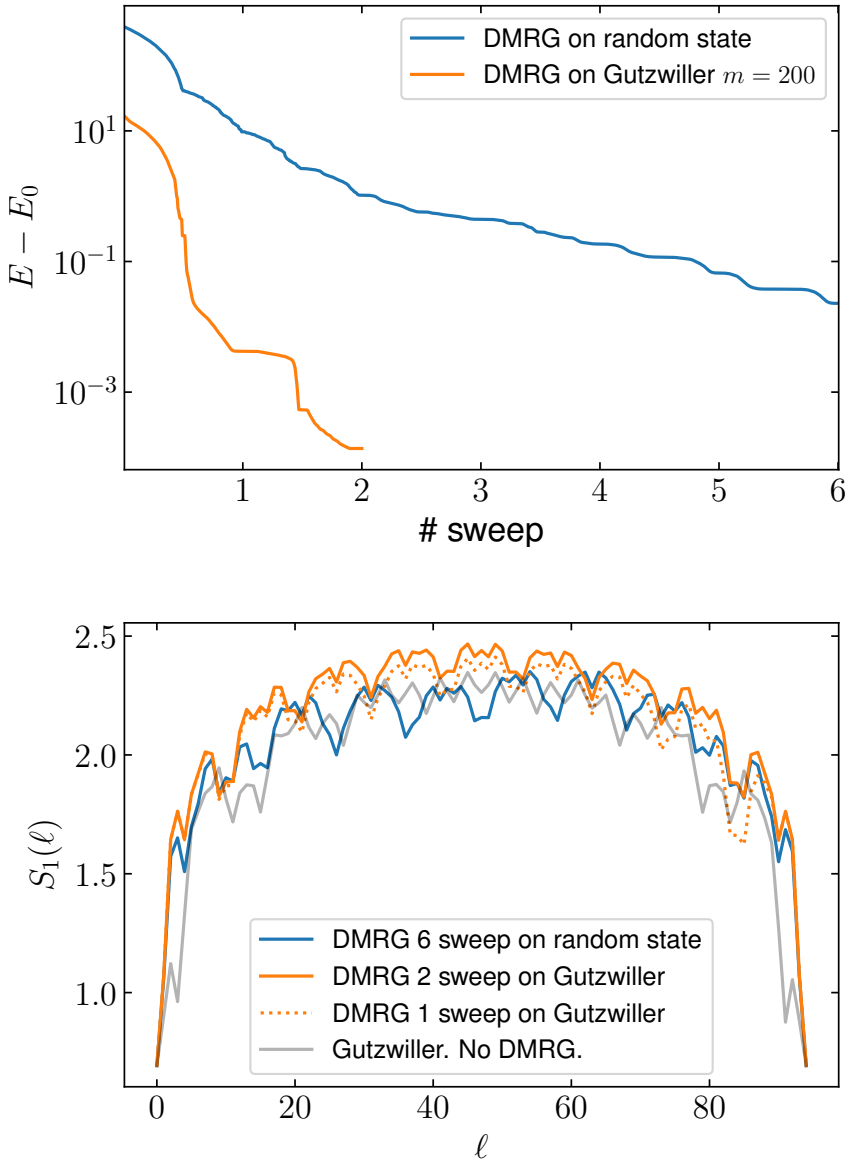

Figure 5.4: For a triangular ladder of size $L = 2 \times 48$. The DMRG has done with $J_2 = J_3 = 1.0$, $J_1 = 0.8$, and $K_1 = 1.0$, a total of $M = 900$ states are kept as the bond dimension of DMRG and Gutzwiller state while the initial parton MPSs has $m = 200$ state each with hopping amplitude $t_2 = t_3 = 1.0$, $t_1 = 0.7$. (top panel) comparison of measured energies during sweeps of DMRG between a random state and the Gutzwiller state. (bottom panel) Entanglement entropies at each cut.

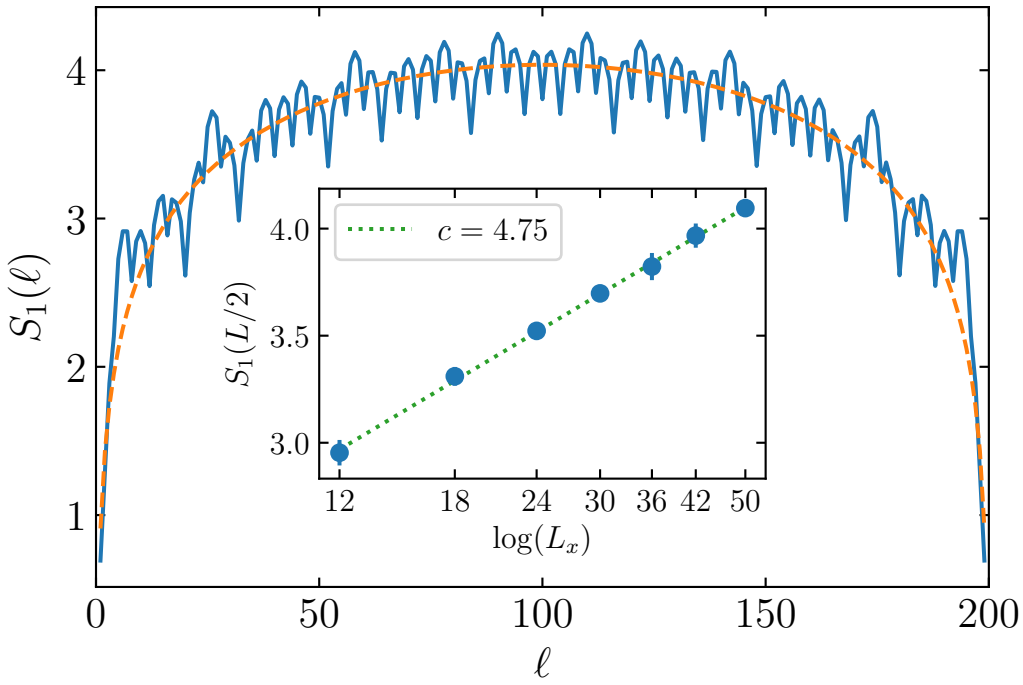

Figure 5.5: The entanglement entropy cuts for various system sizes for the open boundary condition 4–leg ladder on a cylinder. The theory suggests a central charge of $c = 5$. The direct fit on system size of $L = 4 \times 50$ comes out as a central charge of ≈ 4.6 and fit on the average mid–lattice entropies for different sizes show a central charge of ≈ 4.75

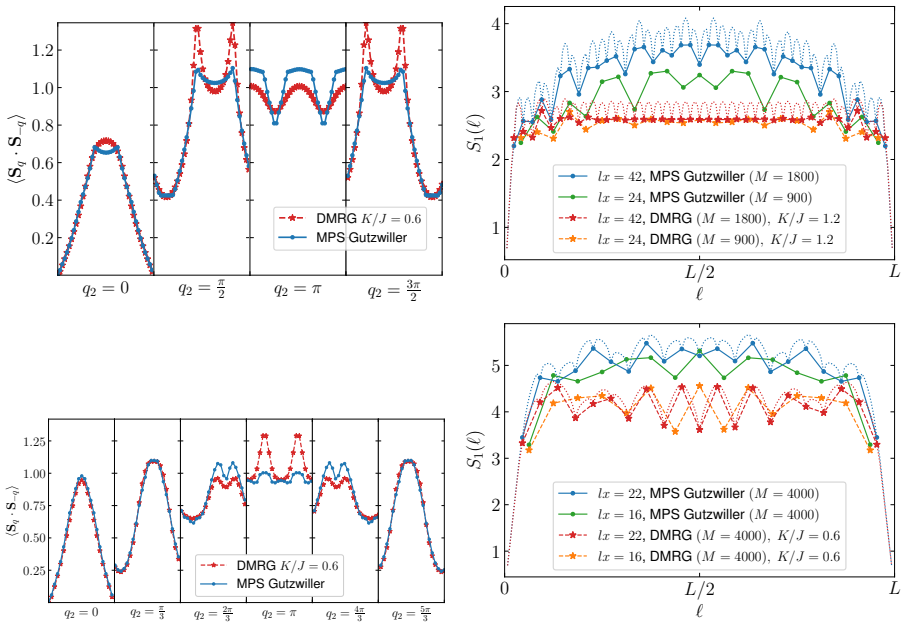

Figure 5.6: The Gutzwiller projected state before and after two sweeps of DMRG. The entanglement entropy has completely flattened and and the spin–spin correlations features are rounded up for the most part. This suggests that the suggested SBM phase is not the correct ground state of 4–leg triangular ladder.

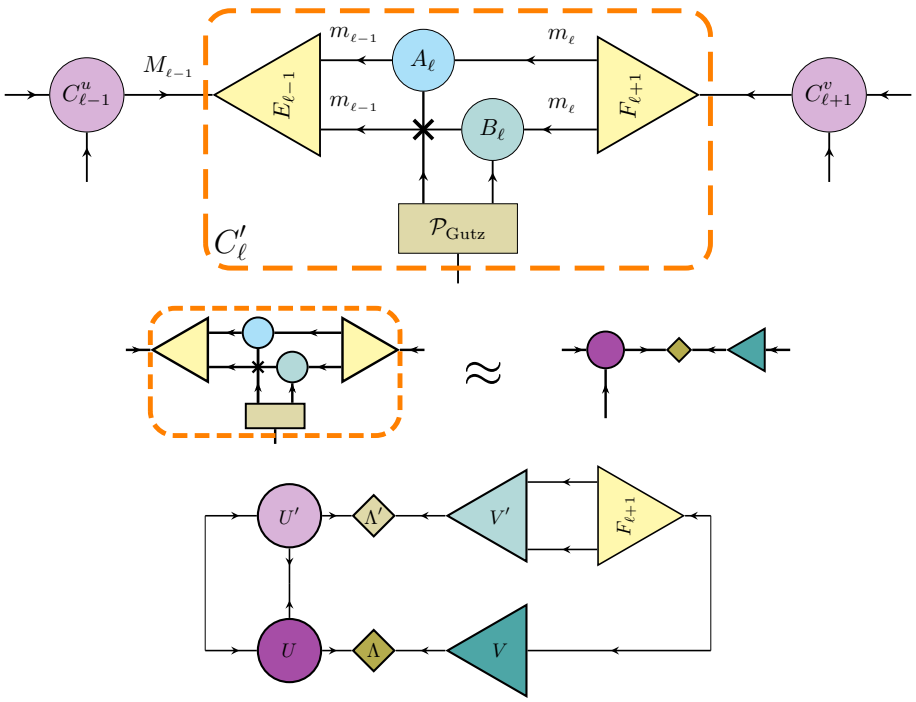

Figure 5.7: (a) The gutzwiller projected MPS tensor network with center of orthogonality at site ℓ, i.e. all tensors on sites on the right/left are right/left isometry when the physical leg is grouped with the right/left leg (b) The generated error can then be calculated. The svd step is the middle figure. Finally the tensor contraction corresponding to fidelity of approximated state at step l compared to doing step ℓ exactly are show underneath. The colors match the svd–truncation figures making the argument easier to follow.

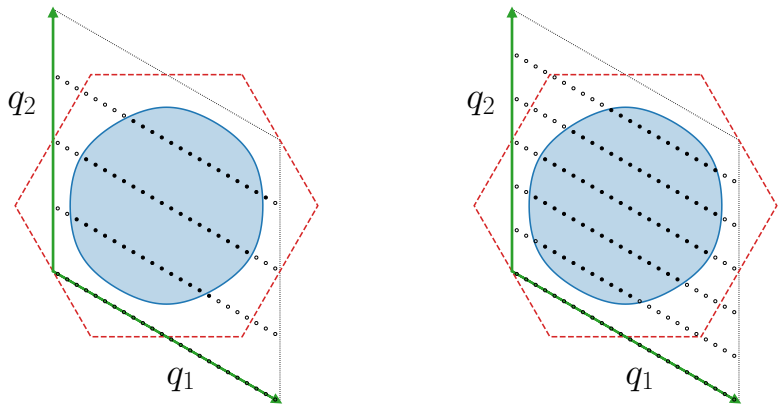

Figure 5.8: The Brillion zone of the 4–leg (left) and 6–leg (right) triangular ladders with 24 sites in the other dimemsion. The halffilling is shown in filled blue colors and the discrete state are filled for the 4×12 and 6×12 sites.

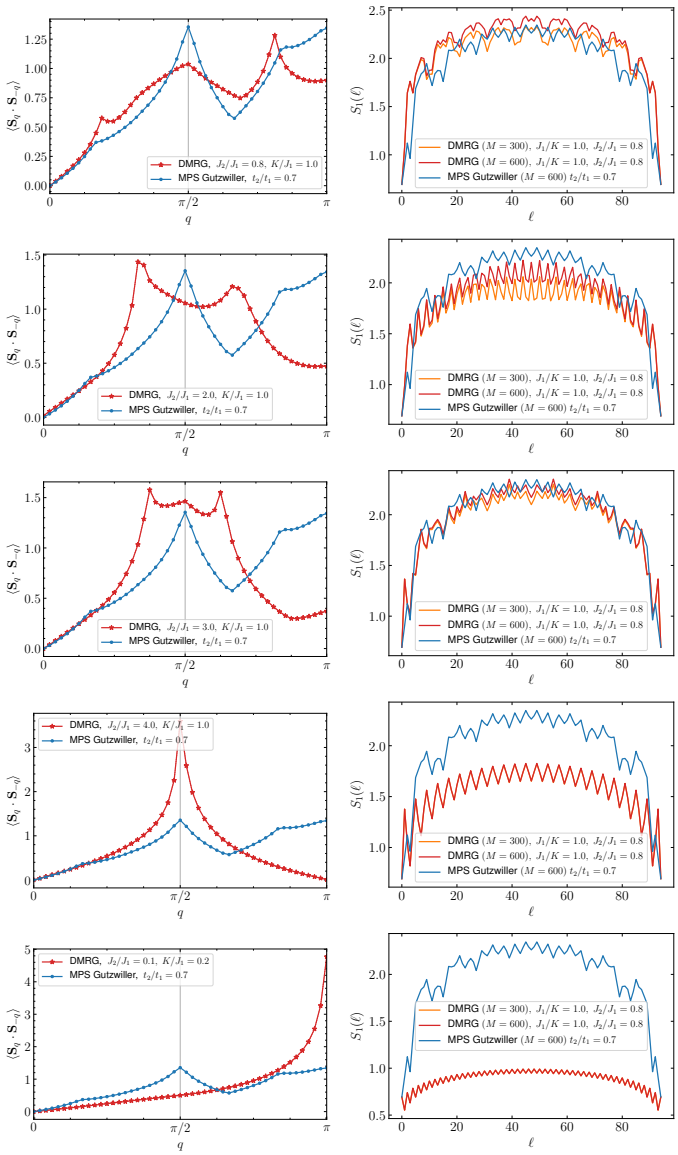

Figure 5.9: Exploring the phase diagram of 2–legs ladder by applying 2 sweeps of DMRG on a single two–band gutzwiller state. The spin–spin structure factors are shown on the left and von Neumann entorpy of system cuts are shown on the right. All rows have $k = j_1$. The first row $j_2/j_1 = 0.8$ corresponds to the large wave–vector SBM, the second row j_2/j_1 correspond to VBS-3 state, the third row corresponds to the $j_2/j_1 = 3.0$ corresponds to the small wave–vector SBM phase between VBS-2 and VBS-3, and the fourth row $j_2/j_1 = 4.0$ corresponds to the VBS-2 state. Note that a drop in the entanglement entropy dome happens when the phase has a lower central charge.

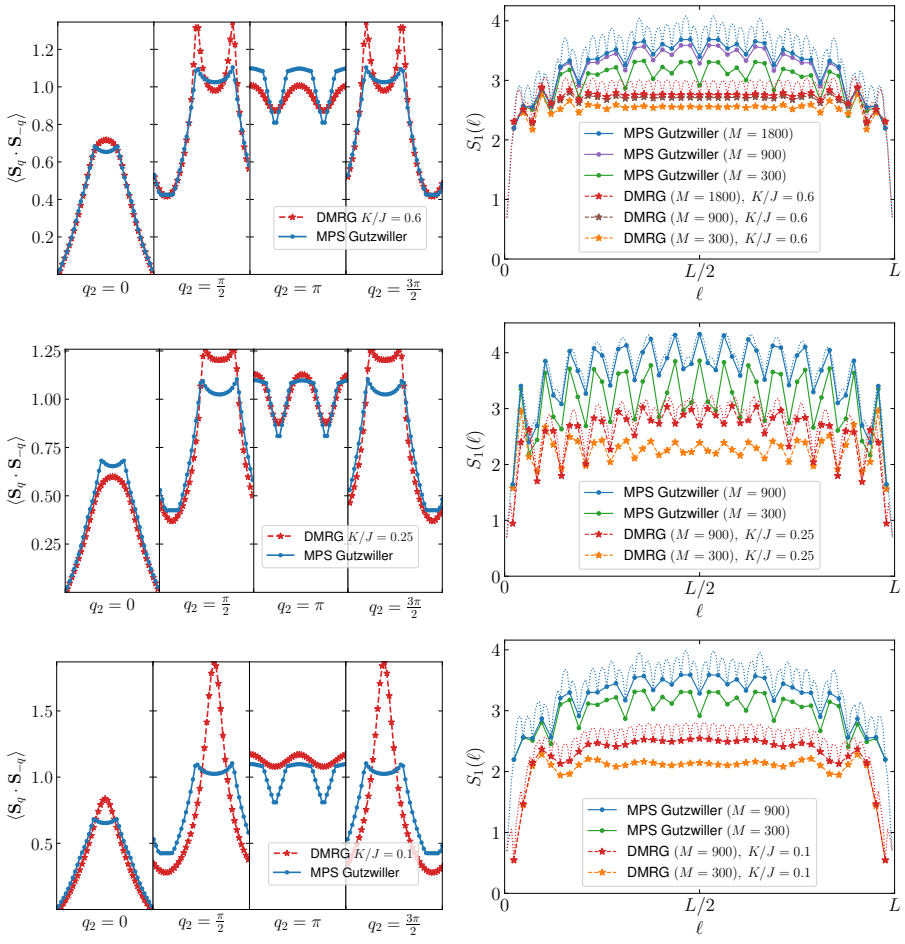

Figure 5.10: Exploring the phase diagram of 4–legs ladder along the line of isotropic J by applying 3 sweeps of DMRG on a single three–band gutzwiller state that is the projection of isotropic hopping fermionic ground states. The spin–spin structure factors are shown on the left and von Neumann entorpy of system cuts are shown on the right. The first row $K/J = 0.6$ corresponds to the tentative SBM phase, the second row $K/J = 0.25$ correspond to VBS state, the third row $K/J = 0.1$ corresponds to the rung state.

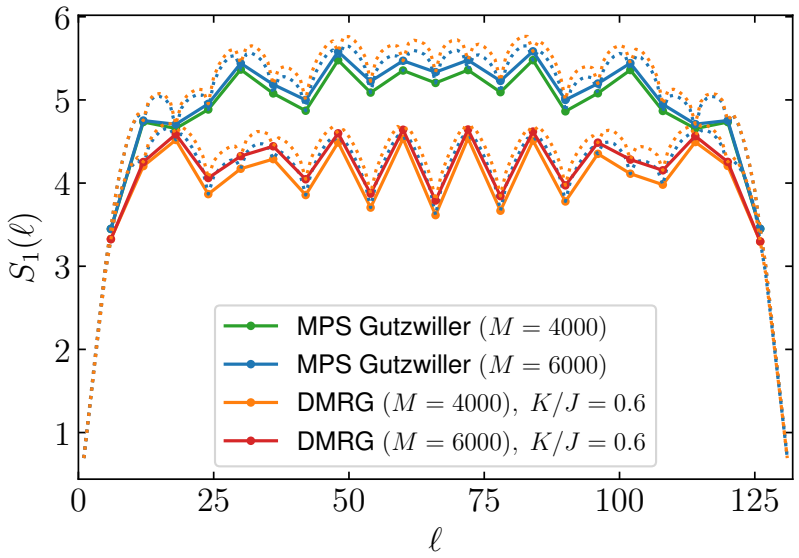

Figure 5.11: von Neumann entropy for a system size of 6×22

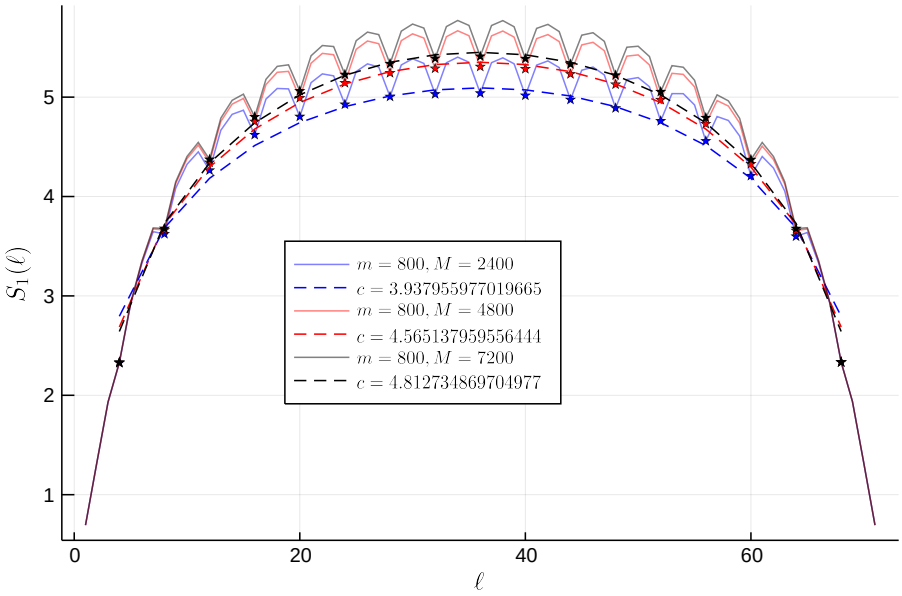

Figure 5.12: von Neumann entropy for a system size of $4times18$ for antiperiodic boundary condition in x–direction and periodic boundary condition in y–direction.

Chapter 6

Conclusion and remarks

The field of quantum spin liquids will remain one of most active areas of research in condensed matter physics for the foreseeable time. This thesis presented two small but significant contributions to this subject.

In chapter 4 we presented a convincing numerical evidence that the ground state of the simple kagome strip Heisenberg model can be described as an intriguing C1S1 spin liquid phase, a marginal instability of the spin Bose metal (i.e., U(1) spinon Fermi surface with no flux) on this ladder. We emphasize that by employing fully controlled numerical and analytical techniques we can understand the realized exotic phase very thoroughly in terms of gapless fermionic spinons—indeed the ability to develop such a complete understanding of an exotic phase of matter in a simple nearest-neighbor Heisenberg spin model is exceedingly rare. We have also demonstrated the contrast between our results and similar $c = 2$ fixed points previously realized in frustrated spin ladders. In particular, our finding is accessed through a non–perturbative description of only nearest neighbor Heisenberg

antiferromagnet, possesses incommensurate wavevectors, and exists as a stable extended quantum phase at zero temperature.

There are multiple questions that still remain to be answered. While the simplest Dirac–spin–liquid–like starting point on this kagome strip leads to a fully gapped state at the mean–field level, it would be interesting to search for other possible two-band scenarios with the hope of connecting our results to recent work suggesting a gapless state in the 2D kagome Heisenberg antiferromagnet [55, 70, 87]. More generally, it is interesting to ask *why* a state such as the C1S1 would be realized in our model: Previous realizations of the spin Bose metal itself involved interactions appropriate for *weak Mott insulators* with substantial charge fluctuations [125, 17, 99], while the simple Heisenberg model of our work is appropriate only in the strong Mott regime. Thus, perhaps our work can give some guidance on realizing exotic spin liquid states with emergent fermionic spinons in simple models of frustrated quantum antiferromagnets.

To investigate the structure change of state going through Gutzwiller projection, in chapter 5 we investigated the MPS representation of the Gutzwiller projection variational wavefunctions and introduced an efficient method to generate large–scale MPSs suitable for the study of spin–liquid states. The Gutzwiller zipper method is an extremely useful alternative to the conventional approaches of VMC and DMRG/ED studies. In a sense, this is an evolved method combining the power of both methods making it more practical in the study of QSLs. A particularly important reason is the fact that the variational wavefunction itself is the outcome of the Gutzwiller zipper algorithm and as a result the

same wavefunction can be fed into any tensor network algorithm of choice. Such comparisons undoubtedly make the derived conclusions more convincing.

Despite the fact that the Gutzwiller zipper method suffers from an orthonormality issue, we have shown that in practice, it performs remarkably well. As a case study we tested this approach on ladders of triangular lattice with an SU(2) symmetric Hamiltonian and disproved the possibility of the SBM phase for a region of the suggested phase diagram in literature.

Finally, we emphasize that while an efficient algorithm focused on matrix product states was presented here, the generalization of such strategies to larger tensor networks may as well be achieved and turn out to be quite useful. A possible extension as an initial step could be an infinite MPS algorithm. Studies of 2D systems on a cylinder with iMPS algorithms are increasingly more common in the community. Therefore, a variational iMPS on a cylinder could open new pathways toward the study of 2D QSLs. The Gutzwiller projection on the 2D tensor networks such as PEPS could also be simply constructed, though much more costly. A thorough investigation of the accuracy and efficiency of methods could also be a future direction.

Bibliography

[1] Ian Affleck, Tom Kennedy, Elliott H. Lieb, and Hal Tasaki. Rigorous results on valence-bond ground states in antiferromagnets. *Phys. Rev. Lett.*, 59:799–802, Aug 1987.

[2] Ian Affleck, Tom Kennedy, Elliott H. Lieb, and Hal Tasaki. Valence bond ground states in isotropic quantum antiferromagnets. *Communications in Mathematical Physics*, 115(3):477–528, Sep 1988.

[3] P. W. Anderson. The resonating valence bond state in la2cuo4 and superconductivity. *Science*, 235(4793):1196–1198, 1987.

[4] P.W. Anderson. Resonating valence bonds: A new kind of insulator? *Mater. Res. Bull.*, 8(2):153–160, 1973.

[5] Frank Arute, Kunal Arya, Ryan Babbush, Dave Bacon, Joseph Bardin, Rami Barends, Rupak Biswas, Sergio Boixo, Fernando Brandao, David Buell, Brian Burkett, Yu Chen, Zijun Chen, Ben Chiaro, Roberto Collins, William Courtney, Andrew Dunsworth, Edward Farhi, Brooks Foxen, and John Martinis. Quantum supremacy using a programmable superconducting processor. *Nature*, 574:505–510, 10 2019.

[6] P. Azaria, C. Hooley, P. Lecheminant, C. Lhuillier, and A. M. Tsvelik. Kagomé lattice antiferromagnet stripped to its basics. *Phys. Rev. Lett.*, 81:1694–1697, Aug 1998.

[7] P. Azaria, P. Lecheminant, and A. A. Nersesyan. Chiral universality class in a frustrated three-leg spin ladder. *Phys. Rev. B*, 58:R8881–R8884, Oct 1998.

[8] L. Balents, M. P. A. Fisher, and S. M. Girvin. Fractionalization in an easy-axis kagome antiferromagnet. *Phys. Rev. B*, 65:224412, May 2002.

[9] Leon Balents. Spin liquids in frustrated magnets. *Nature*, 464:199–208, 2010.

[10] Leon Balents and Matthew P. A. Fisher. Weak-coupling phase diagram of the two-chain hubbard model. *Phys. Rev. B*, 53:12133–12141, May 1996.

[11] B Bauer, L D Carr, H G Evertz, A Feiguin, J Freire, S Fuchs, L Gamper, J Gukelberger, E Gull, S Guertler, A Hehn, R Igarashi, S V Isakov, D Koop, P N Ma, P Mates,

H Matsuo, O Parcollet, G Pawłowski, J D Picon, L Pollet, E Santos, V W Scarola, U Schollwöck, C Silva, B Surer, S Todo, S Trebst, M Troyer, M L Wall, P Werner, and S Wessel. The ALPS project release 2.0: open source software for strongly correlated systems. *Journal of Statistical Mechanics: Theory and Experiment*, 2011(05):P05001, may 2011.

[12] B. Bauer, L. Cincio, B.P. Keller, M. Dolfi, G. Vidal, S. Trebst, and A.W.W. Ludwig. Chiral spin liquid and emergent anyons in a kagome lattice mott insulator. *Nature Communications*, 5(1), Oct 2014.

[13] R. J. Baxter. *Exactly Solved Models in Statistical Mechanics*, pages 5–63. 1985.

[14] A. A. Belavin, A. M. Polyakov, and A. B. Zamolodchikov. Infinite conformal symmetry in two-dimensional quantum field theory. *Nuclear Physics B*, 241(2):333–380, July 1984.

[15] H. Bethe. Zur Theorie der Metalle. *Zeitschrift fur Physik*, 71(3-4):205–226, March 1931.

[16] Samuel Bieri, Laura Messio, Bernard Bernu, and Claire Lhuillier. Gapless chiral spin liquid in a kagome heisenberg model. *Phys. Rev. B*, 92:060407, Aug 2015.

[17] M. S. Block, D. N. Sheng, O. I. Motrunich, and M. P. A. Fisher. Spin Bose-Metal and Valence Bond Solid Phases in a Spin-1/2 Model with Ring Exchanges on a Four-Leg Triangular Ladder. *Physical Review Letters*, 106(15):157202, April 2011.

[18] Matthew S. Block, Ryan V. Mishmash, Ribhu K. Kaul, D. N. Sheng, Olexei I. Motrunich, and Matthew P. A. Fisher. Exotic gapless mott insulators of bosons on multileg ladders. *Phys. Rev. Lett.*, 106:046402, Jan 2011.

[19] C. Broholm, R. J. Cava, S. A. Kivelson, D. G. Nocera, M. R. Norman, and T. Senthil. Quantum spin liquids. *Science*, 367(6475):eaay0668, Jan 2020.

[20] N. Bultinck, M. Mariën, D. J. Williamson, M. B. Şahinoğlu, J. Haegeman, and F. Verstraete. Anyons and matrix product operator algebras. *ArXiv e-prints*, November 2015.

[21] N. Bultinck, D. J. Williamson, J. Haegeman, and F. Verstraete. Fermionic matrix product states and one-dimensional topological phases. *prb*, 95(7):075108, February 2017.

[22] N. Bultinck, D. J. Williamson, J. Haegeman, and F. Verstraete. Fermionic projected entangled-pair states and topological phases. *Journal of Physics A Mathematical General*, 51(2):025202, January 2018.

[23] P. Calabrese and J. Cardy. Entanglement entropy and quantum field theory. *Journal of Statistical Mechanics: Theory and Experiment*, 6:06002, June 2004.

[24] P. Calabrese and J. Cardy. Entanglement entropy and conformal field theory. *Journal of Physics A Mathematical General*, 42:504005, December 2009.

[25] Davide Castelvecchi. Quantum computers ready to leap out of the lab in 2017. *Nature*, 541:9–10, 01 2017.

[26] D. Ceperley, G. V. Chester, and M. H. Kalos. Monte carlo simulation of a many-fermion study. *Phys. Rev. B*, 16:3081–3099, Oct 1977.

[27] Hitesh J. Changlani, Dmitrii Kochkov, Krishna Kumar, Bryan K. Clark, and Eduardo Fradkin. Macroscopically degenerate exactly solvable point in the spin-1/2 kagome quantum antiferromagnet. *Phys. Rev. Lett.*, 120:117202, Mar 2018.

[28] Eric Chitambar, Debbie Leung, Laura Mančinska, Maris Ozols, and Andreas Winter. Everything you always wanted to know about locc (but were afraid to ask). *Communications in Mathematical Physics*, 328(1):303–326, Mar 2014.

[29] Chung-Pin Chou, Frank Pollmann, and Ting-Kuo Lee. Matrix-product-based projected wave functions ansatz for quantum many-body ground states. *Physical Review B*, 86(4), Jul 2012.

[30] L. Cincio and G. Vidal. Characterizing topological order by studying the ground states on an infinite cylinder. *Physical Review Letters*, 110(6), Feb 2013.

[31] Sidney Coleman and Jeffrey Mandula. All possible symmetries of the s matrix. *Phys. Rev.*, 159:1251–1256, Jul 1967.

[32] Philippe Corboz, Glen Evenbly, Frank Verstraete, and Guifré Vidal. Simulation of interacting fermions with entanglement renormalization. *Physical Review A*, 81(1), Jan 2010.

[33] Eyal Cornfeld, L. Aviad Landau, Kirill Shtengel, and Eran Sela. Entanglement spectroscopy of non-abelian anyons: Reading off quantum dimensions of individual anyons. *Physical Review B*, 99(11), Mar 2019.

[34] A J Daley, C Kollath, U Schollwöck, and G Vidal. Time-dependent density-matrix renormalization-group using adaptive effective hilbert spaces. *Journal of Statistical Mechanics: Theory and Experiment*, 2004(04):P04005, apr 2004.

[35] Stefan Depenbrock, Ian P. McCulloch, and Ulrich Schollwöck. Nature of the spin-liquid ground state of the s=1/2 heisenberg model on the kagome lattice, Aug 2012.

[36] Michele Dolfi, Bela Bauer, Sebastian Keller, Alexandr Kosenkov, Timothée Ewart, Adrian Kantian, Thierry Giamarchi, and Matthias Troyer. Matrix product state applications for the alps project. *Computer Physics Communications*, 185(12):3430–3440, Dec 2014.

[37] W. Dür, G. Vidal, and J. I. Cirac. Three qubits can be entangled in two inequivalent ways. *pra*, 62(6):062314, December 2000.

[38] Richard P Feynman. Simulating physics with computers. *International journal of theoretical physics*, 21(6/7):467–488, 1982.

[39] Matthew P. A. Fisher and Leonid I. Glazman. Transport in a one-dimensional luttinger liquid, 1996.

[40] M. T. Fishman and S. R. White. Compression of correlation matrices and an efficient method for forming matrix product states of fermionic Gaussian states. *prb*, 92(7):075132, August 2015.

[41] W. M. C. Foulkes, L. Mitas, R. J. Needs, and G. Rajagopal. Quantum monte carlo simulations of solids. *Rev. Mod. Phys.*, 73:33–83, Jan 2001.

[42] Thierry Giamarchi. *Quantum Physics in One Dimension*. Oxford University Press, New York, 2003.

[43] A. O. Gogolin, A. A. Nersesyan, and A. M. Tsvelik. Bosonization and strongly correlated systems, 1999.

[44] Shou-Shu Gong, Wei Zhu, Leon Balents, and D. N. Sheng. Global phase diagram of competing ordered and quantum spin-liquid phases on the kagome lattice. *Phys. Rev. B*, 91:075112, Feb 2015.

[45] Shou-Shu Gong, Wei Zhu, and D. N. Sheng. Emergent chiral spin liquid: Fractional quantum hall effect in a kagome heisenberg model. *Scientific Reports*, 4(1), Sep 2014.

[46] D. Gottesman. An Introduction to Quantum Error Correction and Fault-Tolerant Quantum Computation. *ArXiv e-prints*, April 2009.

[47] Claudius Gros. Physics of projected wavefunctions. *Annals of Physics*, 189(1):53 – 88, 1989.

[48] J. Haegeman, J. I. Cirac, T. J. Osborne, I. Pižorn, H. Verschelde, and F. Verstraete. Time-Dependent Variational Principle for Quantum Lattices. *Physical Review Letters*, 107(7):070601, August 2011.

[49] J. Haegeman, M. Mariën, T. J. Osborne, and F. Verstraete. Geometry of matrix product states: Metric, parallel transport, and curvature. *Journal of Mathematical Physics*, 55(2):021902, February 2014.

[50] Jutho Haegeman, Christian Lubich, Ivan Oseledets, Bart Vandereycken, and Frank Verstraete. Unifying time evolution and optimization with matrix product states. *Physical Review B*, 94(16), Oct 2016.

[51] F. D. M. Haldane. Exact jastrow-gutzwiller resonating-valence-bond ground state of the spin-$\frac{1}{2}$ antiferromagnetic heisenberg chain with $1/r^2$ exchange. *Phys. Rev. Lett.*, 60:635–638, Feb 1988.

[52] F. D. M. Haldane. Model for a quantum hall effect without landau levels: Condensed-matter realization of the "parity anomaly". *Phys. Rev. Lett.*, 61:2015–2018, Oct 1988.

[53] M. B. Hastings. Dirac structure, rvb, and goldstone modes in the kagomé antiferromagnet. *Phys. Rev. B*, 63:014413, Dec 2000.

[54] Wen-Yu He, Xiao Yan Xu, Gang Chen, K.T̃. Law, and Patrick A. Lee. Spinon fermi surface in a cluster mott insulator model on a triangular lattice and possible application to 1t-tas2. *Physical Review Letters*, 121(4), Jul 2018.

[55] Y.-C. He, M. P. Zaletel, M. Oshikawa, and F. Pollmann. Signatures of Dirac Cones in a DMRG Study of the Kagome Heisenberg Model. *Physical Review X*, 7(3):031020, July 2017.

[56] Yin-Chen He, D. N. Sheng, and Yan Chen. Obtaining topological degenerate ground states by the density matrix renormalization group. *Phys. Rev. B*, 89:075110, Feb 2014.

[57] Michael Hermele, Ying Ran, Patrick A. Lee, and Xiao-Gang Wen. Properties of an algebraic spin liquid on the kagome lattice. *Physical Review B*, 77(22), Jun 2008.

[58] Michael Hermele, T. Senthil, Matthew P. A. Fisher, Patrick A. Lee, Naoto Nagaosa, and Xiao-Gang Wen. Stability of $u(1)$ spin liquids in two dimensions. *Phys. Rev. B*, 70:214437, Dec 2004.

[59] C. Hubig, I. P. McCulloch, and U. Schollwöck. Generic construction of efficient matrix product operators. *Physical Review B*, 95(3), Jan 2017.

[60] Katharine Hyatt, James R. Garrison, and Bela Bauer. Extracting entanglement geometry from quantum states. *Physical Review Letters*, 119(14), Oct 2017.

[61] Yasir Iqbal, Federico Becca, and Didier Poilblanc. Projected wave function study of Z_2 spin liquids on the kagome lattice for the spin-$\frac{1}{2}$ quantum heisenberg antiferromagnet. *Phys. Rev. B*, 84:020407, Jul 2011.

[62] Yasir Iqbal, Federico Becca, Sandro Sorella, and Didier Poilblanc. Gapless spin-liquid phase in the kagome spin-$\frac{1}{2}$ heisenberg antiferromagnet. *Phys. Rev. B*, 87:060405, Feb 2013.

[63] Yasir Iqbal, Didier Poilblanc, and Federico Becca. Vanishing spin gap in a competing spin-liquid phase in the kagome heisenberg antiferromagnet. *Phys. Rev. B*, 89:020407, Jan 2014.

[64] Yasir Iqbal, Didier Poilblanc, and Federico Becca. Spin-$\frac{1}{2}$ heisenberg J_1-J_2 antiferromagnet on the kagome lattice. *Phys. Rev. B*, 91:020402, Jan 2015.

[65] Yasir Iqbal, Didier Poilblanc, and Federico Becca. Comment on "z_2 spin liquid phase on the kagome lattice: a new saddle point", by tao li [arxiv:1601.02165 (2016)], 2016.

[66] Sergei V. Isakov, Matthew B. Hastings, and Roger G. Melko. Topological entanglement entropy of a bose–hubbard spin liquid. *Nature Physics*, 7(10):772–775, Jul 2011.

[67] H. C. Jiang, Z. Y. Weng, and D. N. Sheng. Density matrix renormalization group numerical study of the kagome antiferromagnet. *Phys. Rev. Lett.*, 101:117203, Sep 2008.

[68] Hong-Chen Jiang, Matthew S. Block, Ryan V. Mishmash, James R. Garrison, D. N. Sheng, Olexei I. Motrunich, and Matthew P. A. Fisher. Non-fermi-liquid d-wave metal phase of strongly interacting electrons. *Nature*, 493(7430):39–44, Dec 2012.

[69] Hong-Chen Jiang, Zhenghan Wang, and Leon Balents. Identifying topological order by entanglement entropy. *Nature Physics*, 8(12):902–905, Nov 2012.

[70] Shenghan Jiang, Panjin Kim, Jung Hoon Han, and Ying Ran. Competing spin liquid phases in the s=$\frac{1}{2}$ heisenberg model on the kagome lattice. *SciPost Physics*, 7(1), Jul 2019.

[71] CL Kane. Lectures on bosonization. *Boulder Summer School lectures*, 2005.

[72] T. Karzig, C. Knapp, R. M. Lutchyn, P. Bonderson, M. B. Hastings, C. Nayak, J. Alicea, K. Flensberg, S. Plugge, Y. Oreg, C. M. Marcus, and M. H. Freedman. Scalable designs for quasiparticle-poisoning-protected topological quantum computation with Majorana zero modes. *prb*, 95(23):235305, June 2017.

[73] A. Kitaev and J. Preskill. Topological Entanglement Entropy. *Physical Review Letters*, 96(11):110404, March 2006.

[74] Alexei Kitaev. Anyons in an exactly solved model and beyond. *Annals of Physics*, 321(1):2 – 111, 2006. January Special Issue.

[75] A.Yu. Kitaev. Fault-tolerant quantum computation by anyons. *Annals of Physics*, 303(1):2–30, Jan 2003.

[76] Wing-Ho Ko, Hong-Chen Jiang, Jeffrey G. Rau, and Leon Balents. Ordering and criticality in an underscreened kondo chain. *Phys. Rev. B*, 87:205107, May 2013.

[77] F. Kolley, S. Depenbrock, I. P. McCulloch, U. Schollwöck, and V. Alba. Phase diagram of the J_1-J_2 heisenberg model on the kagome lattice. *Phys. Rev. B*, 91:104418, Mar 2015.

[78] C. Krumnow, J. Eisert, and Ö. Legeza. Towards overcoming the entanglement barrier when simulating long-time evolution, 2019.

[79] T. D. Ladd, F. Jelezko, R. Laflamme, Y. Nakamura, C. Monroe, and J. L. O'Brien. Quantum computers. *Nature*, 464(7285):45–53, Mar 2010.

[80] Hsin-Hua Lai and Olexei I. Motrunich. Effects of impurities in spin bose-metal phase on a two-leg triangular strip. *Phys. Rev. B*, 79:235120, Jun 2009.

[81] Hsin-Hua Lai and Olexei I. Motrunich. Two-band electronic metal and neighboring spin bose-metal on a zigzag strip with longer-ranged repulsion. *Phys. Rev. B*, 81:045105, Jan 2010.

[82] Patrick A. Lee, Naoto Nagaosa, and Xiao-Gang Wen. Doping a mott insulator: Physics of high-temperature superconductivity. *Rev. Mod. Phys.*, 78:17–85, Jan 2006.

[83] Sung-Sik Lee. Stability of the u(1) spin liquid with a spinon fermi surface in $2+1$ dimensions. *Phys. Rev. B*, 78:085129, Aug 2008.

[84] Sung-Sik Lee. Low-energy effective theory of fermi surface coupled with u(1) gauge field in $2+1$ dimensions. *Phys. Rev. B*, 80:165102, Oct 2009.

[85] Sung-Sik Lee and Patrick A. Lee. U(1) gauge theory of the hubbard model: Spin liquid states and possible application to $\kappa-(\mathrm{BEDT-TTF})_2\mathrm{cu}_2(\mathrm{CN})_3$. *Phys. Rev. Lett.*, 95:036403, Jul 2005.

[86] Michael Levin and Xiao-Gang Wen. Detecting topological order in a ground state wave function. *Physical Review Letters*, 96(11), Mar 2006.

[87] H. J. Liao, Z. Y. Xie, J. Chen, Z. Y. Liu, H. D. Xie, R. Z. Huang, B. Normand, and T. Xiang. Gapless spin-liquid ground state in the $s = 1/2$ kagome antiferromagnet. *Phys. Rev. Lett.*, 118:137202, Mar 2017.

[88] Elliott Lieb and Daniel Mattis. Ordering energy levels of interacting spin systems. *J. Math. Phys.*, 3(4):749–751, 1962.

[89] Hsiu-Hau Lin, Leon Balents, and Matthew P. A. Fisher. n-chain hubbard model in weak coupling. *Phys. Rev. B*, 56:6569–6593, Sep 1997.

[90] Andreas W W Ludwig, Didier Poilblanc, Simon Trebst, and Matthias Troyer. Two-dimensional quantum liquids from interacting non-abelian anyons. *New Journal of Physics*, 13(4):045014, Apr 2011.

[91] Amir M-Aghaei, Bela Bauer, Kirill Shtengel, and Ryan V. Mishmash. Signatures of gapless fermionic spinons on a strip of the kagome heisenberg antiferromagnet. *Physical Review B*, 98(5), Aug 2018.

[92] Ookie Ma and J. B. Marston. Weak ferromagnetic exchange and anomalous specific heat in $\mathrm{zncu}_3(\mathrm{OH})_6\mathrm{cl}_2$. *Phys. Rev. Lett.*, 101:027204, Jul 2008.

[93] George B Martins and Wolfram Brenig. Static holes in the geometrically frustrated bow-tie ladder. *Journal of Physics: Condensed Matter*, 20(41):415204, sep 2008.

[94] I. P. McCulloch. Infinite size density matrix renormalization group, revisited, 2008.

[95] Max A. Metlitski and Subir Sachdev. Quantum phase transitions of metals in two spatial dimensions. i. ising-nematic order. *Phys. Rev. B*, 82:075127, Aug 2010.

[96] Ashley Milsted, Jutho Haegeman, Tobias J. Osborne, and Frank Verstraete. Variational matrix product ansatz for nonuniform dynamics in the thermodynamic limit. *Physical Review B*, 88(15), Oct 2013.

[97] Ryan V. Mishmash, Matthew S. Block, Ribhu K. Kaul, D. N. Sheng, Olexei I. Motrunich, and Matthew P. A. Fisher. Bose metals and insulators on multileg ladders with ring exchange. *Physical Review B*, 84(24), Dec 2011.

[98] Ryan V. Mishmash, Matthew S. Block, Ribhu K. Kaul, D. N. Sheng, Olexei I. Motrunich, and Matthew P. A. Fisher. Bose metals and insulators on multileg ladders with ring exchange. *Phys. Rev. B*, 84:245127, Dec 2011.

[99] Ryan V. Mishmash, Iván González, Roger G. Melko, Olexei I. Motrunich, and Matthew P. A. Fisher. Continuous mott transition between a metal and a quantum spin liquid. *Physical Review B*, 91(23), Jun 2015.

[100] R. Moessner and S. L. Sondhi. Resonating valence bond phase in the triangular lattice quantum dimer model. *Phys. Rev. Lett.*, 86:1881–1884, Feb 2001.

[101] Olexei I. Motrunich. Variational study of triangular lattice spin-1/2 model with ring exchanges and spin liquid state in $\kappa-(\mathrm{ET})_2\mathrm{cu}_2(\mathrm{CN})_3$. *Phys. Rev. B*, 72:045105, Jul 2005.

[102] N. Nagaosa. *Quantum field theory in strongly correlated electronic systems*. 1999.

[103] Engineering National Academies of Sciences and Medicine. *Quantum Computing: Progress and Prospects*. The National Academies Press, Washington, DC, 2019.

[104] Tai-Kai Ng, Shaojin Qin, and Zhao-Bin Su. Density-matrix renormalization-group study of s=1/2 heisenberg spin chains: Friedel oscillations and marginal system-size effects. *Phys. Rev. B*, 54:9854–9861, Oct 1996.

[105] Michael A. Nielsen and Isaac L. Chuang. *Quantum Computation and Quantum Information*. Cambridge University Press, 2000.

[106] M. R. Norman. Colloquium: Herbertsmithite and the search for the quantum spin liquid. *Rev. Mod. Phys.*, 88:041002, Dec 2016.

[107] B. Odom, D. Hanneke, B. D'Urso, and G. Gabrielse. New measurement of the electron magnetic moment using a one-electron quantum cyclotron. *Phys. Rev. Lett.*, 97:030801, Jul 2006.

[108] R. Orús. A practical introduction to tensor networks: Matrix product states and projected entangled pair states. *Annals of Physics*, 349:117–158, October 2014.

[109] Sebastian Paeckel, Thomas Köhler, Andreas Swoboda, Salvatore R. Manmana, Ulrich Schollwöck, and Claudius Hubig. Time-evolution methods for matrix-product states. *Annals of Physics*, 411:167998, Dec 2019.

[110] Ingo Peschel. Calculation of reduced density matrices from correlation functions. *Journal of Physics A: Mathematical and General*, 36(14):L205–L208, Mar 2003.

[111] F. Pollmann, A. M. Turner, E. Berg, and M. Oshikawa. Entanglement spectrum of a topological phase in one dimension. *prb*, 81(6):064439, February 2010.

[112] Ying Ran, Michael Hermele, Patrick A. Lee, and Xiao-Gang Wen. Projected-wave-function study of the spin-1/2 heisenberg model on the kagomé lattice. *Phys. Rev. Lett.*, 98:117205, Mar 2007.

[113] N Read and Bulbul Chakraborty. Statistics of the excitations of the resonating-valence-bond state. *Physical review. B, Condensed matter*, 40:7133–7140, 11 1989.

[114] Daniel S. Rokhsar and Steven A. Kivelson. Superconductivity and the quantum hard-core dimer gas. *Phys. Rev. Lett.*, 61:2376–2379, Nov 1988.

[115] Subir Sachdev. Kagome´- and triangular-lattice heisenberg antiferromagnets: Ordering from quantum fluctuations and quantum-disordered ground states with unconfined bosonic spinons. *Phys. Rev. B*, 45:12377–12396, Jun 1992.

[116] A. W. Sandvik. Computational Studies of Quantum Spin Systems. In A. Avella and F. Mancini, editors, *American Institute of Physics Conference Series*, volume 1297 of *American Institute of Physics Conference Series*, pages 135–338, November 2010.

[117] Lucile Savary and Leon Balents. Quantum spin liquids: a review. *Reports on Progress in Physics*, 80(1):016502, Nov 2016.

[118] U. Schollwöck. The density-matrix renormalization group in the age of matrix product states. *Annals of Physics*, 326:96–192, January 2011.

[119] N. Schuch, I. Cirac, and D. Pérez-García. PEPS as ground states: Degeneracy and topology. *Annals of Physics*, 325:2153–2192, October 2010.

[120] N. Schuch, D. Pérez-García, and I. Cirac. Classifying quantum phases using matrix product states and projected entangled pair states. *prb*, 84(16):165139, October 2011.

[121] N. Schuch, D. Poilblanc, J. I. Cirac, and D. Perez-Garcia. Topological order in PEPS: Transfer operator and boundary Hamiltonians. *ArXiv e-prints*, October 2012.

[122] T. Senthil. Theory of a continuous mott transition in two dimensions. *Phys. Rev. B*, 78:045109, Jul 2008.

[123] B. Sriram Shastry. Exact solution of an s=1/2 heisenberg antiferromagnetic chain with long-ranged interactions. *Phys. Rev. Lett.*, 60:639–642, Feb 1988.

[124] Yao Shen, Yao-Dong Li, Hongliang Wo, Yuesheng Li, Shoudong Shen, Bingying Pan, Qisi Wang, H. C. Walker, P. Steffens, M. Boehm, and et al. Evidence for a spinon fermi surface in a triangular-lattice quantum-spin-liquid candidate. *Nature*, 540(7634):559–562, Dec 2016.

[125] D. N. Sheng, O. I. Motrunich, and M. P. A. Fisher. Spin Bose-metal phase in a spin-(1)/(2) model with ring exchange on a two-leg triangular strip. *prb*, 79(20):205112, May 2009.

[126] D. N. Sheng, Olexei I. Motrunich, Simon Trebst, Emanuel Gull, and Matthew P. A. Fisher. Strong-coupling phases of frustrated bosons on a two-leg ladder with ring exchange. *Phys. Rev. B*, 78:054520, Aug 2008.

[127] Y. Shimizu, K. Miyagawa, K. Kanoda, M. Maesato, and G. Saito. Spin liquid state in an organic mott insulator with a triangular lattice. *Phys. Rev. Lett.*, 91:107001, Sep 2003.

[128] S. Singh, R. N. C. Pfeifer, and G. Vidal. Tensor network decompositions in the presence of a global symmetry. *pra*, 82(5):050301, November 2010.

[129] S. Singh, R. N. C. Pfeifer, and G. Vidal. Tensor network states and algorithms in the presence of a global U(1) symmetry. *prb*, 83(11):115125, March 2011.

[130] B. Swingle and J. McGreevy. Renormalization group constructions of topological quantum liquids and beyond. *ArXiv e-prints*, July 2014.

[131] Tiamhock Tay and Olexei I. Motrunich. Possible exciton bose liquid in a hard-core boson ring model. *Phys. Rev. Lett.*, 105:187202, Oct 2010.

[132] Tiamhock Tay and Olexei I. Motrunich. Possible realization of the exciton bose liquid phase in a hard-core boson model with ring-only exchange interactions. *Physical Review B*, 83(20), May 2011.

[133] Gérard Toulouse. The frustration model. In Andrzej Pekalski and Jerzy A. Przystawa, editors, *Modern Trends in the Theory of Condensed Matter*, pages 195–203, Berlin, Heidelberg, 1980. Springer Berlin Heidelberg.

[134] Matthias Troyer and Uwe-Jens Wiese. Computational complexity and fundamental limitations to fermionic quantum monte carlo simulations. *Phys. Rev. Lett.*, 94:170201, May 2005.

[135] A. M. Turner, F. Pollmann, and E. Berg. Topological phases of one-dimensional fermions: An entanglement point of view. *prb*, 83(7):075102, February 2011.

[136] J Vannimenus and G Toulouse. Theory of the frustration effect. II. ising spins on a square lattice. *Journal of Physics C: Solid State Physics*, 10(18):L537–L542, sep 1977.

[137] F. Verstraete, J. J. García-Ripoll, and J. I. Cirac. Matrix Product Density Operators: Simulation of Finite-Temperature and Dissipative Systems. *Physical Review Letters*, 93(20):207204, November 2004.

[138] F. Verstraete, V. Murg, and J. I. Cirac. Matrix product states, projected entangled pair states, and variational renormalization group methods for quantum spin systems. *Advances in Physics*, 57:143–224, March 2008.

[139] F. Verstraete, D. Porras, and J. I. Cirac. Density Matrix Renormalization Group and Periodic Boundary Conditions: A Quantum Information Perspective. *Physical Review Letters*, 93(22):227205, November 2004.

[140] Ch. Waldtmann, H. Kreutzmann, U. Schollwöck, K. Maisinger, and H.-U. Everts. Ground states and excitations of a one-dimensional kagomé-like antiferromagnet. *Phys. Rev. B*, 62:9472–9483, Oct 2000.

[141] Dave Wecker, Matthew B. Hastings, and Matthias Troyer. Progress towards practical quantum variational algorithms. *Physical Review A*, 92(4), Oct 2015.

[142] Dave Wecker, Matthew B. Hastings, Nathan Wiebe, Bryan K. Clark, Chetan Nayak, and Matthias Troyer. Solving strongly correlated electron models on a quantum computer. *Physical Review A*, 92(6), Dec 2015.

[143] X.G. Wen. *Quantum Field Theory of Many-Body Systems: From the Origin of Sound to an Origin of Light and Electrons*. Oxford Graduate Texts. OUP Oxford, 2004.

[144] Steven R. White. Density matrix formulation for quantum renormalization groups. *Phys. Rev. Lett.*, 69:2863–2866, Nov 1992.

[145] Steven R. White. Density-matrix algorithms for quantum renormalization groups. *Phys. Rev. B*, 48:10345–10356, Oct 1993.

[146] M. M. Wolf, G. Ortiz, F. Verstraete, and J. I. Cirac. Quantum Phase Transitions in Matrix Product Systems. *Physical Review Letters*, 97(11):110403, September 2006.

[147] S. Xu and B. Swingle. Accessing scrambling using matrix product operators. *ArXiv e-prints*, February 2018.

[148] Xiao Yan Xu, K.T̃. Law, and Patrick A. Lee. Pair density wave in the doped t-j model with ring exchange on a triangular lattice. *Physical Review Letters*, 122(16), Apr 2019.

[149] S. Yan, D. A. Huse, and S. R. White. Spin-liquid ground state of the s = 1/2 kagome heisenberg antiferromagnet. *Science*, 332(6034):1173–1176, Apr 2011.

[150] Hong Yao and Steven A. Kivelson. Exact chiral spin liquid with non-abelian anyons. *Physical Review Letters*, 99(24), Dec 2007.

[151] T. Zhou and D. J. Luitz. Operator entanglement entropy of the time evolution operator in chaotic systems. *prb*, 95(9):094206, March 2017.

[152] Yi Zhou, Kazushi Kanoda, and Tai-Kai Ng. Quantum spin liquid states. *Reviews of Modern Physics*, 89(2), Apr 2017.

Appendix A

Fundamentals

A.1 Fourier transform conventions

Let us first go over the discrete fourier transform. For a function defined over discete points $0, \ldots, N-1$ with spacing a between them, we can assume it to be a periodic function on the interval $[0, L)$ where $L = Na$ is the size of system. The allowed momenta in the interval $[0, 2\pi)$ are

$$k = 2\pi \frac{na}{L} \qquad \text{where} \qquad n = 0, \ldots, N-1 \tag{A.1}$$

we can also have $n = -\frac{N}{2}, \ldots, \frac{N}{2} - 1$ if we like to define the fourier transform function over the $[-\frac{\pi}{2}, \frac{\pi}{2})$ interval. The symmetric factor fourier transform is defined

$$\tilde{f}(k) = \frac{1}{\mathcal{V}^{1/2}} \sum_{x=0}^{N-1} \mathrm{e}^{-\mathrm{i}kx} \; f(x) \tag{A.2}$$

$$f(x) = \frac{1}{\mathcal{V}^{1/2}} \sum_{k=0}^{K} \mathrm{e}^{\mathrm{i}kx} \; \tilde{f}(k) \tag{A.3}$$

where we defined $K = 2\pi(N-1)a/L$ and $\mathcal{V}$ is the factor that corresponds to the volume of the space, and here is $\mathcal{V} = N$. In order to show this we perform the transform and inverse transform

$$f(x) = \frac{1}{\mathcal{V}} \sum_{x}^{N-1} \left(\sum_{k}^{K} \mathrm{e}^{\mathrm{i}k(x-x')} \right) f(x') \tag{A.4}$$

the expression in the paranthesis should be equal to $\mathcal{V}\delta_{x,x'}$. This is just a geometric series

$$\sum_{k}^{K} \mathrm{e}^{\mathrm{i}km} = \frac{1 - \mathrm{e}^{\mathrm{i}Nkm}}{1 - \mathrm{e}^{\mathrm{i}km}} \tag{A.5}$$

where we introduced $m = x - x'$ which can take values $-(N-1), \ldots, N-1$. Since Nk is always an integer multiple of 2π, the numerator is always zero. The denominator is nonzero for $m \neq 0$ and for $m = 0$ we can use the L'Hospital's rule to find the limit $m \to 0$. Therefore for the expression of Kronecker delta function we have

$$\delta_{x,x'} = \frac{1}{N} \sum_{k}^{K} \mathrm{e}^{\mathrm{i}k(x-x')}, \qquad \delta_{k,k'} = \frac{1}{N} \sum_{x}^{N-1} \mathrm{e}^{-\mathrm{i}(k-k')x} \tag{A.6}$$

If we now consider the continuous space $[0-L)$ we use the notion of number of sites in real space. Any integrable periodic function will have a fourier series with the allowed values of momenta

$$k = 2\pi \frac{n}{L}, \qquad \text{where} \qquad n \in \mathbb{Z} \tag{A.7}$$

the fouries series transform and inverse are defined as

$$\tilde{f}(k) = \frac{1}{\mathcal{V}^{1/2}} \int_{L} \mathrm{e}^{-\mathrm{i}kx} \; f(x) \; \mathrm{d}x \tag{A.8}$$

$$f(x) = \frac{1}{\mathcal{V}^{1/2}} \sum_{k=-\infty}^{\infty} \mathrm{e}^{\mathrm{i}kx} \; \tilde{f}(k) \tag{A.9}$$

where the factor $\mathcal{V}$ again corresponds to volume of space which is $\mathcal{V} = L$ for the case of fourier series. To show this again we have to perform the transform and inverse

$$f(x) = \frac{1}{\mathcal{V}} \int_L \left(\sum_{k=-\infty}^{\infty} \mathrm{e}^{\mathrm{i}k(x-x')} \right) \, f(x') \tag{A.10}$$

the term in paranthesis should be $\mathcal{V}\delta(x - x')$. Indeed it a geometric series

$$\sum_{k=-\infty}^{\infty} \mathrm{e}^{\mathrm{i}kx} = \lim_{N\to\infty} \frac{\sin((2N+1)\pi x/L)}{\sin(\pi x/L)} \tag{A.11}$$

This function is a dirac comb, which is an infinite series of equidistant Dirac delta functions. To show this we multipy this function together with an analytic function $h(x)$ and integrate by closing the contour C at the upper half of the plane. There exist infinite number of poles on the real line at $x = mL$ for $m \in \mathbb{Z}$, so we get

$$g(x) \equiv \sum_{k=-\infty}^{\infty} \mathrm{e}^{\mathrm{i}2\pi nx/L} \tag{A.12}$$

$$\begin{aligned} \int_{-\infty}^{\infty} g(x)h(x) \, \mathrm{d}x &= \Im \left[\sum_m \oint_C \frac{\exp\left(\mathrm{i(2N+1)}\pi \mathrm{z/L}\right)}{\cos(m\pi)\frac{\pi}{L}(z - mL)} h(z)\mathrm{d}z \right] \\ &= \Im \left[\pi\mathrm{i} \sum_m \frac{L}{\pi} \frac{\exp\left(\mathrm{i(2N+1)m}\pi\right)}{\cos(m\pi)} h(mL) \right] \\ &= L \sum_m h(mL) \end{aligned} \tag{A.13}$$

we therefore conclude the following equation for the Dirac comb function

$$\frac{1}{L} \sum_{k=-\infty}^{\infty} \mathrm{e}^{\mathrm{i}2\pi nx/L} = \sum_{m=-\infty}^{\infty} \delta(x - mL). \tag{A.14}$$

If we start by the transformed function and apply inverse and then transform again we will find another equality for the Kronecker delta function for $n, n' \in \mathbb{Z}$ that shows up in case of fourier series

$$\frac{1}{L} \int_0^L \mathrm{e}^{-\mathrm{i}\frac{2\pi}{L}(n-n')} \, \mathrm{d}x = \delta_{n,n'} \tag{A.15}$$

If the function is not periodic and is defined over the whole real space, then we get the continuous fourier transform

$$\tilde{f}(k) = \frac{1}{\mathcal{V}^{1/2}} \int_{-\infty}^{\infty} \mathrm{e}^{-\mathrm{i}kx}\ f(x)\ \mathrm{d}x \tag{A.16}$$

$$f(x) = \frac{1}{\mathcal{V}^{1/2}} \int_{-\infty}^{\infty} \mathrm{e}^{\mathrm{i}kx}\ \tilde{f}(k)\ \mathrm{d}k \tag{A.17}$$

In this case $\mathcal{V} = 2\pi$ to see this we need to look at the Dirac delta function definition as the fourier transform of constact function

$$\frac{1}{2\pi} \int_{-\infty}^{\infty} \mathrm{e}^{\mathrm{i}kx}\ \mathrm{d}k = \delta(x) \tag{A.18}$$

there are various way to show this, a simple approach is

$$\begin{aligned} \frac{1}{2\pi} \int_{-\infty}^{\infty} \mathrm{e}^{\mathrm{i}kx}\ \mathrm{d}k &= \frac{1}{2\pi} \int_{0}^{\infty} 2\cos(kx)\ \mathrm{d}x \\ &= \lim_{k\to\infty} \frac{1}{\pi} \frac{\sin(kx)}{x} \\ &= \lim_{k\to\infty} k\,\mathrm{sinc}(kx) = \delta(x) \end{aligned} \tag{A.19}$$

or we can make use of the fourier transform of the (un–normalized) Gaussian $\mathrm{e}^{-x^2/2\sigma^2}$ which has hight 1 at $x = 0$ and take the $\sigma \to \infty$ limit, which results in a normalized Gaussian function over k with std limit to zero.

$$\begin{aligned} \frac{1}{2\pi} \int_{-\infty}^{\infty} \mathrm{e}^{\mathrm{i}kx} \mathrm{e}^{-x^2/2\sigma^2}\ \mathrm{d}x &= \frac{1}{2\pi} \int_{-\infty}^{\infty} \mathrm{e}^{-(x-\mathrm{i}k\sigma^2)^2/2\sigma^2} \mathrm{e}^{-k^2\sigma^2/2}\ \mathrm{d}x \\ &= \lim_{\sigma\to\infty} \frac{\sigma}{\sqrt{2\pi}} \mathrm{e}^{-k^2\sigma^2/2} = \delta(k) \end{aligned} \tag{A.20}$$

As for the choice of conventions, generally different choice of where to put factor and sign is used for different purposes, so the choice of fourier transform is always mentioned.

A.2 correlation functions vs density matrices

For free theories there is direct connection between two–point correlation functions and their corresponding density matrices [110]. That is due to the fact that in free theories all correlation function of any number of operators reduces to two–point correlation functions, according to Wick's theorem. As the correlation function should also be generated by the reduced density matrix $\langle O\rangle = \mathrm{tr}(\rho O)$, the reduced density matrix is also exponential of a free theory.

For free paring-free fermionic theories of the form $H = -\sum T_{ij} c_i^\dagger c_j$ the reduced density matrix should be of the form

$$\rho \propto \mathrm{e}^{-\mathcal{K}}, \qquad \mathcal{K} = \sum_{ij} c_i^\dagger \ \hat{\mathcal{K}}_{ij} \ c_j \tag{A.21}$$

It is therefore not surprising that the same unitary diagonalization of the density matrix also diagonalizes the correlation matrix $\Lambda_{ij} = \langle c_i^\dagger c_j\rangle$. To show this explicitely, $U^\dagger \hat{\mathcal{K}} U = \mathcal{E}$ where we define the diagonal eigenvalue matrix $\mathcal{E} = \mathrm{diag}(\varepsilon_1, \cdots, \varepsilon_N)$. The correlation function, writing the creation and annihilation operators in terms of the new diagonal operators, $c_i = U_{ik} f_k$, is now

$$\begin{aligned}\Lambda_{ij} = \langle c_i^\dagger c_j\rangle &= \sum_{k,k'} \frac{1}{Z}\,\mathrm{tr}\left(\exp\Big(-\sum_k \varepsilon_l f_l^\dagger f_l\Big)\ U_{ki}^* U_{jk'} f_k^\dagger f_{k'}\right) \\ &= \sum_k U_{ki}^* U_{jk}\ \frac{1}{\mathrm{e}^{\varepsilon_k}+1}\end{aligned} \tag{A.22}$$

therefore the correlation matrix is

$$\Lambda = \Big(U(\mathrm{e}^{\mathcal{E}}+1)^{-1}U^\dagger\Big)^T \tag{A.23}$$

comparing with $\hat{\mathcal{K}} = U\mathcal{E}U^\dagger$ we arrive at the relation between the density matrix and the correlation function

$$\hat{\mathcal{K}}^T = \ln\left(\Lambda^{-1} - 1\right) \tag{A.24}$$

What about a Hamiltonian with pairing? If the Hamiltonian has the form of $H = \sum T_{ij} c_i^\dagger c_j + \frac{1}{2}\sum(\Delta_{ij} c_i^\dagger c_j^\dagger + \text{h.c.})$ then we should use the bogoliubov tranformation to diagonalize the Hamiltonian and the relation should be established between the real fermion (Majorana) correlation function and density matrix. For the density matrix it has the form

$$\rho = \propto \mathrm{e}^{\frac{\mathrm{i}}{4}\mathcal{A}}, \qquad \mathcal{A} = \sum_{ij} \eta_i \ \hat{\mathcal{A}}_{ij} \ \eta_j \tag{A.25}$$

where $\hat{\mathcal{A}}$ is an anti–symmetric matrix. If we anti–diagonalize the matrix with an orthogonal bogoliubov transformation, meaning $O^T \hat{\mathcal{A}} O = \begin{pmatrix} & \mathcal{E} \\ -\mathcal{E} & \end{pmatrix}$ where again the diagonal eigenvalue matrix is defined as $\mathcal{E} = \mathrm{diag}(\varepsilon_1, \cdots, \varepsilon_N)$. For the correlation function we now have

$$M_{ij} = \langle \eta_i \eta_j \rangle = \sum_{kk'} \mathrm{tr}\left(\exp\left(\frac{1}{2}\sum \varepsilon_i (\mathrm{i}\zeta_i \zeta_{i+N})\right) O_{ik} O_{jk'} \zeta_k \zeta_{k'}\right) \tag{A.26}$$

$$= \sum_{kk'} O_{ik} \begin{pmatrix} I & \tanh(\mathcal{E}/2) \\ -\tanh(\mathcal{E}/2) & I \end{pmatrix} O^T_{kj} \tag{A.27}$$

therfore we can write down the majorana correlation matrix

$$M = I + O \begin{pmatrix} & \tanh(\mathcal{E}/2) \\ -\tanh(\mathcal{E}/2) & \end{pmatrix} O^T \tag{A.28}$$

The usual complex fermionic correlation matrices can be writen in terms of the Majorana correlations $M = \begin{pmatrix} M^{1,2} & M^{2,2} \\ M^{2,1} & M^{2,2} \end{pmatrix}$

$$\Lambda_{ij} = \langle c_i^\dagger c_j \rangle = \frac{1}{4}\Big(M^{1,1} + M^{2,2} + \mathrm{i}(M^{1,2} - M^{2,1})\Big) \tag{A.29}$$

$$\Pi_{ij} = \langle c_i^\dagger c_j^\dagger \rangle = \frac{1}{4}\Big(M^{1,1} - M^{2,2} - \mathrm{i}(M^{1,2} + M^{2,1}\Big) \tag{A.30}$$

and the conversly the Majorana correlation function with respect to

$$M = \frac{1}{2}\begin{pmatrix} \Re(\Lambda+\Pi) & \Im(\Lambda-\Pi) \\ -\Im(\Lambda+\Pi) & \Re(\Lambda-\Pi) \end{pmatrix} \tag{A.31}$$

Same as in the hopping only case can compare the correlation matrix with $\hat{\mathcal{A}} = O\begin{pmatrix} & \mathcal{E} \\ -\mathcal{E} & \end{pmatrix}O^T$ therefore we have the relations

$$\hat{\mathcal{A}} = \ln\left(M(2-M)^{-1}\right) \tag{A.32}$$

A.3 Bogoliubov transformation

We are dealing with Gaussian (free) bosonic or fermionic theories of the from

$$H = \sum_{i,j} a_i^\dagger T_{ij} a_j + \frac{1}{2}\sum_{ij} a_i^\dagger \Delta_{ij} a_j^\dagger + \text{h.c.} \tag{A.33}$$

where the i, j goes over N sites of the system. The creation and annihilation operators $a, a^\dagger$ respectively, can be bosonic or fermoinic. In case of fermions the anit–comutation relations

$$\{a_i, a_j^\dagger\} = \delta_{ij}, \qquad \{a_i, a_j\} = 0, \tag{A.34}$$

and in the case of bosons we have the commutation relations

$$[a_i, a_j^\dagger] = \delta_{ij}, \qquad [a_i, a_j] = 0. \tag{A.35}$$

The hermiticity of H requires the hopping matrix T to be hermitian, that is $T = T^\dagger$ and the pairing matrix Δ to be symmetric for bosons $\Delta^\dagger = \Delta^*$ and anti–symmetric for fermions $\Delta^\dagger = \Delta^*$.

The Bogoliubov transformation is a linear transformation of creation and annihilation operators that leaves the particle (boson or fermion) algebra invariant. Let us show

by A, A^* the column vector [1] of all annihilation and creation operators respectively

$$A = \begin{pmatrix} a_1 \\ \vdots \\ a_N \end{pmatrix} \qquad A^* = \begin{pmatrix} a_1^\dagger \\ \vdots \\ a_N^\dagger \end{pmatrix} \tag{A.36}$$

and by $A^T, A^\dagger$ their transpose respectively

$$A^T = \begin{pmatrix} a_1 & \dots & a_N \end{pmatrix} \qquad A^\dagger = \begin{pmatrix} a_1^\dagger & \dots & a_N^\dagger \end{pmatrix} \tag{A.37}$$

the Bogoliubov transformation now generates $\gamma_k, \gamma_k^\dagger$ which obey the same particle algebras

$$\gamma_k = u_{ki}\ a_i + v_{ki}\ a_i^\dagger, \qquad [\gamma_k, \gamma_{k'}]_\mp = 0, \qquad [\gamma_k, \gamma_{k'}^\dagger]_\mp = \delta_{kk'} \tag{A.38}$$

With this definition the Hamiltonian can be written in matrix form in terms of the creation and annihilation vectors

$$H - \frac{1}{2}\operatorname{tr}(T) = \frac{1}{2}\begin{pmatrix} A^\dagger & A^T \end{pmatrix}\begin{pmatrix} T & \Delta \\ \pm\Delta^* & \pm T^* \end{pmatrix}\begin{pmatrix} A \\ A^* \end{pmatrix} \tag{A.39}$$

the $+$ corresponds to bosons and $-$ to the fermions. The constant trace term shows up because we switch half of the T matrix. The Bogoliubov transformation with the matrix notation is

$$\Gamma = \begin{pmatrix} U & V \end{pmatrix}\begin{pmatrix} A \\ A^* \end{pmatrix}, \qquad \Gamma^* = \begin{pmatrix} V^* & U^* \end{pmatrix}\begin{pmatrix} A \\ A^* \end{pmatrix} \tag{A.40}$$

where Γ (same notation as A) is the column vector of annihilations for the Bogoliubov particles and U, V are $N \times N$ matrices representing the transformation.

[1] These are not usual vectors over a field. The $a_i a_j^\dagger$ don't constitute a field because the multiplication is not commutative. Therefore, to be pedantic, the lists should be called modules overs the ring of creation and annihilation operators.

The conditions for the Bogoliubov particles to respect the corresponding algebra is

$$[\gamma_k, \gamma_{k'}]_\pm = \sum_{ij} u_{ki} v_{k'j} [a_i, a_j^\dagger] \pm v_{ki} u_{k'j} [a_i^\dagger, a_j]$$
$$= \sum_i u_{ki} v_{k'i} \pm v_{ki} u_{k'i} = 0 \tag{A.41}$$

$$[\gamma_k, \gamma_{k'}^\dagger]_\pm = \sum_{ij} u_{ki} u_{k'j}^* [a_i, a_j^\dagger] \pm v_{ki} v_{k'j}^* [a_i^\dagger, a_j]$$
$$= \sum_i u_{ki} u_{k'i}^* \pm v_{ki} v_{k'i}^* = \delta_{kk'} \tag{A.42}$$

the conditions can also be written more conveniently in matrix form

$$UV^T \pm VU^T = 0, \qquad UU^\dagger \pm VV^\dagger = I_N \tag{A.43}$$

where the $+$ is for fermions and $-$ is for bosons.

The conditions also conveniently determine the inverse of the Bogoliubov transformation

$$\begin{pmatrix} \Gamma \\ \Gamma^* \end{pmatrix} = \begin{pmatrix} U & V \\ V^* & U^* \end{pmatrix} \begin{pmatrix} A \\ A^* \end{pmatrix}, \qquad \begin{pmatrix} A \\ A^* \end{pmatrix} = \begin{pmatrix} U^\dagger & \pm V^T \\ \pm V^\dagger & U^T \end{pmatrix} \begin{pmatrix} \Gamma \\ \Gamma^* \end{pmatrix} \tag{A.44}$$

one can check that the inverse transform matrix is indeed the right inverse of the transform matrix using the conditions of Eqns. (A.43).

In case of fermions, one can diagonalize the extended Hamiltonian matrix using the usual unitary rotation with eigendecomposition and read the U, V matrices and the corresponding eigenvalues. There will be a double spectrum and the final Hamiltonian is of the form

$$H - \frac{1}{2}\operatorname{tr}(T) = \begin{pmatrix} \Gamma^\dagger & \Gamma \end{pmatrix} \begin{pmatrix} \mathcal{E} & \\ & -\mathcal{E} \end{pmatrix} \begin{pmatrix} \Gamma \\ \Gamma^* \end{pmatrix} \tag{A.45}$$

with the final Hamiltonian of the form, $\mathcal{E} = \{\varepsilon_1, \cdots, \varepsilon_N\}$

$$H = \sum_i \varepsilon_i \gamma_i^\dagger \gamma_i \tag{A.46}$$

A.3.1 transformation for real bosons and real fermions

The transformation is more natural to be considered in terms of real bosons and real femions. The real operators are

$$a_i = (\eta_i + \mathrm{i}\eta_{i+N})/2, \qquad a_i^\dagger = (\eta_i - \mathrm{i}\eta_{i+N})/2 \tag{A.47}$$

and the inverse relations

$$\eta_i = a_i + a_i^\dagger, \qquad \eta_{i+N} = \mathrm{i}(a_i^\dagger - a_i) \tag{A.48}$$

or written as a matrix, where the $\eta_\Re$ and $\eta_\Im$ are introduced as the real part and imaginary part of the complex particles

$$\begin{pmatrix} \eta_\Re \\ \\ \eta_\Im \end{pmatrix} = \begin{pmatrix} I & I \\ \\ -\mathrm{i}I & \mathrm{i}I \end{pmatrix} \begin{pmatrix} A \\ \\ A^* \end{pmatrix}, \qquad \begin{pmatrix} A \\ \\ A^* \end{pmatrix} = \frac{1}{2} \begin{pmatrix} I & \mathrm{i}I \\ \\ I & -\mathrm{i}I \end{pmatrix} \begin{pmatrix} \eta_\Re \\ \\ \eta_\Im \end{pmatrix} \tag{A.49}$$

The real operators are hemitian $\eta = \eta^\dagger$ and they inherit the commutation relations from the complex operators. For real boson

$$[\eta_i, \eta_j] = 2\mathrm{i}\ (\delta_{i,j-N} - \delta_{i-N,j}) \tag{A.50}$$

or as a matrix of bilinear form $\Omega_{i,j} \equiv [\eta_i, \eta_j]$

$$\Omega = \begin{pmatrix} & I_N \\ \\ -I_N & \end{pmatrix} \tag{A.51}$$

and for the real fermions (Majoranas)

$$\{\eta_i, \eta_j\} = 2\delta_{ij} \tag{A.52}$$

and as a matrix of bilinear form $\Omega_{i,j} \equiv \{\eta_i, \eta_j\}$

$$\Omega = \begin{pmatrix} I_N & \\ & I_N \end{pmatrix} \tag{A.53}$$

What is the most generic Bogoliubov transformation $\zeta_k = P_{ki}\eta_i$ that leaves the new particles ζ to follow the same algebras?

For fermions we have

$$\{\zeta_k, \zeta_{k'}\} = P_{ki}P_{k'j}\{\eta_i, \eta_j\} = 2P_{ki}P_{k'i} = 2\delta_{kk'} \tag{A.54}$$

Therefore the general bogoliubov transformation of real fermions is a member of orthogonal group, i.e. $P \in \mathrm{O}(2N)$. Another way to realize that Bogoliubov transformation are operators that leave the bilinear form invariant that is $P\Omega P^T = \Omega$.

For the boson we have

$$\begin{aligned} [\zeta_k, \zeta_{k'}] &= P_{ki}P_{k'j}[\eta_i, \eta_j] \\ &= 2\mathrm{i}\ (P_{ki}P_{k'i+N} - P_{ki}P_{k'i-N}) = 2\mathrm{i}\ (\delta_{k,k'-N} - \delta_{k-N,k'}) \end{aligned} \tag{A.55}$$

or in terms of the bilinear form matrix, linear transformations that leave the bosonic bilinear form (symplectic matrix) invariant, $P\Omega P^T = \Omega$, therefore the allowed transformations are members of the symplectic group $P \in \mathrm{Sp}(2N)$.

The relation between the real particle bogoliubov transformation and complex particle trasnformation is easily to find. If we show the real transformation as $P = \left(\begin{smallmatrix} A & B \\ C & D \end{smallmatrix}\right)$

then the complex particle would because

$$\begin{aligned}\gamma_k &= \frac{1}{2}(\zeta_k + \mathrm{i}\zeta_{k+N}) = \frac{1}{2}\sum_i^{2N}\left(P_{ki}\ \eta_i + \mathrm{i}P_{k+N,i}\ \eta_i\right) \\ &= \frac{1}{2}\sum_i^{N}\Big(A_{ki}\ \eta_i + B_{ki}\ \eta_{i+N} + \mathrm{i}(C_{ki}\ \eta_i + D_{ki}\ \eta_{i+N})\Big) \\ &= \frac{1}{2}\sum_i^{N}\Big(\Big[(A+D)+\mathrm{i}(C-B)\Big]_{ki}\ a_i + \Big[(A-D)+\mathrm{i}(C+B)\Big]_{ki}\ a_i^\dagger\Big)\end{aligned} \tag{A.56}$$

one can now read U, V matrices of the complex transformation from the above equations.

The Hamiltonian needs to be rewritten in terms of the real particles. For fermions

$$H_{\text{fermion}} = \begin{pmatrix}\eta_\Re & \eta_\Im\end{pmatrix}\ \frac{\mathrm{i}}{2}\begin{pmatrix}\Im(T+\Delta) & \Re(T-\Delta) \\ -\Re(T+\Delta) & \Im(T-\Delta)\end{pmatrix}\begin{pmatrix}\eta_\Re \\ \eta_\Im\end{pmatrix} \tag{A.57}$$

and for bosons we have

$$H_{\text{boson}} = \begin{pmatrix}\eta_\Re & \eta_\Im\end{pmatrix}\ \frac{1}{2}\begin{pmatrix}\Re(T+\Delta) & -\Im(T-\Delta) \\ \Im(T+\Delta) & \Re(T-\Delta)\end{pmatrix}\begin{pmatrix}\eta_\Re \\ \eta_\Im\end{pmatrix} \tag{A.58}$$

Now, in case of fermions we would like an orthogonal transformation $P \in \mathrm{O}(2N)$ which anti-diagonalizes the Hamiltonian. By that we mean

$$P^T\hat{H}P = \begin{pmatrix} & \mathcal{E} \\ -\mathcal{E} & \end{pmatrix} \tag{A.59}$$

Note that the same orthogonal transformation also diagonalizes the square matrix, that is

$$P^T\hat{H}^2P = -\begin{pmatrix}\mathcal{E}^2 & \\ & \mathcal{E}^2\end{pmatrix} \tag{A.60}$$

so one can diagonalize the square matrix and read off the the orthogonal transformation and the square of the eigenvalues.

A.3.2 translationally invariant systems

In case of translational invariance, where there are multiple species at each site (shown by greek letters) that is if $T_{\alpha\beta;ij} = t_{\alpha\beta}(j-i)$ and $\Delta_{\alpha\beta;ij} = d_{\alpha\beta}(j-i)$, where d, t are functions of distance. It is always prefered to use the fourier transform before the bogoliubov transformation. This leaves the Bogoliubov transformation only in-between different flavors of particles at each site and signifincantly reduce the computation.

A.3.3 The BCS Hamiltonian

For a translationally invariant system with hopping in each spin sector and the most general possible pairing amplitudes we have the Hamiltonian,

$$H = H_t + H_\Delta - \mu^\alpha \sum_{\mathbf{x}} f^\dagger_{\mathbf{x}'\alpha} f_{\mathbf{x}\alpha}$$

$$H_t = \sum_{\mathbf{x},\mathbf{x}'} t^\alpha(\mathbf{x}-\mathbf{x}')\ f^\dagger_{\mathbf{x}'\alpha} f_{\mathbf{x}\alpha}$$

$$H_\Delta = \sum_{\mathbf{x},\mathbf{x}'} \Delta^{\alpha\beta}(\mathbf{x}-\mathbf{x}')\ f^\dagger_{\mathbf{x}'\alpha} f^\dagger_{\mathbf{x}\beta} + \text{h.c.}$$

The chemical potential and pairing terms are already hermition, so the only hermiticity condition is $t(\mathbf{x}-\mathbf{x}') = t^*(\mathbf{x}'-\mathbf{x})$.

The translational invariance allows for the usual diagonalization of the hopping term in momentum space

$$H_t = -\sum_{\mathbf{k}} t^\alpha_{\mathbf{k}}\ f^\dagger_{\mathbf{k}\alpha} f_{\mathbf{k}\alpha}, \qquad t_{\mathbf{k}} \equiv \sum_{\mathbf{r}} t(\mathbf{r}) \mathrm{e}^{\mathrm{i}\mathbf{k}\cdot\mathbf{r}}. \tag{A.61}$$

For now we assume singlet pairing which means $\Delta^{\uparrow\uparrow} = \Delta^{\downarrow\downarrow} = 0$ and $\Delta \equiv \Delta^{\uparrow\downarrow} = -\Delta^{\downarrow\uparrow}$, the pairing terms in the Hamiltonian can now be written as $\Delta(f^\dagger_{\mathbf{x}\uparrow} f^\dagger_{\mathbf{x}'\downarrow} - f^\dagger_{\mathbf{x}\downarrow} f^\dagger_{\mathbf{x}'\uparrow}) +$

(h.c.), so each terms creates(annihilates) a singlet pair. The pairing term can also be written in momentum space as

$$H_\Delta = \sum_{\mathbf{k}} \Delta_{\mathbf{k}} (f^\dagger_{\mathbf{k}\uparrow} f^\dagger_{-\mathbf{k}\downarrow} - f^\dagger_{\mathbf{k}\downarrow} f^\dagger_{-\mathbf{k}\uparrow}) + \text{h.c.}, \qquad \Delta_{\mathbf{k}} \equiv \sum_{\mathbf{r}} \Delta(\mathbf{r}) \mathrm{e}^{\mathrm{i}\mathbf{k}\cdot\mathbf{r}} \tag{A.62}$$

more comments on $\Delta_{\mathbf{k}}$ properties for the case of singlet pairing.

The Hamiltonian can now be written in the BdG form, defining $\xi^\alpha \equiv -(t^\alpha + \mu^\alpha)$

$$H = \sum_{\mathbf{k}} \begin{pmatrix} f^\dagger_{\mathbf{k}\uparrow} & f_{-\mathbf{k}\downarrow} \end{pmatrix} \begin{pmatrix} \xi^\uparrow_{\mathbf{k}} & \Delta_{\mathbf{k}} \\ \Delta^*_{\mathbf{k}} & -\xi^\downarrow_{-\mathbf{k}} \end{pmatrix} \begin{pmatrix} f_{\mathbf{k}\uparrow} \\ f^\dagger_{-\mathbf{k}\downarrow} \end{pmatrix} + \sum_{\mathbf{k}} \xi^\downarrow_{\mathbf{k}} \tag{A.63}$$

here we also choose a real $\Delta_{\mathbf{k}}$ (explain why), so ignoring the constant term the Hamiltonian can be diagonalized using the Bogoliubov transformation. Defining $\xi^\pm_{\mathbf{k}} \equiv (\xi^\uparrow_{\mathbf{k}} \pm \xi^\downarrow_{-\mathbf{k}})/2$ we can write the matrix part of the Hamiltonian as

$$h_k = \xi^-_{\mathbf{k}} + \xi^+_{\mathbf{k}} \tau^z + \Delta_{\mathbf{k}} \tau^x \tag{A.64}$$

Now since the Hamiltonian is in the x, z plane a simple SU(2) rotation about the y axis with the rotation matrix $U_k \equiv \mathrm{e}^{\mathrm{i}(\theta/2)\tau^y}$ where $\theta = \arctan(\Delta/\xi^+)$ diagonalizes the Hamiltonian. The eigenvalues are $E_\pm = \pm E_{\mathbf{k}} \equiv \sqrt{(\xi^+_{\mathbf{k}})^2 + \Delta^2_{\mathbf{k}}}$ and the eigenvectors define the Bogoliubov particles as

$$\begin{pmatrix} \gamma_{\mathbf{k}\uparrow} \\ \gamma^\dagger_{-\mathbf{k}\downarrow} \end{pmatrix} = U_{\mathbf{k}} \begin{pmatrix} f_{\mathbf{k}\uparrow} \\ f^\dagger_{-\mathbf{k}\downarrow} \end{pmatrix} \qquad U_k \equiv \mathrm{e}^{\mathrm{i}(\theta/2)\tau^y} = \begin{pmatrix} \cos(\theta/2) & \sin(\theta/2) \\ -\sin(\theta/2) & \cos(\theta/2) \end{pmatrix} \tag{A.65}$$

These particles are fermions because the transformation is unitary. More generally, if we rename the elements unitary matrix $U_{\mathbf{k}}$ as follows

$$U_{\mathbf{k}} \equiv \begin{pmatrix} u_{\mathbf{k}} & v_{\mathbf{k}} \\ -v_{\mathbf{k}} & u_{\mathbf{k}} \end{pmatrix}, \qquad \Longrightarrow \qquad \begin{aligned} \gamma_{\mathbf{k}\uparrow} &= u_{\mathbf{k}} f_{\mathbf{k}\uparrow} + v_{\mathbf{k}} f^\dagger_{-\mathbf{k}\downarrow} \\ \gamma^\dagger_{-\mathbf{k}\downarrow} &= u_{\mathbf{k}} f^\dagger_{-\mathbf{k}\downarrow} - v_{\mathbf{k}} f_{\mathbf{k}\uparrow} \end{aligned} \tag{A.66}$$

The final diagonalized Hamiltonian in terms of the Bogoliubov particles (dropping constant terms) is then

$$H = \sum_{\mathbf{k}} (E_{\mathbf{k}} + \xi_{\mathbf{k}}^{-})\ \gamma_{\mathbf{k}\uparrow}^{\dagger}\gamma_{\mathbf{k}\uparrow} + (E_{\mathbf{k}} - \xi_{\mathbf{k}}^{-})\ \gamma_{\mathbf{k}\downarrow}^{\dagger}\gamma_{\mathbf{k}\downarrow} \tag{A.67}$$

For the case of $\xi_{\mathbf{k}}^{\uparrow} = \xi_{\mathbf{k}}^{\downarrow}$ which implies $\xi_{\mathbf{k}}^{-} = 0$, the ground state is simply given by no Bogoliubov quasiparticles, i.e. $\gamma_{\mathbf{k}\alpha}|\mathrm{BCS}\rangle = 0, \forall\, \mathbf{k}, \alpha$, so the BCS ground state can is proportional to $(\prod_{\mathbf{k}} \gamma_{\mathbf{k}\uparrow}\gamma_{\mathbf{k}\downarrow})|0\rangle$. By the insertion of the definition of Bogoliubov quasiparticles, the not yet normalized ground state is

$$|\mathrm{BCS}\rangle \propto \prod_{\mathbf{k}} (u_{\mathbf{k}} + v_{\mathbf{k}} f_{\mathbf{k}\uparrow}^{\dagger} f_{-\mathbf{k}\downarrow}^{\dagger})|0\rangle \tag{A.68}$$

we can derive representation of the ground state by defining a new parameter $g_{\mathbf{k}} \equiv \frac{v_{\mathbf{k}}}{u_{\mathbf{k}}} = \tan\frac{\theta}{2}$, and using the fact that the pairing terms commute,

$$|\mathrm{BCS}\rangle \propto \prod_{\mathbf{k}} (1 + g_{\mathbf{k}} f_{\mathbf{k}\uparrow}^{\dagger} f_{-\mathbf{k}\downarrow}^{\dagger})|0\rangle = \mathrm{e}^{\sum_{\mathbf{k}} g_{\mathbf{k}} f_{\mathbf{k}\uparrow}^{\dagger} f_{-\mathbf{k}\downarrow}^{\dagger}}|0\rangle \tag{A.69}$$

Now by restricting the BCS ground state to N fixed number of particles, with equal number $N/2$ for each $\uparrow, \downarrow$ species, we have

$$|\mathrm{BCS}\rangle_N \propto \left(\sum_{\mathbf{k}} g_{\mathbf{k}} f_{\mathbf{k}\uparrow}^{\dagger} f_{-\mathbf{k}\downarrow}^{\dagger}\right)^{N/2} |0\rangle \tag{A.70}$$

writing the Fourier transform of g as $g_{\mathbf{k}} = \sum_{\mathbf{x}} \phi(\mathbf{x}) \exp(-\mathrm{i}\mathbf{k}\cdot\mathbf{x})$, the real space wavefunction becomes

$$|\mathrm{BCS}\rangle_N \propto \left(\sum_{\mathbf{x},\mathbf{x}'} \phi(\mathbf{x}-\mathbf{x}') f_{\mathbf{x}\uparrow}^{\dagger} f_{\mathbf{x}'\downarrow}^{\dagger}\right)^{N/2} |0\rangle \tag{A.71}$$

evaluated at the configuration of $N/2$ spin up at positions $\mathbf{x}_1, \ldots, \mathbf{x}_{N/2}$ and spin downs at positions $\mathbf{x}_{N/2+1}, \ldots, \mathbf{x}_N$ we have

$$\psi(\mathbf{x}_1, \ldots, \mathbf{x}_{N/2}; \mathbf{x}_{N/2+1}, \ldots, \mathbf{x}_N) = \langle 0 | f_{\mathbf{x}_N \downarrow} \ \cdots \ f_{\mathbf{x}_{N/2+1}\downarrow} \ f_{\mathbf{x}_{N/2}\uparrow} \ \cdots \ f_{\mathbf{x}_1 \uparrow} \left(\sum_{\mathbf{x},\mathbf{x}'} \phi(\mathbf{x} - \mathbf{x}') f^\dagger_{\mathbf{x}\uparrow} f^\dagger_{\mathbf{x}'\downarrow} \right)^{N/2} |0\rangle \tag{A.72}$$

now we can pass the double fermions terms so that the $\uparrow$ spins meet their corresponding partner in each permutation term which lead to no sign change. Ignoring one general sign term depending on whether $N/2$ is odd or even, we can bring all the $\downarrow$ spins out and now the remaining $N/2$ spin $\downarrow$ fermions should find their partner by passing and odd or even number of fermions based on the permutation of each specific term. This results in the following $N/2$ determinant

$$\psi(\mathbf{x}_1, \ldots, \mathbf{x}_{N/2}; \mathbf{x}_{N/2+1}, \ldots, \mathbf{x}_N) = \begin{vmatrix} \phi(\mathbf{x}_{\uparrow,1} - \mathbf{x}_{\downarrow,1}) & \phi(\mathbf{x}_{\uparrow,1} - \mathbf{x}_{\downarrow,2}) & \cdots & \phi(\mathbf{x}_{\uparrow,1} - \mathbf{x}_{\downarrow,N/2}) \\ \phi(\mathbf{x}_{\uparrow,2} - \mathbf{x}_{\downarrow,1}) & \phi(\mathbf{x}_{\uparrow,2} - \mathbf{x}_{\downarrow,2}) & \cdots & \phi(\mathbf{x}_{\uparrow,2} - \mathbf{x}_{\downarrow,N/2}) \\ \vdots & \vdots & \ddots & \vdots \\ \phi(\mathbf{x}_{\uparrow,N/2} - \mathbf{x}_{\downarrow,1}) & \phi(\mathbf{x}_{\uparrow,N/2} - \mathbf{x}_{\downarrow,2}) & \cdots & \phi(\mathbf{x}_{\uparrow,N/2} - \mathbf{x}_{\downarrow,N/2}) \end{vmatrix} \tag{A.73}$$

that can be used for Variational Monte Carlo purposes. The only problem is whether or not this is normalized.

If the system is not translationally invariant, the same procedure can be followed except that the U, V are now full vectors derived from the eigenstates of real space hopping and pairing Hamiltonian and ϕ is a matrix given by $(U^\dagger)^{-1} V^\dagger$. Derive and show!

Appendix B

Tensor Network states

B.1 The AKLT class

The AKLT models has been introduced as the parent Hamiltonian for a particular class of states constructed from valence bonds that does not break translational symmetry of the original lattice [1, 2]. The authors call these states *valence bond solid* or VBS, since the valence bonds follow the lattice bond structure.

The simplest example is the 1D AKLT chain of spin–1s. We can start by writing the 3 dimensional Hilbert space of each site in terms of the symmetrized (triplet) pair of spin–$\frac{1}{2}$ as the symmetric tensor $\phi_{\alpha,\beta} = (\phi_\alpha \otimes \phi_\beta + \phi_\beta \otimes \phi_\alpha)/\sqrt{2}$ where $\phi_1, \phi_2 = 1, 2 = \uparrow, \downarrow$ are a basis for spin–$\frac{1}{2}$ Hilbert space. We can create a valence bond between two sites in this state by choosing a pair of indeces β, γ and multiply the state by the anti–symmetric tensor $\epsilon^{\beta\gamma}$. The result is the state $\psi_{\alpha\delta} = (\phi_{\alpha\beta} \otimes \phi_{\gamma\delta})\epsilon^{\beta\gamma}$ that can be written in terms of

Ising configuration as

$$\psi_{\alpha,\delta} = \frac{1}{2}\Big(|\alpha\uparrow\downarrow\beta\rangle + |\uparrow\alpha\downarrow\beta\rangle + |\alpha\uparrow\beta\downarrow\rangle + |\uparrow\alpha\beta\downarrow\rangle \\ -|\alpha\downarrow\uparrow\beta\rangle - |\downarrow\alpha\uparrow\beta\rangle - |\alpha\downarrow\beta\uparrow\rangle - |\downarrow\alpha\beta\uparrow\rangle \Big). \tag{B.1}$$

which is the sum of over all possible terms with one valence bond (singlet) between the two neighboring sites. Here we have 4 possible choices for singlets, if we had three sites there was 8 possible choice and in general 2^L. This is exactly the AKLT state on a lattice of size L, it is define as

$$\psi_{\alpha\beta} = (\phi_{\alpha\beta_1} \otimes \phi_{\alpha_2\beta_2} \otimes \cdots \otimes \phi_{\alpha_L,\beta})\epsilon^{\beta_1\alpha_2}\cdots\epsilon^{\beta_{L-1}\alpha_L}. \tag{B.2}$$

This is a remarkable state because it ensures the symmetry between exchange of the two spin–$\frac{1}{2}$s on each site while maintaining a singlet bond between neighboring sites! A pictorial representation of this states is shown in Fig B.1.

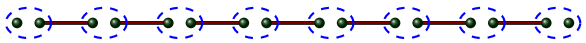

Figure B.1: A pictorial representation of the AKLT chain state. The dots are spin–$\frac{1}{2}$s, the blue dashed circle indicates the symmetrization procedure and the solid lines are singlets. Note that the ordering of dots inside a lattice site is irrelevant since they are enclosed in the symmetrization operator.

So, we know that from the four spin–$\frac{1}{2}$s of every pair of neighboring spin–1s on the chain, two of them are in a singlet state, therefore the total spin of these two sites can only be $0, 1$. This means that the P_2 operator which projects to the spin–2 sector exactly vanishes on these states. It is then natural to define the following Hamiltonian

$$H = \sum_i \mathrm{P}_2(\mathbf{S}_i, \mathbf{S}_{i+1}) = \sum_i \left(\frac{1}{2}(\mathbf{S}_i\cdot\mathbf{S}_{i+1}) + \frac{1}{6}(\mathbf{S}_i\cdot\mathbf{S}_{i+1})^2 + \frac{1}{3}\right) \tag{B.3}$$

which, by definition, has the AKLT state as its ground state.

The authors have shown that the constructed VBS state is the unique ground state of the period system with the above Hamiltonian with a finite gap. For an open system all four possible $\psi_{\alpha\beta}$ are ground states, notice the *dangling* spins at the ends of the open boundary system. It is quite surprising how the SO(3) symmetric ground state of a system made out of spin–1s exhibits *fractional* edge states that essentially behave as spin–$\frac{1}{2}$. This, probably, has been the first rigorous example of *symmetry protected topological* or SPT phase in one spatial dimension.

This construction can be generalized to higher dimensions and more complicated lattices. For example in 2D, a similar construction leads to spin–3/2s on a honeycomb lattice with the Hamiltonian projecting to neighboring spins to the space of spin–3. More generally, an AKLT state for spin–s can defined in terms of the basis of $n = 2s$ spin–$\frac{1}{2}$s at each site living on a lattice with exactly n neighbors. The state can be constructed in two different ways: we can either (i) start by combining all n spin–$\frac{1}{2}$ on every site to form a spin–s and then pick one spin–$\frac{1}{2}$ index from each pair of neighboring sites and multiply by the anti–symmetric tensor which correspond to making a valence bond or a singlet, or (ii) start with a set of neighboring singlets for each bond and then project down the spin–$\frac{1}{2}$s into a spin–s state. The Hamiltonian is then constructed from the projection operators of neighboring spin–s sites into spin–$(2s)$ and because each neighboring sites has one singlet pair by construction, the VBS state is clearly a ground state of this Hamiltonian.(improve/check, does it make sense?)

B.2 Quantum states as tensors

Let us start from the most general possible quantum state $|\psi\rangle$ for a physical system consisting of N sites, each with a local Hilbert space h_i where $\dim(h_i) = d$. Picking the local basis e_i, we have

$$|\psi\rangle = \sum_{e_i,\ldots,e_N} C^{e_i,\ldots,e_N} |e_i,\ldots,e_N\rangle . \tag{B.4}$$

Note that the state is represented by a set of complex numbers that change with change of basis, therefore the quantum state can be understood as a N–tensor represented in the chosen basis by its coefficients.

B.3 Symmetry in tensor network states

B.4 The Matrix Product States

For a quantum state defined on a chain, at every site we assign a $M_i \times M_{i+1}$ matrix $A_i^{e_i}$ (provided that M is large enough!) and then rewrite the coefficient as the product of these matrices. The new representation is called a Matrix Product State (MPS),

$$|\psi\rangle = \sum_{e_i,\ldots,e_j} \mathrm{Tr}(A_1^{e_1} \cdots A_N^{e_N}) |e_i,\ldots,e_j\rangle \tag{B.5}$$

The MPS is representation given by $d \times N$ matrices that are local to site i instead of the general N–tensor. Although looking more complicated at first it has a few advantages over the usual representation. Symmetries of states are more natural to study for a MPS. Topological nature of a phase is reflect in the transformation properties of local matrices. And also the MPS also allows for a compression scheme for a class of states that obey the *area law* which contain states that are ground states of some local Hamiltonian.

[TODO] Derivation of MPS

- Group/space of A Matrices.
- How to generate them.

It is easy to start with Eq. B.4 and generate the A matrices by singular value decomposition of the coefficient tensor. The process is as follows,

- At 1st level we start by a tensor with N legs of dimension d. By separating the leftmost leg and considering this tensor as a linear map from d dimensional space to a d^{N-1} dimensional space and performing the SVD we get the matrices of leftmost site as U and then a new tensor to be used at the next level.
- At level ℓ we start by a tensor with one bond leg with dimension $d^{\min(N-\ell,\ell)}$ and $N-\ell$ physical legs that has dimensions $d^{N-\ell}$. We then reinterpret this tensor as a linear map between $d^{\min(N-\ell,\ell)} \otimes d$ space (by considering the bond leg and the remained leftmost leg together) and the remaining physical legs that has the total dimension $d^{N-\ell-1}$. We then perform SVD. The resulted U are the matrices at site ℓ and $S * V^\dagger$ are the tensor for the next level. This process (if no truncation is required) can also be done by a QR decomposition where the singular values are not generated at all.
- At the last level N, the SVD is no longer necessary since we need to take the whole tensor as the matrices at site N.

We can perform almost the same exact procedure from the right, this alone implies that an MPS representation is not unique. In fact the space of exact MPS representation is much larger than the states.

[TODO] Graphical representation of MPS For a better understanding one can combine all A matrices for each site into a rank–3 tensor, $A_i^{a_i,a_{i+1}}$ where the i is called **physical index** that have the dimension of local Hilbert space d, and the a_i and a_{i+1} are called **bond index** with dimensions M_i and M_{i+1} respectively. The **bond dimension** is a property of the MPS.

B.4.1 The canonical form

An MPS is in *canonical form* with its center of orthogonalization at site ℓ_0 if all the matrices at a given site left of the center form a left isometry ($A_x^\dagger A_x = I$ for all $x < \ell_0$) and all the matrices at a given site right of the center, form a right isometry ($A_x A_x^\dagger = I$ for all $x > \ell_0$). The canonical MPS is useful because an SVD on the matrices at the center can be interpreted as the Schmidt decomposition of the MPS itself (see Fig).

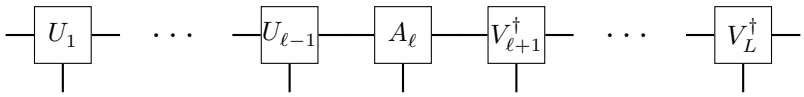

Figure B.2: A canonical MPS before and after and SVD on the center of orthogonalization.

The singular value decomposition can be performed in two different ways depending on how to make a matrix out of the three–leg tensor: when the physical index σ is bundled with the left bond index, there will be $n \equiv \min(m_l d, m_r)$ singular values that correspond to Schmidt values at link ℓ, and when the physical index σ is bundled with the right bond index, there are $n' \equiv \min(m_l, d m_r)$ singular values that correspond to Scmidth values at link $\ell - 1$

$$A_{\ell_0}^{l,\sigma,r} = U^{(l,\sigma),n} S_{\ell_0}^{n,n} V^{\dagger n,r} = U^{l,n'} S_{\ell_0-1}^{n',n'} V^{\dagger n',(\sigma,r)}. \tag{B.6}$$

If we assume the singular values of a given matrix at site A_{ℓ_0} are descending fast enough a truncation on the singular values is an optimal approximation locally for that matrix. However we do not expect such truncation to be the optimal approximation for a generic MPS, since the left(right) matrices weren't isometries to begin with, so the resulting column(row) vectors in the left(right) vector space are not necessarily orthonormal.

The effect of truncation at a given site for a generic MPS depends on the size of the overlap between left(right) vectors in the left(right) vector space. Note that if the overlaps are large, one should not even expect the singular values to drop fast enough! and a reasonable truncate may not be possible at all.

The situation for a canonical MPS at the center is the best it can be, the truncation of singular values is an optimal approximation of the state represented by that MPS.

Tensor product of MPS states

If we start with two MPSs A, B made out of matrices A_i^α, B_i^β respectively, their tensor product MPS, $C = A \otimes B$, can be found by the tensor product of the matrices. The new MPS thus has a very large bond dimension $M_l = m_l(A)m_l(B)$ which is not practical at all. However, if the two MPS were canonical with the same center, then the tensor product MPS is also canonical with centers at the same position. This allows us to optimally perform truncation on the tensor product MPS without explicitly making it.

Let's start with the two MPSs centered at the first site. At any step ℓ, we follow these steps

1. we first make the matrix C'_ℓ that is the tensor contraction of A_ℓ, B_ℓ, that are tensor with dimensions $(m_{\ell-1} \times d \times m_\ell)$, and the carry from previous step $E_{\ell-1}$ that is a $(M_{\ell-1} \times m^2_{\ell-1})$ tensor (see Fig). This step at best takes

$$\mathcal{O}(M_{\ell-1}m^2_{\ell-1}m_\ell d + M_{\ell-1}m_{\ell-1}m^2_\ell d^2) \approx \mathcal{O}(m^4) \tag{B.7}$$

2. we then bundle the physical dimension with the left index, perform SVD , $C'_\ell = U_\ell S_\ell V^\dagger_\ell$ and truncate. The SVD is on a $(dM_{\ell-1} \times m^2_\ell)$ matrix, which at best takes

$$\mathcal{O}(\min(d^2 M^2_{\ell-1}m^2_\ell, dM_{\ell-1}m^4_\ell)) \approx \mathcal{O}(m^4) \tag{B.8}$$

3. the matrices of the truncated tensor product MPS at this site are then identified as the left isometries, that is $C_\ell \coloneqq U_\ell$,

4. and the rest of the SVD defines the carry matrix for the next step $E_\ell \coloneqq S_\ell V^\dagger_\ell$

The procedure is initialized by defining $E_0 = 1$ and is terminated reaching the last step and defining $C_L \coloneqq C'_L$. The resulted MPS is canonical with center at the last site L.

While the above method produces the desired MPS, it is not very efficient. So, can we do better than $\mathcal{O}(m^4)$?

We can avoid making the matrix and performing a full SVD by defining the matrix–vector multiplication function and then feed it to a sparse SVD solver. To analyze the scaling of the matrix–vector multiplication and the sparse SVD method, we start with the best tensor contraction possible for the multiplication to the right vector (see Fig). It can be done in

$$\mathcal{O}(dm_{\ell-1}m^2_\ell + d^2 m^2_{\ell-1}m_\ell + d^2 m^2_{\ell-1}M_{\ell-1}) \approx \mathcal{O}(m^3) \tag{B.9}$$

multiplication to the left vector takes

$$\mathcal{O}(M_{\ell-1}m_{\ell-1}^2 + dm_{\ell-1}^2 m_\ell + d^2 m_{\ell-1}m_\ell^2) \approx \mathcal{O}(m^3) \tag{B.10}$$

so both direction can be done in $\mathcal{O}(m^3)$ but since we need M_ℓ singular values, then we have to perform at least $\mathcal{O}(m)$ number of the above multiplications, which leaves us with $\mathcal{O}(m^4)$ again. In practice, this approach works even worse than the straightforward method!

Iterative sparse SVD solvers

The simplest appraoch to find the largest singular values of a large matrix is by converting the SVD problem to an eigen problem and then solve that using the existing efficient eigensolvers. For a matrix $A_{m\times n}$ There are two ways to do this

1. In the augmented method one solves for the eigen problem of the following matrix

$$B = \begin{pmatrix} 0 & A_{n\times m} \\ A^\dagger_{m\times n} & 0 \end{pmatrix} \tag{B.11}$$

   Assuming $n < m$, the matrix B has $2n$ nonzero eigenvalues that are $\pm s_i$ where s_i are the n singular values of A.

2. The $A^\dagger A$ or $AA^\dagger$ method, solves for those eigen problems. The singular values of A are the square root of the found eigenvalues, so the accuracy for small singular values is not perfect!

B.4.2 Symmetry and Matrix Product States

The symmetry properties of the original state can be translated to the language of MPS in a straightforward manner. For example, translational symmetry, parity, and

time–reversal symmetry (in case of periodic boundary conditions) would imply $A_i^\alpha = A_j^\alpha$, $A = A^T$, and $A = A^*$ respectively.

The implementation of local (internal) symmetries are also relatively easy as they put specific constraints on the form of the A matrices. To see how this works we discuss a common example, the S^z_{tot} (or fermion number n_{tot}) conserving states.

Imagine an MPS for a chain of N sites of spin–1/2 Hilbert space. Let's say the S^z_{tot} is conserved, N is even, and the ground state is a total singlet (as in the ground state of the Heisenberg model for a bipartite lattice or a spin–liquid state). These states live in subset of the original Hilbert space (where the $S^z_{\text{tot}} = 0$) so we can restrict our representations to only explore this smaller subspace. The questions is how does this restriction translate to the MPS representation?

In a general case with no symmetries, the MPS representation at some site $n < N/2$ consists of two matrices which are linear maps between bond vector spaces, $V_n \to V_{n-1}$, where the bond dimensions are $\dim V_{n-1} = 2^{n-1}$ and $\dim V_n = 2^n$. Defining m as the number of down spins on the left of site n,

$$m \coloneqq \frac{1}{2}\left((n-1) - 2\sum_{i=1}^{n-1} S_i^z\right) \tag{B.12}$$

we can think of the left bond vector space V_{n-1} as the direct sum of smaller vector spaces with constant m denoted by V^m_{n-1},

$$V_{n-1} = \bigoplus_{m=0}^{n-1} V^m_{n-1}, \qquad \dim V^m_{n-1} = \binom{n-1}{m} \tag{B.13}$$

and similarly for the right bond vector space. V_n This decomposition doesn't do much for the representation of some general state, since all linear maps of the form $V_n^{m'} \to V_{n-1}^m$

should be present. However, for a state that has the symmetry, the matrix corresponding to spin $\uparrow$ only has of matrices with $m + m' = N/2 - 1$, and the the matrix corresponding to spin $\downarrow$ only has matrices with $m + m' = N/2$ and the rest of the linear map can be considered zero. This means:

- For the $\uparrow$ matrix, instead of a single matrix $A_n^{\uparrow}\colon V_n \to V_{n-1}$ we can use the following set of smaller matrices

$$A_n^{\uparrow,m}\colon V_n^{(N/2-m-1)} \to V_{n-1}^m, \qquad m = 0, \ldots, n-1 \tag{B.14}$$

- For the $\downarrow$ matrix, instead of a single matrix $A_n^{\downarrow}\colon V_n \to V_{n-1}$ we can use the following set of smaller matrices

$$A_n^{\downarrow,m}\colon V_n^{(N/2-m)} \to V_{n-1}^m, \qquad m = 0, \ldots, n-1 \tag{B.15}$$

in terms of the original matrices we can think that they consist of certain non-zero blocks according to the symmetry rule. This reduces the complexity of representation and algorithm based on the representations.

B.4.3 Tensor Product of MPS States

In practice we may sometimes need to make an MPS representation of a state that is given as a tensor product of two other states each given by their respective MPS representation. This is particularly useful, when we have a system with non–interacting flavors of spin per site or a system with non–interacting flavors of fermions, as we can solve for each individual flavor separately and then glue the MPSs together. For a spin system

we have

$$|\psi\rangle_a \otimes |\psi\rangle_b = \sum_{\{a\}\times\{b\}} (A_1 \cdots A_N)(B_1 \cdots B_N)(|a_1, \ldots, a_N\rangle \otimes |b_1, \ldots, b_N\rangle) \tag{B.16}$$

the naive approach would be to make the tensor product of A and B matrices but this approach would hugely increase the bond dimension of the MPS which is not practical. Instead we can use the direct sum, with the bond dimension being the sum of the two bond dimensions. The only problem is that now the result of multiplication of matrices is no longer a number but a 2×2 matrix instead. This is not a problem from the definition we see that it is diagonal and we only need to multiply the two numbers (they correspond to the coefficients of individual configurations that make up the new state).

As for the fermions the situation is a little more complicated, because we need to recover the Fock space convention and one has to include a negative sign when an odd number of fermion swaps are required. Let's first describe how to keep track of fermion number parity in an MPS representation. Same as with the symmetry, here we think of the left bond vector space at site n as the direct sum of two vector spaces with odd$(-)$ and even$(+)$ left fermion number parity, that is V_{n-1}^+ (V_{n-1}^-) is the vector space of all states on the left of site n where the number of fermions are even(odd),

$$V_{n-1} = V_{n-1}^+ \oplus V_{n-1}^-, \qquad \dim V_{n-1}^+ = \dim V_{n-1}^- = 2^{n-2} \tag{B.17}$$

and the same for the right bond vector space V_n. Now

- The matrix $\uparrow$ or $n_i = 1$ changes the fermion parity from left to right. So instead of $A_n^1 \colon V_n \to V_{n-1}$, we use the following two smaller matrices

$$A_n^{1,+-} \colon V_{n-1}^+ \to V_n^-, \qquad A_n^{1,-+} \colon V_{n-1}^- \to V_n^+ \tag{B.18}$$

- The matrix $\downarrow$ or $n_i = 0$ leaves the fermion parity from left to right intacet. So instead of $A_n^0 \colon V_n \to V_{n-1}$, we use the following two smaller matrices

$$A_n^{0,++} \colon V_{n-1}^- \to V_n^-, \qquad A_n^{0,--} \colon V_{n-1}^- \to V_n^- \tag{B.19}$$

These other than keeping track of fermion parity, they will also compress the MPS representation and may be employed in algorithms as well.

Now we can glue MPS states for multiple flavors of fermions together. Let us start with two flavors $f^\dagger$ and $c^\dagger$ and assume $c^\dagger$ fermions are in a MPS format that keeps track of parity. At site n we have four matrices corresponding to physical dimension where each of those are given by two matrices that keep track of left $c^\dagger$ fermion number parity.

B.4.4 The Matrix Product Operator (MPO)

The Hamiltonian H at bond $(i, i+1)$ can be decomposed into a part that has support only on sites $[1, i]$ which we call L^i, a part that has support only on sites $[i+1, N]$ which we call R^i and n_i number of parts that have support across the bond. So we can write the Hamiltonian as

$$H = L^i \otimes I^{(i+1)\to N} + \sum_{a_i}^{n_i} \ell_{a_i}^i \otimes r_{a_i}^i + I^{1\to i} \otimes R^i \tag{B.20}$$

where as ususal I stands for the identity operator and $I^{i\to j}$ is the tensor product of identities from i to j. The above Hamiltonian decomposition may be written as a formal vector

product of two $m_i \equiv n_i + 2$ size vectors Λ^i and P^i

$$H = \left[\begin{array}{c|ccc|c} L^i & \ell_1^i & \dots & \ell_{n_i}^i & I \end{array}\right] \otimes \left[\begin{array}{c} I \\ \hline r_1^i \\ \vdots \\ r_{n_i}^i \\ \hline R^i \end{array}\right] = \Lambda^i \otimes P^i \tag{B.21}$$

In order to find the MPO representation at ith site we need to find the formal matrix $W_{\alpha\beta}$ such that we can write

$$H = \Lambda_\alpha^{i-1} \otimes W_{\alpha\beta}^i \otimes P_\beta^i = \Lambda_\alpha^i \otimes W_{\alpha\beta}^i \otimes P_\beta^{i+1} \tag{B.22}$$

Writing the same Hamiltonian at Eq. B.20 with operators at the ith site explicitely we can related to the decomposition at bond $(i-1, i)$,

$$\begin{aligned}
H &= L^i \otimes I^{(i+1)\to N} + \sum_{a_i}^{n_i} \ell_{a_i}^i \otimes r_{a_i}^i + I^{1\to i} \otimes R^i \\
&= \left(L^{i-1} \otimes I^i + I^{1\to(i-1)} \otimes \sum_{d_i} H^i + \sum_{b_i} \ell_{b_i}^{i-1} \otimes \mathcal{O}_{b_i}^i \right) \otimes I^{(i+1)\to N} \\
&+ \sum_{c_i} I^{1\to(i-1)} \otimes \mathcal{O}_{c_i} \otimes r_{c_i}^i + \sum_{d_i} \ell_{d_i}^{i-1} \otimes \mathcal{O}_{d_i} \otimes r_{d_i}^i \\
&+ I^{1\to(i-1)} \otimes I^i \otimes R^i
\end{aligned} \tag{B.23}$$

$$\begin{aligned}
&= \left(\Lambda_1^{i-1} \otimes I^i + \Lambda_{m_{i-1}}^{i-1} \otimes H^i + \sum_{b_i} \Lambda_{b_i}^{i-1} \otimes \mathcal{O}_{b_i}^i \right) \otimes P_1^i \\
&+ \Lambda_{m_i}^{i-1} \otimes \sum_{c_i} \mathcal{O}_{c_i} \otimes P_{c_i}^i + \sum_{d_i} \Lambda_{d_i}^{i-1} \otimes \mathcal{O}_{d_i} \otimes P_{d_i}^i \\
&+ \Lambda_{m_{i-1}}^{i-1} \otimes I^i \otimes P_{m_i}^i
\end{aligned} \tag{B.24}$$

Here, All terms with support only on site i are labeled as H^i, where the indexes d_i runs over the number of terms that has support both left and right of ith site, c_i runs over terms that start at site i and b_i over terms that finish at site i. This means that $n_i = |d_i| + |c_i|$ and $n_{i-1} = |d_i| + |b_i|$ and that W^i is a $m_{i-1} \times m_i$[1] formal matrix.

The formal MPO matrix would take the following form, note that the following matrix form is simplistic meant just for general understanding.

$$W^i = \left(\begin{array}{c|cccc|c} I & 0 & 0 & 0 & 0 & 0 \\ \hline \mathcal{O}_{b_i} & 0 & 0 & 0 & 0 & 0 \\ \hline 0 & \mathcal{O}_{d_i} & & & 0 & 0 \\ 0 & & \mathcal{O}_{d_i} & & 0 & 0 \\ 0 & & & \mathcal{O}_{d_i} & 0 & 0 \\ \hline H^i & 0 & 0 & 0 & \mathcal{O}_{c_i} & I \end{array}\right) \tag{B.25}$$

In this sense the above calculations suggest the following algorithm, which can be thought of as automata machine

A few examples are in order, the MPO for the quantum Ising model in transverse field is

$$W^i_{\text{QITF}} = \begin{pmatrix} I & & \\ S^z & & \\ hS^x & gS^z & I \end{pmatrix}. \tag{B.26}$$

[1] or $(n_{i-1}+2) \times (n_i+2)$

For the same model but with next nearest neighbors the above algorithm generates the following MPO

$$W^i_{\text{QITFnnn}} = \begin{pmatrix} I & & & & \\ S^z & & & & \\ S^z & & & & \\ 0 & I & & & \\ hS^x & 0 & gS^z & g'S^z & I \end{pmatrix} \tag{B.27}$$

It should be noted that this may not be the most compact MPO representation. For example the following two MPOs also generate the same nnn qitf Hamiltonian but they 4×4 instead

$$W_1 = \begin{pmatrix} I & & & \\ S^z & & & \\ 0 & I & & \\ hS^x & gS^z & g'S^z & I \end{pmatrix}, \qquad W_2 = \begin{pmatrix} I & & & \\ g'S^z & & & \\ gS^z & I & & \\ hS^x & 0 & S^z & I \end{pmatrix}. \tag{B.28}$$

Another important example is interaction with exponential decay, in the case of QITF model the following MPO generates the exponential decay of Ising terms with powers of λ

$$W_{\text{QITFexp}} = \begin{pmatrix} I & & \\ S^z & \lambda I & \\ hS^x & gS^z & I \end{pmatrix} \tag{B.29}$$

So one might ask how can we find the most compact expression of MPO matrix given a Hamiltonian? One can in principle use the singular value decomposition technique to reduce the size of the MPO matrix. More efficient and generic approached for MPO reduction exist [59]. Regardless of the method, a compact MPO is an important step of the DMRG

or other MPS based methods, as these algorithms usually scale with $\mathcal{O}(W^2)$, where W is the dimensions of MPO on the state space.

B.4.5 MPO for ring exchange operator

To demonstrate the MPO construction, here we lay out the details for a fairly complicated operator, the ring exchange operator. The Hamiltonian for the ring exchange operator is defined based on the permutation operator

$$H = \sum_x (P_{x,x+2,x+3,x+1} + \text{h.c.}), \qquad P_{1234}|\sigma_1\sigma_2\sigma_3\sigma_4\rangle = |\sigma_4\sigma_1\sigma_2\sigma_3\rangle \tag{B.30}$$

Lets try to write this Hamiltonian in terms of spin operators. We know that the Heisenberg operators is equal to

$$\mathbf{S}_i \cdot \mathbf{S}_j = \frac{1}{2} P_{ij} - \frac{1}{4} \qquad P_{12}|\sigma_1\sigma_2\rangle = |\sigma_2\sigma_1\rangle \tag{B.31}$$

since the four–spin permutation can be written in terms of two–spin permutations we have

$$P_{ijkl} = P_{ij} P_{jk} P_{kl} \tag{B.32}$$

$$= (2\ \mathbf{S}_i \cdot \mathbf{S}_j + \frac{1}{2})(2\ \mathbf{S}_j \cdot \mathbf{S}_k + \frac{1}{2})(2\ \mathbf{S}_k \cdot \mathbf{S}_l + \frac{1}{2}) = \tag{B.33}$$

$$+ 8\ (\mathbf{S}_i \cdot \mathbf{S}_j)\ (\mathbf{S}_j \cdot \mathbf{S}_k)\ (\mathbf{S}_k \cdot \mathbf{S}_l)$$

$$+ 2\ \Big((\mathbf{S}_i \cdot \mathbf{S}_j)\ (\mathbf{S}_j \cdot \mathbf{S}_k) + (\mathbf{S}_i \cdot \mathbf{S}_j)\ (\mathbf{S}_k \cdot \mathbf{S}_l) + (\mathbf{S}_j \cdot \mathbf{S}_k)\ (\mathbf{S}_k \cdot \mathbf{S}_l)\Big)$$

$$+ \frac{1}{2}\ (\mathbf{S}_i \cdot \mathbf{S}_j + \mathbf{S}_j \cdot \mathbf{S}_k + \mathbf{S}_k \cdot \mathbf{S}_l) + \frac{1}{8} \tag{B.34}$$

lets start by the first term which is the multiplication of three Heisenberg terms with sharing sites

$$(\mathbf{S}_i \cdot \mathbf{S}_j)\ (\mathbf{S}_j \cdot \mathbf{S}_k)\ (\mathbf{S}_k \cdot \mathbf{S}_l) = \tag{B.35}$$

$$+ \frac{1}{16} S_i^z S_l^z + \frac{1}{16} S_i^z S_k^+ S_l^- - \frac{1}{16} S_i^z S_k^- S_l^+ \tag{B.36}$$

$$+ \frac{1}{8} S_i^z S_j^+ S_k^- S_l^z + \frac{1}{8} S_i^z S_j^+ (\frac{1}{2} - S_k^z) S_l^- + 0 \tag{B.37}$$

$$+ \frac{1}{8} S_i^z S_j^- S_k^+ S_l^z - 0 - \frac{1}{8} S_i^z S_j^- (\frac{1}{2} + S_k^z) S_l^+ \tag{B.38}$$

$$+ \frac{1}{16} S_i^+ S_j^- S_l^z + \frac{1}{16} S_i^+ S_j^- S_k^+ S_l^- - \frac{1}{16} S_i^+ S_j^- S_k^- S_l^+ \tag{B.39}$$

$$+ \frac{1}{8} S_i^+ (\frac{1}{2} - S_j^z) S_k^- S_l^z + \frac{1}{8} S_i^+ (\frac{1}{2} - S_j^z)(\frac{1}{2} - S_k^z) S_l^- + 0 \tag{B.40}$$

$$+ 0 + 0 + 0 \tag{B.41}$$

$$- \frac{1}{16} S_i^- S_j^+ S_l^z - \frac{1}{16} S_i^- S_j^+ S_k^+ S_l^- + \frac{1}{16} S_i^- S_j^+ S_k^- S_l^+ \tag{B.42}$$

$$+ 0 + 0 + 0 \tag{B.43}$$

$$- \frac{1}{8} S_i^- (\frac{1}{2} + S_j^z) S_k^+ S_l^z + 0 + \frac{1}{8} S_i^- (\frac{1}{2} + S_j^z)(\frac{1}{2} + S_k^z) S_l^+ \tag{B.44}$$

$$= \frac{1}{16} \times \Big(S_i^z S_l^z + \frac{1}{2} (S_i^- S_l^+ + S_i^+ S_l^-) \tag{B.45}$$

$$+ S_i^z S_k^+ S_l^- - S_i^z S_k^- S_l^+ + S_i^z S_j^+ S_l^- - S_i^z S_j^- S_l^+ + S_i^+ S_j^- S_l^z + S_i^+ S_k^- S_l^z \tag{B.46}$$

$$- S_i^+ S_j^z S_l^- - S_i^+ S_k^z S_l^- - S_i^- S_j^+ S_l^z - S_i^- S_k^+ S_l^z + S_i^- S_j^z S_l^+ + S_i^- S_k^z S_l^+ \tag{B.47}$$

$$+ 2 S_i^z S_j^+ S_k^- S_l^z - 2 S_i^z S_j^+ S_k^z S_l^- + 2 S_i^z S_j^- S_k^+ S_l^z - 2 S_i^z S_j^- S_k^z S_l^+ \tag{B.48}$$

$$+ S_i^+ S_j^- S_k^+ S_l^- - S_i^+ S_j^- S_k^- S_l^+ - 2 S_i^+ S_j^z S_k^- S_l^z + 2 S_i^+ S_j^z S_k^z S_l^- \tag{B.49}$$

$$- S_i^- S_j^+ S_k^+ S_l^- + S_i^- S_j^+ S_k^- S_l^+ - 2 S_i^- S_j^z S_k^+ S_l^z + 2 S_i^- S_j^z S_k^z S_l^+ \Big) \tag{B.50}$$

The second term is two Heisenberg terms with or without sharings, if they share,

$$(\mathbf{S}_i \cdot \mathbf{S}_j)\ (\mathbf{S}_j \cdot \mathbf{S}_k) = \tag{B.51}$$

$$+ \frac{1}{4} S_i^z S_k^z + \frac{1}{4} S_i^z S_j^+ S_k^- - \frac{1}{4} S_i^z S_j^- S_k^+ \tag{B.52}$$

$$+ \frac{1}{4} S_i^+ S_j^- S_k^z + \frac{1}{4} S_i^+ (\frac{1}{2} - S_j^z) S_k^- + 0 \tag{B.53}$$

$$- \frac{1}{4} S_i^- S_j^+ S_k^z + 0 + \frac{1}{4} S_i^- (\frac{1}{2} + S_j^z) S_k^+ \tag{B.54}$$

$$= \frac{1}{4} \times \Big(S_i^z S_k^z + \frac{1}{2} (S_i^+ S_k^- + S_i^+ S_k^-) \tag{B.55}$$

$$+ S_i^z (S_j^+ S_k^- - S_j^- S_k^+) + S_k^z (S_i^+ S_j^- - S_i^- S_j^+) + S_j^z (S_i^- S_k^+ - S_i^+ S_k^-) \Big) \tag{B.56}$$

$$= \frac{1}{4} (\mathbf{S}_i \cdot \mathbf{S}_k + \sum_{\{ijk\}} \epsilon_{abc} S_a^z S_b^+ S_c^-) \tag{B.57}$$

and if they don't share

$$(\mathbf{S}_i \cdot \mathbf{S}_j)\ (\mathbf{S}_k \cdot \mathbf{S}_l) = \tag{B.58}$$

$$+ S_i^z S_j^z S_k^z S_l^z + \frac{1}{2} S_i^z S_j^z S_k^+ S_l^- + \frac{1}{2} S_i^z S_j^z S_k^- S_l^+ \tag{B.59}$$

$$+ \frac{1}{2} S_i^+ S_j^- S_k^z S_l^z + \frac{1}{4} S_i^+ S_j^- S_k^+ S_l^- + \frac{1}{4} S_i^+ S_j^- S_k^- S_l^+ \tag{B.60}$$

$$+ \frac{1}{2} S_i^- S_j^+ S_k^z S_l^z + \frac{1}{4} S_i^- S_j^+ S_k^+ S_l^- + \frac{1}{4} S_i^- S_j^+ S_k^- S_l^+ \tag{B.61}$$

So summing them all up the final answer is

$$P_{ijkl} = S_i^+ S_j^- S_k^+ S_l^- + S_i^- S_j^+ S_k^- S_l^+ + 2S_i^z S_j^z S_k^z S_l^z \tag{B.62}$$

$$+ S_i^z S_j^z (S_k^+ S_l^- + S_k^- S_l^+) - S_i^z S_k^z (S_j^+ S_l^- + S_j^- S_l^+) \tag{B.63}$$

$$+ S_i^z S_l^z (S_j^+ S_k^- + S_j^- S_k^+) + S_j^z S_k^z (S_i^+ S_l^- + S_i^- S_l^+) \tag{B.64}$$

$$- S_j^z S_l^z (S_k^- S_i^+ + S_i^- S_k^+) + S_k^z S_l^z (S_i^- S_j^+ + S_i^+ S_j^-) \tag{B.65}$$

$$+ \frac{1}{2} \times \Big($$

$$+ S_i^z (S_j^+ S_k^- - S_j^- S_k^+) + S_k^z (S_i^+ S_j^- - S_i^- S_j^+) + S_j^z (S_i^- S_k^+ - S_i^+ S_k^-) \tag{B.66}$$

$$+ S_j^z (S_k^+ S_l^- - S_k^- S_l^+) + S_l^z (S_j^+ S_k^- - S_j^- S_k^+) + S_k^z (S_j^- S_l^+ - S_j^+ S_l^-) \tag{B.67}$$

$$+ S_k^z (S_l^+ S_i^- - S_l^- S_i^+) + S_i^z (S_k^+ S_l^- - S_k^- S_l^+) + S_l^z (S_i^+ S_k^- - S_i^- S_k^+) \tag{B.68}$$

$$+ S_l^z (S_i^+ S_j^- - S_i^- S_j^+) + S_j^z (S_i^- S_l^+ - S_i^+ S_l^-) + S_i^z (S_j^+ S_l^- - S_j^- S_l^+) \tag{B.69}$$

$$\Big)$$

$$+ \frac{1}{2} \left(\mathbf{S}_i \cdot \mathbf{S}_j + \mathbf{S}_j \cdot \mathbf{S}_k + \mathbf{S}_k \cdot \mathbf{S}_l + \mathbf{S}_i \cdot \mathbf{S}_k + \mathbf{S}_k \cdot \mathbf{S}_l + \mathbf{S}_i \cdot \mathbf{S}_l \right) + \frac{1}{8} \tag{B.70}$$

Now for the Hamiltonian term $H_{ijkl} = P_{ijkl} + \text{h.c.}$ we get all the terms with three spin interactions to vanish (because they are anti-hermitian) and everything else double so:

$$H_{ijkl} = 2 \times \Big(S_i^+ S_j^- S_k^+ S_l^- + S_i^- S_j^+ S_k^- S_l^+ + 2S_i^z S_j^z S_k^z S_l^z \tag{B.71}$$

$$+ S_i^z S_j^z (S_k^+ S_l^- + S_k^- S_l^+) - S_i^z S_k^z (S_j^+ S_l^- + S_j^- S_l^+) \tag{B.72}$$

$$+ S_i^z S_l^z (S_j^+ S_k^- + S_j^- S_k^+) + S_j^z S_k^z (S_i^+ S_l^- + S_i^- S_l^+) \tag{B.73}$$

$$- S_j^z S_l^z (S_k^- S_i^+ + S_i^- S_k^+) + S_k^z S_l^z (S_i^- S_j^+ + S_i^+ S_j^-) \Big) \tag{B.74}$$

$$+ \mathbf{S}_i \cdot \mathbf{S}_j + \mathbf{S}_j \cdot \mathbf{S}_k + \mathbf{S}_k \cdot \mathbf{S}_l + \mathbf{S}_i \cdot \mathbf{S}_k + \mathbf{S}_k \cdot \mathbf{S}_l + \mathbf{S}_i \cdot \mathbf{S}_l + \frac{1}{4} \tag{B.75}$$

Appendix C

The Variational Monte–Carlo Method (VMC)

C.1 The General idea

Consider a (Hermitian) operator $\mathcal{O}\colon \mathcal{H} \to \mathcal{H}$ and a quantum state $|\psi\rangle \in \mathcal{H}$. We are interested in measuring the expectation value of the operator over the the quantum state defined by

$$\langle \mathcal{O} \rangle = \frac{\langle \psi | \mathcal{O} | \psi \rangle}{\langle \psi | \psi \rangle}. \tag{C.1}$$

The Hilbert space is extremely large and an actual representation of the state and operator is not available to us. However, if we happen to know the action of the operator $\mathcal{O}$ and projections of the state on some basis (spatial sites for example) then we can write the

following

$$\langle \mathcal{O} \rangle = \sum_{\alpha,\beta} \frac{\langle \alpha|\psi\rangle\langle\alpha|\mathcal{O}|\beta\rangle\langle\beta|\psi\rangle}{\langle\psi|\psi\rangle}$$
$$= \sum_{\alpha} \frac{|\langle\psi|\alpha\rangle|^2}{\langle\psi|\psi\rangle} \left(\sum_{\beta} \frac{\langle\beta|\psi\rangle}{\langle\alpha|\psi\rangle}\langle\alpha|\mathcal{O}|\beta\rangle \right) = \sum_{\alpha} p_\alpha f_\alpha(\mathcal{O}) \tag{C.2}$$

where we have defined

$$p_\alpha \coloneqq \frac{|\langle\psi|\alpha\rangle|^2}{\langle\psi|\psi\rangle}, \tag{C.3}$$

$$f_\alpha(\mathcal{O}) \coloneqq \sum_{\beta} \frac{\langle\beta|\psi\rangle}{\langle\alpha|\psi\rangle}\langle\alpha|\mathcal{O}|\beta\rangle = \sum_{\beta} \frac{\langle\beta|\psi\rangle}{\langle\alpha|\psi\rangle}\langle\beta|\mathcal{O}^\dagger|\alpha\rangle^*. \tag{C.4}$$

The parameter $f_\alpha(\mathcal{O})$ can be interpreted as some magnitude of operator $\mathcal{O}$ at configuration α, while p_α has the properties of a probability distribution (in the Kolmogorov sense) over all configurations for the given state ψ. These interpretations make it clear that we can estimate the expectation values of the desired operators by sampling over the configuration space.

C.2 VMC on Gutzwiller Projected Spinons

Here we have two flavors of spinons $c_\uparrow, c_\downarrow$, with the variational wavefunction of free spinons hopping and Gutzwiller projection is implemented through manually exploring(sampling) the single occupancy subspace. The spin operators at site i in terms of the spinons are given by

$$S_i^z = \frac{1}{2}(n_{i\uparrow} - n_{i\downarrow}), \quad S_i^+ = c_{i\uparrow}^\dagger c_\downarrow, \quad S_i^- = c_{i\downarrow}^\dagger c_\uparrow \tag{C.5}$$

The measurements of S^z and correlation functions of S^z is then trivial as it is a diagonal operator in this basis. For non-diagonal operators let us consider the simplest

non-trivial correlation $\langle S_i^+ S_j^- \rangle$, we need to calculate

$$f_\alpha(S_i^+ S_j^-) = \sum_\beta \frac{\langle \beta|\psi\rangle}{\langle \alpha|\psi\rangle} \langle \beta|S_j^+ S_i^-|\alpha\rangle^* \tag{C.6}$$